NANO-PARTICLE BASED PHOTO-CATALYTIC MEMBRANE FOR REMOVAL OF ORGANIC & MICROBIAL POLLUTANTS   IN WATER

BY

ZEINAB AHMED SULIMAN AHMED

A Thesis Submitted in Partial Fulfillment of the Requirements For The Award Of Degree of Doctor Of Philosophy in Industrial Engineering, Department of Manufacturing, Industrial and Textile Engineering, School of Engineering, Moi university-Eldoret, Kenya

January 2025

DECLARATION

Declaration by the Candidate

This thesis is my original work and has not been presented for a degree in any other University. No part of this thesis may be reproduced without the prior written permission of the author and/or Moi University.

Signature: _____ Date   14/8/2024

Zeinab Ahmed Suliman

PHD/IE/5511/21

Declaration by Supervisors

This thesis has been submitted for examination with our approval as University Supervisors.

Signature: _____ Date   14/8/2024

Prof. Josphat Igadwa Mwasiagi

(Moi University, Eldoret, Kenya)

Signature: _____ Date   19/8/2024

Dr. Cleophas Achisa Mecha

(Moi University, Eldoret, Kenya)

DEDICATION

This thesis is dedicated to my family, both near and far, for their unwavering support, encouragement, love, and prayers. I also extend my heartfelt gratitude to my advisors for their invaluable guidance, trust, and assistance.

ABSTRACT

Water is essential for life; however, many people in developing countries, particularly in rural areas, lack access to clean and safe piped water. Untreated potable water often contains biological and chemical pollutants, leading to diseases and even death. Developing eco-friendly technologies using available resources can help address this critical issue. This study aimed to develop and test new nanoparticle-based photocatalytic membranes for point-of-use water treatment systems. Specific objectives were to synthesize and characterize metal-ion-doped TiO_2 photocatalysts coated on polyester membranes, to investigate photocatalytic membrane treatment of wastewater targeting organic and microbial contaminants, to evaluate the disinfection and organic degradation kinetics and synergy of the photocatalytic water treatment, and to assess membrane fouling and reuse potential. TiO_2, ZnO, and Fe_2O_3 were successfully synthesized; synthetic and commercial TiO_2 were doped with ZnO and Fe_2O_3. The target pollutants were reactive blue dye, oxytetracycline (OTC), and *E. coli*. Pure and co-doped photocatalysts were incorporated into polyester membranes via an aqueous heat attachment method to enhance antimicrobial properties, photodegradation of organic pollutants, and antifouling capabilities under sunlight irradiation. The photocatalysts and membranes were characterized using Scanning Electron Microscopy (SEM), Energy-Dispersive X-ray Spectroscopy (EDX), X-ray Diffraction (XRD), Fourier Transform Infrared Spectroscopy (FTIR), and UV–Visible Diffuse Reflectance Spectroscopy (UVDRS). Synthetic feed water containing oxytetracycline (1, 2, and 3 mg/L) and *E. coli* (12×10^4 and 6×10^4 CFU/100 ml) as well as real dam water containing 13×10^3 CFU/100 ml were used for disinfection performance tests. The synergy between the physical filtration of uncoated membranes and the photocatalytic activity of coated membranes (PTFT, PTFC, PTZT, PTZC, and PZ) was evaluated by measuring the synergy index (SI) through log reduction for disinfection and removal efficiency for organic pollutants. The antifouling properties were tested by assessing membrane flux and antifouling performance. Doping enabled visible light absorption, as confirmed by UVDRS analysis TiO_2 displays photo-absorption about 329.9 nm increased by doping to 438.8 nm for TiO_2/Fe_2O_3 and 375.5 nm for TiO_2/ZnO. Solar photocatalytic degradation achieved complete (100%) removal of the dye within 2 hours under solar irradiation for all dye concentrations studied using co-doped photocatalysts. The optimum conditions for degrading OTC were pH 5, flowrate 117 ml/min, and 1 mg/L OTC concentration achieving 96.308% removal. PTZT and PTZC membranes achieved 5-log reduction, the best value observed among uncoated and coated membranes against *E. coli* in both synthetic and dam water. SI for the disinfection of synthetic and real wastewater were 1.11 to 1.24 and 1.07 to 1.09; and SI for photodegradation of OTC were 1.05 to 1.26 and 1.22 to 1.54 for PTZT and PTFT respectively, doping enhanced membrane fouling resistance, extending usage from 2 cycles to 5, 4, 3, 3, and 2.5 cycles for PTFT, PTFC, PTZT, PTZC, and PZ. In conclusion modifying membranes by incorporating photocatalysis nanoparticles can enhance their antifouling capabilities and improve their overall properties, thereby increasing their effectiveness. Based on the study's findings, doping TiO_2 with Fe_2O_3 and ZnO is recommended to combine ZnO's antimicrobial properties with Fe_2O_3's visible light absorbance.

TABLE OF CONTENTS

LIST OF TABLES

LIST OF FIGURES

LIST OF ACRONYMS AND ABBREVIATION

ABBREVIATION	DEFINITION
Ag	Silver
Bq/l	Becquerel per liter
CFU	Colony Forming Units
Cu	Cupper
E. coli	*Escherichia coli*
EDX	Energy-dispersive X-ray analysis
Eg	band gap energy
FWHM	full width at half maximum
g-C_3N_4	graphitic carbon nitride
ISO	International Organization for Standardization
KEBS	Kenya Bureau of Standards
LRV	Log reduction value
mg/l	milligrams per liter
Ncms	Nanostructured Catalytic Membranes
POU	Point-Of-Use
PT	Polyester membranes/ TiO_2
PTZC	Polyester membranes/ TiO_2-ZnO from commercial TiO_2
PTZT	Polyester membranes/ TiO_2-ZnO from synthesis TiO_2
PZ	Polyester membranes/ ZnO

PZC	point of zero net charge
ROS	Reactive oxygen species
RRWTS	Rural Remote Water Treatment System
S. aureus	*Staphylococcus aureus*
SEM	Scanning electron microscopy
FTIR	Fourier transform-infrared Spectroscopy
SSF	Slow Sand Filtration
TFT	TiO_2-Fe_2O_3 from synthesis TiO_2
TFC	TiO_2-Fe_2O_3 From commercial TiO_2
TZT	TiO_2-ZnO from synthesis TiO_2
TZC	TiO_2-ZnO From commercial TiO_2
NP	Nano particles
UV DRS	Ultraviolet-Visible Diffuse Reflectance Spectroscopy
UV	Ultraviolet-Visible Spectroscopy
WHO	World Health Organization
XRD	X-Ray Diffractometer
ZnO	Zinc oxide
$Fe2O_3$	Ferric oxide
μg/l	micrograms per liter

ACKNOWLEDGEMENTS

First and foremost, I would like to express my deepest gratitude and praise to Almighty Allah for guiding and inspiring me throughout my PhD journey.

I am profoundly grateful to my supervisors, Prof. Josphat Igadwa Mwasiagi and Dr. Cleophas Achisa Mecha, for their unwavering support and guidance. Their dedication to providing not only scientific insights but also intercultural lessons has been invaluable, and this work would not have been possible without them.

I extend my heartfelt thanks to the European Commission (EU) for funding this study through the Strengthening Mobility and Promoting Regional Integration in Engineering Education in Africa (SPREE) program (Grant numbers 614586-mobaf-20191-1). Special thanks to the program coordinator and administrator for their support and operation of this scholarship.

My gratitude also goes to the Department of Manufacturing, Industrial, and Textile Engineering (MIT) at Moi University. I appreciate the chair of the department, the postgraduate coordinator, my lecturers for their valuable inputs, and the secretaries and technicians for their assistance.

I am thankful to the Department of Chemical Engineering, the chair of the department, and the technicians for allowing me access to their lab. Similarly, I appreciate the Department of Mechanical Engineering, the chair of the department, and the technicians for providing access to the workshop and assisting with welding and preparing my solar unit. I am also grateful to the Department of Civil Engineering, the chair of the department, and the technicians for granting me access to their lab and providing a space for my unit.

CHAPTER 1

INTRODUCTION

1.1 Background to the study

Water scarcity and contamination pose significant global challenges affecting public health, economic development, and environmental sustainability (Mishra, 2023). Currently, one-third of the global population experiences water shortages, with one billion people lacking direct access to clean drinking water. This issue is exacerbated by factors such as population growth, industrialization, climate change, depletion of natural water reservoirs, and environmental pollution. Since the industrial revolution, improved living standards, intensified agriculture, and manufacturing have driven a steady increase in freshwater demand. These same activities also contribute to the growing quantity and diversity of chemical contaminants in wastewater each year (Jayawardena, 2021; Mufungizi et al., 2024). In most urban and suburban regions of the developed world, water undergoes treatment at centralized facilities and is then distributed directly to homes with residual chlorine content, effectively preventing gastrointestinal infections from waterborne pathogens. However, such services are often unavailable in developing countries and even in some rural and suburban areas of developed countries. These regions lack the economic capacity to maintain centralized water treatment plants that can fully meet their population's needs. The combination of treatment plants and distribution systems is impractical for rural areas in developing nations due to the financial and infrastructural demands required for safe water treatment and delivery. Consequently, these communities frequently rely on untreated natural water sources, such as rivers, lakes, groundwater, or rain (Nunnelley, 2018). To address these concerns, several water purification techniques have been created. Conventional techniques encompass filtration,

sedimentation, flocculation, coagulation, and disinfection (Adesina et al., 2024). Superior pollutant removal is achieved by the use of sophisticated procedures such advanced oxidation processes, membrane filtration, activated carbon filtering, and ion exchange (Chadha et al., 2022). Innovative solutions such as photocatalytic membranes, which combine physical filtration with photocatalytic degradation using materials like titanium dioxide (TiO_2), and solar-powered treatment systems, reduce dependency on conventional energy sources. Point-of-use (POU) systems provide instant access to clean water, especially in places with limited resources or that are distant. All of these systems work together to guarantee the supply of clean drinking water, therefore fostering economic viability and environmental sustainability, particularly in poor countries where the demand is greatest (Anand et al., 2018; Bodzek et al., 2020; Song et al., 2018).

Nanoscience is a fast-expanding field with significant appeal across scientific fields. It examines three-dimensional materials at the nanoscale scale (dimensions ranging from 1 to 100 nm) or having a minimum of one dimension falling inside this range (Fernando et al., 2018; Song et al., 2021). Because of their different actions, which can be attributed to a variety of characteristics including size, shape, charge, and surface area, nanoparticles and nanophotocatalysts are highly adaptable instruments with a wide range of possible uses (Yaqoob et al., 2020). One notable application is their ability to effectively degrade organic pollutants found in wastewater arising from textiles, paper, and plastics industries which pose considerable threats to human health and the environment (Saravanan et al., 2021). When harnessed appropriately, nanoparticles offer promising solutions for the removal of pollutants such as pharmaceuticals (Alizadeh & Baseri, 2022), pesticides (Ahamad et al., 2020), phenols and acid (Irfan et al., 2021), and dyes (Abbasi et al., 2016;

Kumar et al., 2020; Shathy et al., 2022) from industrial wastewater effluents (Bhanvase et al., 2017).

The removal of environmental contaminants such as azo dyes, chlorpyrifos, organochlorine pesticides, nitroaromatics, and more depends heavily on nanoparticles, which include semiconductors, zero-valence metals, and some bimetallic forms. Interestingly, due to their efficacy, metal oxide nano photocatalysts, like SiO_2, ZnO, TiO_2, Al_2O_3, and Fe_2O_3, are used extensively. Titanium dioxide is particularly distinguished as an outstanding photocatalyst, attributed to its cost-effectiveness, non-toxicity, chemical stability, and abundance on earth (Bhanvase et al., 2017; Seneviratne et al., 2021; Umar et al., 2015; Yaqoob et al., 2020). A variety of nanomaterials have demonstrated success in removing heavy metals, organic contaminants, inorganic anions, and microorganisms. The use of nanomaterials and nanoparticles (NPs) has recently gained traction in addressing environmental challenges such as water contaminant treatment and environmental monitoring/sensing. These materials are considered advantageous due to their reactive nanostructures, which have the potential to efficiently convert and remove hazardous/toxic pollutants, transforming them into non-toxic substances (Nasrollahzadeh et al., 2021b).

The photocatalytic process employed in water treatment effectively breaks down various organic substances, encompassing alkanes, lipids, organic acids, aromatics, dyes, pharmaceuticals, and other compounds. These pollutants undergo systematic oxidation, resulting in the formation of low molecular weight intermediates which can be further oxidized, ultimately transforming into environmentally benign byproducts such as carbon dioxide (CO_2), water (H_2O), and other anions (Al-Nuaim et al., 2023), Photodegradation

contributes to the effective removal and transformation of organic contaminants, promoting the purification of water resources (Huang et al., 2024).

The modification of photocatalysts such as TiO_2 or ZnO often employs doping techniques (Nemiwal et al., 2021), such as metal oxide doping. A study by (Karthikeyan et al., 2020) aimed at enhancing photocatalytic properties by reducing the recombination rate of photo-induced electrons and holes, thereby improving the overall efficiency of the photocatalyst. By integrating both TiO_2 and ZnO or Fe_2O_3 and employing this dual doping strategy, it is possible to leverage the advantages of each while mitigating their respective drawbacks (Ali et al., 2021).

The impregnation of photocatalysts into membranes is employed to enhance the antimicrobial properties of the membranes and also degrading the chemicals when they use in water treatment processes (Binazadeh et al., 2023). Various techniques are utilized, including dip coating, electrospinning, sol-gel, layer-by-layer assembly, and the aqueous heat attachment method. In this study, bare and codoped TiO_2 nanophotocatalysts are embedded into the polyester membranes using aqueous heat attachment method. The incorporation of these photocatalysts significantly enhances the photocatalytic efficiency, antifouling capabilities, and durability of the membranes. When exposed to solar energy, these photocatalytic membranes provide an energy-efficient method for degrading organic pollutants and disinfecting water, making them highly suitable for point-of-use water purification and wastewater treatment in both urban and rural settings (Chabalala et al., 2021).

The solar-powered photocatalytic process not only cuts down on electricity usage but also promotes environmental sustainability by minimizing the reliance on non-renewable

energy sources. These membranes can also be applied in air purification systems and on self-cleaning surfaces, showcasing their versatility and potential for widespread environmental benefits. This study's findings underscore the promising future of photocatalytic polyester membranes in various applications, addressing critical water and environmental challenges (Zhang et al., 2023).

Photocatalytic membranes, which contain photocatalyst nanoparticles such as bare titanium dioxide (TiO_2) or codoped photocatalysis like TiO_2-ZnO or TiO_2-Fe_2O_3, significantly improve water treatment by facilitating the photocatalytic degradation of pollutants. These membranes may cleanse water and break down organic pollutants when exposed to light, providing an additional layer of defense against different pollutants. Utilizing solar-powered photocatalytic membranes also promotes sustainability by lessening the reliance on traditional energy sources.

Overall, while conventional filtration methods are effective for basic water purification, advanced membrane technologies provide more comprehensive solutions for eliminating a broad spectrum of contaminants, ensuring safer and more dependable drinking water (Zhang et al., 2023).

Throughout the filtering process, a number of factors affect the photocatalysis-induced degradation of oxytetracycline in aqueous solution using polyester membranes impregnated with a photocatalyst in the presence of sunlight irradiation. Photocatalytic processes are intricate, as numerous independent factors, such as initial pollutant concentration, catalyst loading, pH, filtration time, and water flowrate, can impact the efficiency of degradation as the system's response (Mohsenzadeh et al., 2019). Thus, it is essential to optimize the procedure or end product in order to investigate the relationship

between the independent and response variables (Mehmood et al., 2018). Response Surface Methodology (RSM), which optimizes multiple parameters and displays the correlations between them, appears to be a useful, economical, and effective statistical method for resolving problems (Lotfi et al., 2016). The primary objective of the RSM method is to identify the optimum response and understand how the response varies in a given direction by adjusting the design variables (Zarei & Behnajady, 2019). RSM has been effectively applied to diverse processes for optimization using experimental designs, including the photocatalytic degradation of pollutants using immobilized catalysts within polyester membranes (Jang et al., 2024).

Ensuring drinking water is free from microbial contaminants is critical as even brief exposure to pathogens can cause waterborne diseases. Regulations prioritize verifying water safety by testing indicator organisms, commonly *Escherichia coli* (*E. coli*), for their reliability in detecting fecal contamination. The primary concern is preventing consumption of water contaminated with human or animal feces, emphasizing the need for effective indicator organisms. While no single organism is perfect, *E. coli* is preferred due to its sensitivity in detection, cost-effectiveness, and rapid result turnaround (Organization, 2024).

Combining photocatalytic and filtration processes in water treatment creates a synergistic effect that improves overall efficiency and effectiveness in eliminating contaminants. Photocatalytic processes, utilizing nanoparticles such as titanium dioxide (TiO_2), harness light energy to degrade organic pollutants and disinfect water by generating reactive oxygen species. When integrated with filtration technologies, this approach not only physically removes particles and microorganisms but also chemically breaks down

organic pollutants. This dual approach ensures higher water purity, addressing a wider range of contaminants compared to individual methods. Additionally, utilizing renewable energy sources like solar power to activate photocatalysis enhances sustainability by reducing reliance on traditional energy sources and chemical treatments. Overall, combining photocatalytic and filtration processes offers a promising approach to advancing water treatment technologies towards safer and more environmentally friendly practices (Zhang et al., 2023).

Membrane fouling in water treatment systems occurs when undesired substances accumulate on or within membranes, leading to decreased efficiency and longevity. Mitigating fouling through pretreatment, optimized operational parameters, and cleaning procedures is essential for maximizing membrane reuse and maintaining effective water treatment. Advances in membrane technology, including improvements in materials and design, aim to bolster durability and resistance to fouling, thereby supporting sustainable water purification practices. Additionally, integrating photocatalytic membranes can enhance antifouling properties by leveraging photocatalysis to degrade organic contaminants and minimize fouling, further enhancing the efficiency and longevity of membrane-based water treatment systems (Zhang et al., 2023).

This research emphasized the removal of organic and microbial contaminants from water using photocatalytic membranes designed with enhanced porosity and morphology, aimed at overcoming limitations in wastewater treatment. Utilizing solar-driven photocatalytic membranes with doped titanium dioxide photocatalysts enhances filtration efficiency, reduces membrane fouling, and eliminates the need for electricity-powered UV lamps in water purification processes.

1.2 Statement of the problem

The worldwide shortage of clean, potable water is a significant issue affecting people everywhere, with developing countries facing especially severe challenges in obtaining safe water. Industrial and agricultural activities have introduced a variety of organic and inorganic pollutants into groundwater and surface water sources. Additionally, human and animal sewage contributes to substantial microbial contamination in these waters.

Lack of resources and infrastructure makes the situation worse in many developing countries, depriving many populations of access to clean and consistent water supplies. This situation leads to various health problems, including waterborne diseases, which are particularly harmful to vulnerable populations like children and the elderly.

Addressing these contamination issues is crucial to ensure the availability of clean water, particularly for disadvantaged communities. One promising solution is the use of photocatalytic membranes for removing contaminants. These membranes can revolutionize water treatment by breaking down pollutants at a molecular level through photocatalysis, which accelerates a photoreaction in the presence of a catalyst. This technology can effectively degrade organic pollutants and eliminate microbial contaminants, ensuring the production of safe drinking water.

Photocatalytic membranes are especially beneficial for impoverished communities that suffer the most from water quality issues. These membranes can be used in point-of-use systems, making clean water accessible directly where it is needed. Because of this targeted treatment, there is less reliance on large-scale water infrastructure, which is frequently insufficient in underdeveloped countries.

Furthermore, adopting a solar-powered unit for point-of-use water purification not only saves electricity expenses but also gives an environmentally responsible alternative.

Reducing reliance on fossil fuels and the carbon footprint associated with water treatment, solar-powered purification devices use renewable energy from the sun. This sustainable approach makes clean water more affordable and accessible, making it a practical option for communities with limited resources.

1.3 Justification of the study

The global crisis of clean, potable water is a pressing concern with severe implications for public health, particularly in developing nations. Potable water contaminants, including a wide range of pollutants, pose significant health risks, especially increasing the likelihood of diarrheal diseases and mortality among children. The World Health Organization (WHO) estimates that over 4 million people die each year from drinking contaminated water, with more than 1.5 million of these deaths occurring in children under the age of five (Jackson & Smith, 2018). These alarming statistics highlight the critical need for effective solutions to ensure safe drinking water.

Developing a photocatalytic point-of-use (POU) membrane presents a promising approach to addressing this environmental and public health issue. Photocatalytic membranes have the potential to significantly reduce waterborne contaminants through advanced oxidation processes, offering a sustainable and efficient method for purifying water at the point of consumption. This technology not only addresses the immediate need for clean water but also contributes to long-term environmental sustainability by utilizing solar energy, thus reducing reliance on conventional energy sources (Liang et al., 2022).

The study aims to develop and optimize a photocatalytic POU membrane capable of effectively removing harmful contaminants from water, thereby providing a viable

solution to improve water quality and protect public health. By focusing on the integration of photocatalysis and filtration, this research seeks to enhance the disinfection and degradation of organic pollutants in water, offering a practical and scalable solution for communities lacking access to safe drinking water (Binazadeh et al., 2023).

1.4 Objectives of the study

Main Objective

Development and testing of new Nano-scale photo-catalytic membrane for application in point-of-use water treatment systems.

Specific Objectives

1. To design and characterize metal-ion-doped TiO_2 photo-catalysts on the polyester-based membranes.

2. To investigate photo-catalytic membrane treatment of wastewater targeting organic and microbial contaminants.

3. To evaluate the disinfection and organic degradation kinetics and synergy of the photo-catalytic water treatment.

4. To assess membrane fouling and re-use potential.

1.5 Significant of the study

Having access to clean, safe drinking water is a basic human right and one of the most significant aspects of public health. Lack of access to clean water has a detrimental influence on people's health and significantly affects socioeconomic development, which exacerbates poverty and inequality. To address these urgent problems, there has been an increased focus in recent years on the development of improved water treatment technology. Photocatalytic membranes have become one of these technologies' most

promising applications. These membranes combine the benefits of physical filtration and photocatalytic degradation, effectively removing a broad spectrum of contaminants. When photocatalyst nanoparticles are added to the membrane matrix, they become more effective and have antifouling qualities. This turns the membranes from passive barriers into active surfaces that greatly increase water treatment procedures.

This pressing issue has a possible resolution in the form of a photocatalytic point-of-use (POU) membrane. By leveraging advanced oxidation processes, these photocatalytic membranes can significantly reduce waterborne contaminants, providing a sustainable and efficient method for purifying water at the point of consumption. This technology not only addresses the urgent need for clean water but also supports long-term environmental sustainability by harnessing solar energy, thereby reducing reliance on conventional energy sources. Utilizing a solar unit to activate the photocatalytic process cuts electricity costs and promotes eco-friendliness, while a gravity-fed system eliminates the need for pumps, further conserving energy.

The potential impact of this research on environmental sustainability, public health, and technological innovation makes it significant:

Improvement of Public Health: In order to significantly lower dangerous pollutants in drinking water and thus lower the number of waterborne illnesses and deaths associated with them, especially among children in underdeveloped countries, a photocatalytic POU membrane is being developed.

Environmental Sustainability: Integrating photocatalytic technology with solar energy fosters an eco-friendly approach to water purification. This technology decreases the requirement for electricity from non-renewable sources, thus minimizing the

environmental effect of water treatment procedures.

Technological Innovation: This research enhances the efficiency of water purification systems by combining photocatalysis and filtration. This innovative technique can increase the disinfection and degradation of organic contaminants, paving the path for further breakthroughs in water treatment technologies. TiO_2 can be doped with Fe_2O_3 and ZnO to improve its visible light absorption characteristics. This can be utilized in conjunction with photocatalytic membranes to benefit from the physical filtration and photodegradation processes of photocatalysis.

Policy and Implementation Guidance: The study's findings can inform policymakers and guide the deployment of effective water treatment systems in resource-limited areas. By providing empirical evidence and practical solutions, this research supports the development of policies aimed at improving water quality and accessibility.

Scalability and Practical Application: This study emphasizes the development of practical and scalable solutions for providing safe drinking water. The photocatalytic POU membrane can be implemented in various settings, from individual households to larger community water systems, making it a versatile tool in combating water contamination.

The significance of this study lies in its potential to contribute to global efforts in mitigating waterborne diseases, reducing mortality rates, particularly among vulnerable populations, and promoting sustainable water treatment technologies. The findings from this research could inform policy-making, guide the implementation of water treatment systems in resource-limited settings, and pave the way for further innovations in water purification technologies. Therefore, the development of a photocatalytic POU membrane

is not only scientifically and technologically significant but also socially and environmentally imperative.

1.6 Scope of the study

The focus of this work is the development and implementation of photocatalytic membranes doped with titanium dioxide (TiO_2) paired with iron oxide (Fe_2O_3) or zinc oxide (ZnO) to boost the visible light absorption and overall photocatalytic efficacy. These membranes, developed from polyester/cotton fabric (65%, 35%) provided by Rivatex LTD, Kenya, were tested for their ability to remove microbial and organic contaminants from water. *Escherichia coli (E. coli)* served as the indicator for microbial contamination, while reactive blue dye and oxytetracycline represented organic pollutants. Both synthetic contaminated water and real water samples from a Kesses dam were used to evaluate the membranes' performance. Experimental procedures included photocatalytic testing under sunlight and assessing the membranes' antifouling properties, durability, and efficiency in contaminant removal. The study aimed to ensure the treated water met acceptable drinking water standards by measuring parameters such as turbidity, pH, conductivity, total dissolved solids (TDS), and metal ion and zinc concentrations. This comprehensive approach aims to demonstrate the potential of photocatalytic membranes for addressing water contamination issues, particularly in resource-limited settings, thereby contributing to public health and environmental sustainability.

1.7 Thesis organization

This Thesis is structured into five chapters as outlined below:

Chapter 1 offers an overview of the background related to the research problem and establishes the justification for this study. It also outlines the objectives and significance

of the study.

Chapter 2 delves into existing literature concerning the treatment of potable water, with a particular focus on addressing organic pollutants and disinfection. It examines the application of point-of-use (POU) water treatment technologies as a viable solution for treating drinking water in rural areas. The chapter emphasizes the integration of TiO_2-doped photocatalysis within polyester membranes to facilitate the photodegradation of organic pollutants and the disinfection of water using sunlight irradiation. The chapter also explores the synergistic combination of filtration and photodegradation processes, alongside considerations of membrane fouling and cleaning. Finally, it summarizes the identified research gaps in the field.

Chapter 3 details the methods employed to fulfill the study's objectives. It covers the synthesis of bare and codoped TiO_2 photocatalysts, the photodegradation process of reactive blue dye using these photocatalysts, and the integration of these materials into polyester membranes. Additionally, it discusses the fabrication of a solar-powered point-of-use water treatment system. The chapter includes investigations into the antimicrobial properties of the polyester membranes, the photodegradation of oxytetracycline, the synergistic effects of disinfection and organic degradation, and concludes with an examination of the membranes' antifouling properties and potential for reuse.

Chapter 4 provides a comprehensive analysis of the study's findings. It includes the characterization results of the photocatalysts and both coated and uncoated membranes. The chapter discusses the photodegradation properties exhibited by the photocatalysts and evaluates the antibacterial effectiveness of the polyester membranes. It also examines the photodegradation efficiency of the membranes in removing oxytetracycline and

assesses their disinfection capability against *E. coli* using synthetic feed and real dam water. Additionally, the chapter explores the synergistic index of disinfection and oxytetracycline photodegradation. Lastly, it discusses membrane flux, antifouling outcomes, and the potential reusability of the membranes.

Chapter 5 concludes the study by summarizing its key findings, discussing limitations, and offering recommendations. It highlights the significant discoveries and insights obtained, acknowledging both strengths and challenges encountered during the research. Additionally, the chapter provides practical suggestions based on the study's outcomes and proposes avenues for future research to deepen knowledge and application in this field.

CHAPTER 2

LITERATURE REVIEW

2.1 Overview

Water is a vital requirement for all life forms to survive. However, the absence of safe and clean drinking water is a major concern, particularly for individuals living in rural areas of developing countries. The decrease in available clean water resources is widely recognized, exacerbated by the progress in industry and technology that has increased the release of dangerous effluents into the environment (Achisa, 2014; Chadha et al., 2022). Prior to being discharged, industrial, agricultural, and municipal wastewater must undergo treatment to remove harmful substances such as dyes, pharmaceutical residues, inorganic compounds, and heavy metals. These substances present significant health risks to humans and have the capacity to pollute the environment if not properly managed (Achisa, 2014; Chadha et al., 2022). Numerous clean-energy technologies, including gas and chemical separations, waste and potable water treatment, dehumidification, fuel-cell technology, and electrochemical energy storage, are dependent on the enhancement of membrane-based separations (Ali et al., 2018). Membrane techniques are more environmentally friendly and energy efficient than traditional water and wastewater treatment methods. They can also be used in conjunction with traditional procedures such as coagulation, flocculation, sedimentation, filtration, precipitation, adsorption and disinfection and single-stage processes (Bodzek, 2019). Water pollution is an important environmental issue that affects people all over the world. Industrial process effluents, agricultural pesticide, human outwaste, etc. have led to ground and surface water contamination. Physicochemical and biological processes are the most common approaches for treating wastewater. Coagulation, flocculation, and ozonation are

examples of physiochemical procedures, whereas biological approaches are employed to remove nitrogen, phosphorus, organics, and metal residues. A membrane is a selective barrier that allows particular species in a fluid to be separated using a combination of sieving and sorption diffusion mechanisms. Separation is achieved by selectively allowing the permeation of one or more components of a fluid stream through the membrane while impeding the passage of other components (Kumar & Saravanan, 2017; Rao et al., 1997; Singh et al., 2018). Membranes are utilized in the filtration process to remove pollutants, salts, heavy metal ions, viruses, and various other particles from water. These membranes operate akin to the cellular walls found in human organisms. Membranes act as discerning barriers utilized in the treatment of wastewater, enabling the passage of water while obstructing the movement of undesired impurities (Chadha et al., 2022).

Nanoparticles are defined as three-dimensional materials composed of fundamental units at the nanometer scale (1-100 nm) or having dimensions within this range. Their proven ability to inhibit microbial growth extends across a spectrum of microorganisms, including Gram-positive and Gram-negative bacteria, mycobacteria, and fungi. The effectiveness of nanoparticles against bacterial proliferation varies depending on the type of nanoparticle, primarily due to their abrasive characteristics that damage cell membranes. Additionally, the inherent antibacterial properties of nanoparticles' physical structures contribute significantly to their efficacy. Another mechanism that has been proposed is the enhanced release of antibacterial metal ions from the surface of nanoparticles. Recent research has demonstrated the antibacterial properties of various types of metal-based nanoparticles (NPs). Metal and metal oxide NPs, including silver,

copper, zinc oxide, titanium oxide, copper oxide, and nickel oxide NPs, exhibit antimicrobial activity that varies based on factors such as their composition, surface modifications, inherent characteristics, and the specific microorganisms they target (Biswal & Misra, 2020; Correa et al., 2020; Song et al., 2021). Nanoparticles are used in a variety of disciplines for human wellbeing and, when correctly exploited, hold great potential in the pharmaceutical and biomedical industries. Nanoparticles have different behaviors based on their size, shape, charge, and surface area (Sharmin et al., 2021).

In recent years, there has been an increase in interest in using nanomaterials to build next-generation membranes with improved antifouling and anti-scaling capabilities for water and wastewater treatment. Improvements in membrane structure and transport characteristics are possible thanks to the development of nanomaterials and nanotechnology. The most frequently utilized materials for membrane modifications include silica, zeolites, metals like Ag, Zr, and Ti, metal oxides such as TiO_2, ZrO_2, ZnO, and Al_2O_3, metal-organic compounds, aquaporin (AQP) proteins, and carbon-based materials like graphene, graphene oxide, and carbon nanotubes (CNTs) (Anand et al., 2018; Bodzek et al., 2020; Song et al., 2018). Nanoscale inorganic photocatalysts are incorporated into a membrane matrix to enhance the polymer's properties in photocatalytic membranes. These materials are chosen for their stability, low cost, availability, non-toxicity, unique photocatalytic performance, effectiveness at low concentrations, and potential applications in water and wastewater treatment, TiO_2 has been proven to be an excellent heterogeneous catalyst for photo-degradation of aqueous pollutants and disinfection, however its efficacy is mostly influenced by the initial concentration of pollutants as well as the intensity of light hitting its surface (Bouziane

Errahmani et al., 2021; Kuvarega & Mamba, 2016; Naseem & Waseem, 2022; Santos et al., 2020). Heterogeneous photocatalysis has gained significant traction in environmental remediation applications. Safe semiconductors are the primary materials used to reduce organic contaminants in water. Zinc oxide and titanium oxide have been employed to photocatalytically degrade textile coating effluent under ultraviolet light. Nanocomposites find extensive use in various domains, including wastewater treatment, drug delivery, and life sciences (Naseem & Waseem, 2022).

photocatalytic membranes, which combine physical filtration with photocatalytic degradation using materials like titanium dioxide (TiO_2), and solar-powered treatment systems, reduce dependency on conventional energy sources. These technologies have a synergistic impact in that the combination of photocatalysis and filtration improves not only the degradation of organic pollutants but also the overall efficiency of contaminant removal. Furthermore, the photocatalytic action aids in the reduction of membrane fouling by decomposing organic foulants on the membrane surface, increasing the membrane's lifespan and reuse(Anand et al., 2018; Bodzek et al., 2020; Song et al., 2018).

Point-of-use (POU) systems play a crucial role in ensuring access to clean water, especially in geographically isolated or resource-constrained regions. The significance of these systems is heightened in developing nations where centralized water treatment infrastructure is frequently lacking. By incorporating advanced filtration and photocatalytic degradation, POU systems can effectively remove a wide range of contaminants, including bacteria, viruses, and organic pollutants, ensuring safe drinking water for communities (Nelson et al., 2024).

The synergy of combining photocatalytic membranes with solar-powered systems further enhances the sustainability of these solutions. Solar energy provides a renewable and eco-friendly power source, reducing the reliance on conventional energy and lowering operational costs. This combination in addition of meeting the urgent need for clean water, helps to ensure long-term environmental sustainability by solar energy and reduces greenhouse gas emissions.

Furthermore, the antifouling qualities of photocatalytic membranes are critical in ensuring the efficiency and effectiveness of water treatment systems (Mecha et al., 2018; Mecha et al., 2014).

By preventing the buildup of organic and inorganic fouling agents, these membranes ensure consistent water flow and reduce the need for frequent maintenance and replacement. This translates to cost savings and improved reliability of water treatment solutions, making them more accessible and viable for low-income and resource-constrained communities.

This chapter offers a thorough review of the literature relevant to this study, structured into ten sections. The first section provides an overview of the study. The second section delves into nanomaterials, nanotechnology, and nanophotocatalysis, covering topics such as the synthesis of nanoparticles, photoexcitation, and modification of photocatalysts, synthesis methods of nanophotocatalysts, and the photodegradation of organic and microbial pollutants.

The third section discusses the impregnation of fabric filters with nanophotocatalysts using both in situ and ex situ methods. The fourth section addresses water pollution and contaminants, categorizing them into four types: inorganic, organic, microbial, and

radioactive contaminants. The fifth section explores traditional and modern methods of water purification, including sand filtration, activated carbon, membrane separation processes, chlorination, advanced oxidation processes, and combinations thereof, such as nano-membranes and nanostructured catalytic membranes.

The sixth section investigates Point-Of-Use (POU) devices for treating household water, detailing various types such as ceramic water filters, paper-based water treatment incorporating silver nanoparticles, development and implementation of water treatment systems for rural and remote areas, evaluation of microfiltration membranes impregnated with silver nanoparticles, slow sand filtration, and novel solar-powered nitrogen-doped titanium dioxide photocatalytic membranes.

The seventh section reviews international water standards set by WHO and ISO, as well as national standards established by the Kenya Bureau of Standards. The eighth section discusses the synergy in photocatalysis for water treatment. The ninth section covers issues related to fouling, cleaning, and membrane modification.

2.2 Nanomaterials, nanotechnology and nanophotocatalysis

Nanotechnology is a scientific and engineering technology used at the nanoscale in industries such as compound fabric manufacture, food processing, agricultural processing, engineering, and medical and pharmaceutical applications. Many researchers have shown interest in nanomaterial possibilities for antibacterial work in the last decade. Numerous studies have shown that a variety of metal oxide nanoparticles, such as Al_2O_3, TiO_2, ZnO, CuO, Co_3O_4, In_2O_3, MgO, SiO_2, ZrO_2, and nickel oxide, display toxicity towards a broad spectrum of microorganisms and have the ability to effectively eradicate diverse bacteria. The effectiveness of nanomaterials in diminishing or eradicating cells, as well as their mechanisms of action against bacteria are influenced by multiple factors.

These factors encompass the surface charge, morphology, composition, and nature of the nanomaterials; their concentration, dispersion, and interaction with bacterial cells; the presence of reactive oxygen species; the liberation of antimicrobial ions; the components of the surrounding medium and pH levels; physicochemical characteristics; specific surface-area-to-volume ratios; nanoparticle dimensions; rate of growth; formation of biofilms; features of bacterial cell walls; and the impact of UV light exposure (Hernández-Téllez et al., 2016). Metal nanoparticles' potential as antibacterial agents has been extensively researched, and they are being investigated as an alternate way to overcoming the problem of multidrug resistance in bacteria. The bactericidal properties of nanoparticles stem from physical interaction with the bacterial cell membrane, eliminating the necessity for cellular penetration. Consequently, their application as antimicrobial agents may circumvent mechanisms of bacterial resistance (Fernando et al., 2018). Silver (Ag), zinc (Zn), and copper (Cu) ions, for example, have potent antibacterial properties. The antibacterial properties of Ag have long been known, and they are extremely beneficial in both the textile and medical industries (Koruyucu et al., 2021).

Metal NPs are produced in a number of ways, but they all have significant crystallinity, a huge surface area, and reactive surfaces. The purpose of nanotechnology, which is still in its early stages, is to construct nanostructures or nano-arrays having distinct attributes from bulk or single particle species Antibacterial characteristics are thought to exist in metal oxide NPs (Naseem & Durrani, 2021). Since metal oxides generally have larger bandgaps than other materials, they are especially useful as substrates in the ultraviolet. They're ideal for using as a foundation in a variety of applications because of this feature.

On the other hand, materials with smaller bandgaps are frequently used as secondary parts. Notably, oxides like ZnO and TiO_2 display heightened photocatalytic activity in the UV region, making them popular choices as substrate materials in diverse applications (Satti et al., 2023). Hematite (α-Fe_2O_3), recognized as a type band gap semiconductor with a value of 2.1 eV, has garnered significant interest due to its versatile applications. It is widely employed in various fields such as gas sensors, electrochemistry, pigments, drug carriers, and wastewater treatment. The semiconductor's distinctive properties make it valuable in sensing applications, electrochemical processes, imparting color as a pigment, serving as a carrier for pharmaceutical compounds, and effectively participating in the treatment of wastewater. The diverse range of applications which includes and not limited to dye degradation (Abbasi et al., 2016) and removal of organic pollutants from municipal waste water (Mecha et al 2016) underscores hematite's importance in multiple scientific and industrial domains

Various types of nanomaterials have been reported to successfully remove heavy metals, organic contaminants, inorganic anions, and microorganisms. Nanostructured materials, including nanosorbents, nanoparticles (Pd, Au, Ag, Cu, Fe_2O_3, TiO_2, and others), the TiO_2 photocatalyst is widely used for degrading organic, inorganic (Álvarez et al., 2010) and microbial (Prorokova et al., 2020) pollutants from water. Its performance is attributed to its high stability, low cost, low toxicity, and superior photocatalytic activity compared to other semiconductor materials (Al Zoubi et al., 2021). Despite these benefits, TiO_2 primarily exhibits photocatalytic activity in the ultraviolet (UV) region, constituting only about 5% of the Earth's solar spectrum. Consequently, its effectiveness in the visible range is limited (Bhanvase et al., 2017), TiO_2 exists in three phases, anatase,

rutile and brookite; of these, anatase is considered the most photoactive form. Anatase has strong adsorption of organic compounds and high hole trapping rate; however, rutile and brookite phases also exhibit considerable photoactivity. Incorporating multiple phases of TiO_2 enhances photocatalytic performance and diminishes charge carrier recombination. Anatase is the most thermally stable crystal phase of TiO_2; annealing it at temperatures exceeding 400°C can transform it to rutile (Leary & Westwood, 2011; Yang et al., 2008). Similarly, zinc oxide (ZnO) serves as a photocatalyst due to its potent oxidizing capabilities, non-toxic nature, and cost-effectiveness (Aremu et al., 2021). ZnO exhibits diverse nanostructures, such as nanoneedles and nanocombs (Shekofteh-Gohari et al., 2018).The photocatalytic properties of ZnO can be enhanced by doping (Rheima et al., 2020) since ZnO has a wide band-gap (Munguti & Dejene, 2020; Ramírez-Ortega et al., 2014).

When the TiO_2 surface is exposed to sufficient energy that surpasses its band gap, it initiates redox reactions (Arghavan et al., 2021). Subsequently, electron-hole pairs are generated, potentially instigating redox processes on the TiO_2 surface. However, the economic viability is constrained by suboptimal photoreaction rates and the limited spectral alignment between the TiO_2 absorption spectrum and solar emission spectrum. Additionally, the photocatalytic activity is hampered by rapid charge carrier recombination and sluggish charge carrier interfacial transfer rates (Gurlhosur & Sreekanth, 2018; Mohsenzadeh et al., 2019; Peiris et al., 2021).

Nano-catalytic membrane systems, have demonstrated enhanced effectiveness in addressing environmental challenges such as water contaminant treatment and/or environmental monitoring/sensing. The utilization of nanomaterials and nanoparticles

(NPs) in these applications is viewed favorably due to the unique characteristics of reactive nanostructures that enable them to efficiently convert and/or eliminate hazardous/toxic pollutants, transforming them into non-toxic substances. These innovative materials not only offer higher efficiency but also reduce time requirements, exhibit eco-friendly attributes, and represent low-energy alternatives in a broader context (Nasrollahzadeh et al., 2021a). To embed metal oxide nanoparticles onto textile fibers, three primary techniques are commonly utilized: the initial method is known as the "pad-dry-cure process," followed by ultrasonic irradiation - a highly efficient approach for applying nanoparticles onto the textile fibers' surface and other related substrates. Thermal chemical treatment is the third method. These approaches are primarily based on multistage procedures that take a long time and necessitate the use of binding agents to anchor the nanoparticles to the substrate (El-Nahhal et al., 2016).

2.2.1 Synthesis of nanoparticles

Nanoparticles, typically sized between 1-100 nm, exhibit distinct properties that make them essential in fields such as medicine, electronics, and environmental science. The three main methods used to create nanostructures are bottom-up, top-down, and self-assembly methods as shown in Fig. 2.1. To synthesize nanoparticles, the processing parameters must be managed so that the finished nanoparticles exhibit the following properties (Jamkhande et al., 2019):

(i) Uniform particle size, (ii) Consistent shape, (iii) Same chemical composition and crystal structure, and (iv) Dispersed individually without any agglomeration.
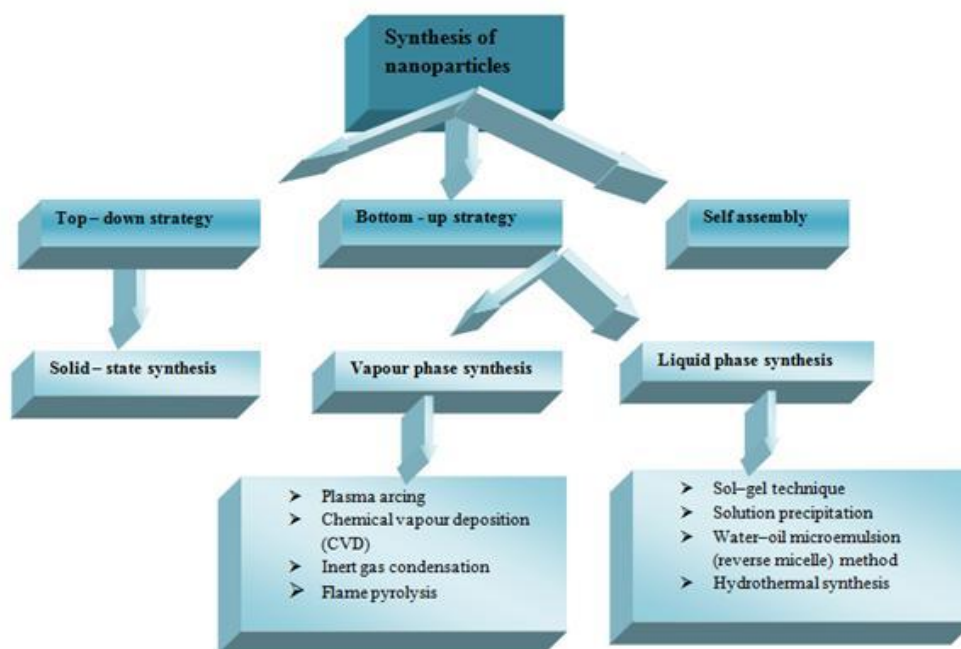
Figure 0-1 synthesis methods of nanoparticles

Physical, chemical, and biological methods are another classification of the nanoparticles synthesis, the physical processes (top down strategy) such as ball milling, laser ablation, and evaporation-condensation are simple and produce high-purity nanoparticles, but they require a significant amount of energy. The chemical approaches (bottom up strategy), such as chemical reduction, sol-gel processes, hydrothermal synthesis, and microemulsions, allow precise control methods, leveraging plant extracts, microorganisms, and enzymatic processes (green synthesis processes), present environmentally friendly and biocompatible alternatives, albeit with slower and less consistent results. Each method comes with its own advantages and drawbacks. These synthesis processes depending on the applications of nanoparticle, including medicine delivery, diagnostic imaging, conductive inks, sensors, water purification, and pollution reduction. As the field progresses, refining these methods and discovering new ones will further unleash (Sadeghi-Aghbash & Rahimnejad, 2022).

2.2.2 Photocatalysis and Photo excitation

There are numerous applications for photocatalysis, which is a heterogeneous process. Potential photocatalysis include a number of oxides with small bandgaps, such as TiO_2, ZnO, SnO_2, Fe_2O_3, and WO_3, or sulfides, such as CdS and ZnS. Free electrons are concentrated in the voltage band of these materials. When materials are exposed to light, photon energy (hv) higher than the bandgap is absorbed by the materials (typically with the ultraviolet illumination). Excited electrons transition to the conduction band, while holes, the positively charged carriers, remain in the valence band once it has been filled, as depicted in Eq. 2.1 (Le, 2018).

$$TiO_2 + hv \rightarrow h^+ + e^- \qquad\qquad 0.1$$
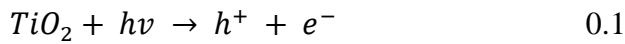
The separation of photogenerated electrons and holes is illustrated in the subsequent phase Eq. 2.2 (Sharma et al., 2017b).

$$e^- + O_2 \rightarrow O_2^{\bullet-} \qquad\qquad 0.2$$

In photocatalytic reactions, the desired final products, akin to other Advanced Oxidation Processes (AOPs), typically include CO_2 and water. Electrons in the conduction band serve as charge carriers for electron acceptors, while hydroxyl groups or organic compounds react with holes in the valence band. Dissolved oxygen (DO) plays a crucial role as a primary electron acceptor, essential for maintaining the separation of electrons and holes. Its presence facilitates photocatalysis by reacting with electrons, leading to the generation of additional reactive oxygen species. As illustrated in Eq. 2.3 – 2.9 (Le, 2018).

$$O_2^{\bullet-} + H^+ \rightarrow OOH^\bullet \qquad\qquad 0.3$$

$$2OOH^\bullet \rightarrow O_2 + H_2O_2 \qquad\qquad 0.4$$

$$OOH^\bullet + O_2^{\bullet-} + H^+ \rightarrow O_2 + H_2 \qquad 0.5$$

$$e^- + OOH^\bullet + H^+ \rightarrow H_2O_2 \qquad 0.6$$

$$H_2O_2 + O_2^{\bullet-} \rightarrow OH^- + OH^+ + O_2 \qquad 0.7$$

$$e^- + H_2O_2 \rightarrow OH^- + OH^+ \qquad 0.8$$

$$contaminant + (\,e^-, h^+\,, OOH^\bullet, OH^\bullet, or\ O_2^{\bullet-}\,) \rightarrow \quad degradation\ products \qquad 0.9$$
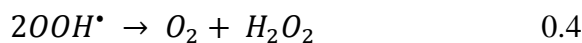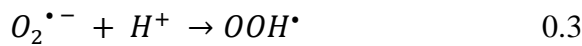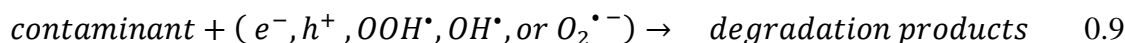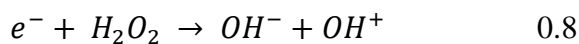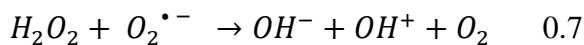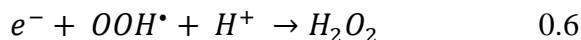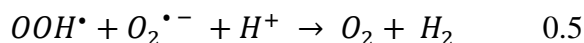
2.2.3 Modified photo-catalysts

Titanium dioxide (TiO_2) is widely regarded for its chemical stability, non-toxicity, and cost-effective production, making it one of the most significant oxides in various photochemical applications, including environmental remediation, water photoelectrolysis, and dye-sensitized solar cells. Despite its benefits, TiO_2 has a bandgap energy of 3.0 - 3.3 e, allowing it to absorb only a small fraction of the solar spectrum (Armaković et al., 2022). The material's economic potential is limited by its low photoreaction rates and the poor overlap between its absorption spectrum and the solar emission spectrum.

 Additionally, the photocatalytic activity is constrained by the rapid charge carrier recombination and low charge carrier interfacial transfer rates (Mohsenzadeh et al., 2019). The photocatalytic materials can be modified to get around these problems. Modified photocatalysts are advanced materials designed to enhance photocatalytic efficiency by improving light absorption, charge separation, and overall catalytic activity. Various strategies include doping with foreign atoms (metals or non-metals) to extend light absorption into the visible range, forming composites of multiple semiconductors for better charge separation, and surface functionalization to attract specific pollutants.

Nanostructuring photocatalysts, such as creating nanoparticles or nanotubes, increases surface area and active sites, while sensitizing with dyes extends light absorption. Core-shell configurations exploit the advantages of combining core and shell components to improve stability and catalytic activity. These improvements enhance the efficiency of photocatalysts in tasks such as environmental cleanup, water purification, and energy transformation. Specifically, they prove to be highly effective in breaking down organic contaminants, purifying water, and generating hydrogen, thus contributing to the resolution of worldwide environmental and energy challenges. As illustrated in Figure 2.2, there exist three categories of alterations (Le, 2018).

2.2.4 Nanophotocatalysts

Nanophotocatalysts, which capitalize on advances in nanotechnology, have transformed the field of photocatalysis by considerably increasing reaction efficiencies. Titanium dioxide (TiO_2) catalysts have great surface area, better charge separation, and configurable band gaps, making them highly effective under natural sunlight. Nanophotocatalysts are applied in water treatment for degrading organic pollutants and disinfecting pathogens, air purification to break down volatile organic compounds and nitrogen oxides, and creating self-cleaning surfaces. They are also important in renewable energy production, such as photocatalytic water splitting to produce hydrogen. Several synthesis procedures, including the sol-gel process, hydrothermal synthesis, chemical vapour deposition, and microwave-assisted synthesis, allow for fine control of nanomaterial characteristics, despite their potential, difficulties like as scalability, stability, and cost persist, focusing future research towards more efficient synthesis procedures, increased durability, and practical integration for long-term environmental

and energy applications (Shafiee et al., 2022).
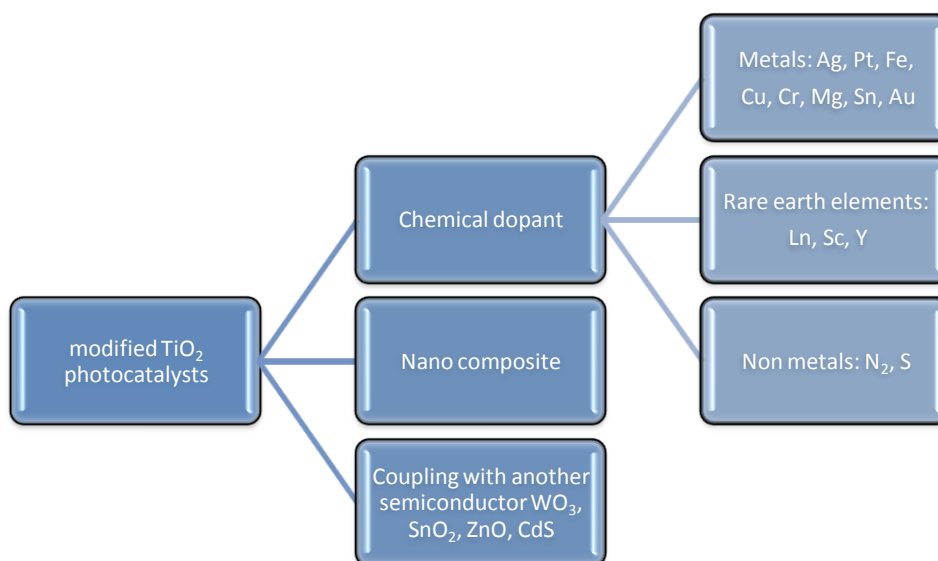
Figure 0-2 Modified methods of TiO$_2$ photocatalysts

Nanocatalysts are also commonly employed in water treatment because they boost catalytic activity at the surface due to their unique traits of having a larger surface area and shape-dependent properties. It improves pollutant reactivity and degradation. For the degradation of environmental pollutants, semiconductor materials, zero-valence metals, and bimetallic nanoparticles are extensively utilized catalytic nanoparticles (Yaqoob et al., 2020).

2.2.5 Synthesis methods of nanophotocatalysts

There are several ways to synthesis the nanophotocatalytic materials as mention in synthesis nanoparticle section, but generally speaking, to make the nanophotocatalytic chemically, it needs chemical precursors (metal salt) and an organic solvent (such as acid, alcohol, or deionized water) works as reducing agent. Then, depending on the process,

the precursor transfers into an inorganic solid by means of chemicals. The most popular method is called sol-gel (Khasawneh, Palaniandy, & Innovation, 2021), and most researchers in the literature have employed it.

Tables 2.1 and 2.2 list some common methods of synthesis (Fe_2O_3/TiO_2 and ZnO/TiO_2), including ultrasound assistance, wet chemical synthesis, hydrothermal hydrolysis, microwave radiation (MWR), and combinations of methods like ultrasonic-assisted sol-gel.

2.2.6 Photocatalytic Degradation of Organic Pollutants

Organic micropollutants have been found in water sources due to their extensive use and discharge. Because many of these stubborn organic pollutants are hazardous, there is growing worry about their potential implications on human health. Advanced oxidation processes (AOPs), such as photocatalysis, have been investigated as potential answers to this problem. It relies on the in situ creation of hydroxyl radicals (.OH) under ambient settings, which have the ability to destroy organic molecules. It uses a semiconductor and a light source (UV or visible light). Heterogeneous photocatalysis is also effective against phenolic compounds and other organic micro-pollutants. Phenol and phenolic chemicals are poisonous, have a high chemical oxygen demand (COD), and are difficult to degrade. The addition of TiO_2 nanoparticles to the adsorption membrane gave the membrane photo catalytic and self-cleaning capabilities, making it more efficient and recyclable (Chabalala et al., 2021). In general, nanomaterials either adsorb or degrade contaminants using a variety of catalytic methods, and photocatalysis are an excellent candidate for water purification; toxic organic contaminants are decomposed into other products. Organic pollutants undergo partial or total mineralization, yielding carbon dioxide, water,

and some inorganic ions.

Table 0-1 Fe_2O_3/TiO_2 synthesis methods

Method	Precursors		organic solvent	Additional materials	Ref.
	TiO$_2$	Fe$_2$O$_3$			
Sol-gel	Titanium isopropoxide (TTIP, >98 %)	Iron (III) chloride hexahydrate (99	Isopropanol (> 98 %),	double distilled water (DDW) + HCl	(Zhu et al., 2004)
Sol-gel	Titanium (IV) butoxide	Fe(NO$_3$)$_3$.9H$_2$O	Ethanol	oxalic acid Deionized distilled water	(Razani et al., 2017)
Sol-gel	Titanium tetra-isopropoxide (TTIP) 97 % purity	Iron (III) chloride nonahydrate (FeCl$_3$)	Ethanol 95 %	37 % hydrochloric acid (HCl)	(Khasawneh et al., 2019)
Sol-gel	Titanium tetra-isopropoxide (TTIP, 97%)	Iron III nitrate nonahydrate (FeN$_3$O$_9$.9H$_2$O)	Ethanol (C$_2$H$_5$OH, 99.5%)	Acetic acid (CH$_3$COOH, 99.8%), and	(Bouziani et al., 2020)
Sol-gel	Titanium (IV) butoxide (Ti (OC(CH$_3$)$_3$)$_4$	Iron (III) nitrate nonahydrate Fe (NO$_3$)$_3$•9H$_2$O	ethylene glycol	Ethanol	(Bootluck et al., 2021)
Sol-gel	TiOCl$_2$	Iron(II) chloride tetrahydrate 99% (FeCl$_2$ •4H$_2$O) + Iron(III) chloride hexahydrate (FeCl$_3$•6H$_2$O)	Ammonium hydroxide solution	--------------	(Khasawneh, Palaniandy, Ahmadipour, et al., 2021)
Ultrasound assisted	Tetrabutyl titanate [Ti (OC$_4$H$_9$)$_4$, 98%]	Iron (III) Chloride 6- hydrate powder	Ethanol (46.07 M)	H$_2$SO$_4$ (98%), deionized water	(H. Moradi et al., 2016)
Wet chemical synthesis	TiCl$_4$	FeCl$_3$	CH$_3$OH	HNO$_3$	(Wang et al., 2003)
hydrothermal hydrolysis	Titanium (IV) tetra-tert-butoxide (TTB)	FeCl$_3$ or FeCl$_2$	n-octanol	Deionized water AgNO$_3$	(Zhu et al., 2004)
Ultrasonic-assisted sol-gel	TTIP	FeCl$_3$	Ethylene glycol Isopropanol C$_2$H$_5$OH	TBAB Urea Ethanol	(Abdel-Wahab et al., 2017b)
	TiO$_2$(anatase 99+%)	Fe(NO$_3$)$_3$ · 9H$_2$O	C$_2$H$_5$OH (ethanol)		

Table 0-2 ZnO/TiO$_2$ synthesis methods

Method	Precursors		organic solvent	Additional materials	Ref.
	TiO$_2$	ZnO			
Sol-gel	tetrabutyl titanate (TBOT)	zinc acetate	absolute Ethanol	Hydrochloric acid (36.5wt.%)	(Wang et al., 2013)
Sol-gel	isopropyl orthotitanate (TTIP)	zinc nitrate tetra hydrate	Ehanol	absolute ethanol	(S. Moradi et al., 2016)
Sol-gel	TiO$_2$	zinc nitrate	deionized water	----------	(Yang et al., 2018)
Sol-gel	titanium tetraisopropoxide (TTIP) Ti [OCH(CH$_3$)$_2$]$_4$, 97%	zinc acetate dihydrate, Zn(CH$_3$COO)$_2$.2H$_2$O 99.9% pure	2-isopropanol	nitric acid/ monoethanola mine acted	(Yang et al., 2018)
Sol-gel	titanium tetraisopropoxide	acetic acid6%	Ethanol	------------	(Mohammad i & Ghorbani, 2018)
Sol-gel	titanium n – butoxide	zinc acetate dehydrate	2 methoxy ethanol	sodium hydroxide	(Upadhyay et al., 2019)
Sol-gel	TiCl$_3$	ZnCl$_2$	HCl ammonium hydroxide	NaOH	(Mohsin, 2020)
Sol-gel	titanium (IV) butoxide (TBT: Ti(OC$_4$H$_9$)$_4$	zinc acetate	Ethanol	ethyl acetoacetate HNO$_3$	(Mohamadi Zalani et al., 2020)
Sol-gel	Titanium tetra-isopropoxide [Ti{OCH(CH$_3$)$_2$	Zn(CH$_3$COO)$_2$.2H$_2$O, ≥98%	absolute ethanol [CH$_3$CH$_2$OH, >99%	hydrochloric acid [HCl, 28%	(Ali et al., 2021)
Sol-gel	Tetra-butyl titanate (C$_{16}$H$_{36}$O$_4$Ti, ≥ 98%, for synthesis, TBT)	nitric acid (HNO$_3$, 65%)	absolute ethanol	----------	(Asadzadeh Patehkhor et al., 2021)
Sol-gel	titanium tetrachloride and	zinc chloride	Ethanol	benzyl alcohol	(Sridevi et al., 2021)
Hydrot hermal process	Titanium butoxide (C$_{16}$H$_{36}$O$_4$Ti)	Zn acetate (Zn(CH$_3$COO)$_2$·2H$_2$O	deionized water	----------	(Pei et al., 2016)
microw ave radiatio n (MWR)	potassium titanium oxalate dehydrate (C$_4$K$_2$O$_9$Ti . 2H$_2$O)	Zinc nitratehexahydrate (Zn(NO$_3$)$_2$ .6H$_2$O	deionized water	NH$_4$OH	(Arin et al., 2013)

In general, a semiconductor, such as TiO_2 absorbs light with a wavelength greater than or equal to the semiconductor band gap width, forming electron hole pairs (e^- h^+). The reduction-oxidation (redox) reactions occur when adsorbed species interact with the surface of the nanocatalyst. Furthermore, h^+ vb react with surface-bound water to create percent OH, and e selects oxygen to generate a superoxide radical anion (A. Mecha et al., 2019; Yaqoob et al., 2020). In environmental applications, TiO_2 is one of the most promising semiconductors. The TiO_2 surface is bombarded with enough energy to overcome the band gap to start redox reactions (Mohsenzadeh et al., 2019).

2.2.7 Photocatalytic Degradation of Microbial Pollutants

To make the water safe, disinfection is an important stage in the water and wastewater treatment process. Chlorine and its compounds are commonly used in conventional wastewater treatment plants. Chlorination, on the other hand, has drawbacks, such as the generation of hazardous disinfection by-products (DBPs). As a result, adequate alternative disinfection strategies must be developed and used. Advanced oxidation processes (AOPs), such as semiconductor photocatalysis, are a good alternative disinfectant because they produce highly reactive hydroxyl (OH) radicals that attack and inactivate bacteria without producing DBPs (A. C. Mecha et al., 2019). Photocatalytic degradation of microbial contaminants is an innovative way of cleansing water by employing photocatalysts such as ZnO or TiO_2 to eliminate hazardous microbes. When exposed to light, these photocatalysts release reactive oxygen species capable of degrading microbial cell walls, proteins, and DNA, culminating in total pathogen mineralization.

This method is particularly beneficial because it disinfects without harmful chemicals,

avoiding the creation of dangerous by-products. Its applications include treating wastewater and drinking water, as well as purifying indoor air and hospital environments (Ali et al., 2012). Advances in nanotechnology have improved the efficiency of photocatalysts, allowing for rapid and thorough microbial degradation even under visible light. However, challenges such as efficient light utilization, catalyst recovery, and long-term stability need to be addressed to fully harness its potential for large-scale applications. Ongoing research aims to enhance photocatalyst performance, understand microbial degradation mechanisms, and integrate these technologies into existing purification systems to improve environmental and public health protection (Anjum et al., 2017; Soleimani et al., 2021).

2.3 Impregnation of the Fabric Filter by nanophotocatalysis

Impregnating fabric filters with nanophotocatalysis composites represents a significant advancement in water treatment technology, particularly in enhancing antimicrobial properties, facilitating photodegradation of organic contaminants, and improving overall filter performance. This process can be approached through two main methods: the in situ (one-step) and ex situ (two-step) processes, each offering unique benefits and applications.

2.3.1 The in situ method

The in situ process entails the simultaneous fabrication and impregnation of nanophotocatalysis composites on textiles. In this one-step approach, nanoparticles are created and inserted into the fabric simultaneously. This approach ensures a uniform distribution of nanoparticles within the textile fibers, enhancing the overall photocatalytic activity of the treated material. Figure 2.3 shows the in situ approach, in which

impregnation and synthesis occur simultaneously, resulting in a more cohesive and efficient functionalization of the textile (Román et al., 2020). In situ functionalization provides various advantages, including:

- Uniform distribution enhances photocatalytic capabilities by evenly dispersing nanoparticles throughout the cloth.

- Strong bonding enhances nanoparticle adherence to textile fibers, leading to longer-lasting functionalization

- Effectively reduces processing time and complexity by integrating synthesis and impregnation in one step (Ayar & Sutaria, 2021).

2.3.2 The Ex situ method

The ex situ approach comprises a dual-phase procedure involving the independent synthesis of nanoparticles prior to their integration into textile substrates. Initially, nanoparticles are fabricated through methodologies such as sol-gel, hydrothermal or chemical vapor deposition. Subsequently, these nanoparticles are incorporated into the textile through techniques like dip-coating, spraying, or padding. Figure 2.4 demonstrates the ex situ approach, where the synthesis of nanoparticles is followed by their application to the textile. This approach provides greater control over the size, shape, and composition of the nanoparticles before they are put to the fabric (Román et al., 2020). The ex situ method offers several benefits, including:

- Controlled Synthesis; allows for precise control over nanoparticle characteristics, optimizing their photocatalytic efficiency.

- Versatility; enables the use of various nanoparticles with different properties tailored to specific applications.

- Scalability; facilitates the large-scale production and application of nanoparticles to textiles.

Both in situ and ex situ methods for incorporating nanophotocatalysis composites into textiles offer distinct advantages and can be selected based on the specific requirements of the application. The in situ method streamlines the process and ensures strong nanoparticle integration, while the ex situ method provides precise control over nanoparticle properties and offers greater versatility. Each strategy contributes significantly to increased photocatalytic activity in textiles, leading to improved applications in water purification, air filtration, and antimicrobial fabrics (Ayar & Sutaria, 2021).
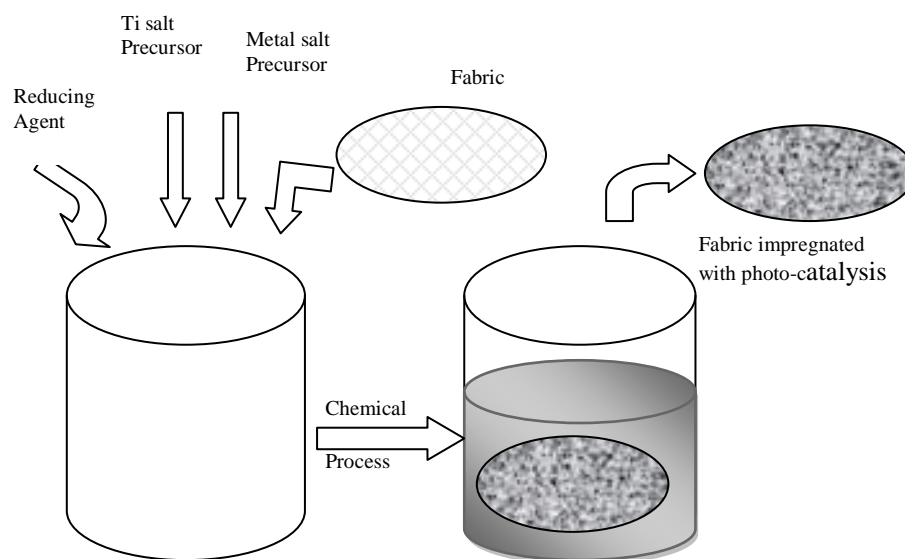
Figure 0-3 Fabric impregnation using in situ method
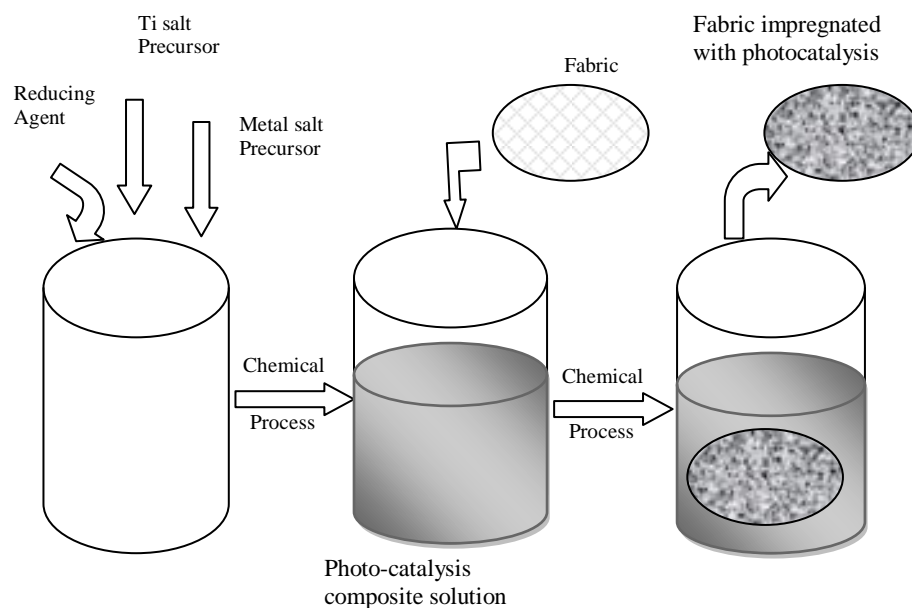
Figure 0-4 Fabric impregnation using ex situ method

2.4 Water pollution & water contaminants

Water pollution is an important environmental issue that affects people all over the world. All living beings in the ecosystem rely on water to survive. Access to clean and safe water is a significant challenge in many impoverished countries. According to the World Health Organization (WHO), approximately 1 billion people worldwide lack a household connection, access to a public standpipe, a protected well or spring, or a rainwater collection source (Jackson & Smith, 2018). The risks of drinking contaminated water are significant, especially for youngsters. The estimation provided by the World Health Organization (WHO) indicates that each year, more than 4 million individuals succumb to the effects of consuming polluted water, with a particularly alarming statistic of over 1.5 million fatalities among children below the age of five (Jackson & Smith, 2018). The ongoing contamination of freshwater reservoirs due to a variety of organic, inorganic, and

microbial impurities represents a notable hazard to the overall water distribution network. Despite the potential of conventional treatment methods in addressing these issues, they frequently prove inadequate in completely eliminating all pollutants and adhering to stringent water quality criteria. Furthermore, present wastewater treatment systems have significant shortcomings, including a high energy requirement, inadequate pollutant removal, and the formation of toxic sludge (Anjum et al., 2019).

Water pollution falls into four categories: inorganic pollutants, organic pollutants, microbiological pollutants, and radioactive contaminants. Inorganic pollutants consist of heavy metals, mineral acids, metal complexes, and cyanides. Organic pollutants encompass substances such as herbicides, pesticides, dyes, medicines, phenols, polyaromatic hydrocarbons, hormone-disrupting compounds, pharmaceuticals, and natural organic matter. Microbial pollutants consist of parasites, bacteria, pathogens, and viruses. Lastly, contaminants with radioactive materials also contribute to water pollution (Chabalala et al., 2021; Sharma & Bhattacharya, 2017).

2.4.1 Inorganic Contaminants

The presence of inorganic contaminants in surface and groundwater remains a significant environmental issue today. Despite various control measures, the release of these contaminants continues to be problematic. These toxins might come from natural geological sources or human activity like farming, mining, and industrialization. While trace amounts of inorganic contaminants might be found in water supplies, levels exceeding the maximum permissible limits can lead to severe health issues, exposure to contaminants can cause harm to various organs, including the liver, kidneys, neurological system, circulatory system, gastrointestinal system, bones, and skin. Dissolved inorganic

pollutants in water can be cationic, anionic, or neutral forms of ions, atoms, or molecules from any element in the periodic table. Inorganic pollution refers to compounds that exist naturally in the environment but have been altered by human activity. These non-carbon-based substances may be detrimental to both human health and the environment (Soni et al., 2020).

Toxic inorganic heavy metals including, lead, cadmium mercury, and arsenic can accumulate in the body and cause a wide range of health problems, including developmental disorders and neurological. Mineral acids, such as hydrochloric acid and sulfuric acid can lower the pH of water, making it caustic and toxic to aquatic life. Other inorganic contaminants, such as nitrates and nitrites, are commonly found in agricultural runoff and can cause serious health problems in infants, such as methemoglobinemia or "blue baby syndrome." Additionally, highly toxic metal complexes and cyanides can contaminate water through industrial processes, mining activities, and improper waste disposal. Addressing these inorganic contaminants is crucial for ensuring safe and clean drinking water problems (Briffa et al., 2020; Masindi & Muedi, 2018).

2.4.2 Organic contaminants

Pesticides, residential garbage, and industrial wastes, among other things, are major anthropogenic causes of organic pollution. Organic material contamination can lead to major health issues such as cancer, hormonal changes, and nervous system disorders. As an example, when chlorine in treated drinking water reacts with naturally existing organic materials, trihalomethanes (THMs) are generated (Sharma & Bhattacharya, 2017). Emissions of organic dyes and heavy metal ions from the paper, leather, and textile sectors pose a significant concern due to their potential mutagenic and carcinogenic

effects. Effluents containing these organic and inorganic substances necessitate treatment prior to discharge into the surroundings to adhere to environmental standards (Naseem & Waseem, 2022). Various semiconductors, including TiO_2, ZnO, Fe_2O_3, C_3N_4, and bismuth-based materials, can facilitate the breakdown of numerous organic pollutants into more readily biodegradable compounds or less harmful molecules, leading to their mineralization into innocuous gases like CO_2 and H_2O (Horikoshi & Serpone, 2020; Moreira et al., 2019).

2.4.2.1 Organic dyes

Reactive dyes have received a lot of attention since they are commonly utilized and water effluent needs to be controlled so that it is disposed of after pretreatment. These dyes are also employed in the coloring and printing of cellulose fibers. What has brought attention to specific dyes is the fact that they, particularly reactive dyes, have been discovered in considerable concentrations in water produced by dyeing and printing operations (Siddique et al., 2011). Therefore, it is critical to create solutions that effectively mitigate the discharge of these dyes into readily accessible water sources. It is imperative that this issue be resolved in order to protect the ecosystem and guarantee the sustainability of water supplies. Various methods, such as adsorption, biological treatment, advanced oxidation processes, and membrane technologies, have been explored for their potential to remove reactive dyes and minimize their impact on water quality (Bagheri et al., 2020; Behera et al., 2021; Samsudin et al., 2015).

Research on the photocatalytic breakdown of dyes, including reactive blue dye, has been published. (Samsudin et al., 2015), different reactive dyes (Kaur et al., 2015), Orange II dye (Lucarelli et al., 2000), using pure TiO_2 under UV light, and methylene blue under

visible light by dye sensitized titania (Samuel & Yam, 2020), also reactive blue 203 dye using ZnO nanoparticles (Bagheri et al., 2020). However, all these studies evaluated the performance of TiO_2 and ZnO separately. There is need to assess the performance of co-doped TiO_2 and ZnO to elucidate synergistic effects.

Dyes have a wide structural variety and are classed depending on their solubility. Dyes are categorized into five commercial series, which include acid dyes, basic dyes, direct dyes, reactive dyes, and disperse dyes (Gupta et al., 2018). Dyes are applied in aqueous solutions and appear colored because they preferentially absorb specific wavelengths of light. Dye molecules consist of two key components: chromophores and auxochromes. Chromophores are responsible for producing the color, while auxochromes enhance the molecule's water solubility, improve its attraction to fibers, and support the chromophores (Adeel et al., 2018).

Approximately 20% of the total dye generated globally is wasted during the dyeing process and dumped into water bodies without treatment, resulting in considerable environmental damage. These dye contaminants possess high toxicity, carcinogenicity, and potentially mutagenic properties (Adeel et al., 2018). Reactive and acid dyes are the most often used dyes in industries. Therefore, eradicating them is vital. Reactive dyes are soluble in water, making it difficult to remove them using typical flocculation and biological breakdown procedures (Çolak et al., 2009).

Dyes can dramatically restrict light penetration into aquatic environments, thereby harming plants and inhibiting photosynthesis (Kim et al., 2015). The elimination of dyes from wastewater and sewage is crucial due to their toxicity, mutagenicity, and carcinogenicity, which stem from aromatic chemicals and can impact all forms of life

(Wang et al., 2009) Researchers have investigated several techniques of dye removal, including adsorption, ozonization, reverse osmosis, and chemical oxidation (Torrades & García-Montaño, 2014). However, conventional processes such as absorption or coagulation are not sufficiently effective, as they often result in incomplete degradation of organic compounds and merely transfer contaminants from one phase to another, methods like sedimentation, filtration, and membrane use are costly and can generate secondary pollutants. Advanced oxidation processes using ultraviolet radiation and catalysts like TiO_2 and ZnO offer a promising alternative due to their high efficiency and non-toxicity (Bagheri et al., 2020).

2.4.2.2 Oxytetracycline (OTC)

Antibiotics make up one of the biggest categories of all the drugs and personal hygiene products. They are regularly excreted or discharged into the environment via direct runoff (Ebele et al., 2017). Recent literature has extensively documented the widespread presence of antibiotics in various environmental matrices, such as sewage treatment plants, surface water, and soils. A major area of research is the photocatalytic degradation of organic pollutants. An illustrative case is oxytetracycline (OTC), a crucial broad-spectrum antibiotic widely employed in livestock globally for both disease prevention and growth promotion (Felis et al., 2020; Wydro et al., 2023).

Oxytetracycline held the highest share of the global antibiotics and antimicrobials market in 2021, valued at USD 4.7 billion. In China exclusively, an estimated 248,000 tons of antibiotics are manufactured on a yearly basis, of which approximately 52% are allocated for veterinary purposes. The excretion of antibiotics in feces or urine, ranging from 40% to 90% in both human and animal recipients, is a notable concern. These excreted

antibiotics exist as either active compounds or glycoconjugates capable of reverting to their original molecules, as highlighted in studies by (Sarmah et al., 2006; Q.-Q Zhang et al., 2015). A comprehensive investigation conducted on 50 samples of livestock dung and compost obtained from eight different regions in China unveiled the presence of 17 distinct antibiotics. Among these antibiotics, oxytetracycline (OTC) exhibited the highest concentration recorded at 416.8 μg/kg, this results in large amounts of residual antibiotics contaminating soil and groundwater, especially through the use of animal manure as fertilizer or leakage (H. Zhang et al., 2015).

OTC can enter water sources from several origins, including effluents from sewage treatment plants, cattle manure dispersed in fields, aquaculture farms, and pharmaceutical industry effluents. The photocatalytic oxidation of OTC using heterogeneous pure semiconductor oxides, such as TiO_2 or metal oxides with band gap energies within the visible light range, is a promising method. A highly effective approach to mitigating the rapid recombination of electron-hole pairs in low-band-gap oxide semiconductors involves the interfacing of two distinct semiconductor materials characterized by staggered conduction and valence bands. This particular configuration enables the separation and accumulation of photoinduced electrons and holes on the respective semiconductors, thus promoting the oxidation and reduction reactions of specific target compounds. Various approaches are employed to enhance catalyst performance, including doping the oxides with metal and/or non-metal elements, surface functionalization, creating composites, and forming nano-heterojunctions (Pelosato et al., 2022).

2.4.3 Microbial contaminants

The existence of biological entities like algae, bacteria, protozoa, or viruses leads to contamination of the water. Each of these organisms possesses the capability to introduce distinctive challenges in the aquatic environment. Algae, being minute, single-celled organisms, are prevalent in water bodies. The taste and smell of water might alter due to excessive algae development, and it can also block filters and produce unwelcome slime on carriers. At times, they may release toxins that are harmful to the skin, nervous system, and liver. Similarly, bacteria are single-celled microorganisms that can contaminate water with various harmful strains. Typhoid, dysentery, cholera, and gastroenteritis can all be caused by them. Some nonpathogenic bacteria can produce taste and odor problems. Protozoans, like bacteria, are single-celled and tiny creatures. Certain protozoans are frequently present in rivers, lakes, and streams treated with sewage. These organisms can lead to symptoms like diarrhea, stomach cramps, nausea, fatigue, dehydration, and headaches. Viruses are the tiniest living entities capable of infecting and infecting others. Viruses such as *hepatitis* and *polio* are frequently found in polluted water (Sharma & Bhattacharya, 2017). TiO$_2$ photocatalysts can eradicate bacteria in water, introducing a new method for photocatalytic microorganism inactivation. Reactive oxygen species (ROS) play a crucial role in this process, as they effectively inactivate bacteria. This capability complements their effectiveness in degrading various organic and inorganic pollutants, making ROS a highly successful strategy for comprehensive water treatment (Wang et al., 2012).

In practice, determining the presence of all of the different harmful organisms in water is time-consuming. Therefore, specific organisms like *E. coli* are utilized as indicators to

signal the possible presence of pathogens. These indicator organisms are sensitive to environmental changes. The goal is to produce permeate that is free from any traces of *E. coli.* The assumption behind the use of indicator species is that enteric bacterial pathogens will have comparable survival characteristics to the indicator organisms. As a result, water quality requirements are expressed in terms of these indicator organisms (Achisa, 2014b). The guidelines set forth by the World Health Organization stipulate that potable water must adhere to a standard of 0 % presence of *E. coli* per 100 ml of processed water (Frisbie et al., 2012). In the realm of scientific inquiry, the predominant focus of laboratory investigations concerning photocatalytic disinfection revolves around the utilization of *E. coli* as a key metric for identifying the potential existence of waterborne pathogens (A. Mecha et al., 2019).

2.4.4 Radioactive Contaminants

Radioactivity is the energy released when certain atoms and isotopes undergo nuclear decay. Protons and neutrons are bundled together in small bundles to form atomic nuclei, which are located in the heart of atoms. There are numerous naturally occurring pollutants in sources of public drinking water. As an illustration, trace amounts of radioactive uranium and radium can dissolve in water and are present in practically all rocks and soil. Groundwater can also naturally contain radon, a radioactive gas produced by the decomposition of radium (Sharma & Bhattacharya, 2017). Radon and gross alpha radiation are produced by the disintegration of several radioactive elements. The decay of uranium and thorium in the Earth's crust can lead to the release of massive alpha particles into drinking water. While these radiations do not constitute a health danger outside the human body, ingestion has been found to be detrimental, particularly with continuous

exposure (Ho et al., 2020).

Reverse osmosis and ion exchange are useful technologies for removing radionuclides from drinking water, hence improving its quality (Woolf et al., 2023). However, communities with inadequate water purification infrastructure and lower-income areas are at higher risk of exposure to radionuclides, raising significant environmental justice concerns (Karim et al., 2020).

2.5 Water purification

Water purification is essential for ensuring safe drinking water and maintaining public health. Physical filtration, sedimentation, and chemical disinfection are traditional ways for purifying water, and they successfully remove particle matter, pathogens, and other impurities. However, these technologies have limitations in dealing with developing contaminants such pharmaceuticals, personal care products, and other micropollutants. Advanced oxidation processes (AOPs) offer an effective solution by generating highly reactive species like hydroxyl radicals, which can break down various organic pollutants. Commonly employed AOPs include techniques such as ozonation, the Fenton reaction, and UV/H_2O_2 treatment, all of which enhance the degradation of persistent pollutants. Photocatalysis, a specific type of AOP, uses semiconductor materials such as titanium dioxide (TiO_2) under light irradiation to produce reactive species that can decompose organic compounds and disinfect water. This approach is highly promising due to its efficiency, non-toxic nature, and potential for solar-driven applications, making it a sustainable option for water treatment. Integrating photocatalysis with traditional methods can further improve the removal efficiency of contaminants and reduce reliance on chemical disinfectants. Collectively, these advanced techniques offer comprehensive

solutions for tackling complex water pollution challenges, ensuring higher water quality standards and addressing the limitations of conventional water purification methods (Binazadeh et al., 2023).

Water disinfection has significantly reduced the threats to public health posed by microbiologically polluted drinking water. Harmful microorganisms are inactivated using several disinfection techniques utilized in drinking water treatment. It examines elements that influence disinfection process efficiency before moving on to the following disinfection processes:

- Pretreatment oxidation by adding oxidants to water early in the treatment process.

- Initial disinfection is a key component of basic drinking-water treatment because granular filter media do not completely eliminate all microbial pathogens.

- Secondary disinfection is employed to maintain the water quality achieved at the treatment plant throughout the distribution system until it reaches the tap.

Pretreatment is one way for removing microorganisms from water. It incorporates operations that affect microbiological water quality before or at the point of input into a treatment plant. Water can be pretreated using a variety of techniques, including roughing filters, microstrainers, off-stream storage, and bank infiltration. Algal cells, excessive levels of turbidity, viruses, and protozoan cysts can all be removed with pretreatment. The different pretreatment solutions can be compatible with a wide range of treatment processes, from simple disinfection to membrane filtration. Additionally, coagulation, flocculation, and sedimentation are used in conjunction with subsequent filtration (Backer et al., 2024).

Coagulation encourages small particles to interact and produce larger particles in

practice; the word refers to particle instability, interparticle collisions, and coagulant addition (i.e. the addition of a material that will generate the hydrolysis products that cause coagulation), Flocculation is the physical process of establishing interparticle interactions that lead to the development of big particles is known as flocculation, Sedimentation is a method of solid–liquid separation in which particles settle due to gravity. Other type of water treatment is the Ion exchange where an undesired ion in the untreated water is swapped out for a solid phase presaturant ion. Calcium, magnesium, and certain radionuclides are removed using this method.

In the treatment of drinking water, many filtering techniques are employed. For microbial infections, filtration can serve as a reliable and efficient barrier. The most used filtration method for treating drinking water is granular media filtration. Under ideal circumstances, coagulation, flocculation, sedimentation, and granular media filtration can remove protozoan pathogens with chlorine-resistant cysts, slow sand filtration Water is gravity-fed through a sand filter without any coagulation pretreatment Due of slow sand filtration's capacity to eliminate parasites, interest in it has grown as a result of numerous disease outbreaks caused by protozoan infections that are resistant to chlorine over the previous 20 years (Achisa, 2014b; Chhabra & Gurappa, 2019; LeChevallier & Au, 2004). A variety of approaches, or a combination of them, can be used to remove, suppress, or kill microorganisms as shown in Fig. 2.5

Physical destruction process	• Heating and UV light irradiation. • . Boiling or solar energy.
physical seperation procedure	• Gravity separation and filtering. • Coagulation, flocculation, sedimentation, and floatation are examples of the former. • membranes, ceramic filters, and slow sand filters are examples of the latter.
Chemical destruction and prevention multiplication	• chemical agents is the most common method • Chlorine gas, chlorine dioxide, sodium hypochlorite, monochloramine, bromine, iodine, ozone, hydrogen peroxide, silver, and copper are among the most regularly utilized chemicals.
Biological destruction process	• occurs in a gravity-operated slow sand filter. • The water is actively treated by natural bacteria and protozoa in the filter's top layer.

Figure 0-5 Approaches used to remove, suppress, or kill microorganisms

(a) Traditional Methods

Water purification has long relied on traditional methods, which can effectively remove various contaminants but often fall short in eliminating all types of pollutants. Key water treatment technologies that are essential to guaranteeing access to clean and safe drinking water are filtration and membrane processes. The physical removal of pollutants from water through filtration involves the use of porous materials such as sand, gravel, or activated carbon to capture particles, sediments, and certain microorganisms. Traditional filtration may not be able to remove all pathogens or dissolved chemicals, even while it is efficient for bigger contaminants.

Conversely, membrane processes use semi-permeable membranes to molecularly segregate pollutants. The pore size and pressure requirements of various techniques vary, including reverse osmosis, ultrafiltration, nanofiltration, and microfiltration.

Microfiltration and ultrafiltration remove suspended solids, bacteria, and some viruses, while nanofiltration and reverse osmosis eliminate dissolved salts, heavy metals, and organic pollutants, providing a more advanced level of purification (Shmeis, 2018).

- **Filtration**

2.5.1 Sand Filtration

2.5.1.1 Overview

Filtration methods have a long-standing history of utilization in water purification dating back to ancient civilizations, effectively targeting the removal of various impurities such as sand, silt, turbidity, scale, and other suspended particles. It is well-documented in historical records that as early as 2000 BC, ancient India employed sand and gravel filters for water treatment purposes. Additionally, the Romans showcased their utilization of natural filtration techniques by strategically constructing canals in close proximity to lakes, facilitating the passage of water through the canal walls for purification (Abdiyev et al., 2023).

Within the realm of traditional water treatment methods, slow sand filtration (SSF) emerges as a particularly noteworthy approach that significantly contributes to the provision of potable water and the mitigation of WASH (Water, Sanitation, and Hygiene) challenges. The enduring appeal of SSF lies in its operational efficiency and cost-effectiveness, rendering it a practical solution for ensuring the availability of clean drinking water in resource-constrained regions. Notably acknowledged by reputable institutions such as the U.S. Environmental Protection Agency (USEPA) and the World Health Organization (WHO) as a financially feasible and reliable technique, SSF continues to find application in rural settings and even some urban areas on a global scale

(Agrawal et al., 2021).

The distinguishing characteristics of SSF encompass its uncomplicated design, minimal energy demands, gradual filtration pace, and the notable absence of chemical pre-treatment requirements. Routine maintenance tasks for SSF typically entail surface scraping or periodic removal of sand to uphold the efficacy of the filtration layers. Despite the array of benefits associated with SSF, the current reliance on this method for meeting drinking water needs is limited to approximately half a million individuals residing in developing nations (Haig et al., 2011).

2.5.1.2 Filter media and its characteristics

Slow Sand Filtration (SSF) uses sand as the primary filter medium, supplemented by layers of pebbles and gravel to cleanse water. Sand, which can be sourced locally or purchased, is crucial to the effectiveness of SSF. Common sands used include coarse sand, fine sand, quartz/silica sand, and Accusand silica. Each sand type has unique properties affecting filtration efficiency. For instance, Accusand silica effectively removes viruses like MS2 and PRD-1, while silica sand achieves over 70% removal of organic matter (OM), a 90% reduction in chemical oxygen demand (COD), and significantly lowers levels of *Escherichia coli*, *total coliforms* (TCs), and salmonella. However, pre-assessment is often necessary to determine the most suitable sand type for specific pollutants (Verma et al., 2017).

The SSF column typically consists of a stratified arrangement starting with diminutive rocks at the base, succeeded by pebbles, and culminating in coarse sand at the uppermost layer. Certain configurations incorporate a substrate of underdrain gravel, followed by coarse sand, and topped with iron-oxide-coated sand. Conversely, some variations feature

a homogeneous sand layer. In order to sustain uniform filtration, effluent is introduced into the filter using mechanisms such as float valves or overflow pipes. Diffuser plates or perforated PVC discs, positioned above the sand bed, ensure uniform distribution of wastewater and protect the schmutzdecke layer—a biological layer crucial for filtration efficiency. Screen filters below the sand media help prevent the release of suspended particles that could impair filter performance (Bourne et al., 2006; Verma et al., 2017)

The efficacy of SSF is heavily influenced by key filter media properties such as bulk density, particle density, porosity, effective diameter (de), and coefficient of uniformity (UC). The effective size (de or d10) of the sand, defined as the screen opening size that allows 10% of the total sand sample mass to pass, is a critical parameter. A lower UC value indicates less uniform sand, which is preferred in SSF for enhanced performance. Larger effective sizes tend to decrease dissolved oxygen (DO) recoveries but also reduce the need for backwashing. Conversely, finer media with smaller grain sizes improve the removal of total suspended solids (TSS) and turbidity, though they require more frequent cleaning (Elbana et al., 2012; Pizzi, 2010).

The strategic layering and characteristics of filter media directly influence SSF's filtration efficiency. Uniformity in sand media is not desirable, as a lower UC value enhances the filter's performance. Larger effective sizes reduce the necessity for backwashing and lower DO recoveries, while finer grains increase filtration efficiency but necessitate more frequent maintenance. Studies show that SSF's filtration efficiency improves with a decrease in grain size of the filter medium. For instance, finer media correlate with better TSS removal and turbidity reduction. However, this also means that the filter medium needs to be cleaned more often when using smaller grains (Verma et al., 2017).

2.5.1.3 Cleaning of the sand filter

Regular cleaning may not consistently yield the intended outcomes within the framework of Slow Sand Filtration (SSF). Although it is generally advised against, backwashing could be considered in cases where the turbidity of the effluent and the concentrations of suspended solids (SS) surpass the values recommended by the World Health Organization (WHO), set at 5 NTU and 100 mg/L, respectively. The frequency of backwashing is determined by various factors, which encompass the attributes of the treated water, like the levels of total suspended solids (TSS) and biochemical oxygen demand (BOD), alongside the qualities of the sand and gravel materials employed during the filtration procedure. In situations where routine maintenance may not be feasible, particularly in remote regions, alternative approaches can be implemented. Strategies like pretreating wastewater, reducing loading rates, and increasing dosing frequency have the potential to uphold the satisfactory performance of SSF. These adaptations play a crucial role in ensuring the continuous effectiveness of SSF in water purification, even when adhering to standard maintenance procedures proves to be challenging, consequently, although SSF stands as a resilient and dependable technique, its efficiency can be further optimized through strategic adjustments to maintenance and operational protocols, especially when dealing with demanding conditions (Jaeel & Abdulkathum, 2018; Verma et al., 2017).

2.5.2 Activated Carbon

Activated carbon (AC) is a material of significant versatility and effectiveness that finds widespread application in a variety of purification processes owing to its remarkable capacity for adsorption, expansive surface area, and intricately structured pore network.

This particular section offers an exhaustive examination encompassing the genesis, categorization, operational mechanisms, benefits, and drawbacks of AC, with a specific emphasis on its utilization within biological activated carbon (BAC) filtration systems, thereby accentuating its paramount importance and adaptability across diverse industrial sectors (Dos Santos et al., 2022).

2.5.2.1 Formation and Mechanisms of Activated Carbon

Activated carbon is generated via processes of carbonization and activation carried out at elevated temperatures. The carbonization process entails heating raw carbon-based materials, such as wood, coal, coconut shells, or peat, without oxygen to eliminate volatile components. Following this, the material undergoes activation, where it is exposed to oxidizing agents like steam or carbon dioxide at temperatures between 600 and 1200°C. This activation step is essential for enhancing the pore structure and surface area of the material, thereby improving its adsorption capabilities. The efficiency of adsorption by activated carbon depends on the quantity of well-developed pores and the distribution of pore sizes in relation to the molecular weight of the organic substances being adsorbed. Adsorption of natural organic matter (NOM) primarily occurs in mesopores and large micropores. Granular activated carbon (GAC), a widely utilized form of activated carbon, effectively adsorbs smaller molecular weight fractions of NOM (Z. Lu et al., 2020).

2.5.2.2 Classification of Activated Carbon

Activated carbon can be classified based on its physical form, method of preparation, and intended use:

(a) Physical Form

Activated carbon comes in different forms, each designed for specific purposes. Powdered Activated Carbon (PAC) consists of fine particles, usually under 0.18 mm in size, allowing for rapid adsorption due to its large surface area. Granular Activated Carbon (GAC), with larger particles ranging from 0.2 to 5 mm, is frequently used in water and air filtration systems due to its robust structure and ease of handling. Extruded Activated Carbon (EAC) has a cylindrical shape and is suitable for particular industrial applications, while Bead Activated Carbon (BAC) is spherical in shape and is preferred for applications that require consistent flow (Z. Lu et al., 2020).

(b) Method of Preparation

There are two ways to produce activated carbon: chemically or physically. The process of physical activation includes the carbonization of raw materials followed by their activation using gases such as steam or carbon dioxide, thereby improving both the pore structure and surface area. Conversely, chemical activation involves saturating raw materials with substances like phosphoric acid or potassium hydroxide prior to carbonization. This approach commonly yields a more elaborate pore structure and is frequently more energy-efficient compared to physical activation (Ganjoo et al., 2023).

(c) Intended Use

Activated carbon is optimized for gas phase applications, such as air purification by removing volatile organic compounds (VOCs), and liquid phase applications, such as water purification, where it effectively removes a wide range of contaminants.

2.5.2.3 Application in Biological Activated Carbon (BAC) Filters

After microbial colonies settle on the carbon surface over time, GAC filters eventually

become BAC filters. These BAC filters remove organic pollutants and inorganic nutrients, including ammonia, phosphorus, and metals from water, through both adsorption and microbial degradation. The performance of BAC filters is heavily influenced by microbial activity, which can extend the service life of GAC through in situ biological regeneration of sorption sites (Dos Santos et al., 2022).

2.5.2.4 Pore Size Classification and Its Importance

Activated carbon pores are classified into three categories based on their size table 2.3.

Table 0-3 Classification of activated carbon by pores size

Classification	Pore Size	Importance
Micropores	< 2 nm	Contribute significantly to the high adsorption capacity of AC
Mesopores	2–50 nm	Essential for the adsorption of larger molecules
Macropores	> 50 nm	Facilitate bacterial adhesion and colonization in BAC filters

For effective BAC filter performance, it is crucial to select GAC with a balanced distribution of these pore sizes. While micropores and mesopores enhance adsorption capacity, macropores are necessary for microbial activity. The current selection criteria for AC in BAC filters often rely on iodine or methylene values, which indicate the presence of micropores and some mesopores but do not account for macropores. This oversight suggests a need to reassess the selection criteria to optimize both adsorption and microbial degradation in BAC applications (Z. Lu et al., 2020).

2.5.2.5 Factors Influencing BAC Performance

The biodegradation of organic matter in BAC filters is influenced by several factors: higher microbial biomass and growth rates enhance degradation efficiency, while a diverse and stable microbial community structure is beneficial. Additionally, operational conditions such as preozonation, temperature, backwashing, and filter characteristics significantly impact microbial activity. For instance, some commercial GACs are specifically manufactured with larger pore sizes to promote bacterial growth, further optimizing the biodegradation process (Z. Lu et al., 2020).

2.5.2.6 Advantages of Activated Carbon

Activated carbon boasts numerous advantages: it possesses a high adsorption capacity, effectively removing a wide spectrum of contaminants; it is versatile, apt for both gas and liquid phase applications; its regenerability allows for multiple reuse cycles, ensuring long-term cost-effectiveness; it is non-toxic, ensuring safety in water and air purification without introducing harmful substances; and it exhibits efficiency in removing impurities even at low concentrations, making it a robust choice across various industrial and environmental settings (Ganjoo et al., 2023).

2.5.2.7 Disadvantages of Activated Carbon

However, the utilization of activated carbon is accompanied by several challenges. Firstly, high-quality activated carbon can be costly, restricting its application in certain contexts. Secondly, activated carbon has a finite adsorption capacity; once saturation occurs, regeneration or replacement is necessary. Thirdly, the handling and disposal of used activated carbon require meticulous attention to prevent environmental contamination. Moreover, activated carbon exhibits selective effectiveness, with some

contaminants proving resistant to adsorption. Lastly, the regeneration process can be energy-intensive and may not completely restore the material's initial adsorption capacity, posing additional operational challenges in its sustainable use.

The use of activated carbon in purification and filtration processes spans across water purification, air purification, and chemical purification, highlighting its critical role in maintaining environmental and industrial standards. Its formation through carbonization and activation processes, classification based on physical form, method of preparation, and intended use, and its application in BAC filters underscore its multifaceted utility. While it offers numerous advantages, the associated challenges necessitate ongoing research and innovation to maximize its effectiveness and sustainability in addressing global purification needs (Ganjoo et al., 2023).

2.5.3 Membrane separation process

Membrane separation is a widely used technique for treating water globally. It may be found in large stations in cities and towns using current style and technology, as well as more basic and traditional methods in remote and extremely underdeveloped places. It is the most popular method used today for treating wastewater and surface water. Currently, it is used to remove dissolved solids, bacteria, organic and inorganic contaminants, suspended materials, and certain microbes from aqueous systems (Msomi, 2015). Other substance is rejected due to size; however the water molecules are permitted to pass (Achisa, 2014b).

Figure 2.5 shows the separation of raw and waste water using membranes, followed by modern and conventional disinfection methods.
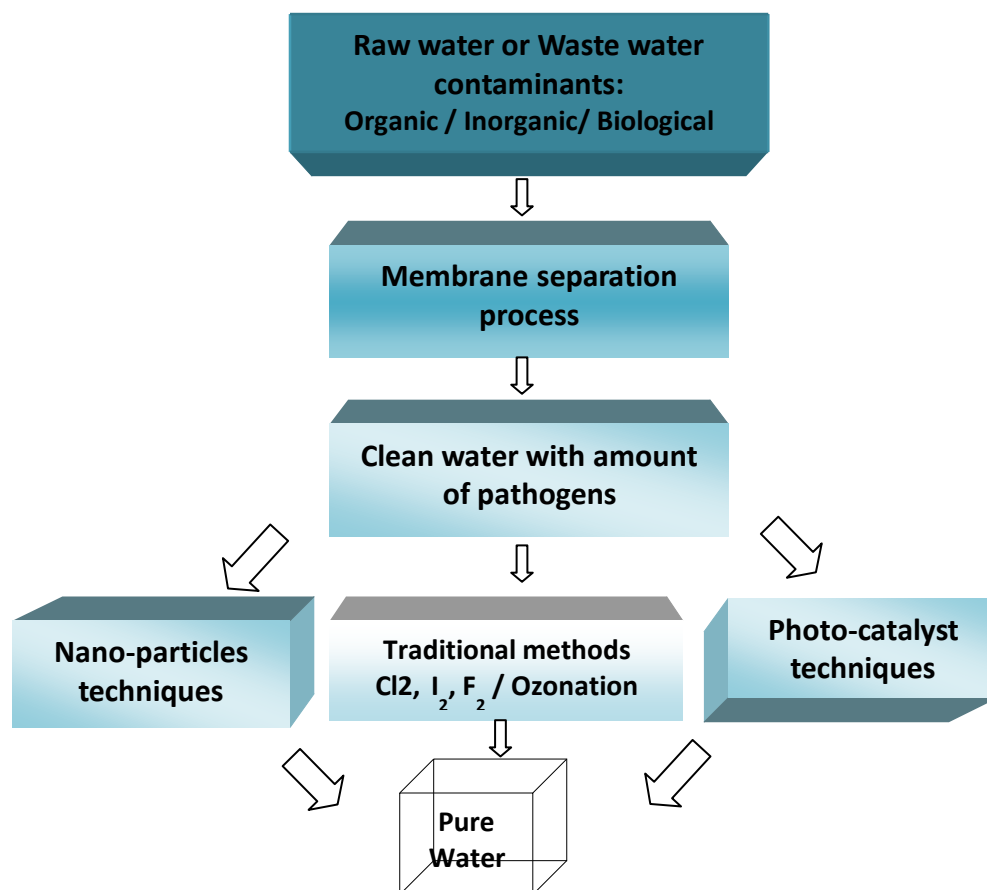
Figure 0-6 Water treatment through membrane followed by disinfection techniques

The size range of materials to be separated and the driving force utilized in separation can both be characterized as industrial membrane processes. Based on what causes the separation, membrane processes are categorized to Reverse osmosis (RO), microfiltration (MF), ultrafiltration (UF), nanofiltration (NF), Electrodialysis, and Dialysis. As listed in Table 2.4 (Chhabra & Gurappa, 2019). The most popular pressure-driven methods for treating water are membrane filtration technologies (Achisa, 2014; Msomi, 2015).

Table 0-4 membranes classification

Process	NF	MF	UF	NF	RO	Electrodialysis	Dialysis
Driving force gradient	Pressure	Pressure	Pressure	Pressure	Pressure	Electric field	Concentration
Separation size rang nm	1 – 10 Angstrom	10^4 - 10^2	$< 10^2$ – 5	~1	< 1	< 5	< 5
force gradient	20 bar	0.5 – 2 bar	0.5 – 2 bar	5 – 12 bar	8 – 70 bar	3 – 7 KWh/m^3 for BW 17 KWh/m^3 for SW	Work by diffusion

- **Chemical Treatment**

2.5.4 Chlorination

Chlorine is widely acknowledged as one of the most cost-efficient and effective disinfectants utilized for inactivating microorganisms in urban water distribution systems. Its usage has led to a substantial decrease in waterborne illnesses such as cholera, typhoid fever, and dysentery, consequently improving public health (Rienzie et al., 2020). The efficacy and affordability of chlorine render it the favored option for disinfecting municipal water (P. Lu et al., 2020).

2.5.4.1 Benefits and Challenges of Chlorine Disinfection

Chlorine disinfection has brought about considerable public health advantages by

managing infectious diseases, yet it also triggers the generation of disinfection by-products (DBPs) when natural organic matter (NOM) in untreated water reacts with chlorine. Notable DBPs encompass trihalomethanes (THMs) and haloacetic acids (HAAs), which pose health risks due to their potential to cause cancer. Persistent consumption of water containing these DBPs, even in minimal amounts, can negatively impact human health, with a specific focus on their cancer-causing characteristics. The creation of THMs in chlorinated water is affected by the composition of untreated water, operational factors, and the residual chlorine in the water distribution system (Srivastav et al., 2020).

2.5.4.2 Chlorination Levels in Drinking Water

When chlorine is introduced into a body of water, a segment of it interacts with both inorganic and organic substances as well as metals that are present, a phenomenon referred to as the chlorine consumption of the water. The chlorine that is not consumed is identified as total chlorine, and this can be further categorized into combined chlorine and free chlorine. Combined chlorine functions as a mild disinfectant; however, its effectiveness diminishes once it binds with inorganic compounds such as nitrates or organic nitrogen-based molecules like urea. Free chlorine, on the other hand, represents the residual chlorine available for deactivating pathogens, serving as an indicator of water quality. Consequently, the total chlorine required is the collective sum of combined chlorine and free chlorine. In instances where water is devoid of impurities, the chlorine consumption is negligible, resulting in the preservation of all chlorine as free chlorine. Nonetheless, in water sources containing organic substances, there is an escalation in chlorine consumption; leading to the formation of combined chlorine through interactions

with inorganic substances like nitrates (Mazhar et al., 2020).

2.5.4.3 Formation of Disinfection By-products (DBPs)

During the process of chlorination, trihalomethanes (THMs) are predominantly generated as disinfection byproducts (DBPs), which encompass chloroform, dibromochloromethane (DBCM), bromodichloromethane (BDCM), and bromoform. These byproducts are created as a result of the reactions occurring between natural organic matters (NOM) precursors like humic and fulvic acids and chlorine as stated by (Thokchom et al., 2020). Among the various THMs formed, chloroform emerges as the most prevalent, yet the existence of bromide in the water, which undergoes oxidation, can also give rise to the production of other THMs. Appendix C1 and C2 showed the Disinfection By-products limits by different organizations (Mazhar et al., 2020).

2.5.4.4 Addressing the DBP Challenge

Addressing the DBP problem involves understanding the extent of their formation, the routes of exposure, and the associated health risks. Control strategies and minimization techniques are crucial in mitigating DBP levels in drinking water. Adopting alternative disinfection methods, such as ozonation or UV treatment, can reduce the formation of DBPs. Additionally, optimizing chlorination practices, such as adjusting the dosage and timing, can minimize DBP production. Improved water treatment technologies and better management practices are essential in reducing the risks associated with DBPs (Kalita et al., 2024).

Chlorine remains an essential disinfectant for ensuring safe drinking water due to its effectiveness and affordability. However, the formation of DBPs poses significant health risks, particularly due to their carcinogenic potential. A comprehensive understanding of

DBP formation, control strategies, and alternative treatment technologies is necessary to ensure the safety and quality of chlorinated drinking water. By addressing these challenges, we can continue to benefit from the advantages of chlorine disinfection while mitigating the associated health risks. The results of this review aim to guide the implementation of effective DBP control measures in municipal water systems, ensuring safer drinking water for communities (Srivastav et al., 2020).

2.5.5 Coagulation and Flocculation

Coagulation and flocculation are important in water treatment because they help to remove suspended particles, turbidity, and pollutants. The key idea underpinning these procedures is the introduction of particular chemicals into the water, which causes particle aggregation and so increases their removability in following treatment phases (Xia et al., 2018).

2.5.5.1 Coagulation

The coagulation process begins with the addition of coagulants, which are chemical agents that negate the negative charges shown by particles in the water. These particles include organic compounds, bacteria, and inorganic components, and are often stable and distributed due to their negatively charged surfaces. Aluminum sulphate (alum), ferric chloride, and polyaluminum chloride are common coagulants.

When coagulants are introduced into the water, the particles become destabilised as their charges are neutralised, allowing them to be closer together. This first phase causes the creation of minute, sticky clusters known as microflocs. The efficacy of the coagulation process is determined by a number of parameters; including the type and quantity of

coagulant employed, water pH levels, temperature, and the characteristics of the particles in the water (Semblante et al., 2018).

2.5.5.2 Flocculation

Following the process of coagulation, the water is subjected to flocculation, which is characterized by a delicate mixing procedure that facilitates the collision and aggregation of microflocs into larger, more stable entities known as flocs. In this stage, the addition of flocculants, chemical substances that assist in the bonding of particles, can be employed to improve the formation of flocs. Among the commonly used flocculants are synthetic polymers such as polyacrylamide.

The process of flocculation typically takes place in a sequence of compartments or tanks, where the water is mixed at progressively decreasing velocities. This gradual mixing process enables the flocs to increase in size and robustness without disintegrating. The increased size of the flocs produced during this phase facilitates their removal through sedimentation, filtration, or other methods of separation (Iwuozor, 2019).

2.5.5.3 Applications and Benefits

Coagulation and flocculation are extensively utilized in municipal water treatment facilities for the purpose of eliminating turbidity, color, and pathogens from potable water. These processes are similarly utilized in wastewater treatment for the purpose of decreasing organic matter and in industrial operations for the treatment of effluents prior to their release. The primary advantages associated with coagulation and flocculation encompasses enhanced water clarity, improved removal of pollutants, and decreased burden on subsequent filtration and disinfection procedures (El-taweel et al., 2023).

2.5.5.4 Challenges and Considerations

Despite their efficacy, the processes of coagulation and flocculation pose numerous challenges. The careful selection and optimization of coagulants and flocculants necessitate a thorough examination of water chemistry and operational parameters. Inaccurate dosing or inappropriate pH levels may lead to subpar performance or the production of excessive sludge. Furthermore, the proper management of sludge generated during these processes is crucial for minimizing environmental repercussions (Kurniawan et al., 2020).

In summary, coagulation and flocculation represent pivotal stages in water treatment aimed at enhancing the elimination of suspended particles and pollutants. By promoting the aggregation and subsequent elimination of particles, these procedures contribute to the generation of pure and safe water for diverse applications. Continuous research and advancements in coagulant and flocculant technologies serve to enhance the effectiveness and sustainability of these indispensable water treatment procedures (El-taweel et al., 2023).

- **Biological Treatment**

2.5.6 Slow Sand Filters

Slow sand filtration is a sustainable and highly effective method of water treatment that leverages natural biological, physical, and chemical processes for water purification. It involves the gradual passage of water through a sand bed, leading to the formation of a biological layer known as the schmutzdecke on the sand surface. This microbial layer, consisting of bacteria, protozoa, and algae, plays a critical role in decomposing organic pollutants and harmful microorganisms, thereby enhancing water quality significantly

(Ranjan & Prem, 2018).

The filtration process in slow sand filters is intricate, the schmutzdecke functions as a biological barrier, decomposing organic substances and pathogens, while the sand bed serves as a physical barrier, capturing suspended particles and solids through mechanisms like straining, sedimentation, and adsorption. The synergy of these processes results in the production of high-quality water with reduced turbidity, decreased pathogen levels, and lower concentrations of organic contaminants (Ranjan & Prem, 2018).

A key advantage of slow sand filters is their simplicity and cost-effectiveness. They demand minimal operational and maintenance efforts, making them especially suitable for rural and resource-limited environments. In contrast to traditional water treatment methods, slow sand filters do not depend on chemical disinfectants, thus averting the generation of harmful disinfection by-products. This characteristic renders them environmentally sustainable and safe for prolonged utilization. Moreover, slow sand filters are recognized for their durability and consistency, delivering reliable performance even amidst fluctuations in raw water quality (Abdiyev et al., 2023).

Nevertheless, slow sand filtration is accompanied by various challenges. Notably, a considerable amount of land is necessary for installing these filters, which may pose feasibility issues in densely populated or urban regions. Additionally, slow sand filters typically exhibit low flow rates, rendering them less appropriate for large-scale water treatment purposes. Regular maintenance is crucial to uphold optimal performance, as periodic cleaning of the schmutzdecke is essential to prevent blockages and sustain filtration efficacy (Abdiyev et al., 2023).

Despite these obstacles, advancements in slow sand filtration technology persist in

enhancing its efficiency and adaptability. Innovations such as pre-treatment procedures to decrease contaminant loads, the utilization of layered filter media to boost filtration effectiveness, and the introduction of intermittent operation methods to prolong filter lifespan have all contributed to the evolution of slow sand filters. Furthermore, integrating slow sand filters with other treatment technologies like membrane filtration and ultraviolet disinfection can further elevate their efficiency and broaden their scope of application (Abdiyev et al., 2023).

In summary, slow sand filtration emerges as a practical and environmentally friendly remedy for water purification, particularly in rural and resource-constrained settings. While challenges exist, continuous research and technological progress offer potential for augmenting the efficiency, scalability, and versatility of slow sand filters, thereby ensuring the delivery of safe and potable water to diverse communities (Maiyo et al., 2023).

2.5.7 Boiling

Boiling water is a straightforward and highly efficient disinfection method necessary for ensuring the safety of water through the eradication of harmful microorganisms. The process entails raising the temperature of the water to its boiling threshold (100°C or 212°F at sea level) and upholding it for a minimum of 20 minutes, contingent upon the altitude and types of pathogens existing (Rosa et al., 2010).

The efficacy of boiling water resides in the elevated temperatures that exterminate or incapacitate microorganisms, such as bacteria, viruses, and protozoa, accountable for ailments like cholera, dysentery, and giardiasis. The application of high heat deforms the proteins and disrupts the cell membranes of these pathogens, thereby neutralizing their

threat. Despite being efficacious against most waterborne pathogens and capable of eliminating certain chemical impurities with lower boiling points than water, boiling does not eradicate chemical contaminants, heavy metals, or salts. Boiling water proves particularly beneficial in exigent circumstances, like natural calamities or regions with restricted access to safe potable water (Rosa et al., 2010). It represents a dependable, simple method that requires no specialized equipment beyond a heat source and a receptacle. The key benefits of boiling water include its simplicity, effectiveness in eliminating most microorganisms, and the absence of any necessary chemical additions. Nonetheless, boiling has a number of limitations, particularly in terms of large-scale applications (Manzoor et al., 2022).

The principal disadvantages entail substantial energy and time demands, rendering it unfeasible or unsustainable for the purification of large water quantities, particularly within resource-constrained environments. Boiling is suitable for minor quantities but unviable for extensive water treatment facilities or the provision of safe water to sizable populations. There exists a probability of recontamination, as boiled water demands proper storage and handling in hygienic, covered vessels to preserve its safety. Furthermore, boiling fails to eliminate chemical pollutants, heavy metals, or dissolved salts from water, thereby requiring supplementary treatments to address these impurities. Moreover, boiling can potentially impact the taste and visual appeal of water due to the evaporation of specific volatile compounds (Akowanou et al., 2016).

In conclusion, while boiling is an effective method for pathogen elimination and the assurance of safe potable water, particularly in emergency situations or for minor applications, its drawbacks in terms of energy consumption, scalability, and the inability

to eliminate chemical impurities limit its utility for comprehensive or long-term water treatment strategies. Adequate storage and treatment of boiling water is critical to preventing recontamination and maintaining continuous safety.

(b) Advanced Oxidation Processes (AOPs)

Advanced Oxidation Processes (AOPs) are chemical treatments that use powerful oxidizing agents to degrade organic contaminants, including those that traditional methods cannot effectively remove.

2.5.8 Ozonation

Ozone-based technology, known as ozonation, proves to be highly efficient in the disinfection of water and the degradation of organic contaminants. It plays a significant role in enhancing the treatment of wastewater by marginally elevating pH levels and the concentration of dissolved oxygen, while concurrently diminishing chemical oxygen demand (COD) and fecal coliforms. Functioning as a potent oxidizing agent, ozone demonstrates exceptional capability in decomposing intricate compounds into simpler molecules via either direct or indirect mechanisms (Bhatta et al., 2015). The application of ozonation, frequently in conjunction with advanced oxidation processes (AOP) such as hydrogen peroxide and ultraviolet light, results in the effective breakdown of a diverse array of pollutants, including pharmaceuticals that are resistant to conventional treatment methods. When compared to chlorination, ozonation exhibits higher efficiency and necessitates lower dosage for disinfection, notably requiring a mere 3 mg/L of ozone for the elimination of 90% of antibiotic-resistant bacteria, as opposed to 30 mg/L of chlorine to achieve a comparable outcome. Moreover, ozone offers notable advantages in the treatment of drinking water, notably enhancing attributes such as color, odor, taste, and

aiding in the elimination of iron and manganese. These advantages establish ozonation as a superior alternative to conventional chlorination approaches for water and wastewater treatment, providing a potent, chemical-free remedy with minimal side effects (Da Silva et al., 2012; Oh et al., 2014; Tripathi & Hussain, 2022).

2.5.8.1 Mechanisms of Inactivation by Ozone

Ozone inactivates bacteria by creating free radicals such as hydroxyl (OH) and superoxide (O_2). These radicals alter bacteria's enzymatic activity and DNA, affecting cell permeability. Ozone specifically targets residues like guanine and thymine, which are very sensitive. According to Bitton (2014), ozone can harm either the nucleic acid core or the protein covering of viruses. Rotaviruses are impacted by both (Tripathi & Hussain, 2022).

2.5.8.2 Advantages of Ozone (O_3)-Based Treatment

In water treatment plants around the world, chlorine is widely used as a major disinfectant. Nonetheless, studies show that chlorine reacts with organic substances in water, producing harmful byproducts such as trihalomethanes (THMs), including chloroform. These THMs have the ability to stimulate the production of cancer-causing free radicals in the human body. According to the U.S. Council of Environmental Quality, the likelihood of cancer is significantly elevated by up to 93 % in individuals who consume water treated with chlorine in comparison to those who ingest non-chlorinated water. As a result, the United States has embraced ozone (O_3) as a disinfectant in more than 280 major water treatment facilities. Ozone exhibits a disinfection potency that surpasses chlorine by over two-fold and operates at a rate 3,000 times swifter (Tripathi & Hussain, 2022). It can be employed independently or in

conjunction with other oxidizing agents or energy sources within sophisticated oxidation procedures (AOPs) for the treatment of groundwater, surface water, or wastewater. The technologies reliant on ozone-based treatment endeavor to enhance the utilization of O_3 for enhanced disinfection and elimination of pollutants from water. The benefits associated with ozone-based water treatment encompass its robust oxidizing capability and rapid reactivity, leading to the immediate eradication of microbes and viruses. This treatment procedure also infuses oxygen into water, eliminates discoloration, odor, and taste, necessitates no supplementary chemicals, supports coagulation, oxidizes manganese and iron, eliminates organic substances, and eradicates algae. Ozone does not generate any enduring odor or taste, effectively exterminates bacteria, and oxidizes materials like iron and sulfur to facilitate straightforward filtration. Furthermore, ozone swiftly reverts to oxygen post-treatment, leaving behind no detectable residues. By integrating biofiltration, ozone treatment enables a reduction in chemical oxygen demand (COD) through minimal dosages, reduces operational expenditures, and maximizes oxygen utilization efficiency, thereby establishing itself as a remarkably efficacious and environmentally sustainable method of water treatment (Epelle et al., 2023; Tripathi & Hussain, 2022).

2.5.8.3 Disadvantages of Ozone (O_3)-Based Treatment

While ozone serves as a highly efficient disinfectant, it is accompanied by certain limitations. Key disadvantages include elevated operational costs and substantial energy demands, potentially restricting its practicality for widespread application. Moreover, ozone treatment systems require specialized machinery and upkeep, leading to an escalation in overall expenses. The production and management of ozone must be

executed with great care due to its highly reactive and potentially unsafe characteristics, necessitating strict adherence to safety protocols. Despite its effectiveness, these drawbacks might render ozone treatment less attractive than traditional disinfection methods in certain scenarios (Epelle et al., 2023; Grignani et al., 2020).

2.5.9 Hydrogen Peroxide (H_2O_2)

Hydrogen peroxide (H_2O_2) is a potent oxidizing agent extensively utilized in water treatment owing to its ability to effectively disinfect and degrade various organic pollutants. This utilization encompasses both the purification of drinking water and the treatment of wastewater, providing significant benefits and posing specific challenges (Anjaneyulu et al., 2024). The primary mechanism of hydrogen peroxide disinfection involves the generation of hydroxyl radicals ($\bullet OH$) upon decomposition, which exhibit high reactivity and the capacity to swiftly oxidize and disintegrate contaminants, such as bacteria, viruses, and organic compounds. These radicals target the cell walls of microbes, resulting in cell lysis and subsequent death, while also transforming organic pollutants into simpler, less hazardous molecules, ultimately yielding carbon dioxide and water. Noteworthy advantages of hydrogen peroxide comprise its robust oxidizing capabilities, environmentally friendly nature as it breaks down into water and oxygen, and wide-ranging disinfection efficacy against bacteria, viruses, and fungi, as well as the absence of detrimental chlorinated disinfection by-products (DBPs) associated with chlorine utilization. Furthermore, when integrated with other advanced oxidation processes (AOPs) like UV radiation or ozone, the effectiveness of hydrogen peroxide is markedly amplified (Cuerda-Correa et al., 2019). Nonetheless, there are several drawbacks linked to its application. The elevated expense of hydrogen peroxide may

render it less financially feasible for large-scale usage. Moreover, meticulous storage and handling are imperative due to its reactive properties, and there exists the potential for the formation of toxic by-products, such as peracetic acid, if utilized incorrectly or in excessive concentrations. Over time, hydrogen peroxide undergoes decomposition, diminishing its efficacy if not promptly utilized, and it lacks a sustained residual disinfectant effect, leaving treated water vulnerable to potential recontamination. In practical terms, hydrogen peroxide is deployed in the treatment of drinking water to eliminate organic impurities and disinfect without producing harmful by-products, in wastewater treatment to disintegrate intricate organic compounds present in industrial discharges and municipal wastewater, and in advanced oxidation processes (AOPs) where it is coupled with UV light or ozone to bolster pollutant breakdown. Additionally, it finds application in managing biofilm formation and microbial proliferation in cooling towers and other water systems. While hydrogen peroxide serves as a versatile and potent tool in water treatment, careful management of its economic viability and handling prerequisites is essential to optimize its advantages. Its role in generating hydroxyl radicals via advanced oxidation processes offers a promising avenue for more efficient and effective water treatment solutions, emphasizing the necessity for ongoing research and development to refine its application and tackle the associated challenges (Jiang et al., 2023; Yeneneh et al., 2024).

2.5.10 Fenton's Reagent

The Fenton reaction, first identified by H.J.H. Fenton in 1894, involves the interaction of ferrous iron (Fe^{2+}) with hydrogen peroxide (H_2O_2) to create hydroxyl radicals ($\cdot OH$). This highly oxidative process is widely used in wastewater treatment to break down

various organic pollutants. When the Fenton reagent (a combination of Fe^{2+} and H_2O_2) is introduced into wastewater, it quickly reacts to produce hydroxyl radicals (Khan et al., 2023), as shown in the following equations:

$$Fe^{2+} + H_2O_2 \rightarrow Fe^{3+} + \bullet OH + OH^- \qquad 0.10$$

$$Fe^{3+} + H_2O_2 \rightarrow Fe^{2+} + HO_2\bullet + H^+ \qquad 0.11$$

$$\bullet OH + RH \rightarrow R\bullet + H_2O \qquad 0.12$$

$$R\bullet + O_2 \rightarrow RO_2\bullet \qquad 0.13$$
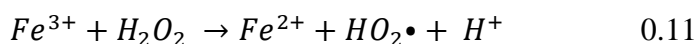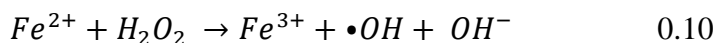
These reactions demonstrate H_2O_2's ability, with Fe^{2+} as a catalyst, to produce hydroxyl radicals that can oxidize and decompose various water contaminants. Hydroxyl radicals are extremely reactive species that can efficiently break down complex organic molecules into simpler, non-toxic substances, making the Fenton process a crucial tool in environmental cleanup and wastewater treatment (Chen et al., 2023).

In addition to the traditional Fenton reaction, Fenton-like reactions have been developed to enhance efficiency and broaden the range of applications. These adaptations use different catalysts, such as ferric iron (Fe^{3+}), other transition metals, or even non-metallic catalysts, to generate hydroxyl radicals under various conditions. These modifications aim to optimize the process for specific types of wastewater or to enhance the degradation efficiency of particular pollutants.

Fenton and Fenton-like reactions offer the advantage of degrading a wide array of organic pollutants, including those resistant to conventional treatment methods. The simplicity of the process, which can be conducted at ambient temperature and pressure, makes it suitable for various applications. Additionally, the reagents used in the Fenton

reaction, such as iron and hydrogen peroxide, are relatively low-cost and readily accessible. However, there are challenges associated with the implementation of Fenton and Fenton-like reactions.

One of the main issues is the need for precise pH control, as the reaction is most effective in an acidic pH range (typically around pH 3). Furthermore, the process generates iron sludge as a by-product, which must be properly managed and disposed of. The efficiency of the reaction can be influenced by the presence of other substances in the wastewater, which may act as scavengers for hydroxyl radicals and reduce their availability for degrading pollutants (Khan et al., 2023).

In summary, Fenton and Fenton-like reactions are highly effective and adaptable methods for wastewater treatment, capable of efficiently degrading a broad spectrum of organic pollutants. The production of hydroxyl radicals through the reaction of H_2O_2 with Fe^{2+} (or other catalysts) allows for the oxidative breakdown of contaminants, providing a valuable tool for environmental remediation. Despite some challenges related to pH control and by-product management, the simplicity, cost-effectiveness, and broad applicability of these reactions make them a significant component of modern wastewater treatment technologies (Liu et al., 2021).

2.5.11 Photocatalysis

2.5.11.1 Overview

Photocatalyst activity relies on the inherent properties of semiconductor materials like titanium dioxide (TiO_2), tungsten oxide (WO_3), and zinc oxide (ZnO), which can generate electron-hole pairs when exposed to light. This process, known as photocatalysis, is an advanced oxidation technique that utilizes light-activated catalysts,

primarily TiO_2, to degrade a wide range of contaminants. When TiO_2 is illuminated, it produces reactive species such as hydroxyl radicals, which are highly effective at breaking down organic pollutants, pharmaceuticals, and endocrine disruptors (Karthikeyan et al., 2020).

Photocatalysis is particularly noteworthy for its ability to address persistent pollutants that are otherwise difficult to remove through conventional water treatment methods. The process can be enhanced by modifying photocatalysts. Incorporating materials like graphene or doping with metals can significantly improve their efficiency and expand light absorption into the visible spectrum, making the process more effective under natural sunlight.

The applications of photocatalysis are diverse, ranging from large-scale water treatment plants to point-of-use systems. In large-scale operations, photocatalysis assists in the degradation of stubborn pollutants and provides an additional layer of disinfection. This is especially valuable in treating industrial wastewater, which often contains complex and resistant contaminants. On a smaller scale, point-of-use systems leverage solar power to purify water in rural or disaster-affected areas, offering a sustainable and accessible solution for clean drinking water.

The technology's advantages are manifold. Its use of sunlight makes it an environmentally friendly and sustainable option. Photocatalysis is also broad-spectrum, capable of targeting a wide array of contaminants and it is non-toxic, ensuring that no harmful byproducts are introduced into the water. These attributes make photocatalysis a promising tool for both developed and developing regions, providing a versatile method for improving water quality.

Despite its potential, there are several challenges that need to be addressed to optimize the use of photocatalysis in water treatment. One of the main issues is the efficient recovery and reuse of photocatalysts. After the photocatalytic process, separating the catalysts from the treated water can be difficult and may require additional steps, which can complicate the process and increase costs. Innovations in catalyst design and system engineering are required to simplify recovery and enhance the practicality of reuse (Karthikeyan et al., 2020).

Another challenge is ensuring adequate light penetration in turbid water. High turbidity levels can block or scatter light, reducing the efficiency of photocatalysis. This is particularly problematic in natural water sources that may contain suspended solids and organic matter. Solutions such as pre-treatment steps to reduce turbidity or the development of photocatalysts that are effective under lower light conditions are being explored to overcome this limitation.

In conclusion, photocatalysis represents a significant advancement in water treatment technology, leveraging the unique properties of semiconductor materials to create a powerful and sustainable method for degrading contaminants. While there are hurdles to overcome, such as catalyst recovery and light penetration in turbid water, ongoing research and technological improvements hold promise for making photocatalysis a cornerstone of future water purification efforts. The ability to use sunlight, its effectiveness against a wide range of pollutants, and its non-toxic nature position photocatalysis as a key player in addressing global water quality challenges (Khader et al., 2024).

2.5.11.2 Titanium dioxide (TiO₂) photocatalysis

Titanium dioxide (TiO₂) photocatalysis is a highly advanced process known as an advanced oxidation process (AOP) that is widely acknowledged for its efficacy in decomposing organic pollutants during water treatment applications. When exposed to ultraviolet (UV) light, TiO₂ generates electron-hole pairs that initiate a series of oxidative reactions. These reactions can break down a wide range of contaminants, including those resistant to conventional treatment methods (Khader et al., 2024).

The initiation of the photocatalytic process occurs upon exposure of the TiO_2 surface to UV light with a wavelength below 385 nm. This process excites electrons from the valence band to the conduction band, creating electron-hole pairs (e^- / h^+). These pairs are highly reactive and can interact with water and oxygen molecules, producing reactive oxygen species (ROS) such as hydroxyl radicals (•OH) and superoxide anions (O_2^-). Such ROS function as potent oxidizing agents capable of disintegrating various organic pollutants into benign byproducts, such as carbon dioxide and water. The key reactions involved in TiO_2 photocatalysis can be delineated as follows:

$$TiO_2 + UV \; or \; visible \; light \; \rightarrow \; TiO_2 \, (e^- + h^+) \qquad 0.14$$

$$h^+ + H_2O \; \rightarrow \; \bullet OH + H^+ \qquad 0.15$$

$$e^- + O_2 \; \rightarrow \; O_2^- \qquad 0.16$$

$$\bullet OH + Organic \; pollutant \; \rightarrow \; degraded \; products \qquad 0.17$$
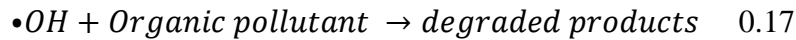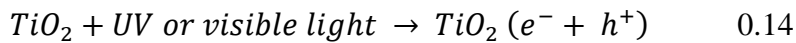
TiO₂ photocatalysis presents numerous advantages for water treatment. Initially, TiO₂ demonstrates chemical stability and non-toxicity, rendering it suitable for environmental use. Furthermore, it is cost-effective and widely accessible. The method effectively

targets a wide array of organic pollutants, such as pharmaceuticals, pesticides, dyes, and endocrine-disrupting substances. Additionally, TiO_2 photocatalysis can serve for disinfection purposes by deactivating bacteria, viruses, and other harmful microorganisms (Armaković et al., 2022).

Furthermore, TiO_2 photocatalysis can be implemented in various setups, including slurry reactors, immobilized systems, and thin films, tailored to the specific treatment requirements. Slurry reactors involve suspending TiO_2 particles in water to maximize the surface area for photocatalysis, necessitating subsequent catalyst separation from treated water. Immobilized systems utilize TiO_2 coated on a substrate, simplifying catalyst retrieval and reuse, albeit potentially reducing the available reaction surface area.

Nonetheless, TiO_2 photocatalysis encounters certain limitations. The reliance on UV light for activation can lead to high energy consumption, especially with artificial UV sources. While natural sunlight is an option, the efficiency of solar-driven TiO_2 photocatalysis is often restricted by the limited UV light fraction in the solar spectrum. Strategies to enhance TiO_2 photocatalytic efficacy have focused on incorporating other elements, like nitrogen, sulfur, or metals, to broaden light absorption into the visible range and enhance efficiency under sunlight.

Another challenge is the recombination of electron-hole pairs, which can significantly reduce ROS production and the overall efficiency of the process. Diverse approaches have been utilized to address this issue, including co-catalysts, innovative TiO_2 nanostructure design, and the application of external fields to enhance charge separation (Dong et al., 2015).

In summary, TiO_2 photocatalysis presents itself as a highly promising and versatile technology for water treatment, effectively degrading a wide range of organic pollutants and providing disinfection capabilities. Despite challenges related to UV light demands and electron-hole recombination, persistent research efforts aim to boost the efficiency and feasibility of this process, establishing it as a progressively viable solution for combating water pollution and ensuring the provision of safe and clean potable water (Dharma et al., 2022).

2.5.11.3 Zinc Oxide (ZnO) Photocatalysis

Zinc oxide (ZnO) photocatalysis is a prominent advanced oxidation process used in water treatment, comparable to titanium dioxide (TiO_2) in terms of its mechanisms and wide-ranging applications. ZnO is a wide-bandgap semiconductor that, when exposed to ultraviolet (UV) light, generates electron-hole pairs. These pairs interact with water and oxygen molecules, producing reactive oxygen species (ROS) such as hydroxyl radicals (•OH) and superoxide anions ($O_2^- \cdot$). These highly reactive ROS can effectively degrade a variety of organic pollutants, including dyes, pharmaceuticals, and pesticides, converting them into harmless byproducts like carbon dioxide and water (Sun et al., 2023).

One of the significant advantages of ZnO photocatalysis is its high photocatalytic activity. ZnO has similar bandgap energy to TiO_2 but offers higher electron mobility, which can enhance the efficiency of photocatalytic reactions. This makes ZnO a potent material for applications not only in water and air purification but also in disinfection processes. ZnO exhibits notable antimicrobial properties, effectively inactivating bacteria, viruses, and other pathogens, making it a valuable tool in ensuring water safety and hygiene (Lee et al., 2016).

Despite its potential, ZnO photocatalysis faces several challenges. The primary limitation is its reliance on UV light, which constitutes only a small fraction of the solar spectrum. This dependence necessitates high-energy input, making the process less energy-efficient and more costly when scaled up Efforts are currently underway to enhance ZnO by modifying its properties to extend its photoresponse into the visible light range. This includes techniques like doping with different metals or non-metals, which aim to utilize more sunlight and enhance the sustainability of the process (Zhang et al., 2023).

Another significant challenge is the rapid recombination of electron-hole pairs in ZnO, which diminishes the availability of reactive oxygen species (ROS) essential for degrading pollutants. Strategies to overcome this include the development of ZnO-based composites with other materials, such as graphene or noble metals, which can act as electron sinks and improve charge separation, thereby enhancing photocatalytic efficiency.

Photocorrosion is another drawback of ZnO, where prolonged exposure to light and the resultant oxidative environment can degrade the ZnO itself, limiting its long-term stability and reusability. Research is focused on creating more stable ZnO structures and coatings that resist photocorrosion, thus extending the material's lifespan in practical applications.

Recent advances have led to the development of ZnO nanostructures, such as nanowires, nanotubes, and nanoparticles, which offer a higher surface area and more active sites for photocatalysis. These nanostructures can significantly improve the degradation rates of pollutants and enhance the overall efficiency of the process.

In summary, ZnO photocatalysis holds great promise for environmental remediation due

to its high photocatalytic activity and strong oxidizing power. While challenges like UV light dependence, electron-hole recombination, and photocorrosion exist, ongoing research and technological advancements are continuously improving the efficiency and practicality of ZnO-based photocatalytic systems. With these developments, ZnO photocatalysis could become a more viable and widespread solution for large-scale water and air purification, contributing significantly to sustainable environmental management (Sun et al., 2023).

2.5.11.4 Ferric Oxide (Fe_2O_3) photocatalysis

Ferric oxide (Fe_2O_3) photocatalysis is a promising technology for water treatment and environmental remediation. Unlike other photocatalysts such as titanium dioxide (TiO_2) and zinc oxide (ZnO), ferric oxide benefits from a narrow bandgap, allowing it to absorb a broader spectrum of visible light, making it more energy-efficient and cost-effective for use under natural sunlight.

When exposed to light, Fe_2O_3 produces electron-hole pairs that migrate to the surface of the photocatalyst, where they engage with water and oxygen to form reactive oxygen species (ROS) such as hydroxyl radicals and superoxide anions. These ROS exhibit high reactivity and are capable of efficiently breaking down diverse organic contaminants into less hazardous byproducts like carbon dioxide and water (Lee et al., 2016).

Moreover, ferric oxide displays notable antimicrobial characteristics, bolstering its suitability for disinfection purposes. Nevertheless, it encounters obstacles such as the swift recombination of electron-hole pairs, leading to diminished efficacy. Furthermore, the holes generated during the photocatalytic process can oxidize the catalyst itself, triggering photocorrosion and compromising its long-lasting stability.

To tackle these challenges, scientists are devising Fe_2O_3-based composites and hybrid materials that enhance the separation of charges, elevate photocatalytic performance, and bolster resistance to photocorrosion. Strategies such as incorporating other elements, pairing with diverse semiconductors, and modifying the surface are under exploration to optimize the efficacy of ferric oxide photocatalysis. By surmounting these hurdles, ferric oxide photocatalysis exhibits substantial promise for sustainable and efficacious environmental remediation and water purification applications (Nunes et al., 2021).

2.5.12 Nano-membranes

Membrane filtration technology produced with nanomaterials is one of the most successful contemporary innovative wastewater treatment approaches. Nanotechnology principles allow new functionality in water treatment membranes, such as catalytic reactivity, high permeability, and fouling resistance, that go beyond current state-of-the-art performance. The advantages of this technique in terms of quality treated water, effective disinfection, and low plant area requirements are the key reasons for its use. In addition, when compared to other treatment methods, it is extremely cost-effective, efficient, and simple to implement. Nanomembrane separation technique is used in wastewater treatment to successfully remove colors, heavy metals, and other impurities. Nanomaterials in new membranes play an important role in the chemical degradation of organic foulants, in addition to particle separation from wastewater. One-dimensional nano-materials (organic and inorganic materials) such as nanotubes, nanoribbons, and nanofibers make up the compositions of these membranes (Anjum et al., 2019). The accumulation of organic matter and traces of organics in wastewater is a big issue, and current methods such as coagulation/flocculation and chlorine technology are unable to

provide satisfactory results. The additional sludge generated by this technology necessitates further processing and disposal. Because of its capacity to generate precise structurally controlled materials for such requirements, nanotechnology offers tremendous potential for filtration applications (Tlili & Alkanhal, 2019).

2.5.13 Nanostructured Catalytic Membranes (Ncms)

Nanostructured catalytic membranes are extensively used in water treatment due to their significant advantages. These membranes offer high uniformity of catalytic sites, enabling precise optimization and control over catalyst contact duration, which facilitates sequential reactions and enhances treatment efficiency. Furthermore, their design simplifies the process of industrial scale-up, making them practical for large-scale applications.

Under both UV and visible-light irradiation, nanostructured TiO_2 films and membranes exhibit a range of beneficial activities. They effectively degrade organic pollutants, inactivate microorganisms, and prevent biofouling, all while physically separating contaminants from water. These capabilities are particularly valuable for maintaining clean and safe water supplies.

One notable advancement in this field is the development of N-doped "nut-like" ZnO nanostructured materials, which are incorporated into multifunctional membranes. These materials significantly boost photodegradation activity under visible light, enhancing the membranes' ability to eliminate a wide array of water pollutants. The incorporation of ZnO also imparts strong antimicrobial properties to the membranes, further improving their effectiveness in water purification.

The combination of these advanced materials ensures that the membranes can

consistently produce clean water with a high flow rate, addressing one of the critical needs in water treatment. The multifunctional nature of these membranes makes them an attractive solution for various water purification challenges, especially in the industrial sector. Their ability to operate efficiently under visible light also aligns with sustainable practices, utilizing natural sunlight to drive the purification process, which is particularly beneficial for remote or off-grid areas. This innovation represents a significant step forward in the water purification industry, promising safer and more efficient treatment solutions (Biswajit et al., 2014; Chorawalaa & Mehta, 2015).

2.6 Point-Of-Use (POU) Devices for household Water Treatment

2.6.1 Overview

In numerous areas within Sub-Saharan Africa, the intersecting issue of inadequate drinking water quality and elevated rates of HIV infection is widespread. The task of providing safe water to the worldwide populace has been recognized by the National Academy of Engineering as a significant Grand Challenge of the field. One possible option, according to the WHO, is to embrace a more decentralized approach to water treatment, with people treating their water in their homes right before consumption. This concept, known as point-of-use (POU) water treatment, has the potential to enhance the microbiological quality of home water while also lowering the risk of diarrheal disease and death, especially among children (Jackson & Smith, 2018).

As per the World Health Organization (WHO), domestic water treatment pertains to the practice of purifying water either at home or at the point-of-use (POU) in settings such as educational institutions, healthcare facilities, and other establishments. The general population is interested in POU household devices that eliminate microbiological

diseases and parasites, as well as harmful compounds, from drinking water and improve its aesthetic quality (removal of taste and odor, turbidity, color). Point-of-use (POU) devices are particularly advantageous in rural regions lacking centralized infrastructure, and their utilization is progressively gaining popularity among consumers. Examples of POU devices that can be installed in homes include in-line filters, reverse osmosis units placed under the kitchen sink, and pour-through pitchers equipped with activated carbon filters (Bitton, 2014).

The three primary types of modern point-of-use water treatment methods that employ nanoparticles in porous media are ceramic, paper, and textile (Fig. 2.7). These systems are gravity fed, which reduces energy costs, and use filtering to remove turbidity.

Ceramics
- A ceramic made from fired clay can be used for ceramic filtration, and research has shown that it is highly effective against bacteria and protozoa.
- Most development
- Market infilteration

Paper
- Cellulose, the most prevalent natural polymer, comprises the majority of paper. It has excellent metal ion sorption properties and is widely accessible, affordable, renewable, and biodegradable.
- New development

Textile
- Altough it is a traditional way, it showspromise for future research because it is:
- cheap
- socialy acceptable
- effictive method

Figure 0-7 point-of-use water treatment methods

Point-of-use (POU) water treatment systems must demonstrate effectiveness, user-friendliness, minimal maintenance requirements, economic feasibility, environmental sustainability, and acceptance in the sociocultural context. Illustrative instances encompass chlorination coupled with secure storage, integrated coagulant-chlorine disinfection mechanisms, solar disinfection, ceramic water filters (CWFs), biosand filters, and combination of traditional method with advanced oxidation process (Hamouda et al., 2012).

2.6.2 Ceramic Water Filters (CWFs): A Practical Solution for POU Water Treatment

CWFs are highly regarded for their practicality and sustainability, particularly in developing countries. They are cost-effective, easy to use, and require minimal maintenance, needing only periodic cleaning. Constructed Wetlands for Wastewater Treatment (CWFs) are composed of a mixture of clay and finely sifted flammable substances, which successfully eradicate microorganisms and decrease cloudiness by means of gravitational filtration using permeable ceramic components. These systems are available in a range of configurations, such as disks, tubes, candles, and containers, rendering them appropriate for a variety of Point-of-Use (POU) scenarios. Silver impregnation is a common enhancement that boosts CWFs' effectiveness, particularly in microbial removal. Silver-modified CWFs can eliminate over 99% of protozoa and between 90 % to 99.999 % of bacteria, significantly lowering the incidence of diarrheal and other waterborne diseases without changing the water's taste or temperature. They are also effective at reducing turbidity. With proper maintenance, commercial ceramic pot filters, widely used in developing countries, can last up to five years without needing

external energy sources or consumables. CWFs have been successfully used in over 20 developing countries, providing safe drinking water to more than 4 million people, thus contributing to public health, social, and economic benefits (Yang et al., 2020).

However, CWFs have limitations. Their relatively low filtration rates and limited ability to remove viruses and chemical pollutants like arsenic and fluoride are significant drawbacks. Despite the increasing body of research and extensive practical implementation observed in recent decades, there remains a paucity of comprehensive evaluations pertaining to the advancements made in this particular field of technology. This exposition aims to provide a concise overview of recent research and practical applications of the Continuous Wavelet Transform (CWF), focusing on key variables and procedures that impact its effectiveness, and to outline the challenges and opportunities for future improvements (Ciawi & Khoiruddin, 2024).

2.6.2.1 Critical Factors for CWF Performance

CWFs are fabricated from a mix of clay and combustible materials like rice husks or sawdust, creating a porous structure during firing. The fabrication process includes raw material selection and processing, mixing and pressing, drying and firing, silver application, and quality testing. Key processes affecting filter effectiveness are well-documented in published reports (Ciawi & Khoiruddin, 2024).

2.6.2.2 Removal of Various Classes of Contaminants

Conventional CWFs primarily target microbial pollutants with relatively large sizes, such as bacteria and protozoa. However, their pore sizes, typically ranging from 0.1 to 100 micrometers, are ineffective at retaining smaller pathogens like viruses and common chemical pollutants through physical filtration. The negatively charged ceramic surface

further limits the capture of viruses and chemical pollutants via adsorption. Studies have shown that Ceramic Water Filters (CWFs) display a decreased efficacy in the removal of viruses, showing minimal variances between silver-infused and non-infused variations. This poses a noteworthy obstacle for traditional CWF systems. Chemical pollutants are typically removed through interactions with the (modified) ceramic surface. Enhancing chemical pollutant removal involves modifying the ceramic surface with specific coatings to increase affinity for target pollutants. For instance, a ceramic disk filter modified with ferric iron was developed to enhance arsenic removal, with its effectiveness being greatly impacted by the amount of ferric iron loaded. Recently, lanthanum (La) has been applied as a novel and effective coating for ceramic materials, targeting both negatively charged arsenate (As (V)) and non-charged arsenite (As (III)). Ceramic materials coated with lanthanum (La) have demonstrated a significant improvement in the adsorption of both As (V) and As (III), resulting in sorption capacities of 24.8 and 10.9 mg/g, correspondingly. The enhancement in removal efficiency can be attributed to the creation of surface precipitates of $LaAsO_4$ and inner-sphere surface complexes involving lanthanum. The chemical composition and properties of the La coating, influenced by the coating process, are critical for optimal pollutant removal (Yang et al., 2020).

2.6.2.3 Virus Removal through Ceramic Surface Modification

Since most viruses hold negative charges in natural aquatic environments, positively charged chemical coatings on ceramic surfaces have been used to enhance virus removal via electrostatic interaction. MgO-amended ceramic filters, for example, were found to enhance the elimination of bacteriophages MS_2 and PhiX174, although their efficacy decreased over time. In a similar vein, ceramic microfilters that were altered with

Zr(OH)x and Y_2O_3 exhibited a notable enhancement in MS_2 removal efficiency, resulting in an elevation of their isoelectric points from below 3.1 to a range spanning from 5.5 to 10. Nevertheless, the efficiency of these filters was compromised by the presence of humic acid and prolonged operation. Furthermore, novel coatings such as nano TiO_2 and nano ZnO have been investigated as potential substitutes for silver as antimicrobial agents, showcasing cost-effective advancements in bacterial removal in small-scale laboratory investigations (Yang et al., 2020).

2.6.2.4 Future Directions and Challenges

Despite these advancements, the development of low-cost, environmentally benign, and effective coatings for ceramic surface modification holds promise for enhanced CWF performance in removing small-sized chemical and microbial pollutants. However, the interaction between coatings and pollutants is strongly influenced by water chemistry, necessitating further research to determine long-term performance under various source waters. Evaluating the safety and leaching behavior of novel coatings is essential before field application (Ciawi & Khoiruddin, 2024).

2.6.2.5 Conclusion

CWFs, produced from locally sourced clay and combustible materials, offer an affordable, effective, low-maintenance, and sustainable POU water treatment solution for developing areas. This review identifies essential elements for CWF performance, including manufacturing methods and source water quality. Two main technical challenges are identified: improving filter flow rate and bacterial removal simultaneously, and enhancing the removal of various chemical and microbial pollutants. Researchers and manufacturers are working to optimize pore properties during manufacturing and employ

novel chemical modifications to improve efficacy. Future research should focus on designing, manufacturing, and applying improved CWFs for POU water treatment in developing countries, aiming to overcome these challenges and enhance overall performance (Yang et al., 2020).

In 2018, Kathryn G. Nunnelley investigated the effectiveness of a novel technique for embedding metallic silver and copper into ceramic media to disinfect bacteria and viruses in drinking water. The study's findings indicate that altering the production method of ceramic water filters can lower costs in raw materials and labor, while also reducing the risk of exposure to potentially harmful silver nanoparticles. Traditionally, silver nanoparticles (AgNP) are painted onto ceramic filters after firing. This research compares this method with a new technique where silver nitrate ($AgNO_3$) is embedded into the ceramic before firing. Lab-based experiments reveal that while AgNP filters initially show higher antimicrobial efficacy, their performance declines over time and they often release silver at concentrations above drinking water standards. In contrast, $AgNO_3$ filters consistently release lower amounts of silver and maintain higher bacterial removal efficacy over time (Nunnelley, 2018).

Although these controlled lab results are promising, they may not fully reflect how these filters would perform in real home-use scenarios, the surface chemistry between the ceramic and silver particles whether nanoparticles or nanopatches might influence the release of silver. Filters made with the same type and amount of silver nanoparticles at different facilities showed varying silver effluent concentrations, possibly due to differences in clay sources or firing protocols. During kiln firing, temperature patterns affect ceramic formation and the silver-ceramic interface. Van der Waals forces might

cause the nanosilver to detach easily during filter use, while the textured ceramic surface likely holds the nanopatch more securely. Additionally, chemical interactions such as ion exchange during mixing might lead to metallic nanopatch formation.

Full-scale filters manufactured in South Africa indicated that filters containing $AgNO_3$ were more efficient than those containing AgNP in eliminating *total coliform* and *E. coli*, resulting in log reductions of 4.06 and 4.11 for $AgNO_3$ compared to 3.85 and 3.92 for AgNP. Filters fabricated using copper nitrate ($Cu(NO_3)_2$), although marginally less efficient than AgNP filters, still attained notable log reductions of 3.33 and 3.54 for total coliform and E. coli, respectively. Furthermore, $AgNO_3$ filters discharged considerably lower quantities of silver into treated water, exhibiting average effluent silver concentrations of 2 μg/L, in contrast to 22 μg/L and 12 μg/L for AgNP filters sourced from Dertig and Mukondeni, respectively. This indicates that $AgNO_3$ filters are not only more secure for consumption but may also possess an extended operational lifespan, thereby enhancing their cost-effectiveness.

Economically, $AgNO_3$ offers distinct advantages over AgNPs. $AgNO_3$ costs around \$1 per gram of silver compared to \$2.71 per gram for AgNPs, allowing for either material cost reduction or more silver use to potentially enhance filter performance while maintaining the same price point. Filters produced with equal amounts of silver showed similar average log removal of E. coli, but those with five times more silver via silver nitrate performed better, albeit with increased material costs. A balance could be achieved by using 2.5 times more silver with silver nitrate, optimizing performance against cost. This does not consider additional labor cost savings from eliminating the painting step or health benefits from reduced exposure to genotoxic silver nanoparticles.

Virus inactivation experiments with silver and copper showed that most inactivation occurs within the first 8 hours. At 8 hours, 100 μg/L Ag achieved 0.42-log and 0.91-log inactivation for MS2 and adenovirus, respectively, indicating adenovirus is more susceptible to silver inactivation. This finding suggests adenovirus might be a better indicator for silver's antiviral performance. Similarly, 200 μg/L Cu achieved 0.39-log removal of MS2 and 1.26-log removal of adenovirus.

The use of silver is limited by its relatively low drinking water standard compared to copper. Using copper either as a substitute or alongside silver could extend the effective performance of ceramic water filters. Combining both metals could optimize filter performance for bacteria, viruses, and protozoa while maintaining safe metal concentrations for human consumption. Future research should explore the formation of a silver-copper alloy in ceramic, and evaluate their combined efficacy in real-world conditions (Nunnelley, 2018).

2.6.3 Paper-Based Water Treatment with Silver Nanoparticles

Paper, primarily composed of cellulose, stands as the most abundant natural polymer. Its qualities of being readily available, inexpensive, renewable, and biodegradable, combined with its excellent metal ion sorption capability, make it an attractive material for various applications; including water treatment Cellulose-based paper is similar to some fabrics in that it is a non-woven material. The incorporation of silver nanoparticles (AgNPs) into cellulose has been widely explored for use in products such as bandages, clothing, and food packaging, highlighting its potential for water treatment applications (Dankovich, 2014; Tang et al., 2009).

The most common method for synthesizing silver nanoparticles on cellulosic materials

involves in situ chemical reduction of metal ions, with sodium borohydride often used as the reducing agent (Tang et al., 2009). Dankovich (2012) described a process for creating AgNP paper by immersing sheets of blotting paper in silver nitrate solutions for 30 minutes. These sheets are then rinsed with ethanol to remove any unabsorbed silver nitrate. To form the nanoparticles, the paper is then placed in an aqueous $NaBH_4$ solution for 15 minutes. Finally, the paper is soaked in water for 60 minutes and dried in an oven at 60°C for 2 to 3 hours (Dankovich, 2012).

A more environmentally friendly method for in situ preparation of silver nanoparticles in paper has also been developed using microwave irradiation. In this method, blotting papers are submerged in aqueous solutions of silver nitrate and glucose before being heated in a microwave Microwave irradiation has also been developed as a more ecologically friendly technique for the in situ production of silver nanoparticles in paper or conventional oven. The glucose acts as the reducing agent, leading to smaller and more uniform nanoparticles with a faster reaction time. Transmission electron microscopy (TEM) images have shown that this method produces nanoparticles with an average size of 5.5 nm (Dankovich, 2012). This method is considered more benign than using sodium borohydride while remaining just as effective (Dankovich, 2014).

The antibacterial effectiveness of silver nanoparticles increases with smaller particle sizes, with those under 10 nm being the most effective. Studies have shown that AgNP paper is effective against *E. coli* bacteria, achieving log 7.6 (± 1.3) and log 3.4 (± 0.9) reductions of viable E. coli and *E. faecalis* bacteria, respectively. However, the reduction was only log 0.95 (± 0.5) for some bacteria likely because they remained on the fiber surfaces in the blotting paper. Graphite furnace atomic absorption measurements showed

that the silver content in the effluent was 0.0475 (± 0.0177) ppm, meeting the USEPA guideline for drinking water of less than 0.1 ppm (Dankovich & Gray, 2011).

Gottesman et al. (2010) proposed a technique for depositing silver nanoparticles onto paper through ultrasonication. In this method, the paper is immersed in a solution containing silver nitrate, ethanol, ethylene glycol, and water, followed by irradiation with a high-intensity ultrasonic horn. This approach minimizes silver loss from the coated surface, enhancing the material's durability. The treated papers were effective against both gram-negative and gram-positive bacteria, indicating their potential for water treatment and preventing cross-contamination (Gottesman et al., 2011).

Another approach to embedding silver nanoparticles in paper involves first immobilizing initiators on the paper's surface. A surface-initiated atom transfer radical polymerization technique is then used to graft poly (tert-butyl acrylate) brushes onto cellulose filters, which are subsequently hydrolyzed into poly (acrylic acid). Silver nitrate is then reduced to Ag^+ in situ using sodium borohydride as the reducing agent. These filters have shown good antibacterial activity against *E. coli* (Tang et al., 2009).

In summary, paper, primarily made of cellulose, has shown significant promise for water treatment applications due to its abundance, cost-effectiveness, renewability, and biodegradability. The incorporation of silver nanoparticles onto paper has been explored through various methods, each demonstrating potential for effective water treatment. The use of silver nanoparticles enhances the antibacterial properties of paper, making it a viable option for point-of-use water purification, as research continues, the optimization of these methods will likely lead to more efficient and environmentally friendly water treatment solutions utilizing paper-based materials (Nunnelley, 2018).

2.6.4 Development and Implementation of the Rural Remote Water Treatment System (RRWTS)

Researchers at DUT have formerly developed the Rural Remote Water Treatment System (RRWTS) to serve as an interim resolution for providing potable water to isolated rural areas. This mechanism implements a gravity-operated microfiltration strategy to address numerous obstacles encountered by established industrial membranes. The filtering component utilizes a domestically produced polyester woven fabric microfiltration (WFMF) membrane, known for its resilience and local availability within South Africa. The other accessories required for the system can also be procured locally, making it adaptable to rural environments.

The core of the RRWTS is the WFMF membrane, used to fabricate flat sheet modules. The membrane is robust, easy to handle, and cost-effective. The construction of the module involves fabricating a rectangular PVC support frame with a permeate outlet. Two sheets of the WFMF membrane are glued to either side of the frame; with a mesh spacer incorporated between the sheets to facilitate permeate flow to the outlet. The complete A4-sized module is then assembled and held together by threaded rods inserted through holes drilled in each module to form a membrane pack, increasing productivity. A permeate collection manifold connects the individual permeate outlets from each module to the permeate outlet tap. The membrane pack is immersed in a process feed tank containing the feed solution, and permeate is collected from the permeate outlet valve.

2.6.4.1 Advantages of the RRWTS

According to Pillay and Jacobs (2005), the RRWTS offers several notable advantages.

The membranes are highly durable and require minimal maintenance. The system functions solely on gravity, thereby eliminating the need for electricity or pumps. It is also straightforward to construct with materials that are readily available locally. Notably, the membranes are not only resistant to damage when dried but also benefit from drying as it helps in shedding fouling materials. Cleaning the membranes is simple, requiring only brushing and rinsing with clean water. Additionally, the system effectively removes turbidity, achieving results comparable to those of commercial microfiltration membranes (Pillay & Jacobs, 2005).

2.6.4.2 Operation of the RRWTS

The operation of the RRWTS is simple and user-friendly: raw water is poured into the process feed tank, then the permeate tap is opened to collect the filtered water in a clean container. Afterward, an appropriate amount of disinfectant is added to the collected water. Finally, the drain valve is opened to empty the unit and remove any settled matter.

2.6.4.3 Performance of the RRWTS

Previous research on the permeate quality produced by the RRWTS has confirmed its suitability for potable water treatment in rural areas. Studies carried out by Pillay et al. (2009) and Pillay and Kalu (2010) have comprehensively examined the performance of the RRWTS in terms of both the quality of the permeate and the rate of product flow. RRWTS unit, which was equipped with 15 modules of A4 size and filtered raw water with a turbidity of 60 NTU, generated 40 LMH of permeate on the initial day of operation. Following a month of continuous daily operation without any cleaning, the system yielded approximately 10 LMH. This suggests that the system could supply a household with 30 liters of water per day for one month without requiring cleaning,

depending on the turbidity of the feed water (Pillay, 2009; Pillay & Kalu, 2012).

2.6.4.4 Cleaning of the RRWTS

Studies by Pillay et al. (2009) showed that depending on the raw water quality, the RRWTS could operate effectively for a month before cleaning was required. After this period, the flow rate progressively decreased if not cleaned. The modules could be cleaned by simply brushing them with a bottle brush and rinsing with water. This proved sufficient to remove the fouling layer. This routine maintenance requires no skill and can be performed while the membranes are in the feed tank. Another cleaning option is to allow the module to dry, causing the fouling matter to fall off. No chemical cleaning is required.

2.6.4.5 Drawbacks of the RRWTS

While the RRWTS overcomes several limitations of existing membrane-based methods for providing potable water to remote rural communities, its permeate does not meet international water standards. Consequently, a separate disinfection step using chlorine or other disinfectants is necessary, relying on the user to add the disinfectant to the product water. This poses challenges as users may forget or ignore this step, resulting in the consumption of water that may contain pathogens. Additionally, incorrect dosing of the disinfectant can lead to the formation of disinfection by-products (DBPs) that are carcinogenic and can adversely affect health.

To mitigate these risks, incorporating disinfection capacity into the membrane itself is suggested. Advances in nanotechnology offer new strategies to address this issue. For example, silver, which has antimicrobial properties, can be incorporated into water filters for disinfection purposes. This approach can reduce the dependency on user-added

disinfectants and enhance the overall safety and effectiveness of the water treatment system.

2.6.4.6 Conclusion

The RRWTS represents a significant advancement in providing clean and safe water to remote rural areas. Its robust, locally produced components and gravity-driven operation make it an accessible and practical solution. However, the need for a separate disinfection step highlights the importance of ongoing innovation to improve the system's efficacy and ease of use, incorporating antimicrobial materials like silver into the membrane could provide a more integrated and reliable disinfection method, ensuring safer drinking water for rural communities (Achisa, 2014).

2.6.5 Evaluation of silver nanoparticles impregnated woven fabric microfiltration membranes for potable water treatment

Achisa et al (2014) studied the incorporation of silver nanoparticles (AgNPs) into woven fiber microfiltration (WFMF) membranes to enhance their disinfection efficacy for point-of-use (POU) water treatment systems, specifically targeting rural areas in developing nations. AgNPs were integrated into the WFMF membrane through the chemical reduction of silver nitrate ($AgNO_3$), and the resulting membranes were characterized using various spectroscopic and analytical methods. The primary objective was to assess the antibacterial efficacy of these AgNP-coated membranes against *E. coli* using both raw river water and synthetic feed water.

The antibacterial performance was evaluated using the disk diffusion method, which demonstrated clear zones of inhibition around the coated membranes, while uncoated

membranes showed no such effect. This indicates the strong antimicrobial activity of the AgNPs. The mechanism of disinfection was hypothesized to be the release of silver ions from the AgNPs, which interact with and deactivate *E. coli.*

In flow tests, the coated membranes achieved 100% removal of *E. coli* across a range of concentrations (2,500-77,000 CFU/100 ml), attributed to both size exclusion and the antimicrobial action of the AgNPs. The coated WFMF membranes maintained effective filtration and disinfection for 63 days, achieving log reduction values (LRVs) of four to five, which are acceptable for municipal water treatment. The treated water exhibited turbidity levels below 1 NTU, even for influent concentrations between 40-700 NTU.

One challenge addressed was the leaching of silver over time, a common issue with nanoparticle-enhanced filtration systems. The study found that silver leaching remained well below the maximum accepted value of 0.1 mg/L, ensuring the treated water was safe for consumption. Despite a decrease in silver concentration over time, the membranes retained 100% disinfection efficacy for up to 63 days.

The study also identified several limitations and areas for future research. The silver loading on the membrane was based on literature, and its optimization regarding disinfection efficacy and leaching rate was not investigated. Future studies should explore different nanosilver loadings and reactant ratios. The use of *E. coli* as an indicator organism provided a model for faecal contamination, but further research should include other microorganisms to validate the system's efficacy broadly.

Additionally, the study noted the need to investigate the antifouling properties of the AgNP-coated membranes, as increased hydrophilicity could potentially reduce fouling. Another area for improvement is addressing the loss of disinfection efficacy due to silver

elution, suggesting that future work should focus on extending the lifespan of the filters and controlling silver leaching. An unexpected decrease in flux over time, even with deionized water, was observed and requires further investigation to determine the cause, whether due to silver coating or membrane fouling.

Overall, this study demonstrates the potential of AgNP-coated WFMF membranes in providing safe drinking water in rural areas, highlighting their effective disinfection and filtration capabilities while also identifying key areas for further enhancement to ensure long-term sustainability and performance (Achisa, 2014).

2.2.6 Slow Sand Filtration (SSF): An Effective Point-of-Use Water Treatment Technology

Slow Sand Filtration (SSF) is a point-of-use (POU) technology recommended by the World Health Organization (WHO) for water purification. Unlike large-scale technologies such as Upflow Anaerobic Sludge Blanket (UASB), Sequencing Batch Reactor (SBR), Membrane Bioreactor (MBR), and the activated sludge process, SSF is cost-effective and utilizes readily available materials. SSF can treat various types of water, including wastewater, drinking water, and rainwater. The primary mechanism of SSF is the development of a biologically active layer known as the schmutzdecke, which plays a crucial role in the removal of bacteria and viruses. SSF can achieve up to 4-log removal efficiencies for bacteria and 43-log for viruses. It also demonstrates high removal efficiencies for organic matter $80 - 90\%$, turbidity $> 90\%$, and suspended solids $> 90\%$ (Verma et al., 2017).

The schmutzdecke layer is composed of algae, bacteria, diatoms, protozoans (such as *Paramecium sp.*) and metazoans. Despite its known composition, a more detailed

molecular-level study of the schmutzdecke's characteristics is needed. Research has shown that introducing aluminum hydroxide or iron oxide-coated sand into SSF offers advantages over uncoated sand. Factors such as hydrophobic interactions, hydration and Van der Waals forces, surface roughness, and macromolecular bridging are believed to contribute to bacterial adhesion. The Derjaguin-Landau and Verwey-Overbeek (DLVO) theory best explains bacterial sorption in aqueous systems.

In a study by Ahammed and Davra, placing iron-oxide coated sand within a 40-cm sand layer improved the removal of *E. coli* and *fecal coliform (FC)* bacteria by at least one log10 unit. However, further research is needed to determine whether placing the sand at different depths would yield similar results. Additionally, the fate of metal-coated sand in SSF and its potential human health impacts should be investigated (Ahammed & Davra, 2011).

Some researchers have focused on the chemistry of sand, exploring interactions between sand particles and colloids or theories explaining the removal mechanisms. The zeta potential of sand is also a critical factor influencing SSF performance. Studies have shown that the adsorption of bacteria, bacteriophages, and viruses increases with the zeta potential. Coated sand, which has a more negative zeta potential due to increased organic matter density, enhances the transport of oocysts. Therefore, studying the zeta potential, behavioral interactions and chemical reactions between sand grains and influent characteristics would provide valuable insights into particle-particle interactions and inform future applications (Verma et al., 2017).

Concluding Remarks

SSF is a sustainable option for wastewater treatment and highly beneficial for treating

drinking water in remote areas. The technology relies on a combination of biological and physicochemical mechanisms to purify water effectively. SSF can efficiently remove various pathogens, including *Giardia, Cryptosporidium, Salmonella, E. coli, total coliforms (TC), fecal coliforms (FC), fecal streptococci, bacteriophages, MS2 virus, Echovirus 12,* and *PRD-1* virus. Its versatility allows it to be used for treating drinking water, wastewater, and rainwater.

Further research is necessary to understand the detailed composition and characteristics of the schmutzdecke layer. Studies should focus on optimizing the use of coated sand and exploring the potential human health impacts of metal-coated sand in SSF. Additionally, examining the zeta potential and the interactions between sand grains and influent characteristics will aid in understanding the mechanisms of particle-particle interactions, which has future implications for improving SSF performance.

In summary, SSF is an effective and sustainable POU technology for water purification. Its ability to utilize readily available materials and treat various water types makes it an attractive option for remote and resource-limited areas. Continued research and optimization will enhance its efficacy and expand its applications, contributing to improved water quality and public health globally (Verma et al., 2017).

2.2.7 Novel solar based nitrogen doped titanium dioxide photocatalytic membrane for wastewater treatment

Nelson et al. (2024) have developed a solar-powered point-of-use water treatment system specifically designed to mitigate antimicrobial pollution, using *E. coli* as the primary microbial contaminant indicator. This innovative system leverages solar radiation to activate photocatalysis, employing a visible light-driven photocatalytic membrane. The

membrane was synthesized by immobilizing nitrogen-doped titanium dioxide (N-TiO$_2$) nanoparticles onto a polyvinylidene fluoride (PVDF) membrane, with the performance evaluated based on the removal efficiency of *E. coli*.

UV–Vis spectroscopy revealed a significant red-shifting of light absorbance from 400 nm (typical of titanium dioxide) to 440 nm, indicating a shift into the visible light region due to nitrogen doping. Photoluminescence (PL) spectra showed a low-intensity photoluminescence, suggesting that the nitrogen-doped titanium dioxide had improved charge separation and suppression of charge recombination. The incorporation of nitrogen was further confirmed by several analytical techniques, including a suppressed XRD 101 peak intensity, specific FTIR peaks and bending vibrations at 1420 cm^{-1}, 1170 cm^{-1}, 1220 cm^{-1}, and 1250 cm^{-1}, and an EDX nitrogen elemental composition of 1.26 wt %.

The process of nitrogen doping of titanium dioxide and its immobilization on PVDF membrane was successfully achieved using polyvinyl alcohol (PVA) immobilization and crosslinking with glutaraldehyde. This modification significantly reduced the water contact angle by 81.39 %, indicating enhanced hydrophilicity. FTIR characterization supported this observation, showing a vibrational stretch from 3000 to 3600 cm^{-1}, which confirmed increased hydrophilicity due to the immobilized N-TiO$_2$, PVA, and glutaraldehyde crosslinking. This hydrophilicity is a desirable characteristic, indicating improved antifouling properties of the synthesized membrane.

XRD analysis identified a suppressed PVDF α phase crystallinity in the N-TiO$_2$-PVDF membrane, attributable to the presence of N-TiO$_2$. SEM-EDX confirmed the successful immobilization of N-TiO$_2$ on the membrane surface, with a titanium composition of 0.42

wt % and nitrogen composition of 0.01 wt %.

The N-TiO$_2$-PVDF membrane demonstrated superior performance, achieving an *E. coli* log removal of 8.42 and a relative flux of 0.35 within 75 minutes, outperforming the TiO$_2$-PVDF membrane. This study highlights the potential of N-TiO$_2$-PVDF membranes to utilize natural sunlight for efficient wastewater treatment. Further research is recommended to evaluate the photodegradation capabilities of this system for removing organic pollutants, potentially broadening its application in water purification (Nelson et al., 2024).

2.7 National and international water standards

Water quality standards are vital for guaranteeing safe drinking water and safeguarding public health. These standards are established and regulated by numerous national and international organizations, each defining specific guidelines and criteria for permissible contaminant levels in water. The primary goal of these regulations is to eliminate or substantially reduce contaminants that pose health risks, thus ensuring the safety of drinking water. The guidelines and legislation provide a comprehensive framework for evaluating overall water quality, setting limits for potentially harmful contaminants. Consequently, these standards are fundamental for assessing the effectiveness of various water treatment and distribution systems in maintaining water quality (Slavik et al., 2020).

(a) International Standards

2.7.1 World Health Organization (WHO)

The World Health Organization (WHO) has established comprehensive Guidelines for Drinking Water Quality, which serve as a fundamental framework for many governments and authorities worldwide in creating their national water quality standards. These

guidelines, although not legally binding, offer essential principles and a preventive, risk-based strategy for managing water quality. (Vacs Renwick, 2013) describes the WHO guidelines as a "framework for safe drinking-water," aimed at ensuring the provision of safe drinking water through a detailed preventive approach (Organization, 2022).

The guidelines focus on three key areas: health-based targets, Water Safety Plans, and surveillance and control. Health-based targets define acceptable levels of disease burden, set reference values for water quality characteristics, and establish technology and performance goals. These targets provide a clear understanding of the acceptable risk levels and necessary standards for ensuring safe drinking water.

Water Safety Plans are central to the WHO guidelines, concentrating on the assessment, monitoring, and management of water systems. These plans aim to identify, prevent, and mitigate health risks related to water quality. Effective communication about these risks and the measures taken to address them is also a crucial part of Water Safety Plans.

Surveillance and control are crucial for ensuring that Water Safety Plans are properly implemented and health targets are met. This requires robust inspection protocols and appropriate surveillance techniques. The WHO guidelines recommend a semi-quantitative approach for surveillance, incorporating logical questions and a straightforward scoring system, which complements targeted sampling and subsequent water quality analysis (Slavik et al., 2020).

The WHO guidelines are often more detailed and comprehensive than the national standards in developing countries, making them frequently adopted as the primary, if not the sole, standard in these regions. Their practicality and thoroughness make them particularly valuable for developing countries, where resources and infrastructure for

water quality management may be limited (Saluja et al., 2022).

The WHO Guidelines for Drinking Water Quality offer a robust and practical framework for ensuring safe drinking water. By emphasizing health-based targets, Water Safety Plans, and effective surveillance and control, these guidelines help governments and authorities manage water quality risks and protect public health. Their detailed and practical nature makes them especially useful in developing countries, where they often serve as the main standard for water quality management (Slavik et al., 2020), Tables 2.7, 2.8 and 2.9   presents the WHO standard values for some physical, chemical, and microbial characteristics of the water. Comprehensive guidelines covering inorganic, organic, and microbial parameters can be found in the appendix A It is anticipated that the number of specified parameters will vary between countries and territories, reflecting the specific relevance and importance of these parameters to each region (Organization, 2021).

Table 0-5 Recommended Physical drinking water standards by WHO (Organization, 2021)

Sl. No.	Property of water	UNIT	Maximum value set	Minimum value set	Median value	WHO Guideline value
1	Color	TCU	50	0.5	15	None set
2	Turbidity	NTU	25	0.3	5.0	Not set
3	pH	-	9.7	8.0	8.5	Not set
4	Taste	DN	6.0	2.0	3 .0	Not set
6	Conductivity	μS/cm	2700	170	2500	None specified

The Guidelines for Drinking-water Quality (GDWQ) specify 43 microbial parameters, including bacterial, viral, protozoan, and helminth pathogens, and toxic cyanobacteria. Microbial water safety is verified through indicator organisms, with a guideline value (GV) for *Escherichia coli* (*E. coli*) or *thermotolerant coliforms*. A survey showed that countries and territories designated numerical standards for 24 microbial parameters, with the most common being *E. coli*, *total coliforms, enterococci*, and *Clostridium perfringens*. The typical standard value for these parameters, except heterotrophic bacteria, was zero or absent per specified volume. Additionally, many countries included directives ensuring that drinking water is free from any harmful microorganisms or parasites. These comprehensive guidelines and standards are critical for ensuring the microbiological safety of drinking water and protecting public health from waterborne diseases. Table 2.9 included six Type of micro-organism with their limitation in potable water according to WHO standard (Organization, 2021).

2.7.2 The International Organization for Standardization (ISO)

The International Organization for Standardization (ISO) is a non-governmental organization that oversees a vast network of national standards organizations, each representing a specific country. ISO functions on a not-for-profit basis, funding the advancement, upkeep, and establishment of novel standards by vending these standards in an impartial setting. The management of the organization is overseen by a Central Secretariat situated in Geneva, Switzerland, with its primary objective being the formulation of International Standards that function as pragmatic instruments and exemplary methodologies across diverse industries (Standardization, 2017).

Table 0-6 Quality requirements for potable water standards by WHO (Organization, 2021)

Sl. No.	Property of water	UNIT	Maximum value set	Minimum value set	Median value	WHO Guideline value
1	Total dissolved solids	mg/l	2500	200	1000	Not set
3	Aluminum, as Al^{+++}	mg/l	0.5	0.03	0.2	None set
4	Chloride, as Cl^-	mg/l	1200	20	250	None set
5	Total Iron as Fe	Mg/l	2	0.2	0.3	Not set
6	Sodium, as Na^+	mg/l	400	100	200	Not set
7	Sulphate SO_4	mg/l	800	50	250	Not set
8	Zinc, as Zn^{++}	mg/l	15	1	5	Not set
9	Magnesium, as Mg^{++}	mg/l	1000	10	100	None specified
10	Calcium, as Ca^{++}	mg/l	500	150	30	None specified

Table 0-7 Microbiological limits for potable water by WHO standard (Organization,

2021)

Sl. No.	Type of micro-organism	Maximum value set	Minimum value set	Median value	WHO Guideline value
1	*Clostridium perfringens* (Sulphite-reducing anaerobes)	0 per 100 ml	0 per 100 ml	0 per 100 ml	None specified
2	*Coliform bacteria* (Total)	150 per 100 ml	0 per 100 ml	0 per 100 ml	None specified
3	*Enterococci (Faecal streptococci)*	0 per 100 ml	0 per 100 ml	0 per 100 ml	None specified
4	*Escherichia coli* (Faecal coliforms, Thermotolerant coliforms)	0 per 100 ml	0	0	Must not be detectable in any 100ml sample
5	*Total heterotrophic bacteria* 22°C	10,000 CFU per ml	5 CFU per ml	100 CFU per ml	None specified
6	*Total heterotrophic bacteria* 37°C	500 CFU per ml	0 CFU per ml	100 CFU per ml	None specified

2.7.2.1 The Function of ISO in the Domain of Water Standards

Water, recognized as one of the most fundamental and invaluable resources globally, is indispensable for sustainable progress, renewable energy, agricultural production, and advancements in sanitation and healthcare. ISO standards hold a pivotal role in aligning technology and terminology, facilitating efficient collaboration among nations that share water resources. These standards encompass virtually every facet of water-related matters, ranging from water quality and governance to infrastructure and sanitation (Zhao et al., 2020).

2.7.2.2 The Recipients of Advantages from ISO Standards pertaining to Water

Enterprises: ISO standards aid organizations by furnishing mechanisms for quantifying and refining water utilization, presenting best practices for treating wastewater, and directing water utilities and irrigation methodologies in the sectors of industry, manufacturing, and construction.

Authorities: Policymakers can employ ISO standards to devise governmental strategies that tackle water-related dilemmas like the impacts of climate change and sanitation, thereby enabling them to fulfill domestic and international responsibilities concerning water management (Zhao et al., 2020).

2.7.2.3 Principal ISO Standards for Water

ISO has devised in excess of 1,200 standards associated with water, with numerous others undergoing development. Below are key domains addressed:

Water Quality: Formulated by ISO/TC 147, these nearly 300 standards envelop a wide array of topics from treatment agents to natural mineral waters. They encompass terminology, methods for water sampling, and advisories on the reporting and monitoring of impurities such as minerals and microorganisms.

Water Footprint: ISO 14046, crafted by ISO/TC 207/SC 5, stipulates prerequisites for gauging and disclosing water consumption, establishing an international standard for water usage.

Hydrometry: ISO/TC 113 has approximately 70 standards for quantifying water and sediment in unenclosed channels, bolstering precise water management and preservation efforts.

Agriculture and Irrigation: ISO/TC 23/SC 18 and ISO/TC 282 have introduced standards

for irrigation and reuse of wastewater in agriculture, fostering sustainability and effective water utilization.

Infrastructure: Standards from ISO/TC 30 for quantifying fluid flow aid in water preservation, especially through the ISO 4064 series intended for water meters.

Sludge Management: ISO/TC 275 offers standards for processing, reusing, and overseeing sludge from diverse water treatment frameworks.

Potable Water Distribution and Wastewater Systems: ISO/TC 224 furnishes directives for evaluating, enhancing, and governing drinking water and wastewater amenities via standards like ISO 24510, ISO 24511, and ISO 24512. Additionally, ISO 24518 and other forthcoming standards provide recommendations for crisis management in water utilities.

Piping and Valves: Standards devised by ISO/TC 138, ISO/TC 5/SC 2, and ISO/TC 153 elevate the dependability and efficiency of water supply networks through top-notch pipes, fittings, and valves.

The development and implementation of ISO standards involve technical committees (TCs) composed of experts from various sectors such as industry, non-governmental organizations, governments, and other relevant entities. These TCs are dedicated to specific subject areas, guaranteeing that the standards reflect a consensus on practical solutions and optimal approaches for sustainable water management. To sum up, the significance of ISO standards lies in their role in advancing secure, sustainable, and effective water management practices on a global scale. They establish a shared framework that benefits industries, regulators, and consumers, ensuring the efficient utilization and management of water resources (Standardization, 2017).

(b) National Standards (EAST AFRICAN STANDARD)

2.7.3 Kenya Bureau of Standards (KEBS)

The establishment of East African Standards has been driven by the necessity to standardize the quality requirements for products and services within the East African Community (EAC). The objective of this standardization is to mitigate trade impediments that emerge during the transaction of goods and services within the region. In order to facilitate this process, the EAC established the East African Standards Committee, which holds the responsibility for formulating and issuing these standards. This Committee comprises delegates from the National Standards Bodies of the Partner States, in addition to participants from the private sector and consumer associations. Proposed standards are circulated to relevant stakeholders via the National Standards Bodies, and their input is integrated through consultations before the standards are ultimately ratified, in accordance with the procedures of the Community. The East African Standard for Potable Water delineates the requirements for drinking water to guarantee its safety and appropriateness for human consumption. This standard establishes the permissible thresholds for various physical, chemical, and microbiological parameters that potable water must meet. It encompasses restrictions for pollutants such as toxic metals, microorganisms, and other deleterious substances, with the aim of safeguarding public health. Adherence to this standard ensures that potable water in East African nations remains consistently safe, pure, and dependable for all consumers (STANDARD, 2018)

Ensuring the provision of safe and high-quality drinking water is crucial for human health. It is imperative that drinking water possesses an acceptable appearance, taste, and odor to instill confidence in consumers, mitigate complaints, and deter the utilization of

potentially hazardous water sources. Water safety may be compromised by a variety of factors, encompassing environmental circumstances, the characteristics of the water source, human activities in proximity to the sources, and the methodologies employed for water collection, management, and purification. These variables have the potential to result in physical, chemical, and microbiological pollution, rendering the water unsuitable for human consumption. The primary health hazard linked to drinking water is infectious ailments induced by pathogenic microorganisms such as bacteria, viruses, and parasites (e.g., protozoa and helminths). The principal peril arises from the ingestion of water contaminated with excrement from humans and animals, although alternative origins and pathways of exposure may also be significant. While only a few chemical pollutants are recognized for causing detrimental health consequences due to prolonged exposure through drinking water, certain inorganic elements are indispensable for human nourishment.

Consumers depend on water suppliers to guarantee the caliber and safety of their drinking water, as they lack the capacity to assess this independently. Regulatory bodies play a pivotal role by instituting health-oriented objectives that water service providers must adhere to. This criterion establishes the fundamental criteria for the physical, chemical, and microbiological attributes influencing the safety and quality of drinking water. Adherence to these guidelines is anticipated to safeguard that drinking water persists as a safe and superior commodity for human consumption (EAS, 2014). Tables 2.10, 2.11, and 2.12 present the physical characteristics of potable water, the chemical characteristics that influence its quality, and the microbial limits that impact its safety, respectively. The chemical characteristics affecting potable water safety, including both inorganic and

organic contaminants, are detailed in the appendix B.

Table 0-8 Physical requirements for potable water (EAS, 2014)

Sl. No.	Characteristic	Treated potable water	Natural potable water	Method of test
I.	Color (TCU[a] max)	15	50	ISO 7887
II.	Turbidity (NTU max)	5	25	ISO 7027
III.	pH	6.5 - 8.5	5.5 - 9.5	ISO 10523
IV.	Taste	Not objectionable	Not objectionable	-
V.	Odour	Odourless	Odourless	-
VI.	Conductivity (μS/cm)max	1500	2500	ISO 7888
VII.	Suspended matter	Not detectable	Not detectable	ISO 11923

[a] True colour units (TCU) mean 15 hazen units after filtration.

Table 0-9 Quality requirements for potable water (EAS, 2014)

Sl. No.	Substance or characteristic	Treated potable Water (mg/L max.)	Natural potable water (mg/L max.)	Method of Test
1	Total dissolved solids	700	1500	ASTM D 5907
2	Total hardness, as $CaCO_3$,	300	600	ISO 6059
3	Aluminum, as Al^{+++},	0.2	0.2	ISO 12020
4	Chloride, as Cl^-	250	250	ISO 9297
5	Total Iron as Fe	0.3	0.3	ISO 6332
6	Sodium, as Na^+	200	200	ISO 9964-1
7	Sulphate SO_4	400	400	ISO 22743
8	Zinc, as Zn^{++}	5	5	ISO 8288
9	Magnesium, as Mg^{++}	100	100	ISO 7980
10	Calcium, as Ca^{++}	150	150	ISO 7980

Table 0-10 Microbiological limits for potable water (EAS, 2014)

Sl. No.	Type of micro-organism	Potable water	Method of test
1	Total viable counts at 22 ºC, in mL, max. [a)]	100	ISO 6222
	Total viable counts at 37 ºC, in mL, max. [a)]	50	
2	*Total Coliforms* [b)] in 100 mL	Absent	ISO 4832
3	*E. coli* [b)] in 100 mL	Absent	ISO 9308-1
4	*Staphylococcus aureus* in 100 mL	Absent	ISO 6888-1
5	Sulphite reducing anaerobes in100 mL	Absent	ISO 6461-2
6	*Pseudomonas aeruginosa fluorescence* in 100 mL	Absent	ISO 16266
7	*Streptococcus faecalis* in 100mL	Absent	ISO 7899-2
8	*Shigella* in 100 mL	Absent	ISO 21567
9	*Salmonella* in 100 mL	Absent	ISO 6785

[a] This parameter is for monitoring the system at source. Total time before analysis should be not more than 6 h at 4 ºC. Determination of total viable counts shall start within 12 h after collection of the potable water sample.

[b] During the bacteriological quality control for different types of water supply, refer to Annex A

(c) Synergy and Antifouling

Combining traditional water treatment techniques with Advanced Oxidation Processes (AOPs) and photocatalysis can greatly improve treatment effectiveness and tackle a wider variety of contaminants. Traditional methods such as filtration and chemical disinfection are efficient at removing particulates and pathogens but are less effective against new contaminants like pharmaceuticals. AOPs work by generating reactive radicals that break down resistant organic pollutants, while photocatalysis, which uses light-activated catalysts such as titanium dioxide, creates reactive species to degrade pollutants. This combined approach ensures thorough contaminant removal, enhances efficiency by minimizing the need for chemical disinfectants, and provides antifouling properties to surfaces, thus maintaining the efficiency of filtration systems. This integrated strategy offers a robust solution to both current and emerging water quality issues (Garrido-Cardenas et al., 2020; Khader et al., 2024).

2.8 Synergy in Photocatalysis for Water Treatment

In water treatment, the concept of synergy in photocatalysis involves combining various materials or processes to achieve an enhanced effect, resulting in a more significant outcome than the sum of their individual contributions. This synergistic approach can greatly boost the efficiency and effectiveness of water purification systems, particularly in breaking down stubborn organic pollutants and disinfecting water (J. Feng et al., 2022).

2.8.1 Material Synergy

Combining various semiconductor materials like titanium dioxide (TiO_2), zinc oxide

(ZnO), and tungsten oxide (WO$_3$) creates composite photocatalysts with superior properties. For instance, TiO$_2$/ZnO composites leverage ZnO's wide bandgap and TiO$_2$'s stability and strong oxidizing power, resulting in enhanced light absorption and charge separation for more efficient photocatalytic activity. Additionally, doping photocatalysts with metal ions such as silver (Ag), iron (Fe), or platinum (Pt), or non-metals like nitrogen (N) or carbon (C), can alter their electronic properties. This doping extends light absorption into the visible spectrum and improves charge carrier separation, thus increasing photocatalytic efficiency under natural sunlight, which is vital for sustainable water treatment. Furthermore, integrating graphene-based materials with photocatalysts further boosts their effectiveness. Graphene's exceptional conductivity facilitates rapid electron transfer, reducing electron-hole pair recombination and enhancing overall photocatalytic performance. This synergy significantly improves the degradation of complex organic pollutants and pathogens, making these advanced materials highly effective for water purification applications (J. Feng et al., 2022).

2.8.2 Process Synergy

Integrating photocatalysis with other advanced oxidation processes (AOPs), such as Fenton reactions or ozonation, creates a synergistic effect that enhances contaminant degradation. For instance, combining photocatalysis with Fenton reactions increases the concentration of reactive oxygen species (ROS), like hydroxyl radicals, leading to more efficient pollutant breakdown, similarly, coupling photocatalysis with ozonation boosts ROS generation, further improving the decomposition of persistent contaminants. Additionally, developing hybrid water treatment systems that merge photocatalysis with conventional methods, such as filtration or adsorption, can optimize overall treatment

efficiency. For example, a photocatalytic membrane system can filter particulate matter while simultaneously degrading dissolved organic pollutants. This synergy between physical separation and chemical degradation offers a comprehensive solution for water purification, enhancing both the removal of particles and the breakdown of complex contaminants (Garrido-Cardenas et al., 2020; Khader et al., 2024).

2.8.3 Operational Synergy

Optimizing the design of photocatalytic reactors to enhance light distribution and catalyst exposure significantly improves the synergy between light and photocatalysts. By incorporating reflective surfaces, light guides, or multi-layer catalyst coatings, these reactors can ensure uniform light penetration and maximize the interaction between light and the photocatalyst, thereby boosting overall photocatalytic efficiency. Additionally, harnessing solar energy for photocatalysis offers a sustainable and cost-effective water treatment solution. The synergy between solar light and advanced photocatalysts, especially those engineered to absorb visible light, provides an efficient and environmentally friendly approach to water purification. This is particularly beneficial for remote or off-grid areas, where conventional energy sources may be limited, making solar-utilized photocatalysis a viable and practical option for clean water access.

In conclusion, the synergy in photocatalysis for water treatment involves the strategic combination of materials, processes, and operational techniques to enhance the overall efficiency and effectiveness of water purification systems. By leveraging these synergistic effects, it is possible to develop advanced water treatment technologies that can effectively address the growing challenges of water scarcity and pollution, providing safe and clean water for communities worldwide (Behroozi & Xu, 2023).

J. Feng et al. (2022) reported the synthesis of ultrathin $Cu_2V_2O_7/Cu_3V_2O8/g$-C_3N_4 (CVC) heterojunctions via reheating, enhancing adsorption and photocatalysis for dye and antibiotic removal. The thermal etching process increased the CVCs' surface area, while the heterojunctions improved light absorption and charge carrier separation. CVC-2 achieved removal efficiencies of 96.2 % for methylene blue, 97.3 % for rhodamine B, 83.0 % for ciprofloxacin, 86.0 % for tetracycline, and 80.5 % for oxytetracycline. The degradation followed pseudo-first-order kinetics, with significantly higher rate constants than pristine CN. The study provided a reliable reference for using synergistic adsorption and photocatalysis in environmental sewage treatment (J. Feng et al., 2022).

Wei and coworkers (2022) examined the flexible optimization of disinfection doses across three major technologies, confirmed through pilot tests. This approach determined the load distribution for various disinfection units while maintaining standards for color, residual chlorine, and microbial indicators. Using the lowest doses of ozone and chlorine minimized costs and DBP formation. Ozone treatment enhanced the effectiveness of subsequent chlorine disinfection, and the ozone-UV-chlorine process mitigated tailing-off, achieving higher log reductions. Pilot-scale tests showcased the synergistic effects of combining ozone, UV, and chlorine disinfection, indicating significant cost-effectiveness and potential applications in reclaimed water treatment plants (Wei et al., 2022).

Shi et al. (2021), demonstrated that ozone pretreatment in a combined disinfection process effectively eliminates UV-absorbing compounds and chlorine-consuming organics, improving UV irradiation efficiency and reducing the chlorine dosage needed, thereby minimizing DBP production. The combined method achieved a 7 - log reduction in *E. coli* with 3 mg/L ozone, 5 mJ/cm²UV, and 2.5 mg/L chlorine. The sequential ozone-

UV-chlorine system is expected to broaden pathogen inactivation, decrease DBP formation, lower operating costs, enhance operational flexibility, and improve disinfection reliability. These results can help local water industries optimize disinfection strategies and offer valuable insights for safe, efficient water quality control and potential secondary effluent reuse (Shi et al., 2021).

Irani & Amoli-Diva (2020) developed an efficient filtration membrane grafted with Ag-doped $ZnO@Fe_3O_4$ NPs/MWCNTs photocatalyst for removing amoxicillin (AMOX) from pharmaceutical wastewater. The evaluation of the synergistic effect of photocatalysis and filtration showed that the PC-PAA-PA membrane had superior AMOX removal potential and antifouling capability due to its photocatalytic performance. The new membrane demonstrated high permeates flux, excellent photodegradation ability, and low membrane fouling. Triplicate fouling tests indicated the photocatalyst's stability on the membrane surface during operation. These remarkable performances suggest the potential expansion of cost-effective water purification reactors to produce clean water in an energy-efficient manner (Irani & Amoli-Diva, 2020).

Mecha et al. (2017), showcased the combined photocatalytic ozonation process's synergistic effects on disinfecting municipal wastewater. Complete inactivation of all target pathogenic bacteria was achieved due to the positive interaction between photocatalysis and ozonation, resulting in SI values as high as 1.86. This synergy significantly reduced the necessary contact time for disinfection by 50-75% compared to using photocatalysis or ozonation alone. No bacterial regrowth was observed after 24 and 48 hours in the dark, indicating irreversible bacterial cell damage. Although real wastewater required longer contact times than synthetic water, complete inactivation was

still attained. The effectiveness of solar photocatalytic ozonation is expected to further both fundamental research and practical applications of using sunlight for wastewater treatment (Mecha et al., 2017).

Jimenez-Relinque et al. (2022) synthesized S-TiO_2 composites from metallurgical waste via simple precipitation–calcination routes, using titanium isopropoxide precursor (M1) and commercial TiO_2 nanoparticles (M2). While bare TiO_2 samples showed the highest absolute photocatalytic activity, composites with 15–25% TiO_2 content achieved nearly the same efficiency per gram as pure TiO_2. Remarkably, composites like 15M1 and 25M1 outperformed bare TiO_2 in adsorption–photocatalysis, owing to TiO_2 integration into the S crystalline structure. This synergy allows S to act as an efficient adsorbent trap, facilitating the transfer of pollutants to the TiO_2 surface for rapid photodegradation. Optimal TiO_2 loading enhances UV absorption and photocatalytic oxidation. This study illustrates the dual benefits of TiO_2 and steel slag composites in dye wastewater treatment, offering innovative solutions for managing metallurgical waste and water pollution (Jimenez-Relinque et al., 2022).

The integration of solar energy with advanced nanomaterial-based smart systems for water purification is in its nascent stages. More targeted and specific research is crucial to strategically address the potable water needs of millions, while preserving natural water resources for all living beings and future generations on Earth (Verma et al., 2019).

2.9 Fouling, cleaning and membranes modification

Membranes have found use in the water industry as physical barriers to certain size ranges of water pollutants. They function as filters or selective sieves, filtering out particles larger than the membrane pore size while permitting smaller contaminants and water molecules to pass through. Membrane fouling occurs when suspended or dissolved

materials deposit irreversibly on the membrane's exterior surface or holes, reducing the membrane's overall function. Once the membrane filtration process has been fouled, sophisticated and often costly cleaning operations such as forward and reverse flushing, backwashing, air scouring, and back permeation must be conducted. Modification of membrane properties with nanoparticles is one such breakthrough, which can be used to fine-tune performance for specific pollutant types or increase fouling resistance (Kuvarega & Mamba, 2016).

Many low-pressure membrane-based separation techniques, including UF and MF, experience internal fouling as a result of adsorption and pore clogging. However, surface fouling occurs on semi-permeable membranes that are comparatively denser and more compact, as those utilized in NF and RO (AlSawaftah et al., 2021). Natural organic matters (NOM) are one of the most dangerous foulants to low-pressure membranes. While other researchers have concentrated on studying related foulants like colloidal organics, humic substances (HS), biopolymers (BP), polysaccharides (PS), proteins (PN), etc., others have concentrated on the molecular weight (MW) distribution and the hydrophobicity/hydrophilicity of the NOM impact on membrane fouling (Liu et al., 2016; Touati & Tadeo, 2017).

According to the strength of the particles' attachment to the membrane surface, fouling can be categorized as reversible or irreversible. The reversible fouling can either be backwashable or not, as shown in figure 2-8.
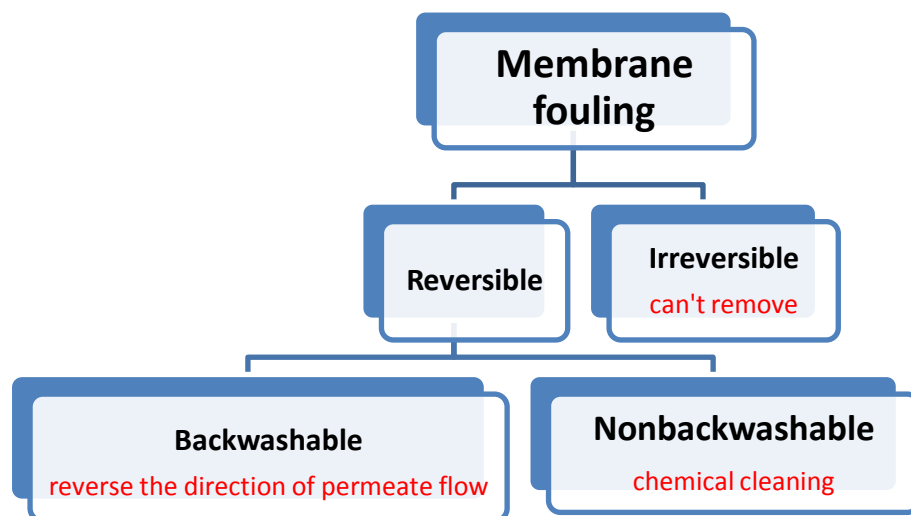
Figure 0-8 Membrane fouling classification

2.9.1 Factors Affecting Fouling
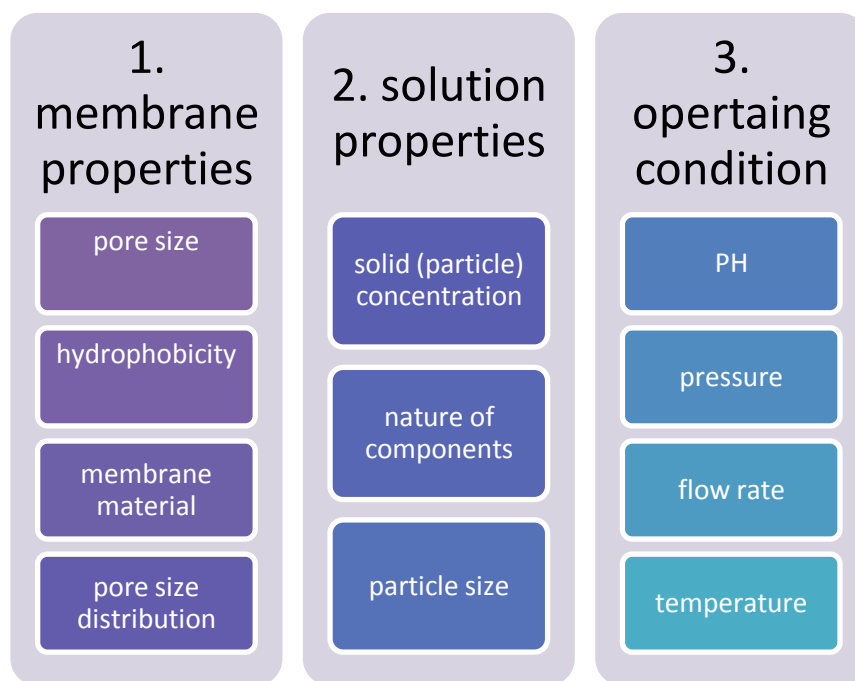
Figure 0-9 Factors affecting fouling

Membrane modification is important for improving membrane performance and reducing

membrane fouling, which is a major issue in all membrane processes (Chabalala et al., 2021). According to the literature, there are three ways to reduce fouling: It has been demonstrated that adding polar functional groups, such as hydroxyl and carbonyl groups, decreases membrane fouling and lengthens membrane life, chemical group's hydroxyl and carbonyl are added to the membrane surface through pre-adsorption of citric acid and sodium bisulfate, nanomaterials like graphene oxides, carbon nanotubes, Titanium Oxide and metal nanoparticles are incorporated into the polymer's structural backbone (Msomi, 2015). They also found that TiO_2 deposition reduced fouling more effectively than blended TiO_2 due to the larger number of particles on the membrane's surface. TiO_2-coated membranes were discovered to filter whey and have high photocatalytic and hydrophilic capabilities in previous studies. They also discovered that increasing UV irradiation time and coating material can help enhance flux until a stable condition is reached. The addition of more photocatalyst results in membrane obstruction and, as a result, a reduction in flux. In the case of many types of wastewater, including as dairy, industrial, and agricultural wastewaters, as well as disinfection, the use of TiO_2- modified membranes offers multiple advantages, including the ability to obtain higher fluxes and superior self-cleaning capabilities. In recent years, there has been a lot of interest in the possibility of using it to change membranes for efficient oily wastewater treatment (Nascimben Santos et al., 2020).

In general nanoparticles are frequently used in filtration membrane materials to reduce biofouling and extend the life of the membrane. Nanoparticles incorporated into the membrane matrix aid to overcome the separation and leaching restrictions of nanoparticles into aqueous solutions. Through photodegradation, nanoparticles,

particularly photocatalytic nanoparticles, have the ability to eliminate the creation of hazardous condensates, which is another major concern in membrane filtering (Chabalala et al., 2021).

2.9.2 Membranes cleaning

Membrane cleaning is a vital maintenance activity crucial for maintaining the effectiveness and durability of membrane-based filtration systems. Membrane fouling, which involves the buildup of undesirable substances on the membrane surface or within its pores, greatly hampers system performance by decreasing permeate flux and raising transmembrane pressure. Proper cleaning restores the membrane's functionality by eliminating these fouling agents, thus improving operational efficiency. The selection of a cleaning method depends on various factors, including membrane configuration, membrane type, chemical resistance, and the type of fouling matter. The main membrane cleaning techniques encompass hydraulic, mechanical, chemical, electrical, and biological methods, each with distinct applications and levels of effectiveness (Terán Hilares et al., 2022).

2.9.2.1 Chemical Cleaning Methods

Chemical cleaning methods are versatile and effective for addressing a wide range of fouling types, with specific chemicals targeting different contaminants. Acid cleaning, utilizing acidic solutions like citric acid or hydrochloric acid, is effective in dissolving inorganic scales and metal oxides, particularly in RO and NF membranes prone to scaling. However, it must be managed carefully to prevent membrane damage due to the corrosive nature of acids. Alkaline cleaning employs solutions such as sodium hydroxide to saponify organic foulants and hydrolyze proteins, making it common for UF and MF

membranes fouled with organic matter and biofilms, although it may not address inorganic scales. Oxidative cleaning uses oxidizing agents like hydrogen peroxide or chlorine to break down organic fouling and are highly effective for biofouling in UF and MF membranes, though it requires careful handling to avoid damaging sensitive RO membranes (Gul et al., 2021).

2.9.2.2 Electrical Cleaning Methods

Electrical cleaning methods, such as electrochemical cleaning, involve applying an electric field across a membrane, which causes charged particles or molecules to migrate towards the oppositely charged electrode, thereby effectively separating them from the membrane surface. This approach is particularly effective for membranes used in electrodialysis and other electrically driven processes, helping to reduce biofouling and scaling. However, it requires membranes specifically designed to withstand the electric field, offering a novel and targeted cleaning solution for certain applications (Achisa, 2014).

2.9.2.3 Biological Cleaning Methods

Biological cleaning methods, which offer targeted cleaning with minimal impact on membrane materials, are still under development and may be slower and more expensive than chemical methods. Enzymatic cleaning utilizes specific enzymes to degrade organic foulants like proteins and polysaccharides, making it suitable for all membrane types and particularly effective against biofouling. This method provides targeted cleaning while maintaining membrane integrity but is often slower and more costly. Bioaugmentation, on the other hand, involves adding beneficial microorganisms to degrade biofouling agents and is primarily considered for UF and MF systems. Although promising for

biofouling control, it requires further research for practical implementation (Terán Hilares et al., 2022).

2.9.2.4 Combined Cleaning Methods

Combined cleaning methods leverage the strengths of multiple techniques to provide comprehensive fouling control, ensuring optimal membrane function and longevity. Physical-chemical cleaning, which combines physical methods like backwashing with chemical cleaning agents, is widely used across all membrane types to address complex fouling scenarios, effectively increasing cleaning efficiency and extending membrane life by tackling both organic and inorganic foulants. Photocatalytic cleaning utilizes photocatalytic nanoparticles integrated into membranes to enhance cleaning through oxidative reactions triggered by light exposure. This advanced technique is effective for UF, NF, and RO membranes, breaking down organic pollutants, reducing biofouling, and increasing the potential for membrane reuse (Yu et al., 2024).

Membrane cleaning methods vary significantly based on the type of membrane and the nature of the fouling. Selecting the appropriate cleaning technique is critical for maintaining membrane performance and extending its operational life. Physical methods are generally preferred for particulate fouling, while chemical methods are more effective against organic and inorganic scales. Biological methods offer targeted cleaning with minimal impact on membrane materials, although they are still under development. Combining different cleaning techniques can provide comprehensive fouling control, ensuring optimal membrane function and longevity (M. A. Ahmed et al., 2023).

2.10 Summary of Findings and Gaps from Literature

Although the synergy and combination of advanced oxidation process with traditional

method like photocatalytic membranes have shown remarkable performance in the treatment of water, there are several challenges that need further research to be resolved, such as:

Transitioning from laboratory-scale experiments to pilot-scale and eventually large-scale implementation is essential for the widespread adoption of advanced water treatment technologies. Pilot-scale testing serves as a bridge between controlled laboratory settings and real-world applications, helping to fine-tune design parameters and operational procedures. The ultimate aim is large-scale deployment in community-scale systems, which would extend benefits to more people and simplify operations, maintenance, and management. This approach takes advantage of economies of scale to lower costs and ensure consistent water quality. Centralized operations allow trained personnel to use standardized practices, improving reliability. This progression turns promising laboratory discoveries into practical solutions, addressing global water issues and providing safe, clean water for communities around the world.

Recent research has focused on the effects of various metal or metal oxide nanoparticles incorporated into titanium dioxide to optimize photocatalytic performance. Investigations have been conducted to determine the ideal ratios of these nanoparticles and the optimal amount of photocatalytic material required. The simultaneous incorporation of multiple metals or metal oxides has also been explored to further enhance photocatalytic properties. Studies indicate that such incorporations can lead to improved degradation of pollutants and more efficient purification of water and air. However, a comprehensive understanding of the interactions between different nanoparticles and titanium dioxide is still needed to develop advanced photocatalytic systems with superior efficiency. These

advancements are essential for creating more effective and sustainable environmental technologies. Addressing these gaps could significantly contribute to global efforts in pollution control and resource management, leading to cleaner and healthier ecosystems.

Existing research underscores the necessity of enhancing solar-powered photocatalytic processes to decrease dependency on electricity and reduce overall treatment costs. Solar energy presents a sustainable and economical alternative, but its application in photocatalytic systems is not yet fully explored. Studies indicate that utilizing solar energy could greatly improve the efficiency and scalability of these treatments, though additional research is needed to achieve this potential fully.

Furthermore, ensuring continuous operation of solar-powered systems during low sunlight periods, such as at night or on cloudy days, poses further challenges. Implementing batteries or alternative energy storage solutions is crucial to maintain operational efficacy. Optimization of these energy storage systems and their integration with photocatalytic processes is still in its early stages and requires significant advancement.

The findings underscored the importance of advancing solar photocatalysis technology alongside the innovation of reliable energy storage solutions. Closing these gaps will enable the development of more dependable and cost-effective photocatalytic systems capable of functioning effectively in various environmental conditions. This holistic approach has the potential to significantly advance pollution control and resource management efforts, promoting cleaner and healthier environments.

Ensuring the stability and longevity of photocatalytic materials is essential for maintaining consistent and durable performance. Further research is needed to enhance

material stability by exploring alternative solutions, refining synthesis methods, and applying protective coatings.

The synergy between filtration and photocatalysis, achieved by impregnating photocatalytic nanoparticles into membranes, has been shown to significantly increase the membranes' efficiency in degrading organic pollutants and enhancing their antimicrobial properties. Research indicates that this integration not only improves pollutant removal but also boosts the membranes' resistance to fouling, thereby extending their reuse potential. The hybrid approach leverages the strengths of both filtration and photocatalysis, leading to a more robust and effective water treatment solution.

However, several gaps remain in the literature. Firstly, the optimal types and ratios of photocatalytic nanoparticles to be used within membranes have yet to be conclusively determined. Further studies are necessary to understand how different nanoparticles interact with various membrane materials and pollutants. Additionally, long-term performance and stability of these hybrid membranes under real-world conditions are not thoroughly investigated, requiring comprehensive field studies to validate laboratory findings.

Moreover, the cost-effectiveness of producing and maintaining these advanced membranes needs to be assessed to ensure practical applicability on a large scale. There is also a need for standardized methods to evaluate the enhanced properties of these membranes, ensuring consistent and reliable performance metrics across different studies. Addressing these gaps will be crucial for advancing the development and implementation of these innovative water treatment technologies.

CHAPTER THREE

MATERIALS AND METHODS

3.1 Materials, reagents and equipment

3.1.1 Materials and reagents

Titanium (IV) tetraisopropoxide 97% (TTIP) (Sigma Aldrich), titanium dioxide (TiO_2) powder and iron (III) nitrate nonahydrate (Fe (NO_3)$_3$·9H_2O) (DLA company), Zinc acetate dihydrate (Zn(CH_3COO)$_2$.2H_2O, 99.5%) (DLA company), isopropanol ((CH_3)$_2$CHOH, (Gelsup company), absolute ethanol (C_2H_5OH) (Eldo lab), sodium hydroxide (NaOH) (Gelsup company), acetone extra pure (CH_3)$_2$CO (LOBA CHEMIE PVT. LTD.), reactive navy blue HER dyes for textile industry (Rift Valley Textiles, Rivatex Ltd). Deionized water, sourced from Eldo Chemical Reagent Company, was employed for all synthesis and treatment procedures. Oxytetracycline was obtained from DLA Company. *Escherichia coli* (*E. coli*) strain ATCC 25922 from DLA Company, Macconkey and nutrient agar from DLA Company. Polyester fabric was supplied by Rivatex Ltd. With physical specification: composition: 65% polyester, 35% cotton, areal density: 0.048 g/m², thickness: 0.9 mm, yarn density: 10 picks/cm (weft), 13 ends/cm (warp).

 All the chemical reagents employed in this study were of analytical grade and were used without additional purification.

3.1.2 Equipment

The equipment utilized in the laboratories at Moi University included: Furnace (CARBOLITE GERO ELF 11/14B 230 V   2600 W 12.5 AMPS 1 PH + N), Oven (mrc), pH meter (HI96107 PH Range 0 ~ 14 pH made in Italy, QC M – 6 - 28), Magmatic stirrer (STONE, STAFFORDS, SS10, R000100860, 230 volt, 50/60 HZ, 50 W, fuses

T1A),Magmatic bar, Hot plate (CAUTION HOT TOP, PRO SCIENTEFIC HPS-7, STIR 60 – 1600 rpm), Digital Ultrasonic Cleaner (LMUC SERIES, RICO SCIENTIFIC INDUSTRIES, WZ – 91B, Tatarpur, Tagore Garden, New Delhi – 27, Model USBT-6 LITERS, 150 W), General purpose UV/Vis Spectrophotometer (BECKMAN COULTER, DU 720), weighing scale (model HZT-A200), Thermometer, Rotary evaporator (model LRE – 201, 220 V/50 HZ, 1.5 KW), Thermo scientific incubator (REF 51028130, SN 42565850, IP 20, 230 V, 50/60 HZ, 1.3 A, 300 W), Tuttnauer Autoclave – steam sterilizer (Model 2540 M, max pr. 2.8 bar, test pr. 4.1 bar, CONT 23 L, 230 V, 6 A, 50 HZ), Paqualab photometer (model ELE INTERNATIONAL), Data- logging solar power meter (PCE – SPM 1, TAIWAN), VWR international shaker & mixer (230 V, 50 HZ, 51 W, 100 – 2500 r.p.m, made in Germany).

3.2 Synthesis and characterization of metal-ion-doped TiO_2 photo-catalysts and impregnation to polyester based membranes

3.2.1 Synthesis of α-Fe_2O_3

The method described by Bouziani et al. (2020) was used with some modifications. Initially, pure α-Fe_2O_3 powder was synthesized via a two-step process. First, Iron III nitrate nonahydrate was dehydrated at 120°C for 2 hours to obtain the base material. Then, this dehydrated substance underwent controlled heat treatment at 350°C, resulting in α-Fe_2O_3 powders. To achieve a fine powder form, the resulting agglomerates were carefully ground using a mortar and pestle, ultimately producing the desired α-Fe_2O_3 powder (Bouziani et al., 2020).

3.2.2 Synthesis of α-Fe$_2$O$_3$-TiO$_2$ (TFT) from synthesized α-Fe$_2$O$_3$ and titanium precursor

The Ultrasonic-assisted sol-gel technique (Abdel-Wahab et al., 2017b) was employed with slight modification. The process commenced by dispersing 0.2 grams (equivalent to 1.25 millimoles) of α-Fe$_2$O$_3$ (prepared in section 3.2.1) in 25 milliliters of isopropanol through 15 minutes of ultrasonic irradiation. Subsequently, this suspension was subjected to mechanical stirring, while TTIP, dissolved in 15 milliliters of isopropanol, was gradually added. After an hour of stirring, a specific quantity of water was introduced, and stirring was continued for an additional 2 hours to guarantee complete hydrolysis of TTIP. To further enhance the reaction, the mixture underwent 30 minutes of ultrasonic treatment in an ultrasonic cleaner. The isopropanol solvent was removed through evaporation under reduced pressure at 50° C employing a rotary evaporator, yielding a residual substance that was subsequently dried at 80° C for duration of 12 hours and ultimately exposed to calcination at 350° C for a period of 2 hours.

3.2.3 Synthesis of α-Fe$_2$O$_3$-TiO$_2$ (TFC) from Fe (NO$_3$)$_3$ .9H$_2$O and commercial TiO$_2$

In accordance with the methodology outlined by (Ahmadi et al., 2020), an initial solution was formulated through the dissolution of iron (III) nitrate nonahydrate (Fe(NO$_3$)$_3$•9H$_2$O) in ethanol, resulting in a 0.6M concentration of iron nitrate. Subsequently, titanium dioxide (TiO$_2$) powder was introduced into the solution under magnetic stirring, while ensuring the beaker remained covered to prevent ethanol evaporation. The solution underwent stirring for duration of 30 minutes, followed by sonication at frequencies of 35 kHz for 15 minutes, and an additional 15 minutes at 130 kHz. Upon removal of the cover,

ethanol was allowed to evaporate overnight on a hot plate maintained at 50°C. The desiccated sample was then subjected to calcination at 300°C for 10 minutes, crushed into a powdered form, and further heated for 6 hours at 300°C in a furnace.

3.2.4 Synthesis of TiO_2

The TiO_2 powder was prepared through sol-gel method as reported in the literature (Bouziani et al., 2020), 55 ml of ethanol, 135 ml of deionized (DI) water, and 0.2 ml of acetic acid were mixed. Subsequently, 18.5 ml of tetraisopropoxide was gradually added to the mixture, which was then stirred with a magnetic stirrer for 48 hours. The resulting precipitate was collected, filtered, rinsed with DI water, and dried at 80° C for 24 hours. The material was then calcined at 500° C for 2 hours, and the resulting agglomerate was gently ground using a mortar and pestle to obtain TiO_2 powder.

3.2.5 Synthesis of ZnO nanopowder

The approach outlined by Wang and colleagues (2013) was implemented with minor adjustments. A blend containing 6.23 grams of zinc acetate, 6 ml of deionized water, and 80 ml of absolute ethanol was meticulously prepared and exposed to magnetic agitation for duration of 30 minutes. Subsequently, the solution obtained was allowed to mature at room temperature until it transformed into a solidified gel. This gel was then desiccated and subjected to calcination at temperatures within the range of 450° C to 600° C for various time frames of 1, 1.5, 2, 2.5, and 3 hours. The resultant conglomerate was delicately pulverized utilizing a mortar and pestle. This series of steps ultimately led to the production of ZnO nanopowder (Wang et al., 2013).

3.2.6 Doping of synthesized and commercial TiO_2 by ZnO

The commercial and synthesized TiO_2 were doped with ZnO using the sol gel method

(Rheima et al., 2020). This was achieved by mixing 25 ml of 0.01 mole TiO_2 nano powder with 25 ml of zinc acetate dehydrate, under magnetic stirring at 80° C for 6 hours. The pH of the mixture was carefully adjusted to 11.5 upon cooling to room temperature by the gradual addition of 10 ml (drop by drop) of 1 M sodium hydroxide solution, with further stirring at 60° C for 60 minutes. The resulting gel product was subsequently extracted and washed using de-ionized water, following by dehydration at 105° C and a final calcination step at 550° C at 3 hours. The agglomerate was gently ground using a mortar and pestle to obtain TiO_2/ZnO nanophotocatalysts (named by TZT for the photocatalysis prepared from TiO_2 synthesized from precursor at the lab and TZC for the photocatalysts synthesized from commercial TiO_2).

3.2.7 Characterization of photocatalysts

The surface morphology of the photocatalysts was assessed through the utilization of Scanning Electron Microscopy (SEM) provided by Zeiss, specifically the Ultra55 model. Examination of the chemical composition was performed using Fourier Transform-Infrared Spectroscopy (FTIR) from the Frontier series by Perkinelmer, with samples analyzed in Attenuated Total Reflectance (ATR) mode across the spectral range of 4000-650cm-1. Elucidation of the structure of the photocatalysts was achieved through X-ray Diffraction utilizing the Smartlab X-Ray Diffractometer, which is capable of conducting Powder X-ray Diffraction (PXRD), High-Resolution X-ray Diffraction (HRXRD), and X-ray Reflectometry (XRR).

The average crystallite sizes of the photocatalysts were determined using the Debye–Scherrer equation 3.1. In this equation, d represents the crystallite size, λ stands for the wavelength of the incident X-ray, β is the full width at half maximum (FWHM) of the

diffraction formula, K is the Scherrer constant (a typical value is 0.94), and θ represents the scattering angle.

The Debye–Scherrer equation is given by:

$$d = \frac{K\lambda}{\beta cos\theta} \qquad 3.1$$

Furthermore, Energy-Dispersive X-ray Analysis (EDX) was utilized for chemical analysis. Optical properties were investigated using a Shimadzu UV-3600 UV–visible spectrophotometer, with baseline correction performed using a calibrated reference sample of barium sulfate to ensure accuracy. The determination of band gap (Eg) values for the photocatalysts was accomplished through the application of Equation (3.2) (Jasso-Salcedo et al., 2014; Achisa C Mecha et al., 2016).

$$E_g = \frac{1240}{\lambda} \qquad 0.2$$

Where: λ is the cut-off wavelength (nm) of the UV–vis absorption spectra.

3.2.8 Degradation of reactive blue dye under visible light irradiation

Photodegradation studies were conducted using three distinct concentrations of Reactive Navy Blue HER dye (1, 2, 3 mg/L) and pH = 7. In individual 20 ml test tubes, 0.02 mg from each photocatalysts was introduced, followed by the addition of the respective concentrations of the blue dye. Subsequently, the test tubes were positioned under direct sunlight irradiation. Samples were collected within a period of 2 hours and the concentration of the dye was determined using UV-visible spectroscopy at λ max=600 nm to see the effect of the initial concentration of the dye and irradiation time.

To observe the impact of pH variations, samples of a 1 mg/L dye solution were prepared under different pH conditions— acidic at pH 3, neutral at pH 7, and alkaline at pH 11. Subsequently, all samples were subjected to identical conditions for analysis.

The photocatalyst degradation efficiency was evaluated as the removal percentage of Reactive blue dye, equation (3.3)

$$Removal\ Efficiency\ (\%) = \frac{C_0 - C_t}{C_0} \times 100\%$$ 0.3

Where: C_o and C_t represent the initial and final concentrations of Reactive blue dye by (mg/L) respectively.

3.2.9 The effect of solution pH

The dye removal rate is significantly affected by the pH of the test solution. In this study, 20 ml of a blue dye solution with a concentration of 1 mg/L was used. To adjust the pH within the range of 3 to 11, precise amounts of 0.1 M HCl and NaOH solutions were added. Subsequently, 0.004 g of each photocatalyst per liter was separately introduced into each container. The solutions were then exposed to a sun light irradiation for 60 minutes for half of them and 120 minutes for the remainder. Afterward, the specimens were separated and filtered, and the absorbance of each solution was measured using a spectrophotometer. This absorbance data was then compared with the initial absorption levels before undergoing the photocatalytic process.

3.2.10 Photocatalyst reusability and stability

The assessment of nanophotocatalyst efficacy in diverse applications and the cost-effectiveness of the photodegradation mechanism rely on critical variables such as strong durability and a straightforward recovery procedure. This study centers on both pure and doped nanophotocatalysts, particularly devoid of any chemical intervention to eliminate contaminants from their surface. Instead, the approach entails allowing the mixture to sediment for numerous hours, succeeded by water segregation and a desiccation process at 60°C, as detailed by (Najafi et al., 2022).

3.2.11 Immobilization of bare and codoped photocatalysts onto polyester membranes

The immobilization of bare ZnO and codoped TiO_2- α-Fe_2O_3 and TiO_2-ZnO photocatalysts onto the polyester membranes was achieved using an aqueous heat attachment method, following a protocol reported by (Sudrajat, 2018) with modifications. Initially, the polyester membranes, sized at 40 cm × 40 cm, underwent a thorough cleaning process with detergent at 80°C for 30 minutes to eliminate impurities. Subsequently, the polyester membranes were rinsed extensively with water to remove the detergent and cleaned with acetone at 25°C for 30 minutes. A further step involved immersing the polyester membranes in a 1 M NaOH solution at 80°C for 5 hours, followed by repeated rinsing with water and drying at 80°C for 24 hours. The cleaned polyester membranes were then immersed in separate photocatalysts suspension at 80°C for 2 hours under magnetic stirring at 200 rpm and dried at 40°C for 24 hours. This immersion-drying process was repeated three times consecutively. The coated membranes underwent curing at 150°C for 30 minutes. Finally, the resulting coated polyester membranes was immersed in water at 80°C for 30 minutes to remove weakly attached particles, dried at 80°C for 24 hours, and stored in a desiccators for subsequent use. (The membranes named by P for uncoated membranes PTFT, PTFC, PTZT, PTZC, and PZ for coated membranes with TFT, TFC, TZT, TZC, and ZnO photocatalysis respectively).

3.2.12 Characterization of the polyester membranes

The optical properties of the membranes were evaluated using a digital microscope (MSX-500Di viewer) to observe any color changes due to the addition of different

photocatalysts. The surface morphologies of the membranes were examined with Scanning Electron Microscopy (SEM) on a Zeiss Ultra55. Additional insights into the chemical composition of the photocatalyst nanopowder and the membranes were provided by Energy-Dispersive X-ray Analysis (EDX). To confirm the effective impregnation of the photocatalysts in the membrane and ensure its purity, the structural characteristics of the photocatalyst nanopowder into the membranes were determined through X-ray Diffraction using a Smartlab X-Ray Diffractometer, capable of PXRD, HRXRD, XRR, etc. he characterization of functional groups on the coated membrane was performed using Fourier Transform Infrared Spectroscopy (FTIR) with a Perkinelmer Frontier instrument in ATR mode, covering the spectral range from 4000 to 650 cm^{-1} to elucidate the chemical compositions of their surfaces.

3.2.13 Development of Point-Of-Use (POU) solar unit devices for household water treatment

The study aimed to provide clean and safe drinking water to remote rural areas by treating raw potable water. To achieve this, a point-of-use solar unit was developed as a water treatment system, as illustrated in Figure 3.1 and 3.2. The main component of the setup is polyester-cotton membranes (65% polyester, 35% cotton) measuring 20 cm by 20 cm, which are either uncoated (control) or coated with titanium dioxide doped with zinc oxide or ferric oxide. The membrane is affixed to a transparent glass container designed to absorb sunlight and activate the photocatalysts. The container includes a tap to collect the clean water.
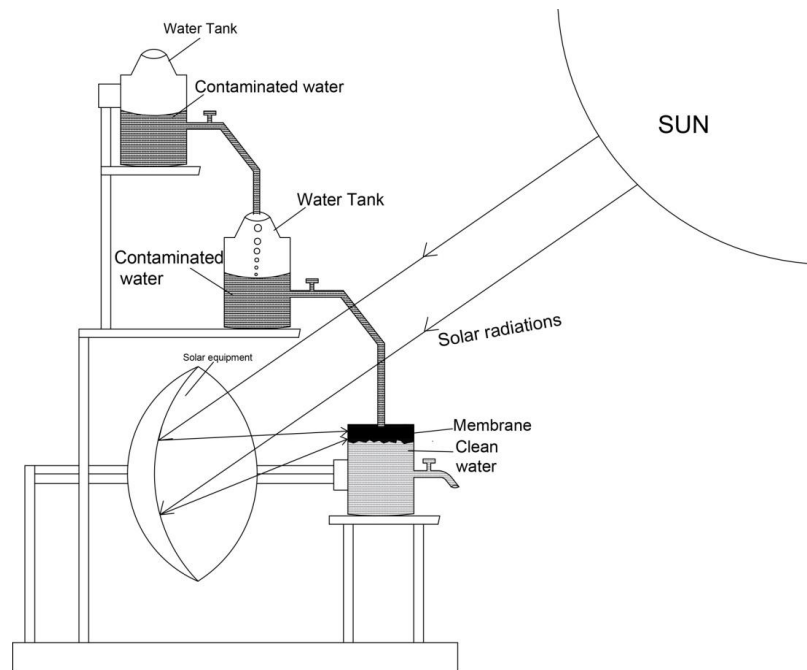
Figure 0-1 Schematic diagram for Point-Of-Use (POU) solar unit devices for household water treatment

Figure 0-2 Photograph of the Point-Of-Use (POU) solar unit device for household water treatment

The feed system of the unit comprises two water tanks positioned vertically, each equipped with taps to control the water flow. This vertical arrangement allows gravity to facilitate smooth water movement between the tanks. The primary purpose of the upper water tank is to regulate and maintain the water level in the lower tank. By doing so, it prevents head loss and ensures that the pressure remains consistent.

A parabolic solar collector, featuring a 60 cm diameter dish, is employed to focus solar radiation onto the membranes. To maximize sunlight exposure throughout the day, the positioning and tilting of the solar collectors are adjusted manually. Refer to Figure 3.3 for a detailed illustration.
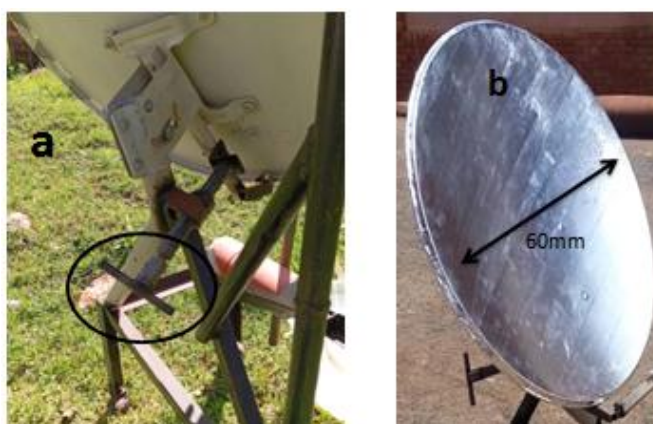
Figure 0-3 (a) adjusting the solar collector (b) the solar collector (dish) diameter

To operate the system, the user aligns the unit towards the sun and manually adjusts the dish until sunlight is focused on the membrane, activating the photocatalysts. Raw water is then poured into the two feed tanks: 3 liters into the lower feed tank (as used in this study) or any constant volume of water, and up to 5 liters into the upper feed tank. The system relies on gravity, eliminating the need for electricity or pumps. Once the glass container tap is opened, the treated water is collected in a clean container.

The experiments were conducted at Moi University, Eldoret Town, Kenya, in September, between 9:00 AM and 3:00 PM. The solar intensity, as measured by a photometer, ranged from 900–950 W/m². In the membrane area, the sunlight was concentrated using a solar concentrator, increasing the intensity to 2000–2150 W/m².

3.3 Treatment of wastewater targeting organic and microbial contaminants

The study focused on removing the organic and microbial contaminants from the feed suspensions, therefore raw dam water and synthetic feed created with distil water spiked with *E. coli* were used as examples of the microbial and oxytetracycline as organic pollutants in water. Because rural residents who typically get their water from dams or rainfall are the target population for the POU (Achisa, 2014b), raw dam water was used. However, seasonal variations in climate can affect the microbial communities in dam water. As a result, the synthesis water included both high and low concentrations of *E. coli*. Furthermore, oxytetracycline was tested as an organic pollutant in synthesis water to evaluate how well the coated membranes degraded any organic pollutants that might be present in dam raw water.

The disinfection test consisted of two parts. In the first part, the antibacterial efficacy of the coated membrane was assessed by exposing it to media containing gram-negative *E. coli* as indicator organisms. In the second part, the disinfection efficacy of the coated filter during water filtration was investigated using dam raw water and synthetic feed as samples with different *E. coli* concentrations (Flow test).

3.3.1 Synthetic feed water with oxytetracycline

Three concentrations of OTC solution (1 mg/L, 2 mg/L, and 3 mg/L) were prepared and filtered through polyester membranes impregnated with TFT, TFC, TZT, TZC, TZ, and

uncoated membranes as a control under concentrated sunlight using the point of use solar unit. The experimental run for about 90 minutes and the samples were collecting after every 30 minutes. The collected samples were analyzed with UV spectroscopy, and the removal efficiency was calculated using equation 3.4 to assess the photodegradation of the coated membrane.

$$OTC\ removal\ efficiency = \frac{C0 - Ct}{C0} * 100 \qquad 0.4$$

Where: C0 denotes the initial concentration of the sample in mg/L before filtration, while Ct signifies the concentration of the sample in mg/L after filtration using the coated membranes under the light.

3.3.2 Experimental design

From the comparison between the results obtaining from section 3.3.1 of the several types of the coated membranes, the polyester membranes coated with Fe_2O_3- TiO_2 from synthesis TiO_2 (PTFT) gave the best performance in degrading oxytetracycline under the sun light irradiation. And because there are other variables affecting the degradation efficiency of the oxytetracycline in addition of the contaminant concentration as depicted in the flow diagram Figure 3.4 Response Surface Method (RSM) based on Central Composite Design (CCD) was employed for conducting experiments. The Design-Expert software, Version 13.0 (Stat Ease, Inc., MN, USA), was utilized for data analysis and response surface optimization. The results obtained were systematically analyzed through Analysis of Variance (ANOVA) to establish relationships between parameters and response variables. The goodness of fit for the experimental data was evaluated using regression models (R^2). The chosen factors for optimization were pH, initial concentration of OTC, and water flowrate. These parameters served as independent

variables, each with three levels (Table 3.1), while the OTC removal efficiency (%) was considered the response variable. A total of 20 experimental runs were conducted according to the centered central composite design, as shown in Table 3.2. The experimental runs included 6 replicate runs at the center, 6 factorial runs, and 8 axial runs, and were calculated using Eq. (3.5).

$$N = 2^k + 2k + C0 = 2^3 + (2*3) + 6 = 20 \qquad \qquad 0.5$$

Where N represents the total number of experiments, k is the number of parameters, 2k accounts for the axial runs, and C0 denotes the center point runs.
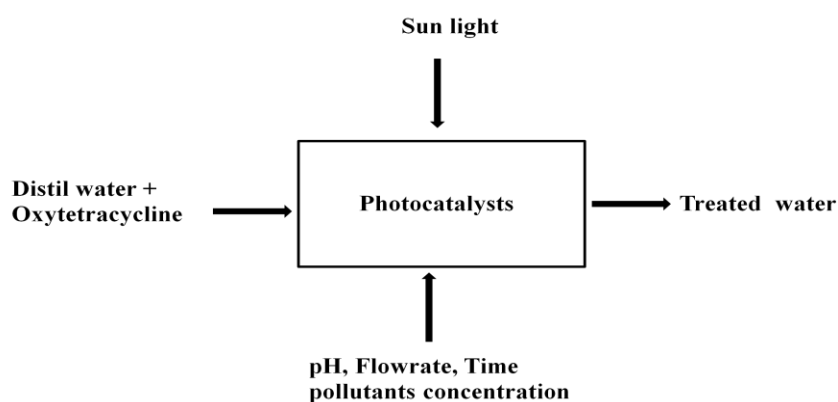
Figure 0-4 Flow diagram of oxytetracycline degradation by photocatalytic membrane

Table 0-1 Ranges and levels of the experimental variables

Experimental variable factors	Label	unit	-alpha	Low (-1)	Central (0)	High (+1)	+alpha
pH	A	…	3.97731	5	6.5	8	9.02269
OTC concentration	B	mg/l	0.318207	1	2	3	3.68179
Flow Rate	C	…	1.68179	-1	0	+1	1.68179

Table 0-2 Matrix of central composite design

Run	Space Type	Factor 1 A:pH	Factor 2 B:oxytetracycline concentration mg/l	Factor 3 C:Flowrate	Removal Efficiency %	
					actual	predicted
1	Axial	9.02	2.00	0.00	48.00	45.60
2	Axial	6.50	0.32	0.00	100.00	100.00
3	Center	6.50	2.00	0.00	55.65	53.07
4	Factorial	5.00	1.00	1.00	91.00	88.42
5	Factorial	8.00	1.00	-1.00	56.50	57.77
6	Factorial	8.00	1.00	1.00	61.50	62.09
7	Factorial	5.00	3.00	1.00	40.00	38.06
8	Axial	3.98	2.00	0.00	63.15	66.49
9	Center	6.50	2.00	0.00	48.00	53.07
10	Center	6.50	2.00	0.00	48.00	53.07
11	Axial	6.50	2.00	-1.68	55.65	54.41
12	Factorial	8.00	3.00	-1.00	48.66	50.57
13	Axial	6.50	2.00	1.68	46.60	48.78
14	Center	6.50	2.00	0.00	55.65	53.07
15	Center	6.50	2.00	0.00	55.65	53.07
16	Center	6.50	2.00	0.00	55.65	53.07
17	Factorial	5.00	3.00	-1.00	50.33	49.08
18	Axial	6.50	3.68	0.00	51.33	51.93
19	Factorial	8.00	3.00	1.00	52.03	51.75
20	Factorial	5.00	1.00	-1.00	96.70	96.31

3.3.3 Disinfection performance of the coated membrane

The antibacterial efficacy of the PTFT, PTFC, PTZT, PTZC, and PZ coated membranes and P uncoated membrane as a control when exposed to media containing gram negative bacteria *Escherichia coli* (*E. coli*) strain ATCC 25922 was investigated using qualitative

techniques, namely the Disk diffusion test and Glass bottle test.

The concentrated culture of bacteria was diluted using a serial dilution method. Initially, 1 gram of concentrated bacteria was dissolved in 9 ml of distilled water to achieve a concentration of 10^0 bacteria. After thorough shaking to ensure complete dissolution, 1 ml from the 10^0 solution was mixed with 9 ml of water to obtain a concentration of 10^1 bacteria. This process was iterated until reaching a concentration of 10^6 bacteria. Figure 3.5 showed the shaker and the bacteria concentrations ($10^0 – 10^6$) CFU/ml.
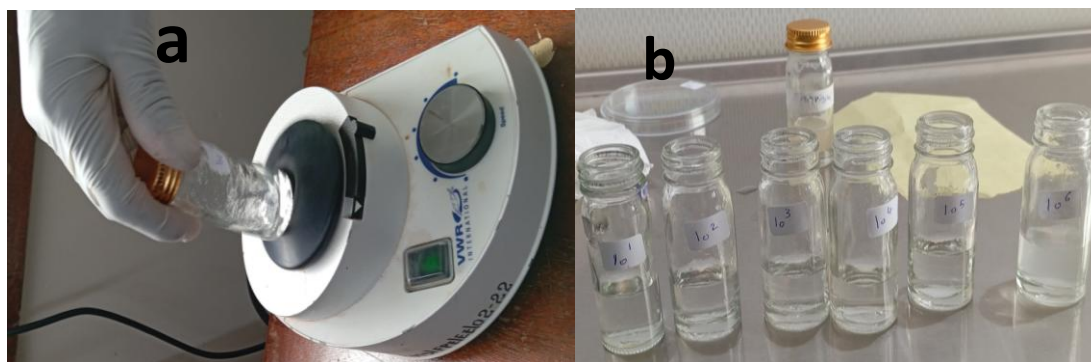
Figure 0-5 Bacteria dilution (a) shaker and (b) the bacteria concentrations ($10^0 – 10^6$) CFU/ml

3.3.3.1 Disk diffusion test

In the disk diffusion test, both membrane pieces coated and uncoated are placed onto a culture plate (macConkey agar) that has been inoculated with bacteria beforehand, thus functioning as a control. Subsequently, compounds diffuse from the discs into the agar medium, forming a concentration gradient. If the compound has antibacterial properties, it will inhibit bacterial growth around the discs, resulting in the formation of an inhibition zone. The diameter of this zone is then measured to evaluate the effectiveness of the tested substance against the bacteria.

The disinfection performance of the coated membrane against *E. coli*, a modified (Amani

et al., 2019) method was employed. Initially, 51.5 grams of MacConkey agar, a selective medium for gram-negative bacteria, was dissolved in 1 litter of distilled water and thoroughly mixed. Coated and uncoated fabric membranes were then cut into 10x10 mm pieces. Subsequently, all materials, including the membranes, agar media, and tools, were sterilized in an autoclave for 15 minutes at 121°C. The cooled agar media was poured into petri dishes (15 ml each) and allowed to solidify. Next, 0.1 ml of *E. coli* at concentrations of *2.45 * 10^5* CFU/ml (high concentration) and *2.45 * 10^3* CFU/ml (low concentration) was evenly distributed on the surface of the media. The membrane pieces were placed in the center of each plate then closed the petri dishes tightly using Parafilm. The plates were incubated for 24 hours at 37°C to allow bacterial growth, after which the inhibition zones were measured using a ruler. Figure 3.6 depicted the disk diffusion test steps and Figure 3.7 depicted growth of *E. coli* in macConoky agar.
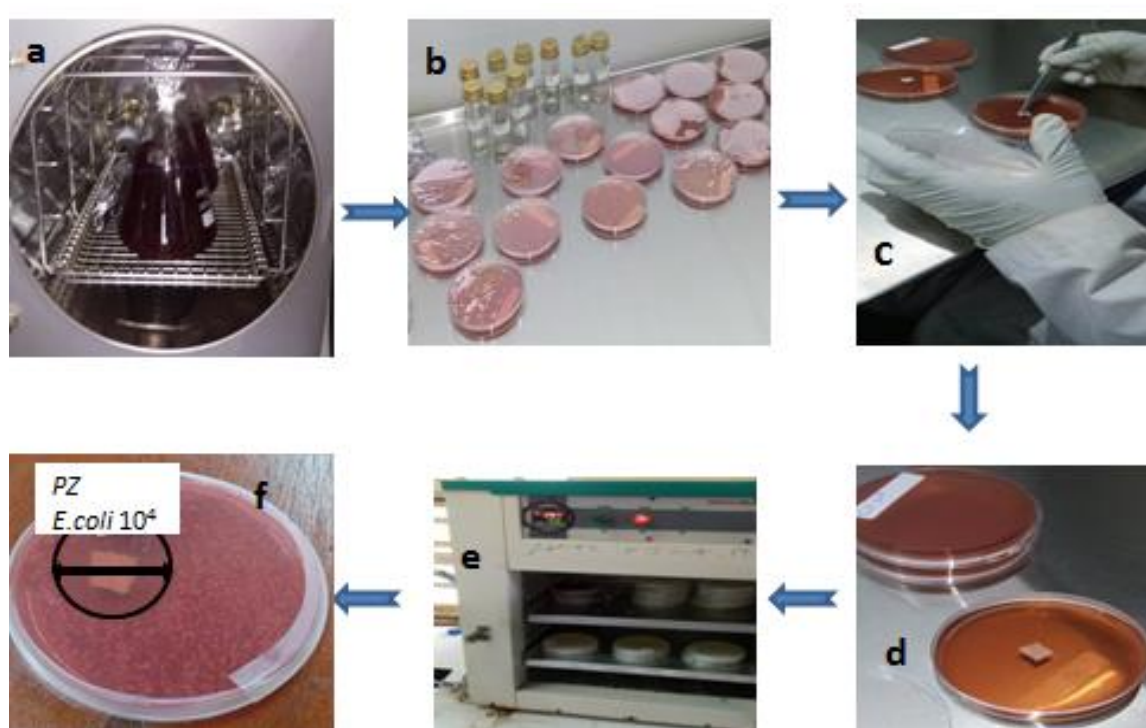
Figure 0-6 Disk diffusion test steps

(a) Autoclave, (b) solidified agar media with 0.1 ml of bacteria, (c) membrane pieces placed in the center of each plate, (d) petri dishes closed tightly using Parafilm (e) incubated (f) bacterial growth after 24 hrs.

Figure 0-7 Growth of *E. coli* bacteria in MacConkey agar culture media

3.3.3.2 Glass bottle test

The Glass bottle test evaluates how effectively a substance disinfects when placed in a liquid containing the specific microorganism targeted for removal. In this method, the substance, possibly containing antimicrobial properties, is submerged in the liquid for a set duration. Throughout this period, the antimicrobial elements diffuse from the substance into the surrounding liquid, potentially halting the growth of microorganisms. Following the test's completion, the liquid is analyzed to determine if the microorganism is present or absent, indicating the substance's effectiveness in disinfection (Achisa, 2014b).

In this study, 0.1 ml of a bacterial concentration of (98000 CFU/ml) was added to a glass bottle and the volume was adjusted to 10 ml. Subsequently, pieces of coated and uncoated membranes, sized 10x10 mm, were placed in the glass bottle and thoroughly mixed. Then, 0.1 ml of the culture was transferred onto agar media using the same culture

method described in section (3.3.3.1). The antibacterial effects were assessed using equation (3.6), which calculates the percentage of microorganism reduction (R). This equation compares the number of bacterial colonies from the control (A) with those from the prepared polyester fabrics (B):

$$R\% = \left(\frac{A-B}{A}\right) * 100 \qquad\qquad 0.6$$

3.3.4 Synthetic feed water containing *E. coli*

Ensuring the absence of microbial contaminants in drinking-water is of paramount importance as even a single exposure to such contaminants can lead to waterborne diseases. Therefore, regulations should prioritize verifying the microbial safety of drinking-water. This verification is typically based on testing indicator organisms, with *Escherichia coli* (*E. coli*) being the preferred choice. Alternatively, *thermotolerant coliforms* can be used, although they are considered less reliable but still acceptable (Organization, 2024).

The primary public health concern regarding microorganisms in water is the consumption of drinking-water contaminated with human or animal feces. Consequently, microbial analysis typically focuses on testing for organisms indicating recent fecal contamination, known as "faecal indicator organisms." While no single faecal indicator organism is ideal, *E. coli* is widely regarded as the most suitable indicator of fecal contamination in drinking-water. This approach considers factors such as complexity, sensitivity of detection, cost, and timeliness of obtaining results (Organization, 2024).

From the bacterial concentration prepared in section (3.3.3), 1 ml of the 10^6 concentration was extracted and added to a glass bottle. The volume was adjusted to 10 ml, and from this solution, 0.1 ml was transferred to a larger container and the volume completed to 10

litters to create synthetic feed with a concentration of bacteria denoted as $12 * 10^4$ CFU/100 ml (high concentration of bacteria). This synthetic feed was then subjected to solar irradiation in a solar unit point of use for 90 minutes, with samples taken at 30-minute intervals. The experiment utilized PTFT, PTFC, PTZT, PTZC, and PZ coated membranes, with uncoated P membranes serving as a control, to compare their disinfectant removal efficiency. Samples were collected and taken to the microbiology lab for testing.

A synthetic feed with a concentration of $6 * 10^4$ CFU/100 ml of bacteria was prepared using the same steps as the high-concentration feed. This feed was then run through the coated and uncoated membranes to investigate their antimicrobial removal efficiency.

For the preparation of culture media, 51.5 grams of MacConkey agar were dissolved in 1 liter of distilled water and thoroughly mixed. The agar media and tools were sterilized in an autoclave for 15 minutes at 121°C. The agar media was then cooled under laminar flow and poured into petri dishes (15 ml each), allowing it to solidify. Subsequently, 0.1 ml from each water sample was evenly distributed on the surface of the media. The plates were incubated for 24 hours at 37°C to facilitate bacterial growth, after which the number of colonies was counted. The antibacterial effects were assessed using equation (3.6) as outlined in section (3.3.3.2).

In municipal water filtration, it is recommended to achieve a log removal value (LRV) of 4 or 5 to ensure effective disinfection (A. Mecha et al., 2019; Wei et al., 2022). The LRV is calculated using the formula (equation 3.7)

$$LRV = log_{10}(Cf/Cp) \qquad 0.7$$

where Cf and Cp represent the concentrations of microorganisms in the influent and

effluent, respectively.

3.3.5 Dam water

To evaluate the effectiveness of point-of-use filtration using coated membranes with real potable water, samples were collected from Kesses dam in Eldoret, Kenya. Analysis was conducted within six hours of collection to prevent the loss of *E. coli* viability. The properties of the raw river water utilized are detailed in Table 3.3. *E. coli* used as a microorganism indicator, measured using a plate count method as detailed in section 3.3.4. Conductivity, Total dissolved solids, and pH measured using portable pH meter. Turbidity, Total Iron as (Fe), and Zinc, as (Zn^{++}) measured using Palin test equipment.

Table 0-3 Properties of raw water collected from Kesses dam

Parameter	unit	Value
E. coli	CFU/ 100 mL	$13 * 10^3$
Turbidity	NTU	16
pH	-	7.92
Conductivity	µS/cm	166
Total dissolved solids	mg/L	83
Total Iron as Fe	mg/L	0.11
Zinc, as Zn^{++}	mg/L	Nil

3.4 Disinfection and organic degradation kinetics and synergy of the photo-catalytic water treatment

In this study, two experimental pathways were utilized to evaluate the disinfection efficiency and organic degradation kinetics, as well as the synergy of photocatalytic

water treatment.

Pathway 1

This pathway involved four experimental groups:

1. Uncoated membrane

2. Titanium dioxide (TiO_2) - coated membrane

3. Zinc Oxide (ZnO) - coated membrane

4. Titanium Dioxide doped with Zinc Oxide (TiO_2/ZnO) - coated membrane

The experiments with uncoated membranes, TiO_2 coated membranes, and ZnO coated membranes were conducted to determine the removal efficiency of each respective filtration process. The TiO_2/ZnO coated membrane experiments were performed to explore potential synergistic effects between different disinfection methods and the kinetics of organic degradation.

Pathway 2

This pathway included three experimental groups:

1. Uncoated membrane

2. Titanium dioxide (TiO_2) - coated membrane

3. Ferric dioxide (Fe_2O_3) - coated membrane

4. Titanium Dioxide doped with ferric Oxide (TiO_2/Fe_2O_3) - coated membrane

The experiments with uncoated membranes and TiO_2, Fe_2O_3 coated membranes were conducted to determine the removal efficiency of the uncoated filtration process and TiO_2 respectively. The TiO_2/Fe_2O_3 coated membrane experiments were carried out to investigate potential synergistic effects between different disinfection methods and the kinetics of organic degradation.

Overall, both pathways aimed to reveal the potential synergistic effects between different disinfection units and the kinetics of organic degradation by comparing the performance of uncoated (filtration process), TiO_2 coated, ZnO coated, and TiO_2 doped with ZnO or Fe_2O_3 coated membranes (filtration and photocatalysis process).

The two pathways in this study addressed two scenarios: disinfection and the kinetics of organic degradation. The effectiveness of microbial removal was measured by the log reduction of microbial indicators. A synthetic feed containing *E. coli* as the microbial indicator, along with real raw water from a dam, was used as the feed for all experiments. All experiments were conducted using the same system to ensure consistency.

Bacterial survival was estimated using the Chick-Watson disinfection model (Jaiaue et al., 2022; Peleg, 2021) equation 3.8.

$$log \left(\frac{N}{N_0}\right) = -kC^n t \qquad 0.8$$

In this model, N_0 represents the initial number of bacteria (CFU/ml), N is the number of bacteria at time t, k is the disinfection rate constant, C is the concentration of the disinfecting agent at time t, and n is the reaction order.

In photocatalytic filtration processes, assuming a stable concentration of the disinfecting agent over time given a fixed catalyst concentration, irradiation source, and filtration rate, the equation could be reformulated as follows:

$$log \left(\frac{N}{N_0}\right) = -k' t \qquad 0.9$$

This model was utilized to fit the data on photocatalytic disinfection, where k' represents the rate constant independent of concentration (min^{-1}).

To assess the efficacy of the combined process, the synergy index (SI) for photocatalytic

filtration was computed using the subsequent formula (Mecha et al., 2017).

$$SI = \frac{LRV_{Fil+Photo}}{LRV_{Fil}+LRV_{Photo}} \qquad\qquad 0.10$$

In this expression, LRV denotes the log reduction value, with the subscripts denoting filtration (Fil) and photocatalysis (Phot).

In the second pathway, the kinetics of organic degradation was assessed using oxytetracycline as an example of an organic pollutant. As mentioned earlier in Section 3.3.1, three concentrations of the antibiotic 1, 2, and 3 mg/l were used in the experiment under sun light irradiation concentrated by the solar unit, the concentration of oxytetracycline was measured using a UV spectrophotometer at a wavelength of 350 nm (λmax 350). The degradation was quantified in terms of removal efficiency, calculated using Equation 3.3.

The Langmuir-Hinshelwood (L-H) equation is frequently used to describe the kinetics of heterogeneous photocatalytic reactions, such as the degradation of pollutants like oxytetracycline. This model aids in comprehending how the reaction rate is influenced by the pollutant concentration and the surface characteristics of the photocatalyst (Eskandari et al., 2023).

The L-H equation for the photocatalytic degradation can be expressed as:

$$r = \frac{kKC}{1+KC} \qquad\qquad 0.11$$

r is the reaction rate (rate of degradation of oxytetracycline).

k is the rate constant of the reaction (when the surface is fully covered by the reactant).

K is the Langmuir adsorption constant of the reactant (oxytetracycline) on the catalyst surface.

C is the concentration of the reactant (oxytetracycline).

Assuming that the reactant is in equilibrium between the solution phase and the surface of the photocatalyst, the surface adsorption adheres to Langmuir isotherm behavior, implying monolayer coverage of the adsorbate on the catalyst surface. Additionally, the reaction rate is dictated by the surface reaction step, with no limitations from mass transfer.

For low concentrations where KC<< 1, the L-H equation simplifies to a pseudo-first-order kinetic model:

$$r = k'C \qquad\qquad 0.12$$

Where $k' = $ kK is the pseudo-first-order rate constant

The rate constant (k') can be calculated from experimental data using the integral method. Therefore, pseudo-first-order kinetics can be employed to fit the experimental data in these processes through linear regression analysis (Bahrudin, 2022) .

$$-ln\left(\frac{C_t}{C_0}\right) = k't \qquad\qquad 0.13$$

The synergy index (SI) for photocatalytic filtration was determined using the following equation (Achisa C. Mecha et al., 2016):

$$SI = \frac{R_{Fil+Photo}}{R_{Fil}+R_{Photo}} \qquad\qquad 0.14$$

In this equation, R represents the percentage removal, with the subscripts indicating filtration and photocatalysis. An SI value greater than 1 signifies a positive synergistic effect of the combined process, while an SI value less than 1 indicates a negative effect.

3.5 Membrane fouling and re-use potential

3.5.1 Membrane flux performance

In this study, a novel multifunctional antifouling membrane was developed by combining filtration technology with photocatalytic processes. This was achieved by using commercially available or lab-synthesized titanium dioxide, doped with either zinc oxide or ferric oxide. The membrane's performance was assessed by evaluating its efficiency in removing oxytetracycline (OTC) under sunlight irradiation using a solar unit.

The flux performance of both uncoated and photocatalyst-coated membranes was evaluated during a 90-minute filtration period under sunlight radiation. The permeate flux (kg/m²h) was determined using equation 3.14, which factors in the mass of permeated water (m), the effective surface area of the membrane (A), and the filtration time (Δt) (Etemadi et al., 2017; Irani & Amoli-Diva, 2020).

$$J = \frac{m}{A\Delta t} \qquad\qquad 0.2$$

3.5.2 Evaluating the membranes antifouling performance

Fouling is a major factor that leads to the reduction of water flux (Wang et al., 2021). Membranes with excellent antifouling properties can significantly extend their lifespan (Cao et al., 2021). To investigate the antifouling properties of the prepared membranes, the previous experiment was extended with additional steps (Pang et al., 2019). The antifouling performance of both uncoated and photocatalyst-coated membranes was evaluated using the recovery ratio of flux (RRF) as a parameter. The membranes were fouled by running dam water through them until a cake layer formed on their surfaces, slowing down the filtration process. This cake layer was then removed, and the membranes were washed with deionized water without any chemical treatment. After

cleaning, the permeate flux (JS) was measured. The permeate flux of deionized water under the same conditions was used as the reference (JR) (Irani & Amoli-Diva, 2020). The RRF was calculated using equation 3.15.

$$RRF \% = \frac{J_S}{J_R} \times 100 \qquad\qquad 0.3$$

3.5.3 Cleaning of the membranes

Fouling requires periodic cleaning of the modules to remove the fouling material from the membrane's surface and pores. The ability to restore the pure water flux after cleaning indicates a successfully cleaned membrane. The choice of cleaning method depends on several factors: the module configuration, membrane type, chemical resistance of the membranes, and the type of fouling material present in the feed (Achisa, 2014b).

Membrane systems can operate for more than 10 cycles without interruption. However, over time, a cake layer forms on the membrane surface, leading to a gradual decrease in flow rate if not cleaned. The formation rate of this layer varies based on whether the membranes are coated or uncoated and the specific characteristics of the membranes. Cleaning the membranes can be easily achieved using the method described by (Achisa, 2014) for cleaning polyester membranes coated with bare and doped Titanium Dioxide photocatalysis. This involves simply brushing the membranes with a bottle brush and rinsing them with water, effectively removing the fouling layer. This straightforward maintenance process requires no special skills, eliminating the need for chemical cleaning.

CHAPTER FOUR

RESULTS AND DISCUSSION

4.1 Synthesis and characterization of metal-ion-doped TiO₂ photo-catalysts and impregnation to polyester based membranes

4.1.1 Characterization of the Photocatalysts

4.1.1.1 SEM and EDX analysis

The surface morphology of iron oxide analyzed using SEM is depicted in Fig. 4.1. The SEM images Fig. 4.1 (a and b) reveal an agglomerated shape morphology, indicating that the nanoparticles exhibit a tendency to cluster and form larger assemblies due to their elevated surface energies (Gurlhosur & Sreekanth, 2018). The EDX analysis Fig.4.1 (c and d) confirms the precise composition of the iron oxide, with 67.92 % iron content and 32.8 % oxygen content, highlighting the successful preparation of the material.
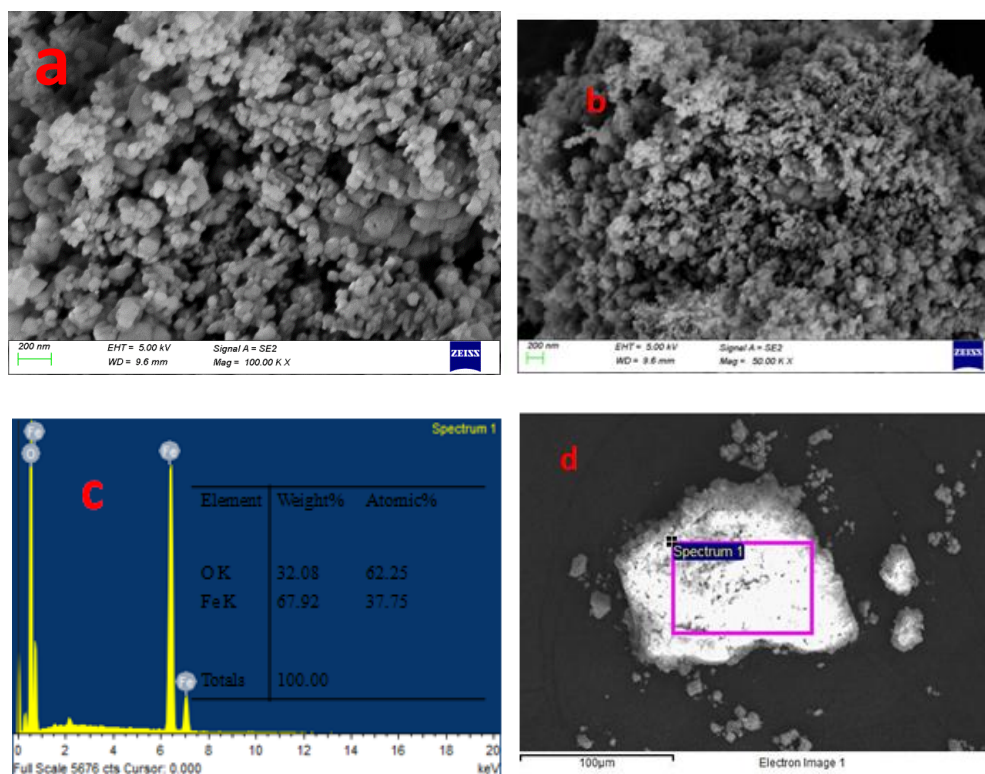
Figure 0-1 SEM & EDX analysis of Fe₂O₃

(a) SEM images (100.00 and 50.00) K X magnification and (b and c) EDX images of synthesis Fe$_2$O$_3$ nonoparticles

Fig. 4.2 (a and b) displays SEM images of the photocatalyst synthesized from the combination of Fe$_2$O$_3$ and a titanium precursor. The images reveal a somewhat porous and agglomerated morphology in the sample, suggesting potential advantages for property enhancement. Notably, both large and small particles of nearly equal sizes were observed in the images (Kumar et al., 2020). The confirmation of elemental composition in the composites was carried out through EDX measurements Fig. 4.2 (c and d), with 7 % iron content, 47.9 % oxygen content and Titanium content 45.10 % providing a comprehensive understanding of the synthesized photocatalyst's constituent elements.
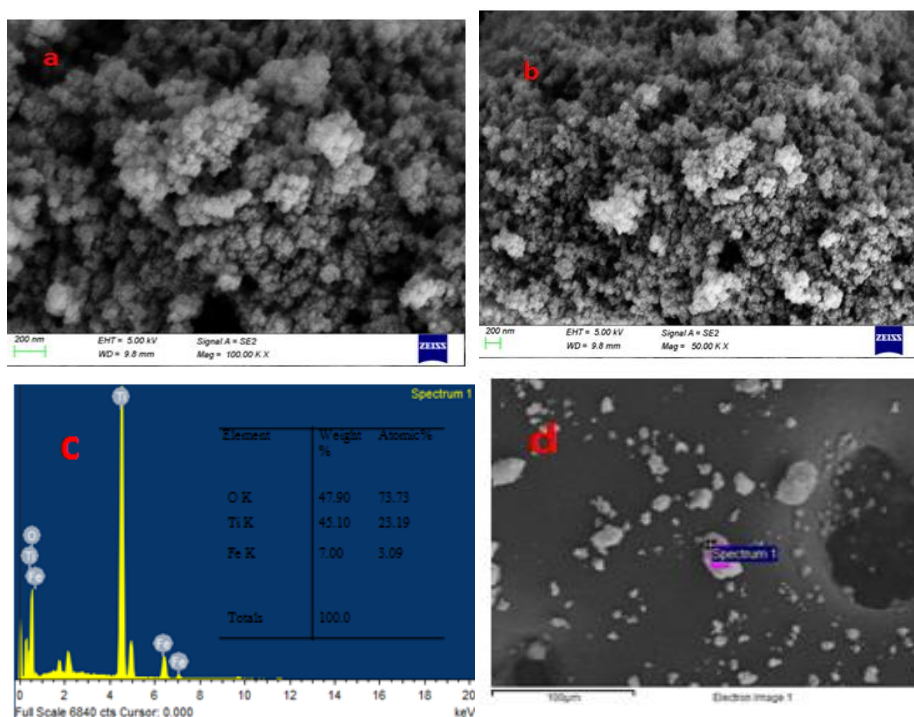
Figure 0-2 SEM & EDX analysis of TFT

(a) SEM images (100.00 and 50) K X magnification and (b and c) EDX images of α-Fe$_2$O$_3$-TiO$_2$ (TFT) from Synthesis Fe$_2$O$_3$ and titanium precursor

Surface morphology analysis was conducted on commercially available TiO_2 nanoparticles doped with synthesized iron oxide. The SEM images in Figure 4.3 (a and b) of the Fe_2O_3-doped TiO_2, revealing a distinctive spherical shape morphology on the nanoparticle surface. At a magnification of 100,000 times, a denser distribution of spherical shapes with minimal empty spaces is evident, Furthermore, Figure 4.3 (a and b) illustrates the occurrence of agglomeration of these spherical shapes, forming clusters within the samples (Gareso et al., 2021).

The confirmation of elemental composition in the composites was carried out through EDX measurements Fig. 4.3 (c and d), with 32.45 % iron content, 44.67 % oxygen content and Titanium content 22.88 % providing a comprehensive understanding of the synthesized photocatalyst's constituent elements.

The findings indicate that the particle size of the photocatalyst synthesized from the Titanium precursor is smaller compared to that of commercially available Titanium, as depicted in figure 4.2 and figure 4.3. The results suggest that an escalation in calcination time leads to heightened material crystallinity. However, it is noteworthy that elevating the calcination time might concurrently result in an increase in crystal grain size.
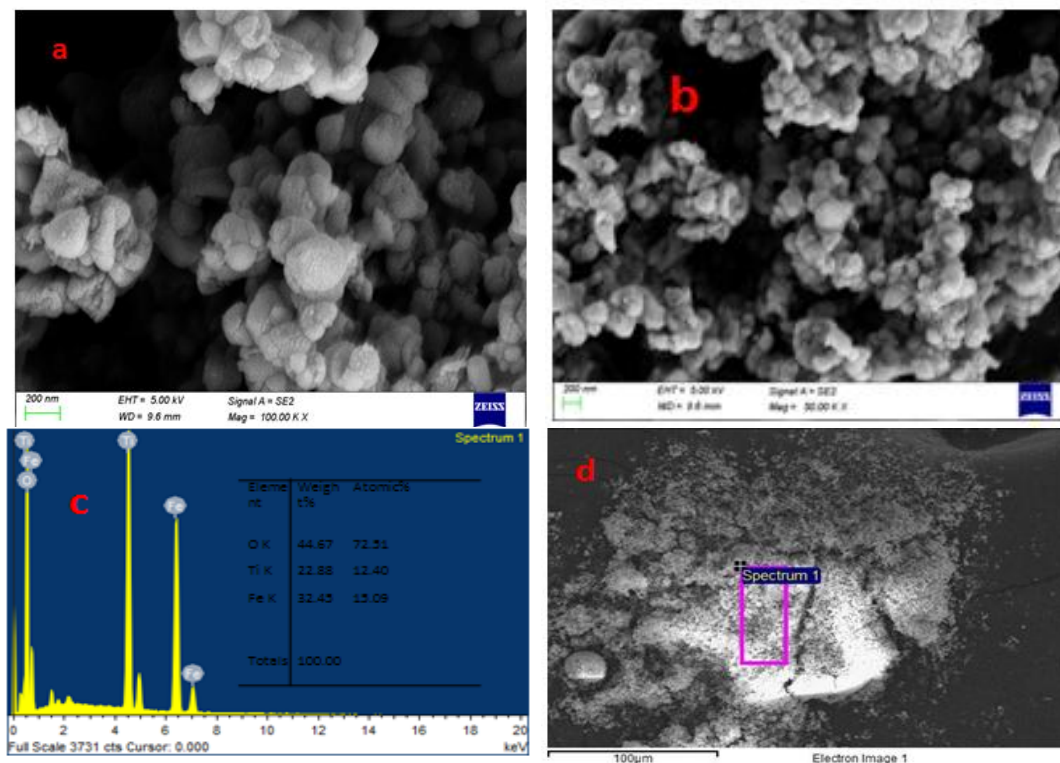
Figure 0-3 SEM & EDX analysis of TFC

(a and b) SEM images (100.00 and 50) K X magnification and (c, and d) EDX images of

α-Fe_2O_3-TiO_2 (TFC) from Fe $(NO_3)_3$ $9H_2O$ and commercial TiO_2

SEM analyses results for TiO_2, TZT, and TZC are shown in Figure 4.4. The presence of TiO_2 was confirmed in all images, while Figure 4.4 (c, d, e, and f) indicated the coexistence of both TiO_2 and ZnO. The observed distribution of elements such as Zn, Ti, and O across the sample confirmed their uniform presence, providing validation for the successful synthesis of ZnO/TiO_2 photocatalysis. Notably, particles of ZnO-TiO_2 produced from synthesized TiO_2 (Figure 4.4 (c and d)) were smaller in size and exhibited a tendency to agglomerate more than particles of ZnO-TiO_2 (Figure 4.4 (e and f)) produced from commercial TiO_2, as evident in the SEM images.
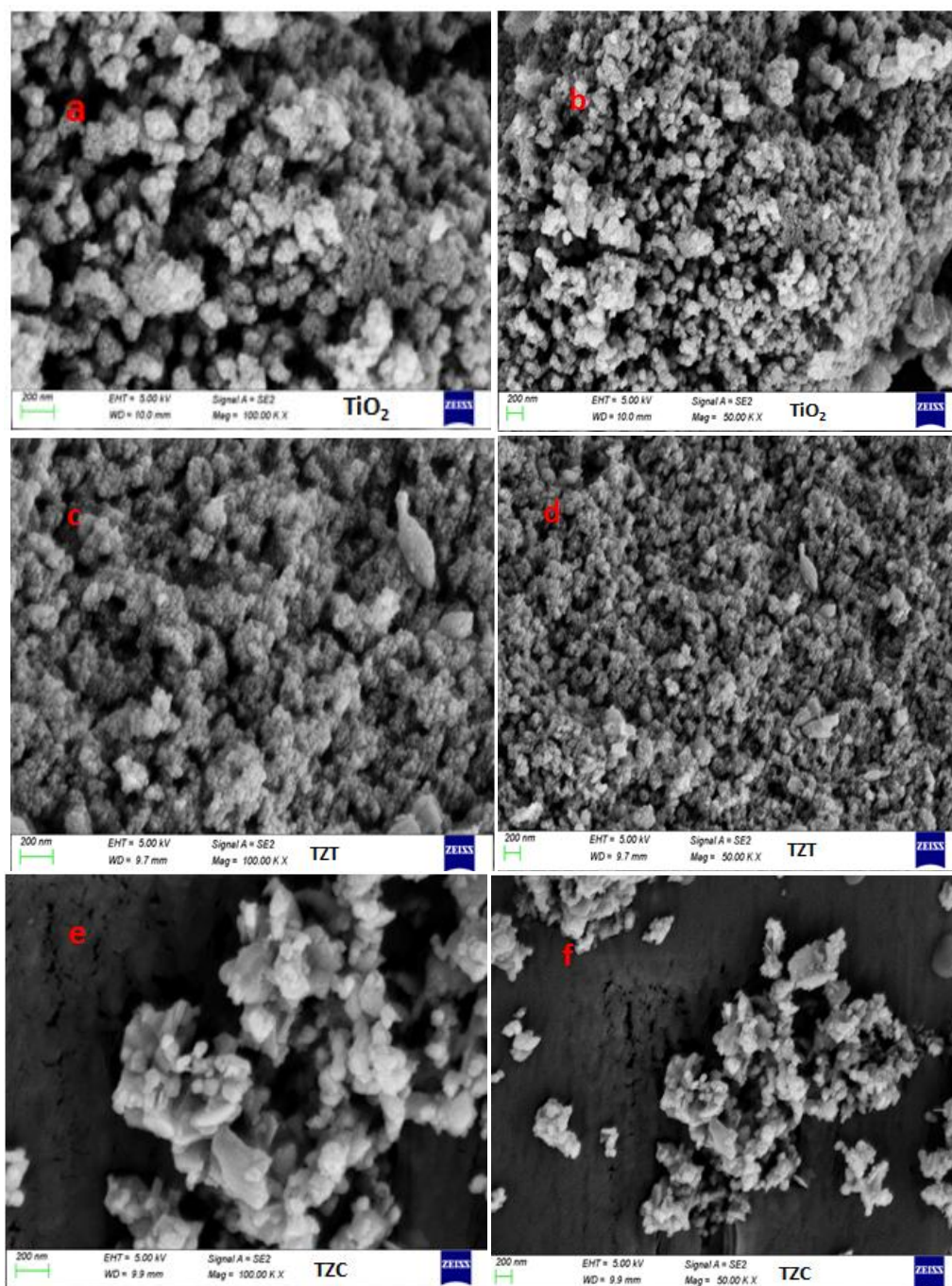
Figure 0-4 SEM analysis of TZT AND TZC

SEM images of (a and b) TiO$_2$, (c and d) TZT, and (e and f) TZC photocatalysts for

100.00 and 50.00 kx respectively

EDX analysis results for TiO$_2$, TZT, and TZC are shown in Fig. 4.5.(a, b, c, d, e, and f)

The EDX spectra unveiled specific peaks indicating the presence of Ti and O for bare

TiO_2 with 59.88 % oxygen content and 40.12 % Titanium content Fig.4. 5.(a, b), and Ti, O, and Zn atoms in the mixed oxide nanophotocatalysis sample with 62.19 % zinc content, 28.2 % oxygen content and 9.6 % Titanium content for TZT Fig. 4.5 (c and d) and 40.51 % zinc content, 44.50 % oxygen content and 14.99 % Titanium content for TZC Fig. 4.5 (e and f) The elemental composition portrayed in the spectrum corresponds with the various stages of Zn-TiO_2 photocatalyst preparation, providing affirmation of the successful integration of zinc into the titanium dioxide structure.

Figure 0-5 EDX analysis of TZC and TZT

EDX images of (a and b) ZnO, (c and d) TZC, and (e and f) TZT photocatalysts
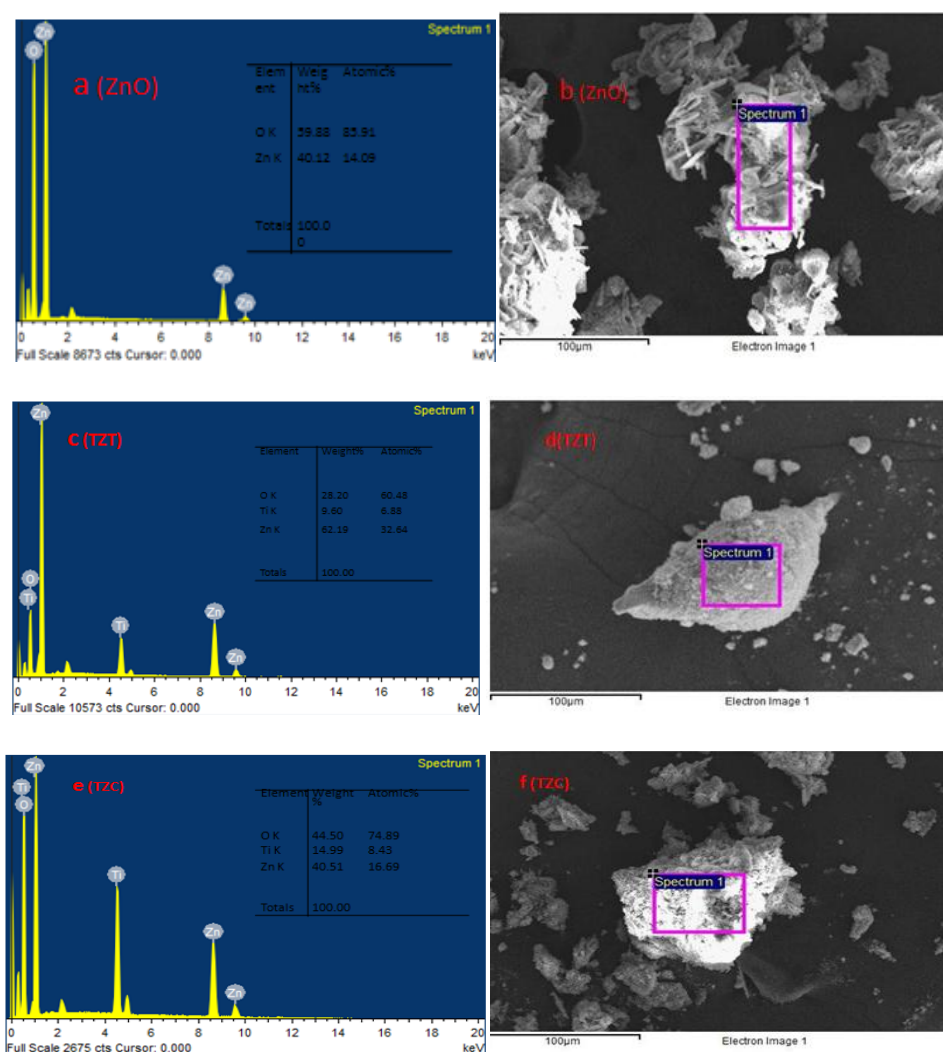
4.1.1.2 FTIR analysis

The FTIR spectra of the synthesized TiO_2, TiO_2-Fe_2O_3 photocatalysts from the commercial and synthesized TiO_2 and the Fe_2O_3, between (400 – 4000) cm^{-1} is shown in Fig. 4.6. The spectra exhibited distinctive peak patterns at 1074 cm^{-1}, 1630 cm^{-1}, and 3439 cm^{-1}, which are indicative of the presence of TiO_2-Fe_2O_3 in the material. The broader peaks observed at 3439 cm^{-1} and 1620 cm^{-1} are attributed to -OH stretching and bending vibrations and are likely to play a significant role in phase formation and stabilization across all nanophotocatalysis, while the strong band below 700 cm^{-1} is associated with the Fe-O stretching mode. Specifically, the Fe-O stretching mode is observed at 556 cm^{-1} and 471 cm^{-1} in pure Fe_2O_3 and in commercial TiO_2 doped with Fe_2O_3 (Dehbi et al., 2020; Kumar et al., 2020), but in the TiO_2-Fe_2O_3 nanophotocatalysis synthesized from precursor materials, it appears as a single stretching peak. Furthermore, a broad band in the 500-600 cm^{-1} range is linked to the vibration of the Ti-O bonds (Talebi et al., 2017).
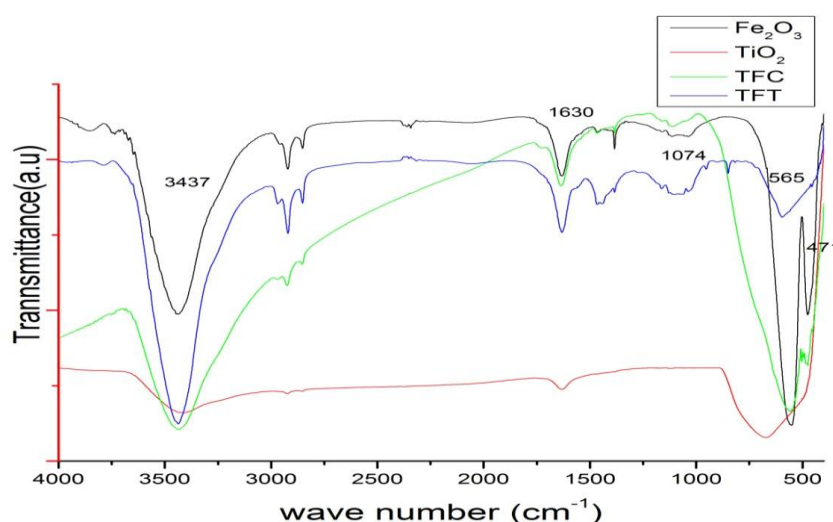
Figure 0-6 FTIR curves of α-Fe_2O_3 nanopowder, TiO_2 photocatalyst, doping TFT and TFC photocatalysts

Figure 4.7 shows the FTIR spectrum revealing minor peaks at 3438 cm^{-1} and 1460 cm^{-1} for ZnO, and 3390 cm^{-1} and 1626 cm^{-1} for TiO_2. This indicates the presence of –OH group stretching vibrations and H–O–H bond deformation attributed to trace amounts of adsorbed water on their surfaces, in agreement with the literature (Laid et al. 2020). For TiO_2, the FTIR spectrum displays a wide band from 472 to 880 cm^{-1}, resulting from the overlap of Ti–O–Ti and Ti–O vibration modes. The prominent peak at 672 cm^{-1} is attributed to Ti–O stretching. In the case of ZnO, characteristic peaks between 456 and 520 cm^{-1} arise from the Zn–O stretching mode. The H–O–H and O–H stretching and bending vibrations produce signals in the ranges of 2852–3800 cm^{-1} and 1600–1682 cm^{-1}, respectively, indicating negligible moisture content in all photocatalysts (Shathy et al. 2022). No additional peaks are detected in the FTIR spectra, confirming the absence of contamination in each photocatalyst, consistent with EDX results.
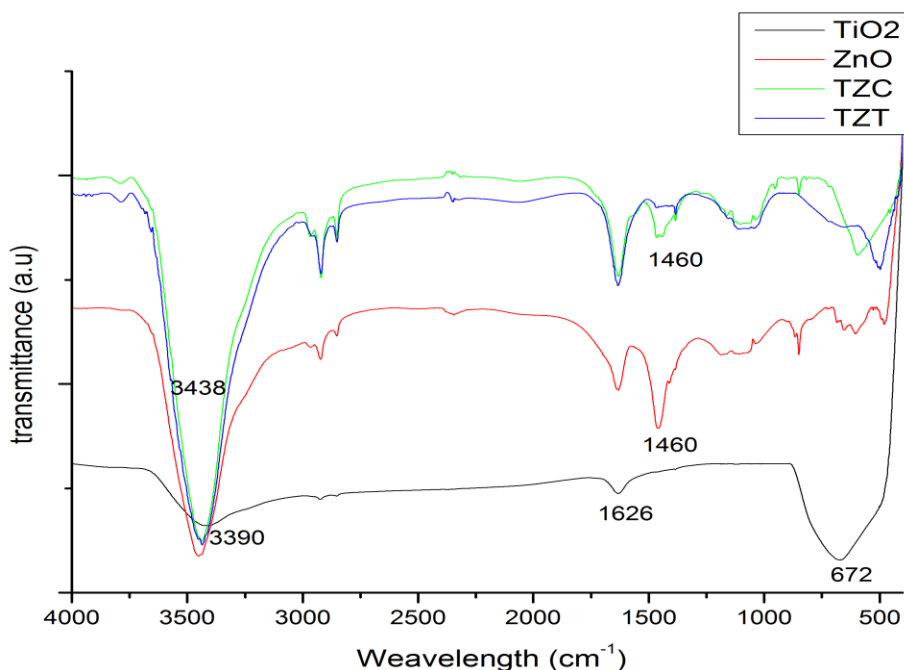
Figure 0-7 FTIR spectra of ZnO, TiO_2, TZC, and TZT photocatalysts

4.1.1.3 XRD analysis

The X-ray diffraction (XRD) analysis results for (α-Fe_2O_3 nanopowder, TiO_2 photocalyst, doping TFT and TFC photocatalysts) are shown in Fig. 4.8. A total of eleven well-defined peaks, all of which can be attributed to the α-Fe_2O_3 phase, commonly known as hematite were observed. The prominent peaks were detected at angles of 24.9, 33.27, 35.39, 41.103, 48.2, 53.9, 57.4, 62.2, 63.8, 71.82, and 75.9 degrees, corresponding to the respective diffraction planes (012), (104), (110), (113), (024), (116), (122), (214), (300), (1010), and (220) of hematite (Asoufi et al., 2018; Lassoued et al., 2018). Furthermore, the presence of two additional peaks at 25.1 and 48.2 degrees, corresponding to the diffraction planes (101) and (200), indicated the presence of the TiO_2 anatase phase within the sample (Abdel-Wahab et al., 2017b; Ijadpanah-Saravy et al., 2014).
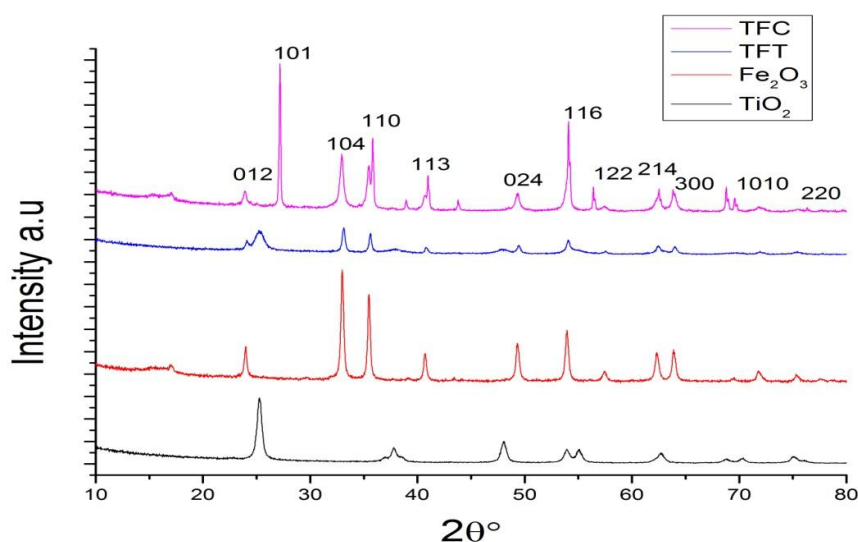
Figure 0-8 XRD curves of α-Fe_2O_3 nanopowder, TiO_2 photocalyst, doping TFT and TFC photocatalysts

XRD analysis results for (TZT, TZC, and TiO_2) are depicted in Fig. 4.9; the XRD pattern of ZnO displays well-defined diffraction peaks at 2θ values of 31.65, 34.18, 36.05, 47.12, 56.34, 62.74, 66.35, 67.84, 69.04, 72.58, and 76.95. These characteristic peaks are

attributed to the (100), (002), (101), (102), (110), (103), (200), (112), (201), (004), and (202) crystallographic planes, respectively, aligning with the wurtzite hexagonal phase of ZnO (JCPDS No. 36-1451). The identified diffraction peaks are in accordance with existing literature (Ma et al., 2013). The XRD pattern's manifestation of narrow and intense diffraction peaks serves as evidence of high crystallinity of the as-prepared nanoflowers (Sharma et al., 2017a). Moreover, the existence of two supplementary peaks at 25.3 and 48.05 degrees, corresponding to the diffraction planes (101) and (200), respectively, signifies the presence of the anatase phase of TiO_2 within the analyzed sample (Abdel-Wahab et al., 2017b; Ijadpanah-Saravy et al., 2014; Theivasanthi & Alagar, 2013). Nevertheless, the identification of three minor crystal peaks at 2θ values of 37.7°, 55.28°, and 62.7°, corresponding to the crystalline planes of (011), (220), and (221), respectively, suggests the presence of a limited amount of rutile phase (with JCPDS No. 80514) in the sample. It is noteworthy that these peaks align with the characteristic peaks of the anatase phase. Intriguingly, the same anatase peaks were also evident in the XRD pattern of pure TiO_2 with JCPDS No. 21.1272 in agreement with the literature (Khasawneh, Palaniandy, Ahmadipour, et al., 2021).
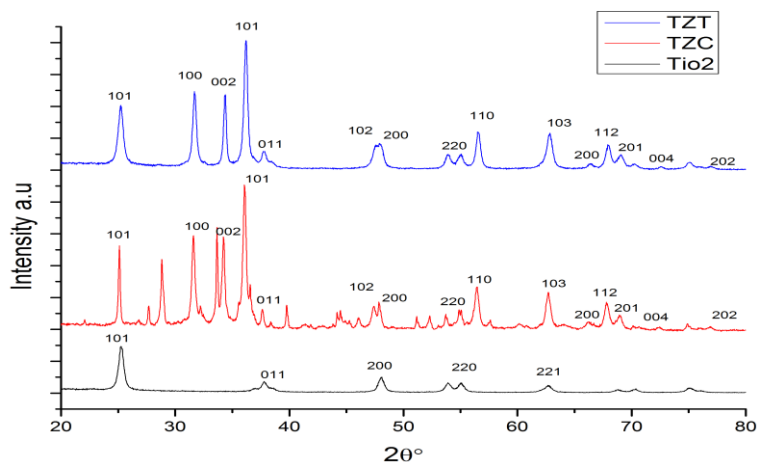
Figure 0-9 XRD curves of TZT, TZC, and TiO_2

The average crystallite sizes of the photocatalysts were determined using the Debye–Scherrer equation were reported in Table 4.

Table 0-1 Crystals size of the photocatalysts

Photocatalyst type	TiO2	Fe$_2$O$_3$	TFC	TFT	ZnO	TZT	TZC
Crystal size	14.83	22.54	38.20	32.30	37.23	21.30	21.40

4.1.1.4 UV-DRS analysis

Fig. 4.10 illustrates the UV–visible diffuse reflectance spectra (DRS) for α-Fe$_2$O$_3$, TiO$_2$, and the two synthesized α-Fe$_2$O$_3$-TiO$_2$ powders. The pristine α-Fe$_2$O$_3$ powder displays broad absorption across the entire UV–visible spectrum, displays photo-absorption about 527 nm, corresponding to band-gap energy of 2.35 eV. In contrast, TiO$_2$/Fe$_2$O$_3$ photocatalysts exhibit extensive optical absorption in both the UV and visible ranges, displays photo-absorption about 438.8 nm, corresponding to band-gap energy of 2.83 eV. While pristine TiO$_2$ powder only demonstrates limited absorption in the UV range. TiO$_2$ specifically displays photo-absorption in the UV-light region below 400 nm, corresponding to band-gap energy of 3.76 eV. Notably, the optical absorptions of the α-Fe$_2$O$_3$/TiO$_2$ composites exhibit a noticeable red-shift in the visible light region compared to TiO$_2$, attributed to the presence of α-Fe$_2$O$_3$ in the composite powders. This observation suggests that α-Fe$_2$O$_3$/TiO$_2$ composites could serve as effective photocatalysts for utilizing sunlight as an energy source for contaminant reduction (Bouziani et al., 2020).
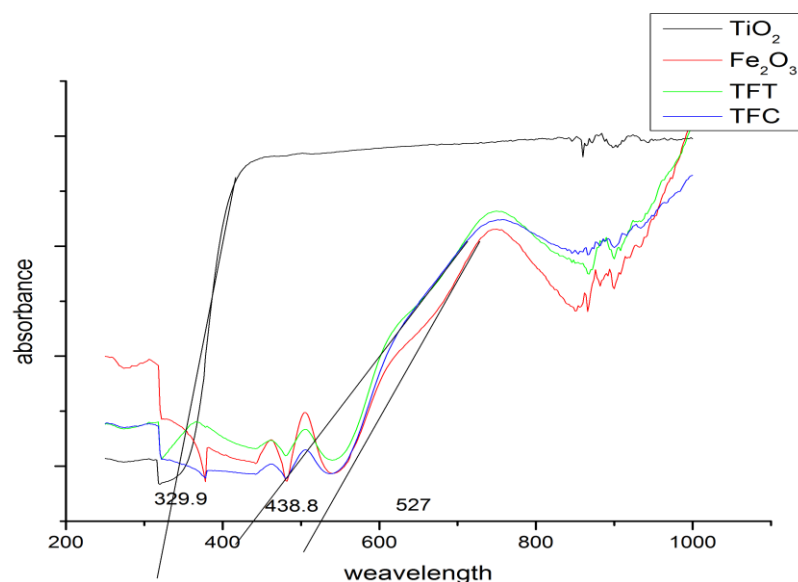
Figure 0-10 UV-DRS curves of α-Fe$_2$O$_3$ nanopowder, TiO$_2$ photocatalyst, doping TFT and TFC photocatalysts

In Figure 4.11, the diffuse reflectance spectra (DRS) obtained from 200-800 nm for DRS TiO$_2$ photocatalysis reveal optical absorption peaks at wavelengths of 329.9 nm, and TZC, and TZT codoped photocatalysis reveal 375.5 nm. The bandgap energy (Eg) for each sample was determined using Eq. (3.1). The calculated energy bandgap values were 3.76 eV and 3.02 eV for pure TiO$_2$ and codoped photocatalysis. The outcomes indicate an increase in wavelength attributed to the incorporation of TiO$_2$ into ZnO. This change in band gap is indicative of the impact of the doping process on the optical properties of the synthesized nanoparticles. Notably, the reduction in band gap is anticipated to enhance catalytic activity. The results agree with the literature (Alizadeh & Baseri 2022).
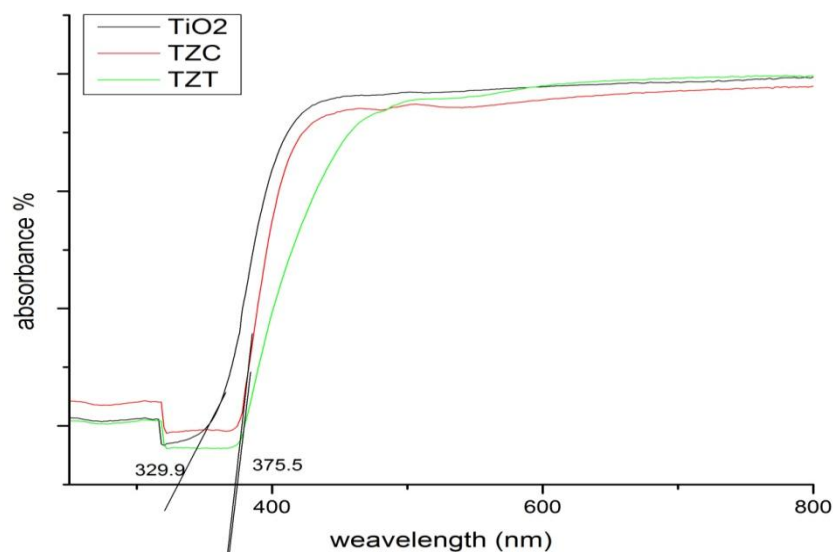
Figure 0-11 UV-DRS curves of TZT, TZC, and TiO_2 photocatalysts

4.1.2 Degradation of reactive blue dye under visible light irradiation

4.1.2.1 The effect of Initial concentration of the dye with the time of irradiation

The evaluation of the photocatalytic organic degradation of the blue dye using several concentrations of the dye (1, 2 and 3 mg/L) for the synthesis TiO_2 and doping TiO_2 with Fe_2O_3 using synthesis and commercial TiO_2 on different irradiation time was conducted and the results are illustrated in Fig (4.12, 4.13, and 4.14). The doped TiO_2 (TFT and TFC) exhibited superior removal efficiency in eliminating the blue dye compared to pure TiO_2 achieving a 100% removal percentage after two hour of sun light irradiation for the doped photocatlysts.
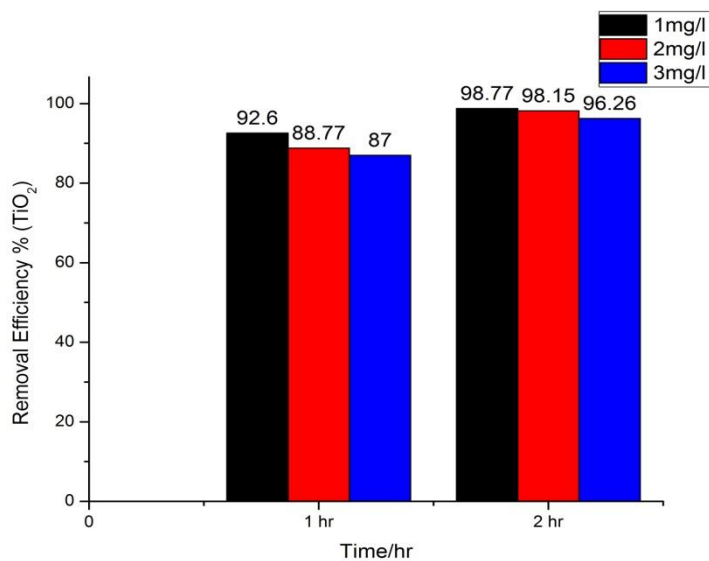
Figure 0-12 Removal efficiency % of blue dye using TiO_2 photocatalyst: Concentration
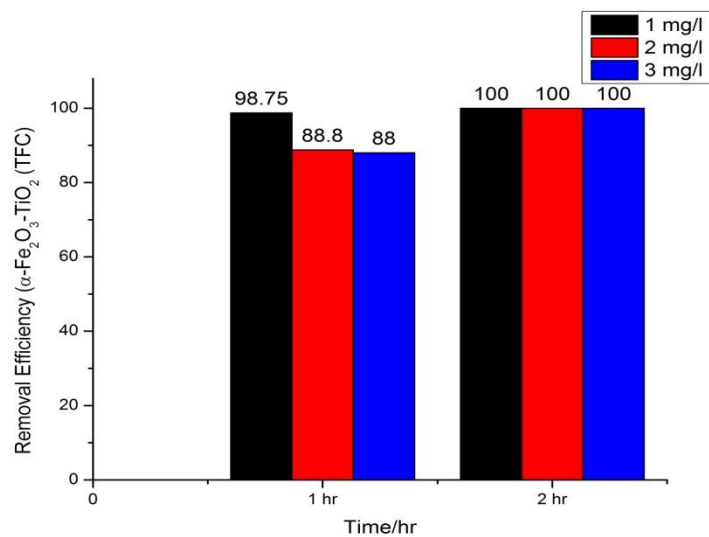
of dye Vs. Time

Figure 0-13 Removal efficiency % of blue dye using α-Fe_2O_3-TiO_2 (TFC) photocatalyst:

Concentration of dye Vs. Time
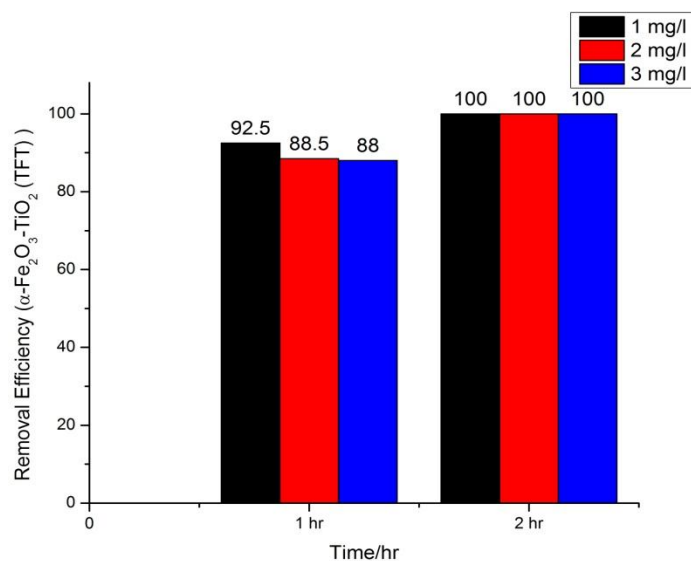
Figure 0-14 Removal efficiency % / hr of blue dye using α-Fe$_2$O$_3$-TiO$_2$ (TFT)

photocatalyst: Concentration of dye Vs. Time

The relationship between the initial concentration of the dye and removal efficiency for the pure ZnO is illustrated in Fig. 4.15. The degradation efficiency increased with increase in exposure time. The highest removal efficiency was 85% at dye concentration of 1 mg/l and 2hr of exposure to sunlight. The degradation efficiency was higher for lower dye concentration as expected. As the dye concentration increases, a decline in catalyst activity occurs, stemming from the accumulation of adsorbed compounds on the catalyst's surface.
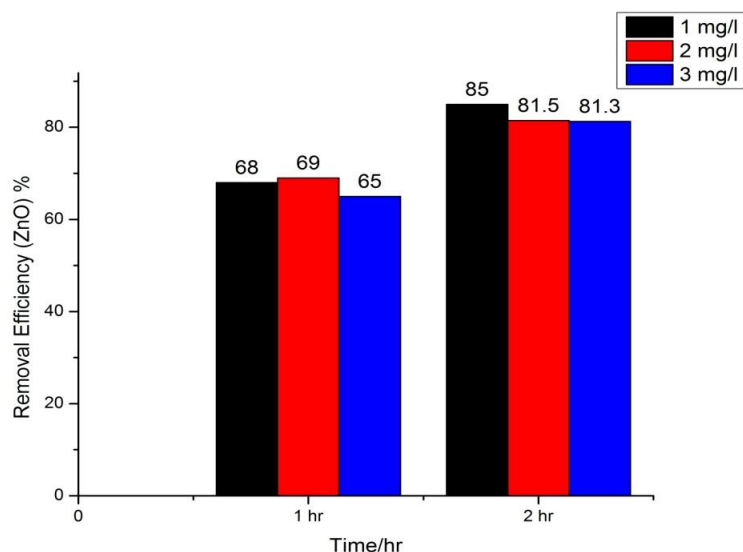
Figure 0-15 Removal efficiency % / hr of blue dye using ZnO photocatalyst:

Concentration of dye Vs. Time

In Figure (4.16 and 4.17), the effect of initial dye concentration on photodegradation for TZC and TZT photocatalysts is illustrated. The final concentrations of the dye were 87, 84, and 82 % for 1, 2, and 3 mg/l concentration of blue dye, respectively for TZC; and 100 % removal efficiency for the three concentrations of dye using TZT. As the blue dye concentration increases, the degradation efficiency decreases due to the reduction in catalyst activity caused by the heightened presence of adsorbed compounds on the catalyst's surface (Alizadeh & Baseri 2022). The removal efficiency of TZT was higher than TZC and reached 100%. This was attributed to the lower band gap (shift towards visible light region) of TZT (3.02 eV) compared to that of TZC (3.22 eV)). This shift resulted in absorption of visible light as confirmed by UV DRS results.

Regarding how the duration of reaction contact influences degradation efficiency. There was a direct correlation between degradation and irradiation time Figure (4.16 and 4.17). The utilization of a solar concentrator further contributes to the degradation process. The removal efficiency for TZC improved from (68, 67.7, and 65.2)% to (87, 84, and 82) %

for 1, 2, and 3mg/l blue dye, respectively as irradiation time was increased from 1 to 2 h. Whereas using TZT, the performance improved to 100% for all the concentrations of reactive blue dye. This demonstrated the efficacy of the synthesized TiO2 doped ZnO nanocatalyst (TZT) in the degradation process.
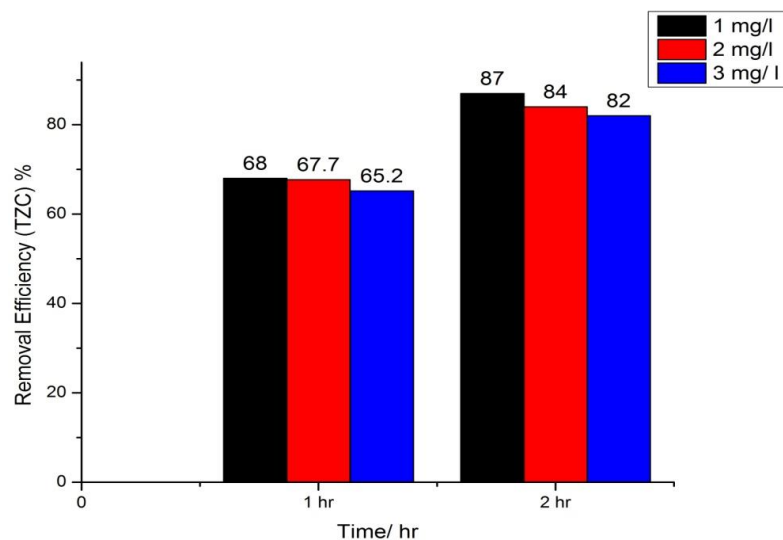
Figure 0-16 Removal efficiency % / hr of blue dye using ZnO - TiO$_2$ (TZC)

photocatalyst: Concentration of dye Vs. Time
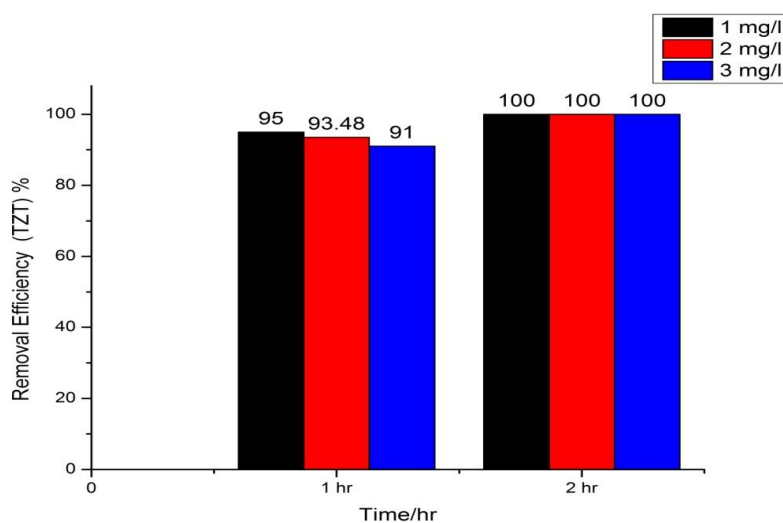
Figure 0-17 Removal efficiency % / hr of blue dye using ZnO - TiO$_2$ (TZT)

photocatalyst: Concentration of dye Vs. Time

4.1.2.2 The effect of solution pH

The resulting removal percentages were plotted as a function of pH in the 3–11 range, as illustrated in Figures 4.18, 4.19, 4.20, 4.21, 4.22 and 4.23. The degradation of Reactive Blue 171 dye was more effective in acidic and neutral pH ranges when utilizing bare (TiO_2, ZnO) or codoped (TFT, TFC, TZT, and TZC) photocatalysts. This observation can be attributed to the point of zero net charge (PZC) of the photocatalysts, which is at pH 6.8. In an acidic solution (pH<6.8), the photocatalysts carry a positive charge, while Reactive Blue 171 exhibits a negative charge due to the sulfonic group present. This favorable electrostatic interaction promotes the adsorption of the anionic Reactive Blue 171 dye onto the surface of the photocatalyst.

In this scenario, the positively charged the photocatalysts actively attract and adsorb more dye molecules onto its active sites, leading to an enhancement in the degradation efficiency of Reactive Blue 171. Previous literature has also linked photocatalytic activity with the adsorption of dye molecules onto the surface of photocatalysts, as reported by (Aguedach et al., 2005; Daneshvar et al., 2003; Najafi et al., 2022; Samsudin et al., 2015).

At elevated pH levels, photocatalysts assume a negative charge as the pH surpasses the point of zero net charge (PZC). The repulsion between the negatively charged photocatalysts and the similarly negatively charged dye molecules impedes the adhesion of dye molecules to the catalyst surface. Consequently, the photodegradation process becomes more challenging, as the degradation facilitated by electron-hole pairs (hv_B^+) and conduction-band electrons (e_{CB}^-) is obstructed. The hydroxyl radicals generated by the photocatalysts play a crucial role in degrading dye molecules. However, in alkaline

conditions, the presence of OH⁻ interrupts the photodegradation process. This interruption occurs because OH⁻ induces the formation of intramolecular hydrogen bonds in electron-donating groups, such as ⁻NH₂ located in the α-position of the carbonyl group of Reactive Blue 171. This leads to increased chemical stability of the dye, making it more resistant to attack by hydroxyl radicals. Consequently, a decrease in photocatalytic activity is observed in alkaline solutions due to these hindrances in the degradation process. This effect has been previously documented, as reported by (Samsudin et al., 2015).
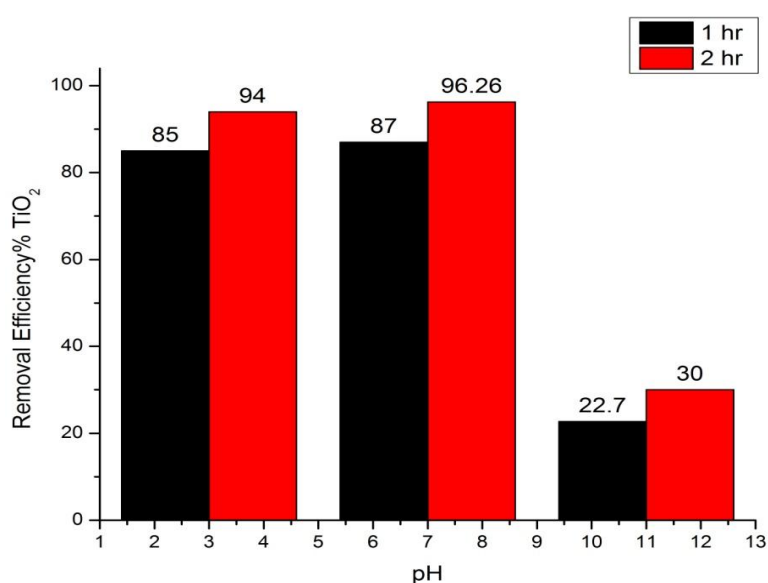
Figure 0-18 Removal Efficiency % of TiO₂ Vs. pH within 1 and 2 hr irradiation time
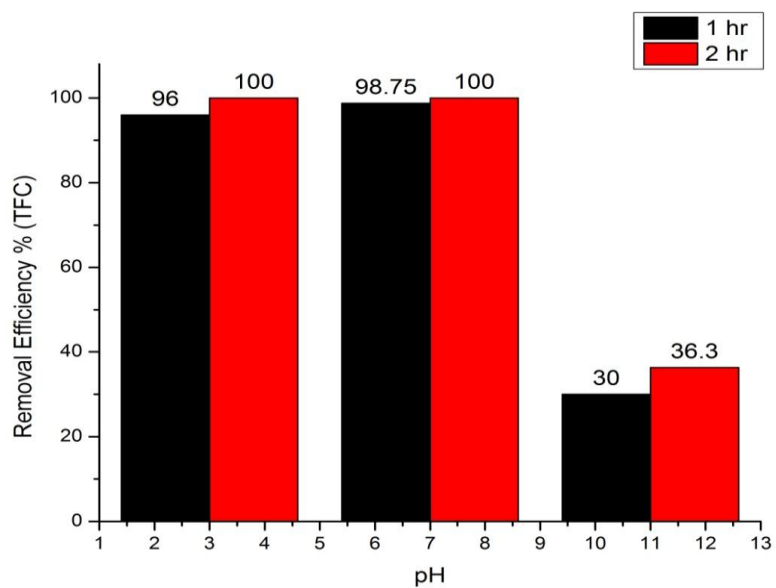
Figure 0-19 Removal Efficiency % of TFC Vs. pH within 1 and 2 hr irradiation time
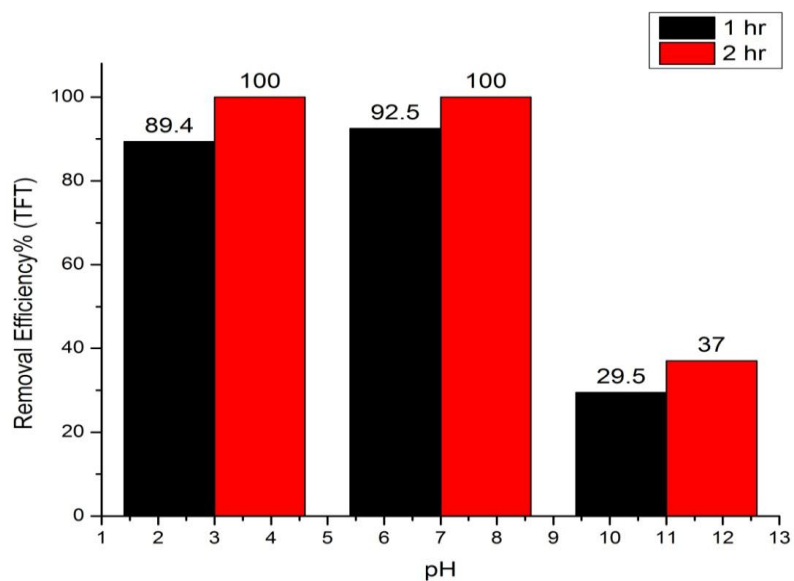
Figure 0-20 Removal Efficiency % of TFT Vs. pH within 1 and 2 hr irradiation time
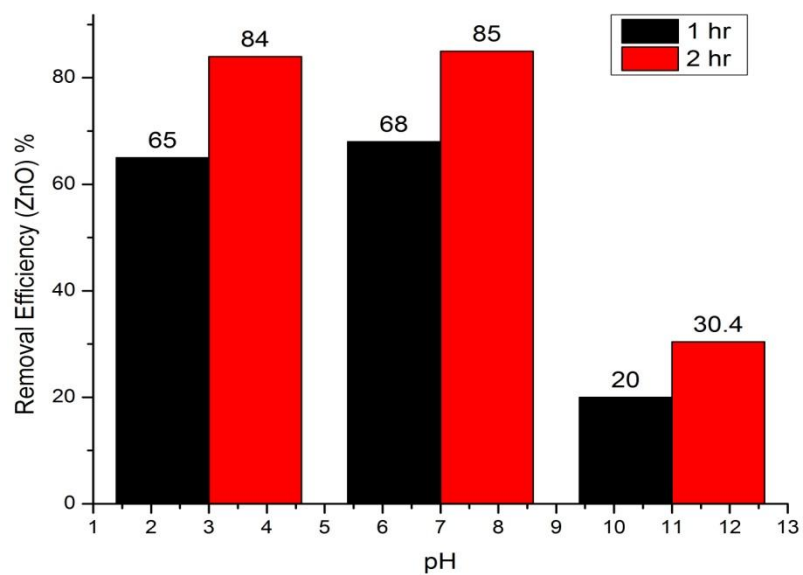
Figure 0-21 Removal Efficiency % of ZnO Vs. pH within 1 and 2 hr irradiation time
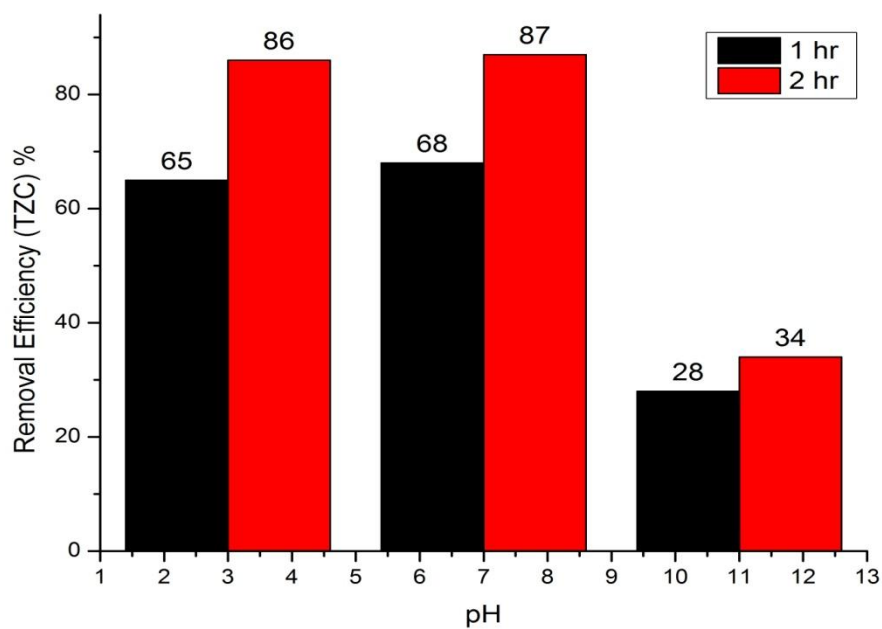
Figure 0-22 Removal Efficiency % of TZC Vs. pH within 1 and 2 hr irradiation time
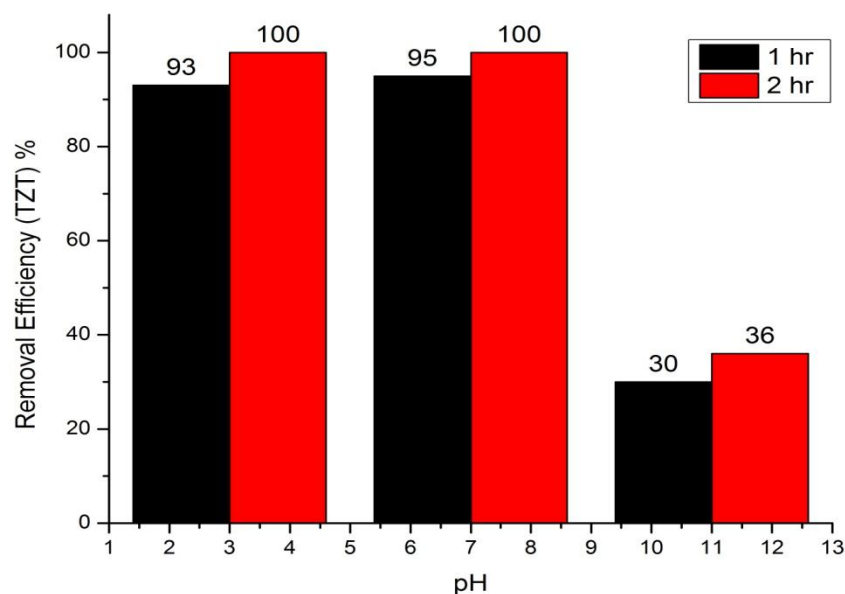
Figure 0-23 Removal Efficiency % of TZT Vs. pH within 1 and 2 hr irradiation time

4.1.2.3 The stability & reusability of nanophotocatalysts

The findings of the study, presented in Figure 4.24, provide insights into the stability and activity of the photocatalyst over four consecutive cycles. This emphasizes the practical importance of understanding how well the catalyst maintains stability and efficacy across multiple usage instances, offering valuable insights into its suitability for large-scale applications with economic and environmental considerations. Notably, the results in Fig. 4.24 indicate that after the fourth cycle, the reactive blue dye removal efficiency has only decreased by about 13.06 % for bare TiO_2, 11.1 % for Fe_2O_3-TiO_2 (TFC), 9.7 % for Fe_2O_3-TiO_2 (TFT), 13 % for ZnO, 12.9 % for ZnO – TiO_2 (TZC), and 11 % for ZnO – TiO_2 (TZT) confirming the significant activity and high stability of the nanocomposite.
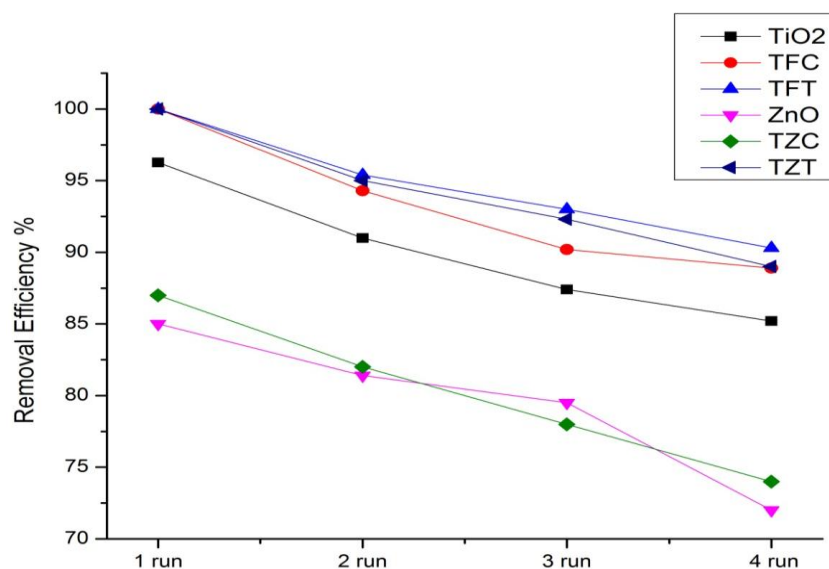
Figure 0-24 Evaluation of the stability

The obtained results from the evaluation of the stability and activity of 1 mg/L initial dye concentration in TiO_2, TFC, TFT, TZC, and TZT in 20 ml solution up to 4 consecutive cycles

4.1.2.4 Comparison of bare and doped TiO_2 nanophotocatalysts with other nanophotocatalysts

The TiO_2 nanophotocatalyst stands out as a unique semiconductor with excellent photodegradation activity. While TiO_2 typically requires a UV source or doping with metal or metal oxide to effectively absorb sunlight irradiation as reported by (Mahmoodi et al., 2018) , even a concentration of 0.004 g/L of TiO_2 demonstrates significant efficiency, removing 96.26% of a 1 mg/L dye solution under sunlight irradiation. Moreover, the introduction of Fe_2O_3 or ZnO through doping enhances its performance, achieving 100% removal efficiency after 120 minutes of sunlight irradiation. Table 4 compiles findings from various studies exploring nanoparticle applications for organic dye removal in wastewater. Notably, codoped TiO_2 emerges as the most promising

option, offering the highest removal efficiency. Its ability to operate under sunlight irradiation is a key advantage, contributing to cost reduction and utilizing clean energy sources.

Table 0-2 Comparison of various nanophotocatalysts removal efficiency of organic dyes considering the source of light and experimental conditions

Nanophotocatalytic type	Photocatalytic Dosage ($g L^{-1}$)	Time (min)	Pollutant	Source of light	Removal/efficiency (%)	Ref.
Anatase Nano-TiO_2	1.00	40	Reactive Blue 4	125 W UV lamp/ sun light	100	(Samsudin et al., 2015)
N-Cu, N-Fe and N codoped TiO_2 and Bare TiO_2	0.06	5	RB 4 dye	100 W halogen lamp	100, 84, 80 and 75	(Kaur et al., 2015)
TiO_2	1.00	120	Procion Navy H-EXL (PN)	UV-LED	100	(Tapia-Tlatelpa et al., 2019)
$CoAl_2O_4$	0.25	150	navy blue	UVA lamps 75Watts	42-67	(El Jabbar et al., 2019)
ZnO	0.01--0.06	20	reactive blue 203	8W UV lamp	99.1	(Bagheri et al., 2020)
TiO_2, Fe_2O_3 and TiO_2-Fe_2O_3	60.00	60	Titan Yellow and Methyl Orange	UV lamp	92.98, 71.67 and 62.89% for TY	(Kumar et al., 2020)
Cu_2SnS_3 + GO	0.40	240	Navy Blue ME2RL	300 W xenon lamp	88	(Shelke et al., 2023)
ZnO	0.004	120	Navy Blue 171	Sun light	85	This work
Bare TiO_2 and TiO_2-Fe_2O_3	0.004	120	Navy Blue 171	Sun light	96.26 and 100	This work (Suliman et al., 2024)
TiO_2-ZnO	0.004	120	Navy Blue 171	Sun light	87 and 100	This work

4.1.3 Characterization of the polyester membranes

4.1.3.1 The optical properties of the polyester membranes

Fig. 4.25 (a…f) displays the digital microscope images of uncoated and coated membranes. Fig 4.25 (a) represented the uncoated membranes, it is polyester/ cotton fabric without any treatment, and it was used as a control to compare with other coated membranes. In Fig. 4.25 (b and c), a noticeable alteration in the color of the membrane fibers is observed, transitioning from white to red. This color change is attributed to the presence of TiO_2- α-Fe_2O_3, providing compelling evidence of a successful impregnation process for the PTFT and PTFC.

Figures 4.25 (d, e, and f) present images of coated polyester membranes with TZT, TZC, and pure ZnO respectively, upon visual examination as shown in the three images a slight change in the color of the membranes is evident, appearing lighter due to the gray hue of ZnO. However, a more detailed assessment of nanolevel surface morphology using Electron Microscopy (SEM) exposes noticeable alterations in the fibers of the coated fabric.
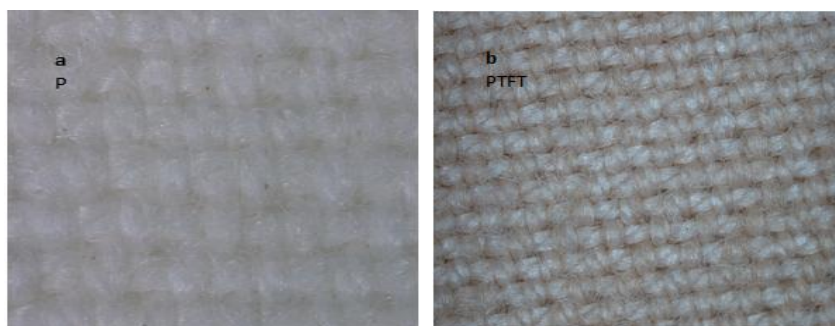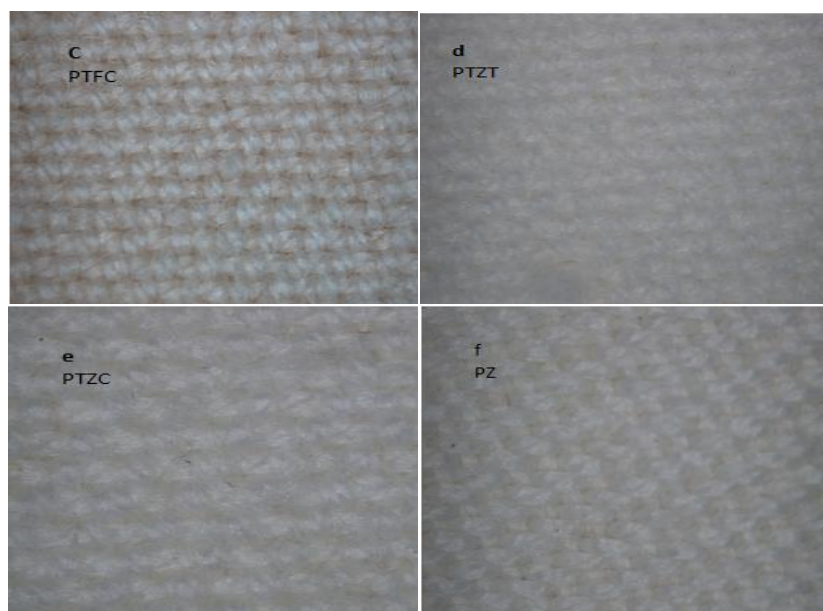
Figure 0-25 Digital microscope images of the membranes

(a) Uncoated membranes and (b) Coated membranes with TFT, (c) Coated membranes with TFC, (d) Coated membranes with TZT, (e) Coated membranes with TZC, and (f) Coated membranes with ZnO

4.1.3.2 SEM and EDX analysis

Fig. 4.26 illustrated SEM micrographs of the coated membrane surface by TFT and TFC captured at magnifications of 100.00 k X and 5.00 k X, The images revealed the presence of a substance on the coated membrane surface, which was hypothesized to be TiO_2- α-Fe_2O_3 NPs.

The images depict a somewhat porous and clustered morphology within the samples, indicating potential benefits for improving properties. Notably, both large and small particles of nearly identical sizes were observed in the images. The results suggest that the particle size of the photocatalyst synthesized from the Titanium precursor is smaller compared to that of commercially available Titanium, which agree with SEM of the TFT and TFC photocatalysts in section (4.1.1) fig (4.2 & 4.3).

EDX analysis of the PTFT and PTFC coated membranes, as depicted in Fig. 4.27,

illustrates the chemical composition. It revealed distinct peaks in the spectrum, confirming the presence of 1.51 % Ti, % 46.60 O, 51.18 % C, and 0.70 % Fe in the PTFT coated membrane and 0.33 % Ti, 46.53 % O, 52.9 % C, and 0.25 % Fe in the PTFC coated membrane. The elemental composition attests solely to the presence of the fabric membrane and photocatalyst material, confirming the high purity and success of the impregnation process.
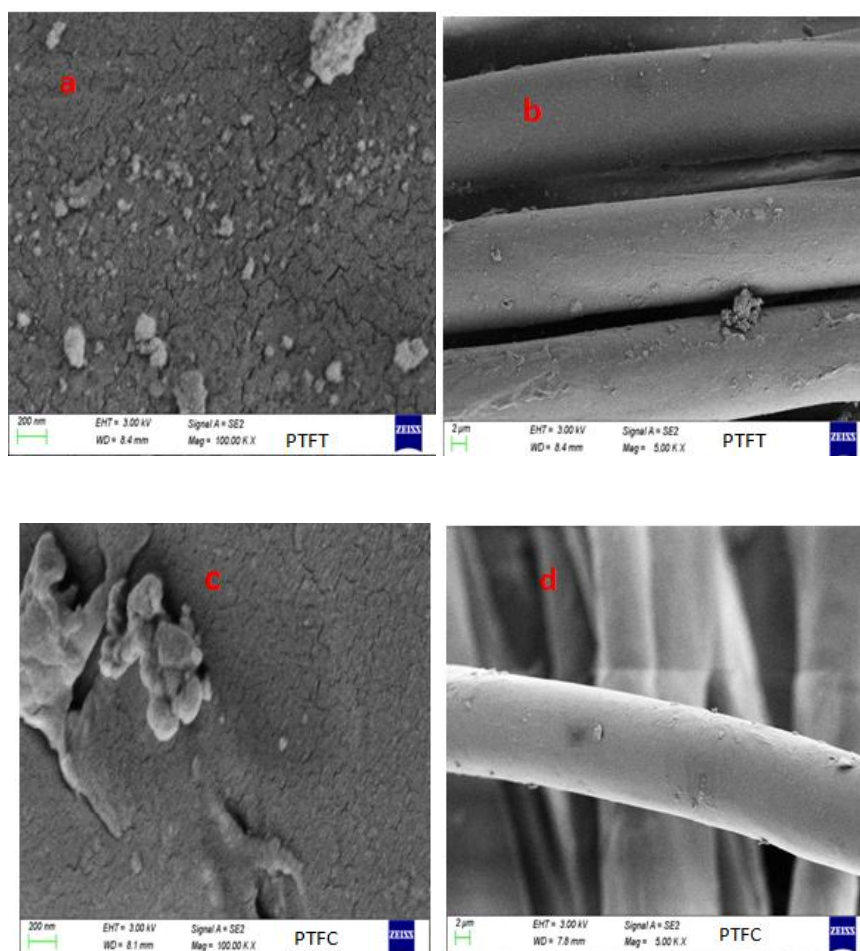
Figure 0-26 SEM images of PTFT and PTFC coated membranes

(a & b) PTFT and (c & d) PTFC at 100kx and 5 kx magnifications
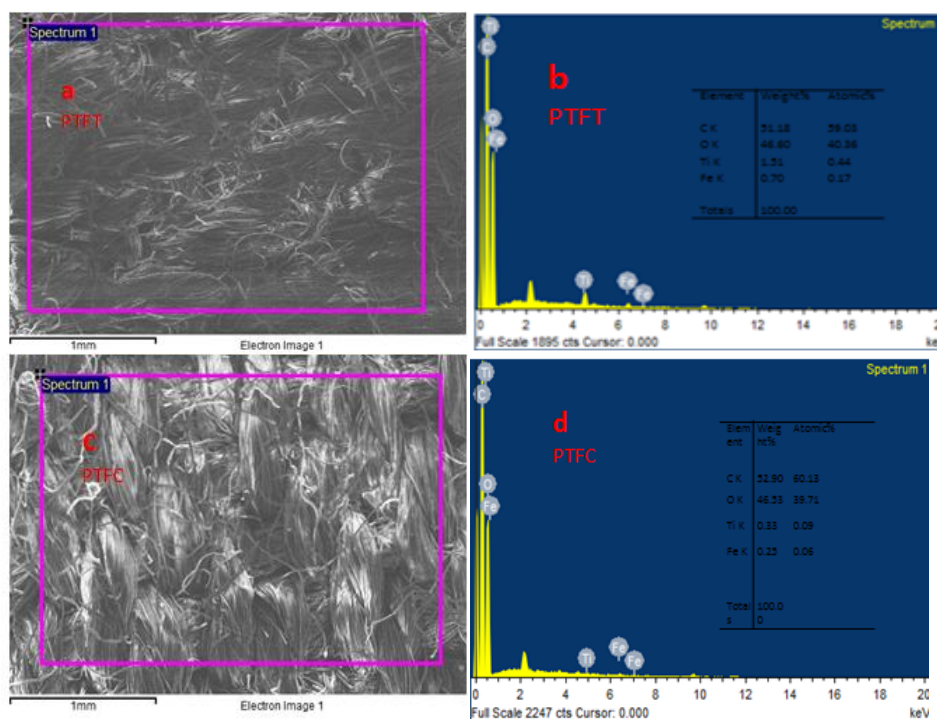
Figure 0-27 EDX images of PTFT and PTFC coated membranes

(a & b) PTFT and (c & d) PTFC showing the chemical composition

SEM images Fig.4.28 of the coated membrane surface by TZT and TZC, captured at magnifications of 100.00 k X and 5.00 k X respectively, depict clusters believed to be TiO_2-ZnO nanoparticles. The images reveal a porous and clustered morphology, suggesting potential enhancements in properties. Interestingly, both large and small particles of nearly identical sizes were observed. The uniform distribution of elements such as Zn, Ti, and O across the sample confirms their presence, validating the successful synthesis of ZnO/TiO_2 photocatalysis. Notably, particles of ZnO-TiO_2 produced from commercial TiO_2 were tended to agglomerate into the membranes surface and made big clusters more compared to particles produced from synthesized TiO_2, as seen in the SEM images.

The chemical composition of the PTZT and PTZC coated membranes is shown by EDX

analysis, as shown in Fig. 4.29. It showed clear peaks in the spectrum, indicating that the coated membrane with mixed oxide nanocomposite contained 0.32 % Ti, 43.36 % O, 51.57 % C, and 4.25 % Zn for PTZT membranes and 0.49 % Ti, % 43.12 O, 53.32 % C, and 0.57 % Zn for PTZC membranes verifies the excellent purity and efficacy of the impregnation process only by attesting to the existence of the fabric membrane and photocatalyst material.
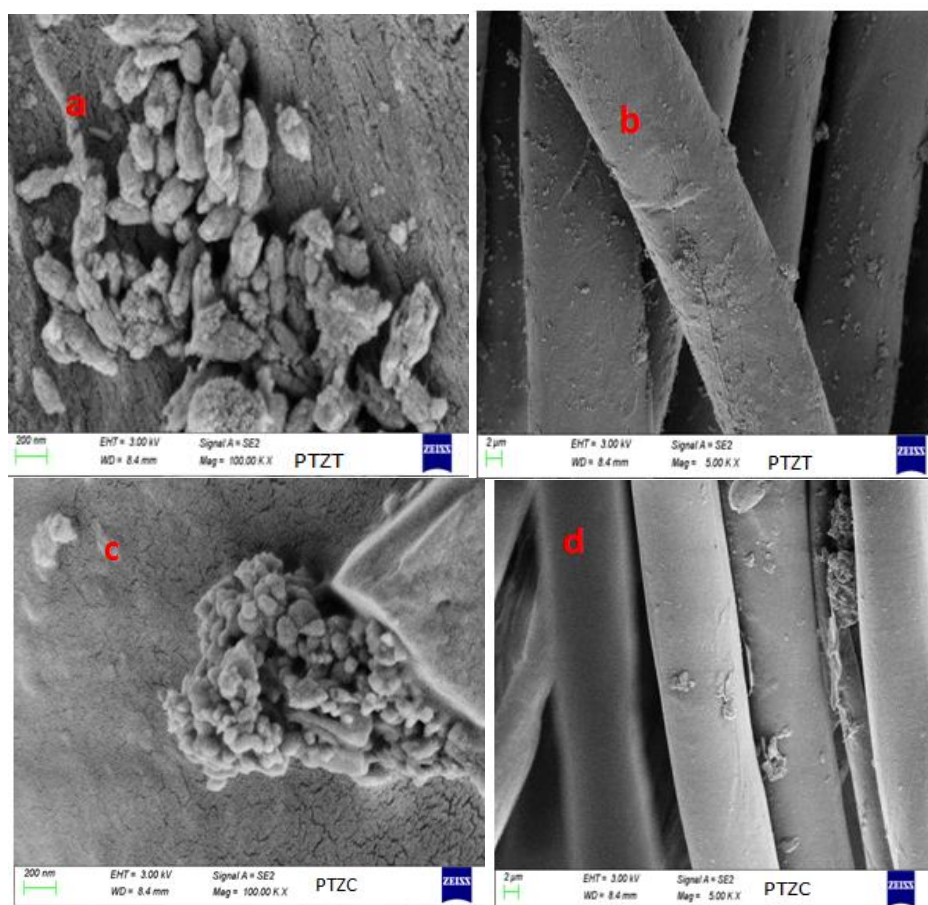
Figure 0-28 SEM images of PTZT and PTZC coated membranes

(a & b) PTZT and (c & d) PTZC at 100kx and 5 kx magnifications
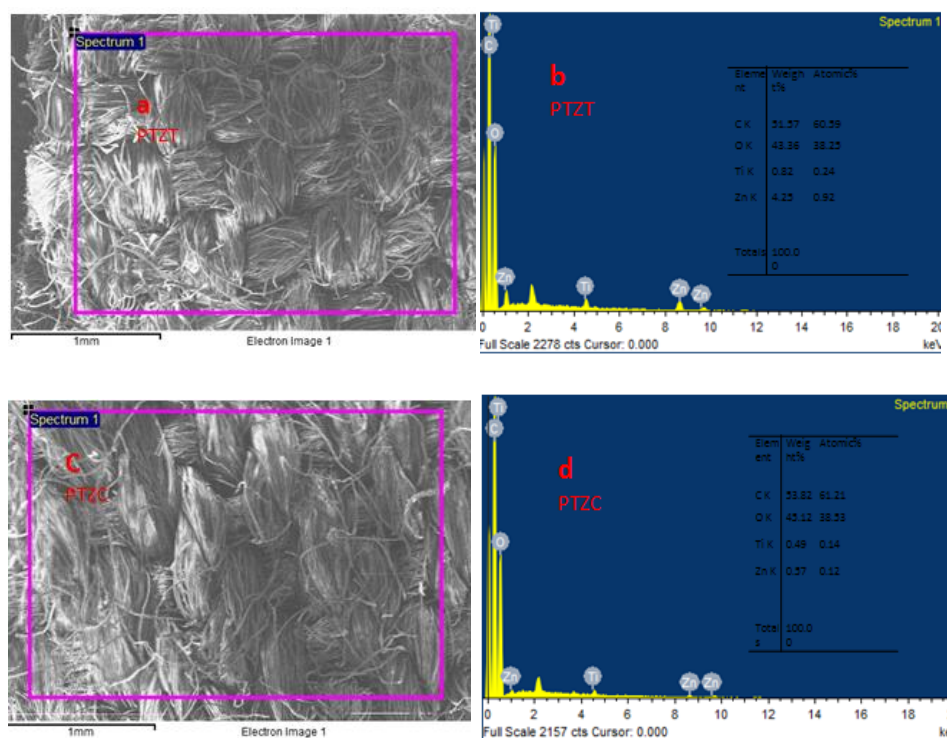
Figure 0-29 EDX images of PTCT and PTZC coated membranes

(a & b) PTZT and (c & d) PTZC showing the chemical composition

In Figure 4.30, the visualization illustrates the presence of ZnO nanoparticles located on the coated polyester membranes. The image showcases the clustering of these nanoparticles on the surface of the coated fabric. These clusters serve as confirmation for the successful synthesis of ZnO on the polyester fabric, providing substantiation for the effective impregnation of cotton fabric with ZnO nanoparticles. Additionally, the even distribution of zinc and oxygen elements on the fiber surface was noted.

EDX tests were used to confirm the elemental composition of the ZnO coated polyester membranes, resulting in a thorough understanding of the constituent elements of the synthesised photocatalyst as depicted in Fig. 4.31 contains 0.93 % Zinc, % 52.93 carbon and 46.12 % oxygen, demonstrating the material's effective processing.
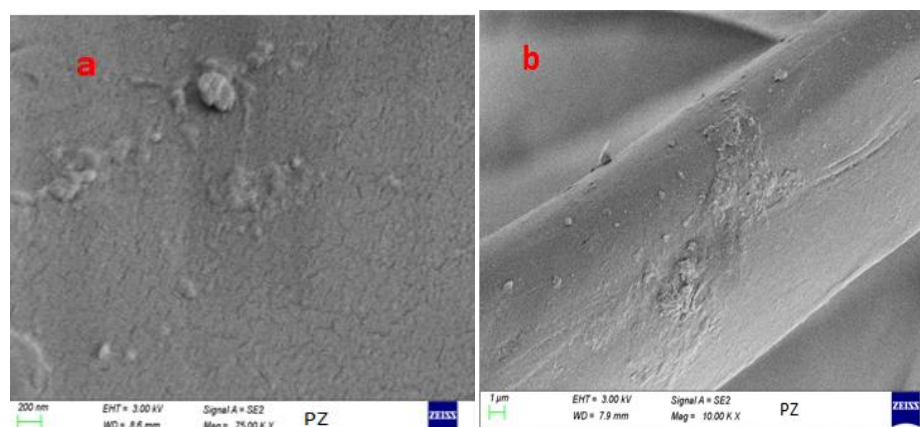
Figure 0-30 SEM images of coated membranes (PZ) at 100kx and 5 kx magnifications
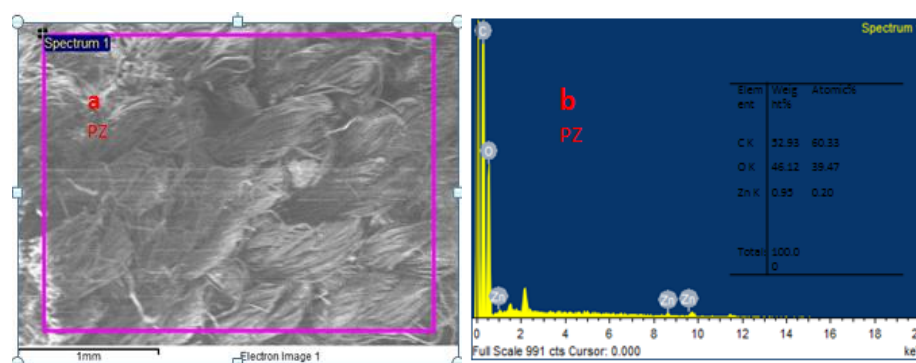
Figure 0-31 EDX images of the coated membranes (PZ) showing the chemical composition

4.1.3.3 XRD analysis

The XRD patterns (Fig.4.32) for PTFT and PTFC coated membranes and uncoated membranes, composed of a blend of polyester and cotton fabric, reveal distinctive features of each material's crystalline structure. The X-ray diffraction pattern of cotton exhibits prominent diffraction peaks at 2θ values of 15 and 22.6, while the polyester pattern shows clear peaks at 2θ values of 16.6, 22.6, and 25.2 (Muthukumar & Thilagavathi, 2012). The diffraction peaks observed in both treated and untreated membranes correspond to the crystal structure of the fabrics, revealing a semi-crystalline nature. This suggests that the treatment applied to the membrane surface does not alter

the original crystalline structure of the untreated textile, irrespective of the heterogeneous modification. The crystallinity observed is indicative of the molecular arrangement and tightness within the fabric (Dong et al., 2020; El-Naggar et al., 2021)
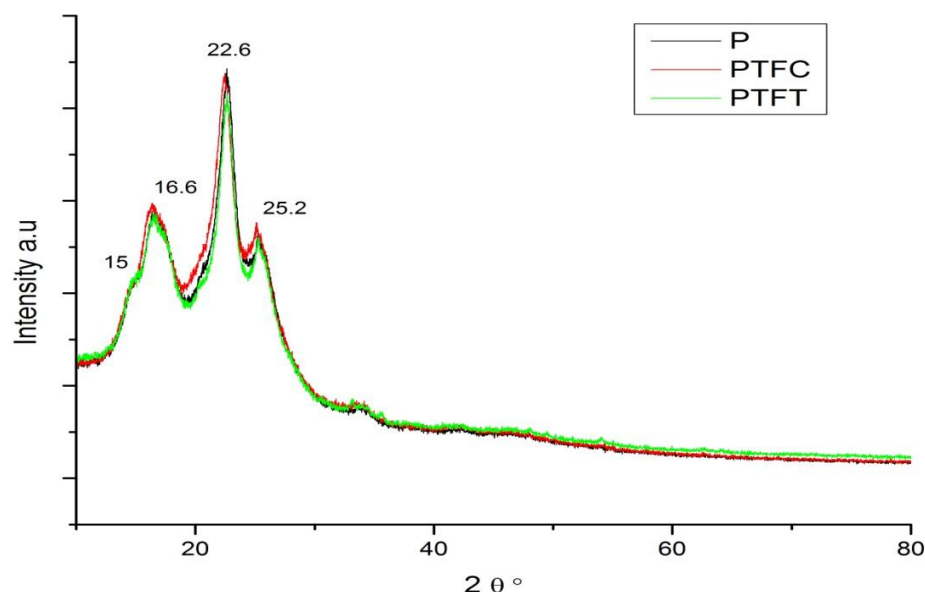
Figure 0-32 XRD curves of PTFT and PTFC coated and P uncoated membranes

The XRD patterns (Fig.4.33) for coated membranes PTZT and PTZC as well as uncoated membranes made of a mixture of polyester and cotton fabric highlight unique aspects of the crystalline structure of each material. While there are distinct peaks in the polyester pattern at 2θ values of 16.6, 22.6, and 25.2, the cotton X-ray diffraction pattern has notable peaks at 22.6 and 15 (Muthukumar & Thilagavathi, 2012). The diffraction peaks seen in the membranes, both treated and untreated, are semi-crystalline because they match the textiles' crystal structure. The diffraction peaks of PTZC are corresponded with diffraction peaks of the uncoated membranes this shows that the original crystalline structure of the untreated textile is not changed by the treatment that is applied to the membrane surface. In the opposite the diffraction peaks of PTZT showed the polyester cotton with shift in peak 16.6 to 16.47 and 15 to 14.4 plus additional peaks at 2θ 31.65,

34.2, 36.11, 47.47, 56.37, 62.6, and 67.7. These characteristic peaks are attributed to the (100), (002), (101), (102), (110), (103), (200), (112), (201), (004), and (202) crystallographic planes, respectively, aligning with the wurtzite hexagonal phase of ZnO (JCPDS No. 36-1451). The identified diffraction peaks are in accordance with existing literature (Ma et al., 2013). Moreover, the existence of two supplementary peaks at 25.2 and 47.47 degrees, corresponding to the diffraction planes (101) and (200), respectively, signifies the presence of the anatase phase of TiO_2 within the analyzed sample (Abdel-Wahab et al., 2017a; Ijadpanah-Saravy et al., 2014; Theivasanthi & Alagar, 2013). According to the EDX study result, the amount of Ti and Zn in the PTZT coated membranes is greater than that of other photocatalysts, which is one explanation for why the diffraction peaks of TZT photocatalysts show in the XRD pattern.
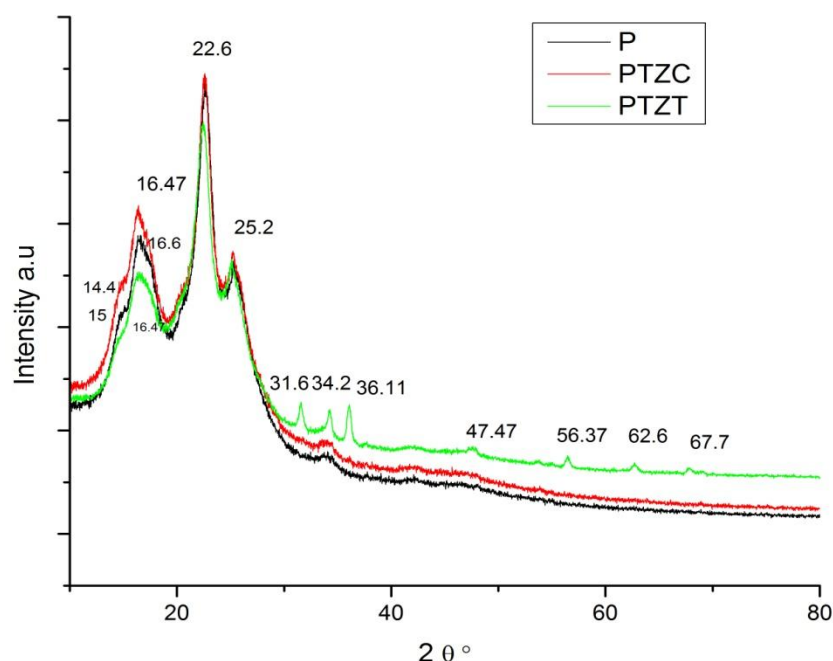
Figure 0-33 XRD curves of PTZT and PTZC coated and P uncoated membranes

Fig.4.34 depicted the X-ray diffraction (XRD) patterns of both PZ coated and uncoated

membranes, composed of a blend of polyester and cotton fabric, display distinct characteristics corresponding to the crystalline structure of polyester and cotton materials. Cotton exhibits clear diffraction peaks at 2θ values of 15 and 22.6, whereas polyester shows notable peaks at 2θ values of 17.1, 22.6, and 25.2 .These semi-crystalline diffraction peaks reflect the inherent crystal structure of the textiles, indicating that the surface treatment applied to the membrane does not alter the original crystalline arrangement of the untreated textile, irrespective of the heterogeneous modification. The observed crystallinity provides valuable insights into the molecular configuration and compactness of the fabric.
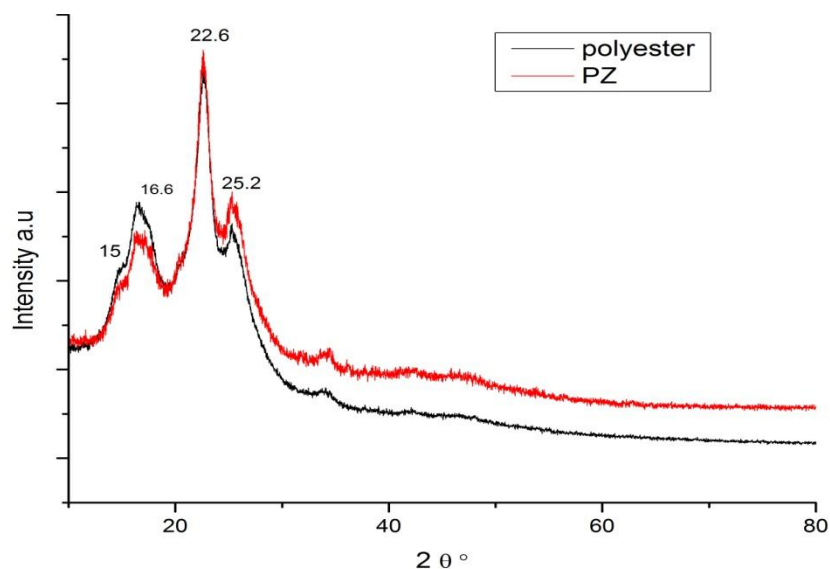
Figure 0-34 XRD curves of PZ coated and P uncoated membranes

4.1.3.4 FTIR analysis

The FTIR analysis of both uncoated and coated fabric was conducted across the range of 500 cm^{-1} to 4000 cm^{-1}, revealing the distinctive features of the cotton and polyester components. The FTIR spectra Fig.4.35, 4.36, and 4.37 displayed characteristic peaks

representing functional groups in the membranes. Notably, peaks at 1162 cm^{-1} and 1709 cm^{-1} were identified in both the uncoated and coated fabric spectra. This confirmation of the presence of these peaks indicated that the membranes were predominantly polyester-based (Agrawal et al., 2020).

Cotton fibers typically display distinctive absorption bands, vibrational modes C=O stretching, C–O stretching, and O–H deformation in the 1,200 to 1,700 cm^{-1} range (Vaideki et al., 2007). The presence of a trace amount of HO-C=O is evidenced by a peak around 2,800 cm^{-1} (Krishnamoorthy et al., 2012). In the spectrum of the cotton-OH sample, a substantial absorption band within the 3600–3000 cm^{-1} range is attributed to the free OH stretching vibration and intra- and intermolecular hydrogen bonds associated with cellulose's chemical structure (Dochia et al., 2018). In the 3000–2800 cm^{-1} range, several narrow bands related to the stretching vibrations of methylene and methine groups are observed, typically showing a single absorption band in samples consisting only of cellulose (Alosmanov et al., 2017; Ma et al., 2021; Salama & El-Sakhawy, 2016). The band width observed between 1700 and 1500 cm^{-1} is influenced not only by the bending vibrations of H–OH bonds due to the presence of adsorbed water but also by peaks associated with asymmetric stretching vibrations of carboxyl groups in pectin acid and pectate. Furthermore, a small peak at 888 cm^{-1} is indicative of the presence of pectin (Alosmanov et al., 2022).

There was no notable distinction in the FTIR peaks observed between the uncoated and coated membranes. Similar findings were reported in other studies, such as (Mecha & Pillay, 2014) where AgNPs-coated polyester membranes showed no significant shift in peaks compared to their uncoated counterparts. This lack of discernible difference was

attributed to the relatively low amount of NPs present on the membranes, leading to an absence of significant chemical bonding. Another expected explanation; the photocatalysis particles were mechanically trapped on the surface of the membranes so they didn't appear in the FTIR pattern.
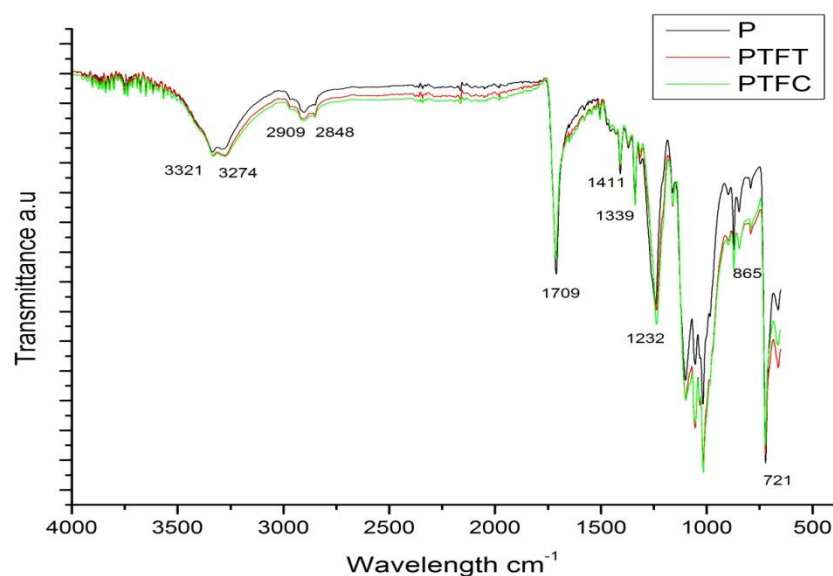
Figure 0-35 FTIR curves of PTFT and PTFC coated and P uncoated membranes
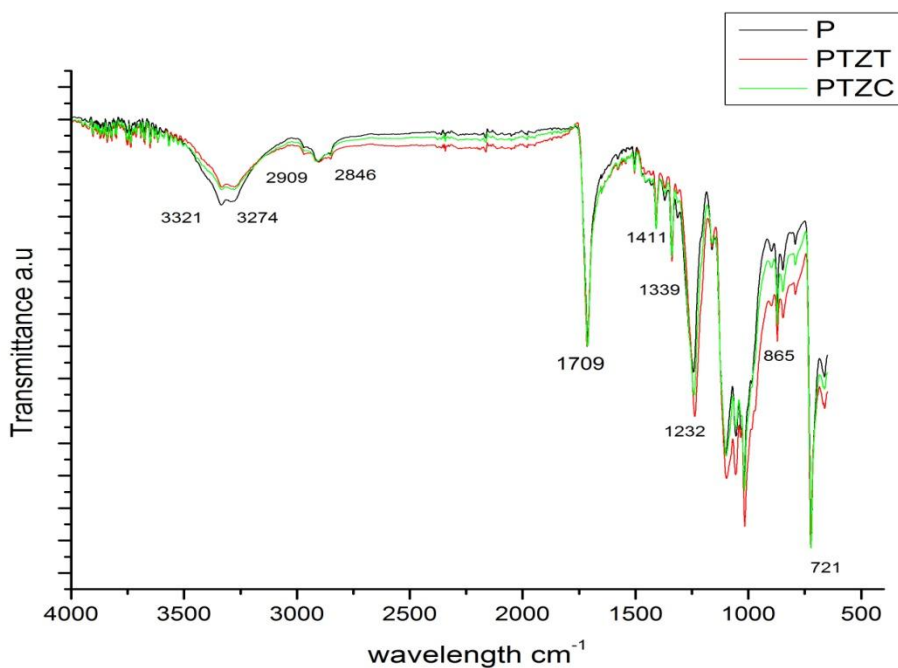
Figure 0-36 FTIR curves of PTZT and PTZC coated and P uncoated membranes
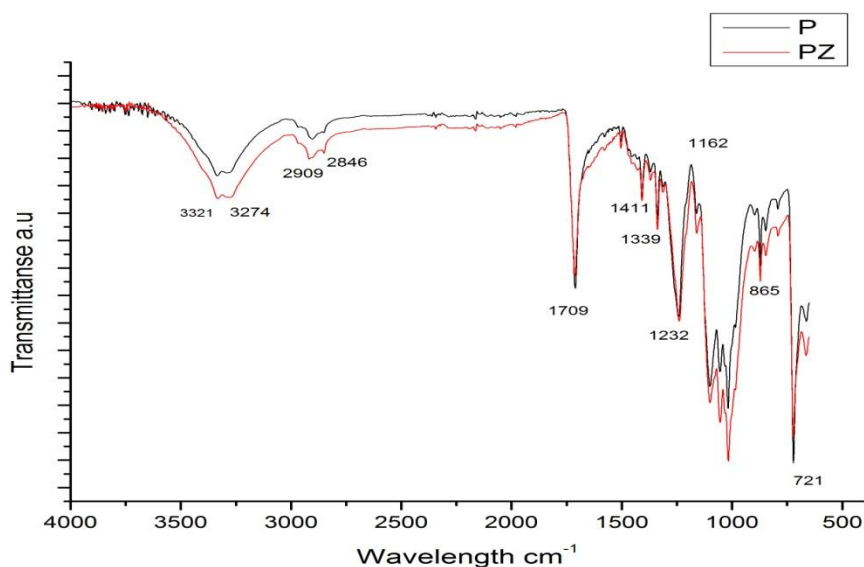
Figure 0-37 FTIR curves of PZ coated and P uncoated membranes

4.2 Treatment of wastewater targeting organic and microbial contaminants

4.2.1 Synthetic feed water with oxytetracycline (OTC)

Figure (4.38), (4.39), and (4.40) illustrate the percentage of removal efficiency for OTC concentrations of 1, 2, and 3 mg/L, respectively, over 30, 60, and 90 minutes using various membrane coatings including PTFT, PTFC, PTZT, PTZC, and PZ, alongside uncoated P membranes. Among these, PTFT and PTZT, both coated with synthesized titanium dioxide through doping, exhibited the highest removal efficiencies. Specifically, they achieved 88.167% (PTFT) and 86.157 % (PTZT) removal for 1 mg/L OTC, 55.654 % (PTFT) and 51.887 % (PTZT) for 2 mg/L OTC, and 51.012 % (PTFT) and 48.668 % (PTZT) for 3 mg/L OTC.

The removal efficiency of the coated membranes with doping synthesis titanium dioxide showed a slight decrease (less than 4 %) when compared to the membranes with doping commercial titanium dioxide. For comparing PTFT and PTFC it decreased 1.5 % for 1 mg/L TOC, 2.51 % for 2 mg/L OTC, and 2.34 % for 3 mg/L OTC concentration. And for

comparing PTZT and PTZC it decreased 2.01 % for 1 mg/L TOC, 2.26 % for 2 mg/L OTC, and 3.35 % for 3 mg/L OTC concentration. Additionally, across all three figures, it was observed that ferric oxide demonstrated faster organic degradation compared to zinc oxide. However, after 90 minutes of operation under direct sunlight irradiation using the solar unit, the removal efficiencies of both ferric oxide and zinc oxide-coated membranes were relatively close to each other. The degradation mechanism is faster in the titanium dioxide doped with ferric oxide because the band-gap energy shifts more towards the visible region 2.83 eV (Bouziani et al., 2020) compared to the titanium dioxide doped with zinc oxide 3.02 eV (Alizadeh & Baseri, 2022).
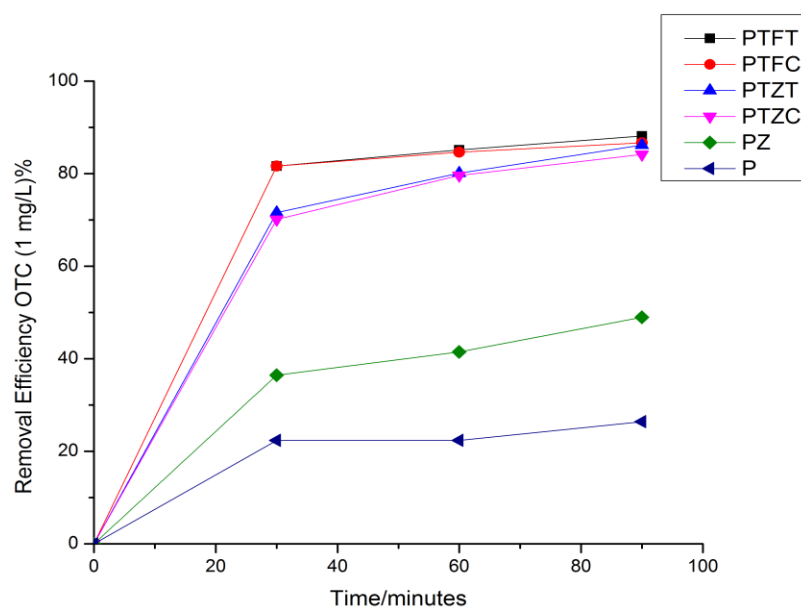
Figure 0-38 Removal Efficiency % of 1 mg/L OTC using coated and uncoated membranes
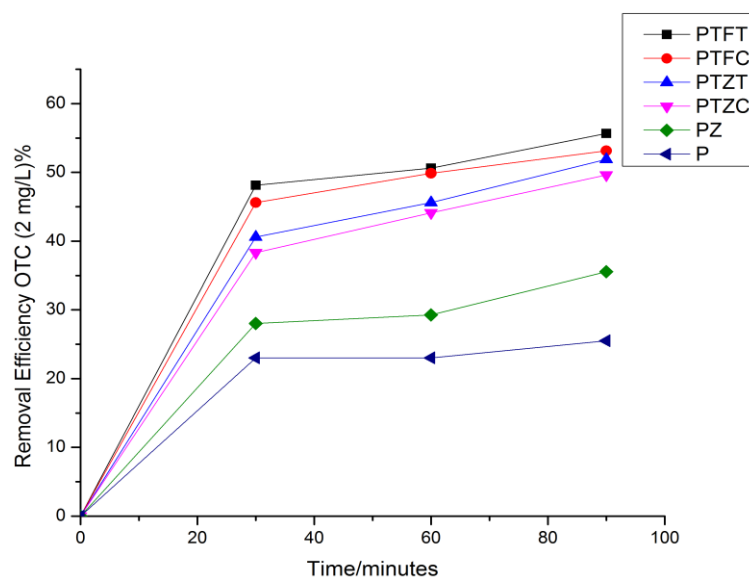
Figure 0-39 Removal Efficiency % of 2 mg/L OTC using coated and uncoated membranes
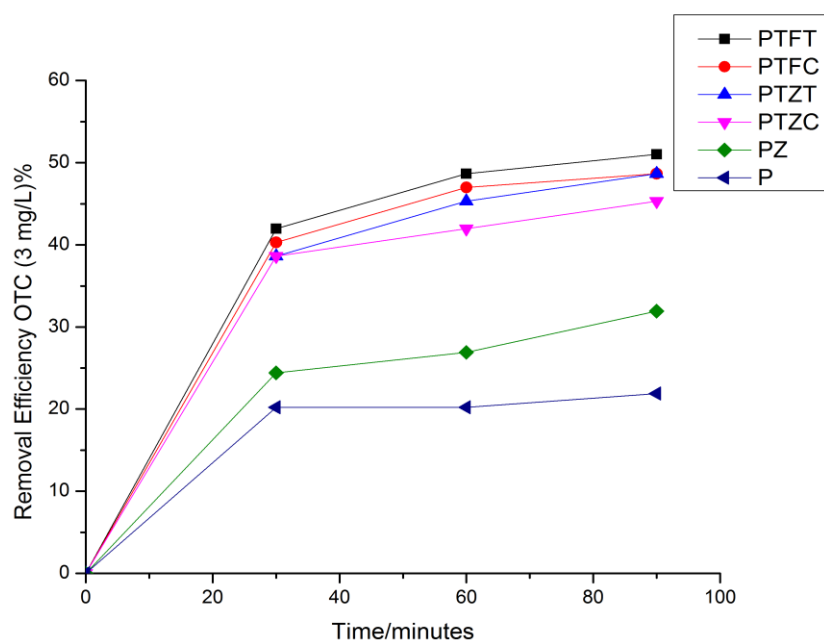
Figure 0-40 Removal Efficiency % of 3 mg/L OTC using coated and uncoated

membranes

4.2.2 Comparison of the removal efficiency of membranes with and without sun light

Table 4.3 presented a comparison of the removal efficiencies of coated membranes under sunlight irradiation using a solar unit versus conditions without sunlight. This allows for an assessment of the effectiveness of sunlight in activating the photocatalysts.

The enhancement in removal efficiency (R %) resulting from the developed membranes indicates an increase in the efficacy of coated membranes in degrading OTC compared to uncoated membranes. This improvement can be quantified using an equation.

$$Increasing\ of\ R\% = R\ \%\ of\ coated - R\ \%\ of\ uncoated \qquad\qquad 0.1$$

Despite the decrease in removal efficiency of the coated membranes in the absence of direct sunlight, the membranes still exhibited functionality. The change in removal efficiency (ΔR %) indicates the decrease in efficiency of the coated membranes with and without direct sunlight, which can be calculated using an equation.

$$\Delta\ R\% = R\%\ under\ sun\ light - R\%\ without\ sun\ light \qquad\qquad 0.2$$

The continued function of photocatalysts in the absence of direct sunlight may be attributed to their nanoscale particle size or to the release of Zn^{2+} and Fe^{2+} ions from ZnO and Fe_2O_3 dissolution (Sethi & Sakthivel, 2017). Additionally, residual energy from prior light exposure could sustain some catalytic activity. Nonetheless, it's crucial to acknowledge that the efficiency of photocatalysts notably diminishes without light, as their primary mechanism hinges on photon absorption to create reactive species.

Table 0-3 Contaminant removal efficiencies of membranes with and without sun light

Membrane Type	R% under sun light			Increasing of R% due to developed membranes			R% without sun light			Δ R% ≡ decreasing of R% due to the absence of the sun light		
	1mg/L	2mg/L	3mg/L	1mg/L	2mg/L	3mg/L	1mg/L	2mg/L	3mg/L	1mg/L	2mg/L	3mg/L
PTFT	88.16	55.65	51.01	61.79	30.14	29.14	38.44	36.82	30.25	49.72	18.83	20.76
PTFC	86.66	53.14	48.67	60.28	27.63	26.79	36.43	35.56	30.25	50.23	17.58	18.42
PTZT	86.16	51.89	48.67	59.78	26.37	26.79	38.44	30.54	26.90	47.72	21.35	21.77
PTZC	84.15	49.63	45.32	57.77	24.11	23.44	36.43	29.28	23.55	47.72	20.35	21.77
PZ	48.98	35.56	31.92	22.61	10.05	10.05	33.91	26.77	21.50	15.07	8.79	10.42

4.2.3 Statistical analysis and modeling of removal efficiency using RSM

To assess the suitability of the first order and second-order models, various analyses were conducted, including normal plots, residual analysis, main effects, contour plot, and ANOVA statistics such as R^2, adjusted R^2, and lack-of-fit. Table 4.4 reveals that the software recommended a quadratic model after validating the lack of fit and reviewing model summary statistics. Further confirmation of model adequacy was performed through ANOVA, which furnished details about quadratic and interaction effects, along with the normal linearized effects of parameter (Esfahani et al., 2014; Zarei & Behnajady, 2019), as summarized in Table 4.3. The model's F-value of 48.90 signifies its significance, with only a 0.01% probability that such a large F-value could result from random variation. "Prob > F" values below 0.0500 indicate the significance of model terms, including main, interaction, and quadratic terms. The lack-of-fit F-value of 0.5317 suggests that the lack of fit is not statistically significant relative to pure error, with a 74.75% chance that this lack of fit could occur due to random noise. A non-significant lack of fit is desirable as it indicates a good fit of the model to the data. The "Predicted R-squared" of 0.9202 is reasonably consistent with the "Adjusted R-squared" of 0.9578, with a difference of less than 0.2. The "Adeq Precision," measuring the signal-to-noise ratio, yields a ratio of 25.476, indicating an adequate signal. Therefore, the model is deemed suitable for predicting experimental data based on these evaluations.

Table 0-4 Sequential model fitting for the OTC removal efficiency

Source	Sum of Squares	df	Mean Square	F-value	p-value	
Mean vs. Total	69625.90	1	69625.90			
Linear vs. Mean	3393.38	3	1131.13	9.11	0.0009	
2FI vs. Linear	880.52	3	293.51	3.45	0.0484	
Quadratic vs. 2FI	**985.95**	**3**	**328.65**	**27.50**	**< 0.0001**	**Suggested**
Cubic vs. Quadratic	39.26	4	9.82	0.7338	0.6012	Aliased
Residual	80.26	6	13.38			
Total	75005.28	20	3750.26			
Lack of Fit						
Linear	1907.96	11	173.45	11.11	0.0078	
2FI	1027.45	8	128.43	8.23	0.0164	
Quadratic	**41.49**	**5**	**8.30**	**0.5317**	**0.7475**	**Suggested**
Cubic	2.23	1	2.23	0.1428	0.7210	Aliased
Pure Error	78.03	5	15.61			
Model Summary Statistics						

Source	Std. Dev.	R²	Adjusted R²	Predicted R²	PRESS	
Linear	11.14	0.6308	0.5616	0.3572	3457.68	
2FI	9.22	0.7945	0.6997	0.5594	2370.19	
Quadratic	**3.46**	**0.9778**	**0.9578**	**0.9202**	**429.14**	**Suggested**
Cubic	3.66	0.9851	0.9528	0.8878	603.47	Aliased

Table 0-5 ANOVA and lack-of-fit (LOF) test for response surface quadratic model of OTC Removal Efficiency %

Source	Sum of Squares	df	Mean Square	F-value	p-value	
Model	5259.86	9	584.43	48.90	< 0.0001	significant
A-pH	526.79	1	526.79	44.07	< 0.0001	
B-OTC concentration	2828.26	1	2828.26	236.63	< 0.0001	
C-Flowrate	38.33	1	38.33	3.21	0.1036	
AB	801.20	1	801.20	67.03	< 0.0001	
AC	74.42	1	74.42	6.23	0.0317	
BC	4.90	1	4.90	0.4098	0.5364	
A²	15.93	1	15.93	1.33	0.2752	
B²	958.22	1	958.22	80.17	< 0.0001	
C²	3.93	1	3.93	0.3285	0.5792	
Residual	119.52	10	11.95			
Lack of Fit	41.49	5	8.30	0.5317	0.7475	not significant
Pure Error	78.03	5	15.61			
Correction Total	5379.38	19				

Upon reviewing the graphical depiction of actual versus predicted values in Fig. 4.41 it becomes evident that the model provides a flawless explanation for the entire experimental range. Assessing model adequacy involves measuring residuals, with the

normal probability plot serving as a crucial tool for evaluating the normality of these residuals, as reported by (Khataee, 2009; Zarei & Behnajady, 2019). The points closely align with the diagonal line, signifying minimal discrepancies and confirming the model's appropriateness for elucidating the studied process. In Fig. 4.42 the marginal difference between data points and the straight line indicates that studentized residuals adhere to a normal distribution (Mohsenzadeh et al., 2019). Additionally, the residual plots almost create a straight line, suggesting normality in the distribution. This reinforces the conclusion that the model is adequate for explaining the underlying process.
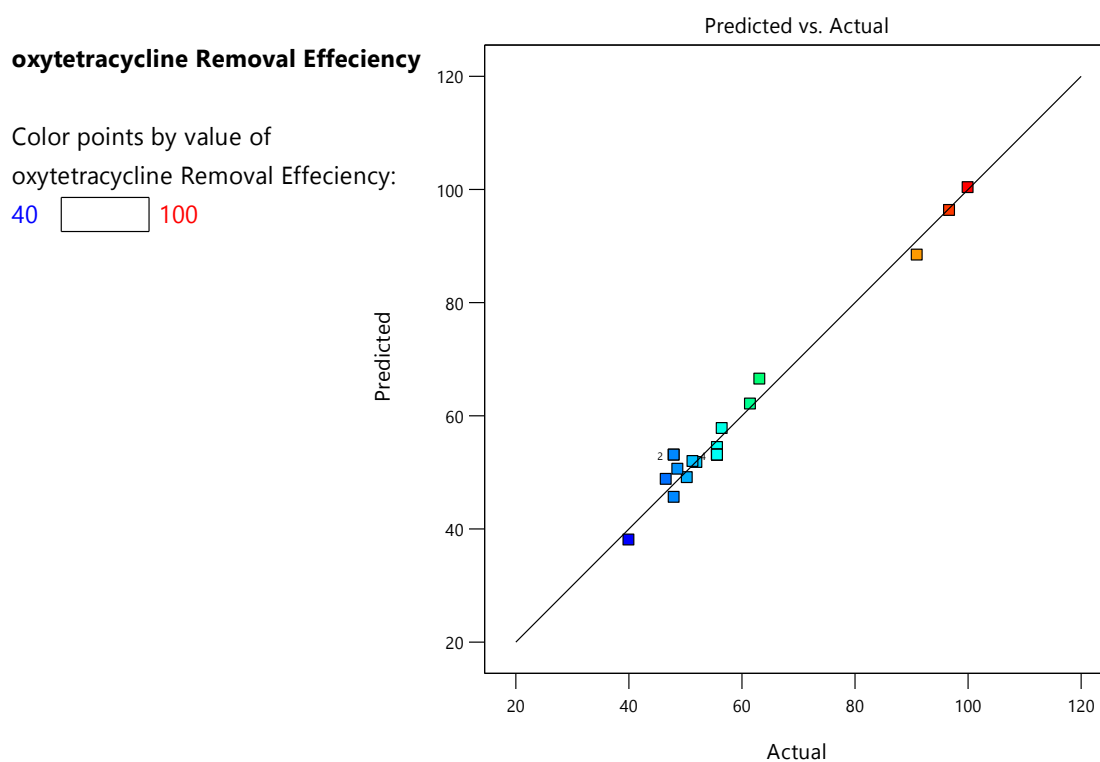
Figure 0-41 Plot of actual vs. predicted values of OTC removal efficiency

oxytetracycline Removal Effeciency

Color points by value of
oxytetracycline Removal Effeciency:

40 [   ] 100
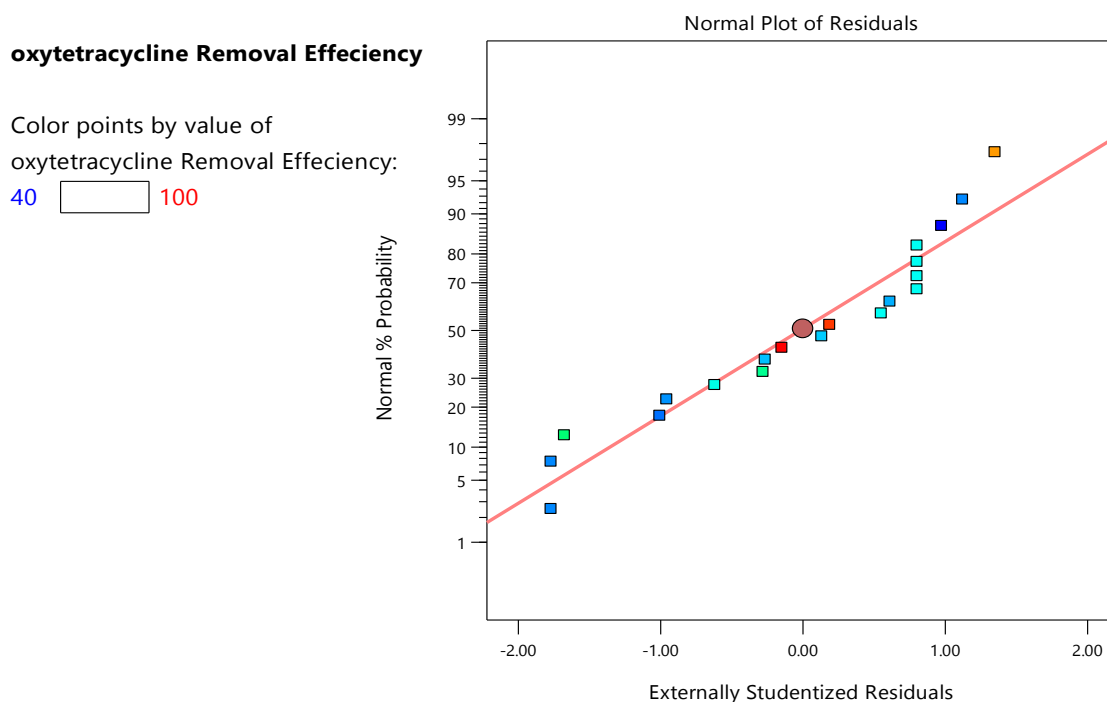
Figure 0-42 Normal probability plots of studentized residuals

4.2.4 Optimization of independent variables

To depict the impacts of OTC concentration, pH, and water flowrate on the response variable (OTC removal efficiency), response surface graphs were created using design expert software. These graphs were generated by altering two independent variables within experimental ranges while maintaining the third variable at the central point. In Fig. 4.43, the flowrate and pH were varied at a 2 mg/l OTC initial concentration. In Fig. 4.44, the OTC concentration and flowrate were changed at pH 6.5. Fig. 4.45 was created by adjusting the OTC concentration and pH at a flowrate of 0.5. These graphical representations illustrate the intricate interactions among the independent variables.

The CCD (Central Composite Design) method was applied to determine the optimal values for various variables influencing OTC removal efficiency. Table 4.6 outlines these optimal values, which collectively result in the maximum efficiency for removing OTC. According to the software calculations, the predicted OTC removal efficiency is

96.308%, aligning well with the experimentally observed removal efficiency of 95%. This underscores the effectiveness of Response Surface Methodology (RSM) in optimizing operational parameters for the heterogeneous photocatalytic process involved in OTC removal. The results affirm that RSM successfully orchestrates interactions among independent variables, leading to an enhanced OTC removal efficiency.

Table 0-6 Optimum values of OTC removal efficiency (%)

pH	OTC concentration	Flowrate	OTC Removal efficiency	Desirability
5	1	-1	96.308	0.938
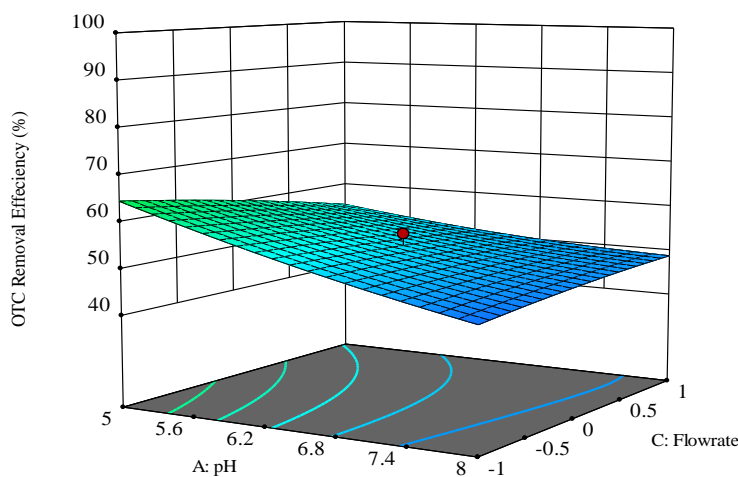
Figure 0-43 3D graphic surface optimization of OTC concentration versus pH and water flowrate; the flowrate and pH were varied at a 2 mg/l OTC initial concentration
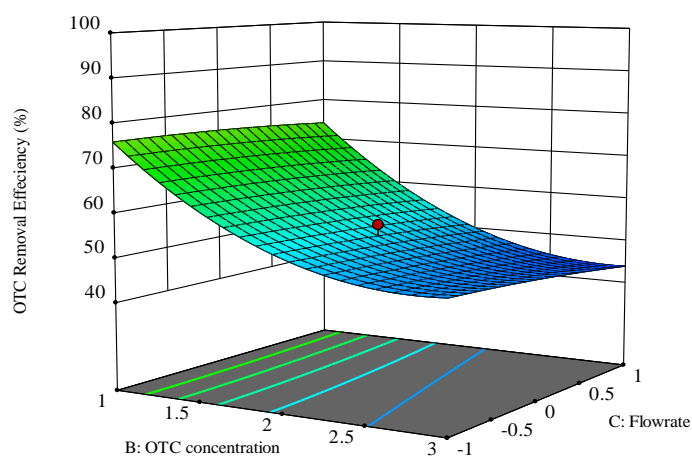
Figure 0-44 3D graphic surface optimization of OTC concentration versus pH and water

flowrate; the OTC concentration and flowrate were changed at pH 6.5
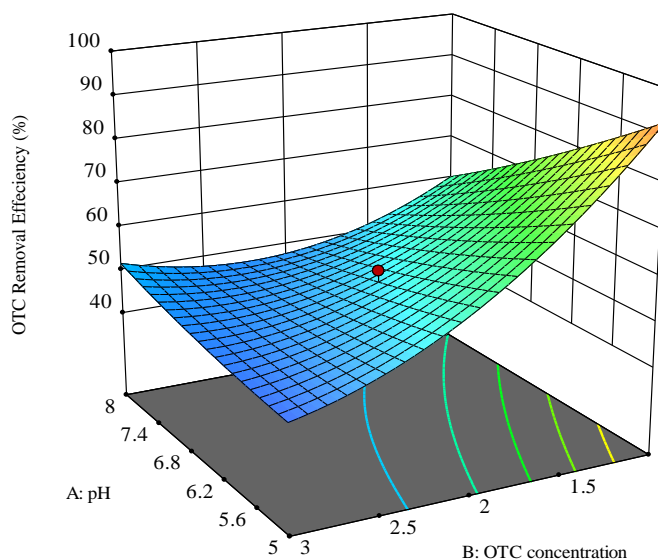
Figure 0-45 3D graphic surface optimization of OTC concentration versus pH and water

flowrate; the OTC concentration and pH were changed at a flowrate of 0.5

4.2.5 Investigation of the disinfection performance of the coated membrane

4.2.5.1 Disk diffusion

Table 4.7 displays the zone of inhibition (in millimeters) for PTFT, PTFC, PTZT, PTZC, and PZ coated membranes, as well as uncoated P membranes, against negative bacteria (*E. coli*) using concentrations of $2.45 * 10^5$ and $2.45 * 10^3$.

In Figure 4.43, the growth of the inhibition zone is clearly depicted for *E. coli* concentration $2.45 * 10^5$ for both coated and uncoated membranes. Notably, around the uncoated membranes, bacterial growth is observed everywhere, even on the membrane itself, indicating the absence of antimicrobial properties in plain polyester. Conversely, for coated membranes, clear inhibition zones are evident around each, varying in length depending on the type of photocatalyst incorporated.

Using a lighter concentration of bacteria, $2.45 * 10^3$ concentrations expands the inhibition zone for coated membranes due to the reduction in bacterial numbers. However, the uncoated membranes still lack an inhibition zone due to their absence of antimicrobial properties.
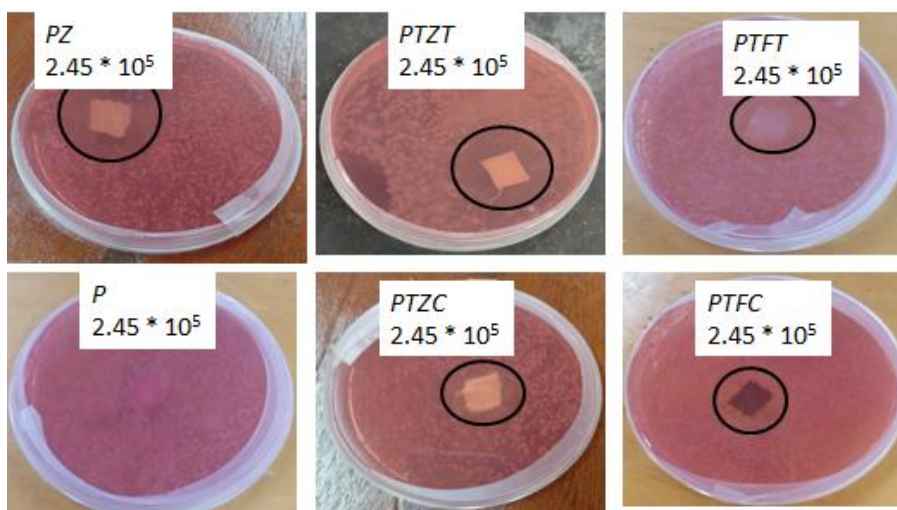
Figure 0-46 Zone of inhibition for the coated and uncoated membranes against *E. coli* $2.45 * 10^5$

Table 0-7 Zone of inhibition in mm for the coated and uncoated membranes against *E. coli* ($2.45 * 10^5$ and $2.45 * 10^3$) CFU/ml concentration

Membranes type	Zone of inhibition in mm *E. coli*	
	$2.45 * 10^5$	$2.45 * 10^3$
P	Zero	zero
PTFT	16	20
PTFC	17	19
PTZT	20	25
PTZC	18	21
PZ	26	30

The generation of reactive oxygen species, such as superoxides and hydroxyl radicals, which penetrate bacterial cells and damage their membranes, is what gives photocatalyst nanoparticles their antibacterial characteristics (Parra-Ortiz & Malmsten, 2022). ZnO nanoparticles have been shown in earlier studies to have strong antibacterial properties on polyester fabric. For example, Rastgoo et al. treated cotton/polyester fabric with ZnO nanoparticles to achieve comprehensive antibacterial and antifungal characteristics (Rastgoo et al., 2017). Amani et al applied corn silk, zinc acetate, or a mix of the two treatments to the polyester fabric samples to increase their antibacterial activity. The treated fabric demonstrated strong antifungal and antibacterial qualities (Amani et al., 2019).

Because ZnO has potent antibacterial capabilities, the polyester membrane coated with it in this study, PZ has the highest inhibition zone against *E. coli* for both concentrations among all coated membranes, 26 and 30 mm inhibition zone of *E. coli* for $2.45 * 10^3$ and $2.45 * 10^5$ concentrations respectively.

When ZnO is doped with TiO_2, the resulting photocatalyst retains its antimicrobial

properties, albeit slightly reduced compared to pure ZnO. However, it still exhibits effective antimicrobial activity. This is because the antimicrobial properties of TiO_2 are inferior to those of ZnO.

The incorporation of TiO_2 doped with ferric oxide into polyester fabric enables the inactivation of gram-negative bacteria such as *E. coli,* Prorokova et al. incorporated photocatalysts of titanium dioxide doped with ferric into polyester fabric and observed inhibition zones when testing the antimicrobial properties of the coated fabric against *E. coli* (Prorokova et al., 2020).

In this study, the coated membranes incorporating TiO_2 doped with Fe_2O_3 photocatalyst nanoparticles demonstrated the smallest inhibition zone compared to both bare ZnO and doped ZnO membranes, (16 and 20 for PTFT) and (17 and 19 for PTFC) mm inhibition zone of *E. coli* for $2.45 * 10^3$ and $2.45 * 10^5$ concentration respectively.

4.2.5.2 Glass bottle test

Table 4.8 elucidates the removal efficiency of *E. coli* $9.8 * 10^5$ CFU/100ml concentration using membranes coated with ZnO, TZT, TZC, TFT, and TFC, as well as the uncoated membrane, as determined through the glass bottle test method. The results showed in Figure 4.45 confirm that the uncoated membranes lack antimicrobial activity, resulting in a zero-removal efficiency of *E. coli*. Conversely, PZ-coated membranes, incorporating Zinc Oxide, exhibit a100% removal efficiency, consistent with expectations and supported by existing literature (Martinaga Pintarić et al., 2020).

Doping ZnO with TiO_2 demonstrated excellent performance for both photocatalysts, PTZT (99.99) and PTZC (99.95), indicates that incorporating Titanium Dioxide into Zinc Oxide does not compromise the antimicrobial efficiency of the membranes. This finding

aligns with prior research (Marra et al., 2017), supporting the notion that doping Zinc Oxide does not diminish its antimicrobial effectiveness against *E. coli*.

The PTFT and PTFC membranes exhibited antimicrobial efficiency of 92.97% and 91.3%, respectively. This effectiveness stems from the combined action of both photocatalysts, TiO_2 (Zhang et al., 2019) and Fe_2O_3 (Granados et al., 2021). Indeed, both doping photocatalysts contributed to the overall antimicrobial function of the membranes.

Table 0-8 the removal efficiency of *E. coli* using the Glass bottle test

Membranes type	P	PTFT	PTFC	PTZT	PTZC	PZ
E. coli Removal Efficiency %	0.00	92.97	91.30	99.99	99.95	100
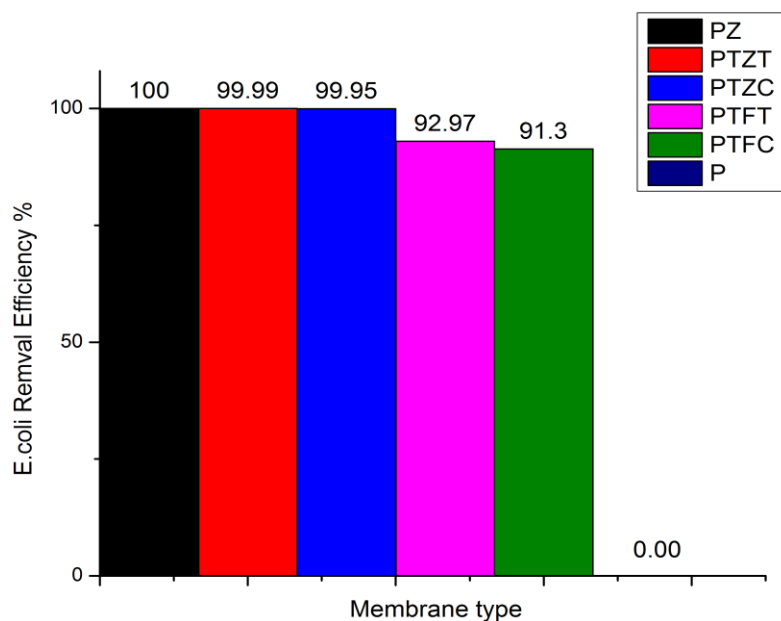
Figure 0-47 the removal efficiency of *E. coli* using the Glass bottle test

4.2.6 Flow Feed (Dam water and Synthetic feed water with *E. coli*)

The disinfection efficiency of three different feed concentrations of water was evaluated. The concentrations were as follows: high ($12 * 10^4$ CFU/100 ml) and medium ($6 * 10^4$ CFU/100 ml) for synthetic feed and $13 * 10^3$ CFU/100 ml for dam water. The removal efficiency (%) and Log Reduction Value (LRV) were calculated and are presented in Table 4.9.

Table 0-9 disinfection efficacy of the synthetic feed and dam water

| Membranes type | Synthetic feed *(E. Coli)* | | | | Dam water *(E. Coli)* | |
| | $12 * 10^4$ CFU/100ml | | $6 *10^4$ CFU/100ml | | $13 * 10^3$ CFU/100ml | |
	Removal %	LRV	Removal %	LRV	Removal %	LRV
P	64.60	0.45	63.50	0.44	65.00	0.46
PTFT	98.20	1.70	98.00	1.70	98.50	1.80
PTFC	98.00	1.70	97.50	1.60	98.30	1.77
PTZT	99.999	5.00	99.999	5.00	99.999	5.00
PTZC	99.999	5.000	99.999	5.00	99.999	5.00
PZ	99.95	3.30	99.90	3.00	99.96	3.40

For the synthetic feed, the uncoated filters achieved notable *E. coli* removal percentages of 64.6 % and 63.5 % for the high and medium *E. coli* concentrations, respectively. The corresponding Log Reduction Values (LRVs) were 0.45 for the high concentration and 0.44 for the medium concentration. This indicates that the removal efficiency improved as the *E. coli* concentration in the feed water increased. The likely reason for this is that higher concentrations caused more *E. coli* to deposit on the filter surface, enhancing the filtration effectiveness (Achisa, 2014b). The removal efficiency of the dam water

increased to 65 %, and the Log Reduction Value (LRV) became 0.46. This improvement in removal efficiency may be attributed to the lower initial concentration of *E. coli*, which can lead to more effective filtration process. Additionally, the natural turbidity of the dam water might have helped reduce the effective pore size of the membranes, thereby enhancing the removal efficiency.

Zinc oxide demonstrated effective bacterial removal rates in both synthetic feed and dam water, achieving high percentages 99.95, 99.90, and 99.96 respectively. However, its limited sunlight absorption due to a short bandgap hindered its full potential. By incorporating titanium dioxide, the bandgap shifted into the visible light spectrum, enhancing sunlight absorption and bacterial inactivation. UV DRS testing confirmed this shift. Thus, the combination of zinc oxide and titanium dioxide offers improved antimicrobial efficacy, especially in environments with elevated bacterial concentrations (Sethi & Sakthivel, 2017).

For the membranes coated with doped zinc oxide, the disinfectant efficiency increased, achieving nearly complete removal of *E. coli*, approaching 100%. This high removal efficiency is due to the disinfectant properties of zinc oxide photocatalysis (H. M. Ahmed et al., 2023). Both type of doped zinc oxide coatings demonstrated similar results in terms of removal percentage and Log Reduction Value (LRV), regardless of the titanium dioxide doping was synthesized from precursor or from commercial source. The removal percentage for high, medium, and dam water concentrations was 99.999 % with corresponding LRVs of 5.

For the membranes coated with titanium dioxide doping with ferric oxide, there was an increase in removal percentage and Log Reduction Value (LRV) due to the antimicrobial

properties of the TiO_2 (Chand et al., 2020; Khashan et al., 2021) and Fe_2O_3 (Ezealigo et al., 2021; Zúñiga-Miranda et al., 2023) photocatalysts. The removal percentages achieved were 98.2 % and 98 % for high concentrations, 98.00 % and 97.50 % for medium concentrations, and 98.5 % and 98.30 % for dam water concentrations for PTFT and PTFC, respectively. The corresponding LRVs were 1.70 for high concentrations, 1.70 and 1.60 for medium concentrations, and 1.80 and 1.77 for dam water concentrations.

To evaluate the performance of coated and uncoated membranes targeting organic and microbial contaminants, synthetic feed with varying concentrations of oxytetracycline (an organic contaminant) was used. The optimal results were achieved using an experimental design program. Additionally, to assess the disinfectant efficiency, synthetic feed with very high ($12 * 10^4$ CFU/100 ml) and medium ($6 * 10^4$ CFU/100 ml) concentrations of *E. coli* (microorganism detector) were tested, alongside dam water samples ($13* 10^3$ CFU/100 ml).

The purpose of the solar unit point-of-use system is to treat raw water by degrading chemical contaminants and disinfecting microbes. Additionally, it aims to ensure that other physicochemical properties of the water (Turbidity, pH, Conductivity, Total dissolved solids (TDS), Total Iron as Fe, and Zinc, as Zn^{++} …etc) meet global water quality standards. Table 4.10 presents the physicochemical properties of the dam water before and after filtration, allowing assessment of whether they conform to the water quality standards. The study used Kenya standard of water (EAS, 2014) and WHO standard.

The turbidity of the dam water was initially reduced from 16 NTU to 4 NTU using uncoated polyester membranes, while this met the Kenyan standard for water quality (5

NTU); it did not meet the WHO standard (< 1 NTU). However, when the coated membranes with titanium dioxide doped with zinc oxide and ferric oxide was used for filtration, the turbidity was reduced to less than 1 NTU, meeting both Kenyan and WHO standards. Filtration with membranes coated with pure zinc oxide achieved a turbidity of 1 NTU, which meets the Kenyan standard and is on the edge of the WHO standard. The results demonstrate that doping titanium dioxide provided the best performance in terms of reducing turbidity.

The properties of the dam water were measured as follows: pH at 7.92, conductivity at 166 µS/cm, and total dissolved solids (TDS) at 83 mg/l. These values meet both national and international water quality standards. Filtration using both coated and uncoated membranes resulted in slight reductions in these values, but all measurements remained within the standards both before and after filtration.

The Total Iron as Fe and Zinc, as Zn^{++} measured after and before filtration to confirm that they were no released of these metals from the coated membranes and also to confirm that they are with the water standardization range.

The amount of iron in the raw dam water was 0.25 mg/l, which is within both national and international water quality standards. Filtration using uncoated polyester membranes and zinc oxide coated membranes reduced the iron content to 0.06 mg/l, demonstrating the effectiveness of these membranes in mitigating iron. When using titanium dioxide doped with zinc oxide or ferric oxide, the iron content was reduced to 0.07 mg/l and 0.09 mg/l, respectively, for both synthetic and commercial titanium dioxide. Although these reductions are still significant, they are slightly less effective than the reductions achieved with uncoated and zinc oxide coated membranes. The slight increase in iron content with

the doped titanium dioxide membranes is not due to iron release from the photocatalysts, as the increase is also observed in membranes coated with titanium dioxide doped with zinc oxide. This suggests that the increase is due to the titanium dioxide mechanism, where large ferric compounds are broken down into smaller components by the photocatalyst, allowing them to pass through the membrane pores. This aligns with studies indicating that titanium dioxide degrades and breaks down chemical contaminant compounds (Haque et al., 2017) and transfer them to safe less harmful compound (Van Thuan et al., 2023).

Table 0-10 the physicochemical properties of the dam water before and after filtration

Parameter	Unit	Raw Water Value	Membranes Type						Water Standard	
			PTFT	PTFC	PTZT	PTZC	PZ	P	KEBS	WHO
Turbidity	NTU	16	0.8	0.8	0.7	0.7	1	4	5	< 1
pH	-	7.92	7.82	7.81	7.88	7.81	7.55	7.89	6.5 - 8.5	6.5-8.5
Conductivity	μS/cm	166	162	166	166	166	167		1500	≤ 400
Total Dissolved Solids (TDS)	mg/L	83	81	83	83	83	83	81	700	< 1000
Total Iron as Fe	mg/L	0.11	0.07	0.09	0.07	0.09	0.06	0.06	0.3	2
Zinc, as Zn^{++}	mg/L	Nil	Nil	Nil	Nil	Nil	Nil	Nil	5	< 3

4.3 Disinfection and organic degradation kinetics and synergy of the photo-catalytic water treatment

The synergistic effect of combining photocatalysis and filtration was evaluated, revealing that the developed membrane outperformed the uncoated membrane (filtration only) in removing microbial and organic contaminants. It is widely recognized that transition metals can react with certain oxidants, thereby enhancing the elimination of organic pollutants and the inactivation of microorganisms (Malvestiti et al., 2024). This highlighted the membrane's effectiveness in producing clean water efficiently. Additionally, the disinfection and photodegradation of organics from each individual process were used as references to quantitatively assess the synergistic effects of both the sequential and combined photocatalysis and filtration processes.

4.3.1 Evaluate the disinfection synergy of the photo-catalytic water treatment

E. coli is the primary bacteria used as an indicator of fecal contamination, commonly employed to monitor and assess the quality of both wastewater and drinking water (Odonkor & Ampofo, 2013; Osuolale & Okoh, 2017). To evaluate disinfection, three concentrations of E. coli were used for the flow test as previously mentioned. The high and medium concentrations were derived from synthetic feed ($12 *10^4$ & $6 *10^4$ CFU/100 ml), while the third ($13 * 10^3$ CFU/100 ml) came from real dam water. The experiment was conducted under sunlight irradiation using both uncoated membranes and photocatalysis-coated membranes as filter media. Water samples were collected, the number of bacterial colonies was counted, and the percentage of microorganism reduction (R) was calculated using Equation 3.5. The synergistic effects of disinfection

processes utilizing filtration and photocatalysis were quantitatively determined using Equation 3.6. These calculations correspond to *E. coli* log reduction values shown in Table 4.11.

Table 0-11 Log-reduction values and synergy indices for the disinfection of synthetic and real feed using uncoated and coated membranes under solar irradiation

process	$12*10^4$ CFU/100 ml			$6*10^4$ CFU/100 ml			$13*10^3$ CFU/100 ml		
	R %	LRV	SI	R %	LRV	SI	R %	LRV	SI
P	64.60	0.45	-	63.50	0.44	-	65.00	0.46	-
PF	71.20	0.54	-	70.30	0.53	-	72.00	0.57	-
PT	75.00	0.60	-	74.50	0.59	-	78.10	0.66	-
PZ	99.95	3.30	-	99.90	3.00	-	99.96	3.40	-
PTZT	99.999	5.00	1.15	99.999	5.00	1.24	99.999	5.00	1.11
PTFT	98.20	1.70	1.07	98.00	1.70	1.09	98.50	1.80	1.07

The percentage of microorganism reduction was 64.6 - 65% for the uncoated membranes (filtration only). For membranes coated with bare ferric oxide, titanium dioxide, and zinc oxide, the reduction percentages were 71.2 - 72 %, 75 - 78.1 %, and 99.95 - 99.96 % respectively. When co-doped photocatalysts were used, the reduction increased to 98.2 - 98.5 % for titanium dioxide doped with ferric oxide. In the case of titanium dioxide doped with zinc oxide, the reductions were very high and almost complete the full percentage 99.999 %, rise by approximately 0.049, 0.099, and 0.039 % compared to zinc oxide alone for high and medium concentrations of synthetic feed and dam water respectively.

The log reduction in filtration for uncoated membranes was between 0.44 and 0.46. Coated membranes showed better performance, with those coated with pure ferric oxide achieving a log reduction between 0.53 and 0.57, and those with titanium dioxide achieving between 0.59 and 0.66. Remarkably, membranes coated with zinc oxide exhibited a significant increase in log reduction, ranging from 3.00 to 3.40, due to its high antimicrobial properties. For codoped membranes, those coated with titanium dioxide doped with ferric oxide achieved log reductions between 1.7 and 1.8. However, the membranes coated with titanium dioxide doped with zinc oxide demonstrated the best performance among all membranes studied, with a log reduction reaching 5.00. This superior performance is attributed to the combination of zinc oxide's unique antimicrobial properties and titanium dioxide's enhanced sunlight absorbance.

Coated membranes with both photocatalysts (Fe_2O_3-TiO_2 and ZnO-TiO_2) achieved SI values more than 1.00 during filtration-photocatalysis processes. This indicates that the combination of photocatalysis and filtration produced synergistic effects, significantly enhancing disinfection performance. Which can be attributed to the interfaces formed between the two materials (ZnO-TiO_2 or Fe_2O_3-TiO_2), providing more active sites for the photocatalytic reaction. According to Cheng et al., the enhanced interfacial structure facilitates better charge transfer and spatial separation of photogenerated charge carriers, thereby enhancing photocatalytic activity. In this hybrid nanostructure, electrons transfer from the conduction band (CB) of ZnO or Fe_2O_3 to that of TiO_2, while holes transfer from the valence band (Vb) of TiO_2 to that of ZnO or Fe_2O_3. This proposed mechanism suggests a synergistic effect in *E. coli* inactivation by the photocatalysts through efficient charge transfer processes (Sethi & Sakthivel, 2017; Tahir et al., 2016).

$$ZnO - TiO_2 + hv \rightarrow TiO_2 + e -_{CB} + h +_{VB} \qquad 0.3$$
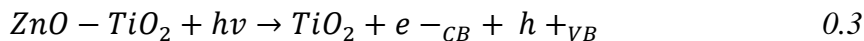
Or in case of Fe_2O_3 the equation will be

$$Fe_2O_3 - TiO_2 + hv \rightarrow TiO_2 + e -_{CB} + h +_{VB} \qquad 0.4$$

$$OH^\bullet + E.coli \rightarrow degraation \ product \qquad 0.5$$
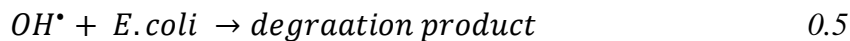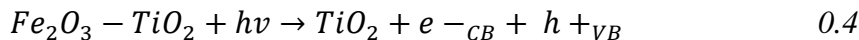
Migration of hole from VB of titania to VB of Zinc Oxide or Ferric Oxide

$$h +_{VB} (TiO_2) \rightarrow VB \ (ZnO) \qquad 0.6$$

Or
$$h +_{VB} (TiO_2) \rightarrow VB \ (Fe_2O_3) \qquad 0.7$$
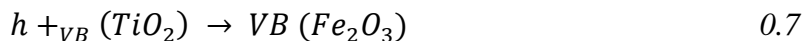
Migration of electron from CB of ZnO or Fe_2O_3 to CB of TiO_2

$$h +_{CB} (TiO_2) \rightarrow CB \ (ZnO) \qquad 0.8$$

Or
$$h +_{CB} (TiO_2) \rightarrow CB \ (Fe_2O_3) \qquad 0.9$$
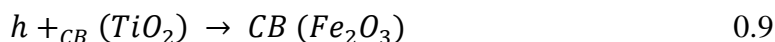
Zinc and Ferric dissolution for inactivation *E. coli*

$$ZnO - TiO_2 + E.coli \ suspuntion \rightarrow Zn^{+2} \qquad 0.10$$

Or

$$Fe_2O_3 - TiO_2 + E.coli \ suspuntion \rightarrow Fe^{+2} \qquad 0.11$$

$$Zn^{+2} + E.coli \rightarrow Diffusion \ of \ of \ Zn^{+2} \ ion \ in \ to \ the \ cell \ membrane \rightarrow cell \ damage \qquad 0.12$$

Or

$$Fe^{+2} + E.coli \rightarrow Diffusion \ of \ of \ Fe^{+2} \ ion \ in \ to \ the \ cell \ membrane \rightarrow cell \ damage \qquad 0.13$$
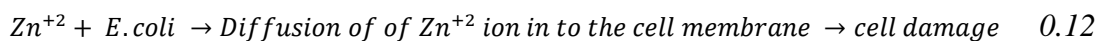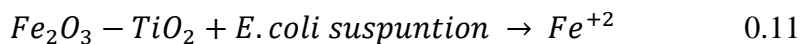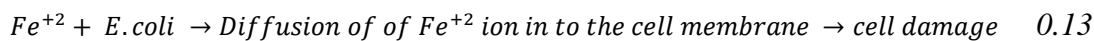
The filtration photocatalytic disinfection findings could not be directly compared to the literature due to changes in water matrix, membrane type, photocatalyst concentrations,

initial bacterial concentrations, and contact times used by other researchers. For example, Mecha and colleagues demonstrated that solar photocatalytic ozonation achieved log reductions ranging from 1 to 2.3 within 15 minutes (Mecha et al., 2017). Sethi and Sakthivel reported that using high concentration (50%) ZnO/TiO_2 samples resulted in complete inactivation, or a 7 log reduction, of *E. coli* cells at 60, 45, 30, 15, and 10 minutes of UV light irradiation, respectively (Sethi & Sakthivel, 2017). Shi and colleagues found that combining ozone (at 3 mg/L) and UV treatment (at 20 mJ/cm²) resulted in a 6.0 log reduction in *E. coli* inactivation (Shi et al., 2021). Recently, Nelson et al. reported an 8.42 log reduction after 100 minutes of solar light irradiation using N–TiO_2-PVDF (Nelson et al., 2024).

4.3.2 Evaluate the organic degradation kinetics and synergy of the photo-catalytic water treatment

Oxytetracycline (OTC) was used as an organic pollutant in the synthetic feed for the flow test. Three concentrations of OTC—1 mg/L, 2 mg/L, and 3 mg/L—were used to examine the removal efficiency of uncoated membranes (filtration only) and photocatalysis-coated membranes (photodegradation and filtration). The experiments were conducted under identical conditions using sunlight irradiation with a solar unit to concentrate the light and activate the photocatalysis for 90 minutes, with samples taken every 30 minutes.

Table 4.12 showed OTC removal efficiencies and SI values for uncoated membranes P and coated membranes PT, PF, PZ, PTZT, and PTFT. The uncoated membranes removed 26.38% to 21.88% of 1 to 3 mg/L OTC through filtration alone (physical separation). For Coated membranes with bare Fe_2O_3, ZnO, and TiO_2 increased the removal efficiency to 26.9% to 35.42%, 31.93% to 48.99%, and 33.6% to 53.51%, respectively. When using

codoped TiO2-Fe_2O_3 (PTZT) and TiO_2-ZnO (PTFT), the removal efficiency rose significantly to 48.67% to 86.16% for PTZT and 51.01% to 88.17% for PTFT.

The increased removal efficiency in coated membranes is attributed to the combination of physicochemical processes. In uncoated membranes, the removal of organics was solely due to physical filtration. In contrast, coated membranes benefited from both the filtration process and photodegradation from the photocatalysts, enhancing the overall efficiency. The synergy of combining filtration and photodegradation in Fe_2O_3-TiO_2 and ZnO-TiO_2 coated membranes was greater than one, indicating a positive effect in degrading Oxytetracycline.

Table 0-12 OTC removal efficiencies and SI for uncoated membrane P and, PT, PF, PZ, PTZT, and PTFT coated membranes

	30 minutes						60 minutes						90 minutes					
	1 mg/l		2 mg/l		3 mg/l		1 mg/l		2 mg/l		3 mg/l		1 mg/l		2 mg/l		3 mg/l	
	R%	SI	R%	SI	R%	SI	R%	SI	R%	SI	R%	SI	R%	SI	R%	SI	R%	SI
P	22.36	-	23.00	-	20.20	-	22.36	-	23	-	20.20	-	26.38	-	26.77	-	21.88	-
PZ	36.43	-	28.02	-	24.39	-	41.45	-	29.28	-	26.9	-	48.99	-	36.82	-	31.93	-
PF	28.89	-	27.02	-	23.55	-	30.40	-	28.02	-	24.55	-	35.42	-	33.05	-	26.9	-
PT	46.47	-	33.05	-	28.57	-	49.48	-	35.56	-	29.41	-	53.51	-	39.33	-	33.60	-
PTZT	71.59	1.18	40.58	1.07	38.62	1.18	80.13	1.19	45.61	1.09	45.32	1.26	86.16	1.13	51.89	1.05	48.67	1.12
PTFT	81.64	1.54	48.12	1.30	41.97	1.31	85.15	1.51	50.63	1.25	48.67	1.45	88.17	1.47	55.65	1.22	51.01	1.32

The degradation mechanism of Fe_2O_3-TiO_2 and ZnO-TiO_2 coated membranes relies on the combined photocatalytic activity and inherent properties of both Fe_2O_3 (ferric oxide) or ZnO (Zinc Oxide) and TiO_2 (titanium dioxide).

The first step in degradation mechanism of Fe_2O_3-TiO_2 is the photocatalytic activation when exposed to the sunlight irradiation, TiO_2 absorbs photons with sufficient energy to surpass its band gap, causing electrons to move from the valence band to the conduction band and forming electron-hole pairs (Ahmadi et al., 2020).

$$TiO_2 + h\nu \rightarrow TiO_2 \left(e_{cb}^- + h_{vb}^+ \right) \qquad 0.14$$
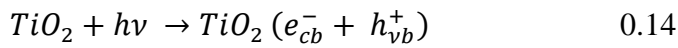
Fe_2O_3, with its narrower band gap, can be activated by visible light and generates electron-hole pairs in a similar manner.

$$Fe_2O_3 + h\nu \rightarrow Fe_2O_3 \left(e_{cb}^- + h_{vb}^+ \right) \qquad 0.15$$
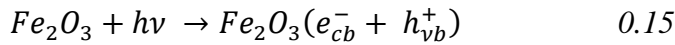
Combining Fe_2O_3 and TiO_2 enhances charge separation. Electrons from the conduction band of TiO_2 can transfer to the conduction band of Fe_2O_3, thereby reducing the recombination of electron-hole pairs.

$$TiO_2 \left(e_{cb}^- \right) + Fe_2O_3 \rightarrow TiO_2 + Fe_2O_3 \left(e_{cb}^- \right) \qquad 0.16$$
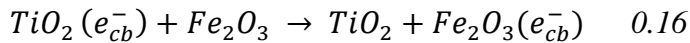
Electrons in the conduction bands can react with oxygen molecules (O_2) dissolved in water to form superoxide radicals (Theerthagiri et al., 2018).

$$O_2 + e^- \rightarrow O_2^{\bullet -} \qquad 0.17$$

$$O_2^{\bullet -} + 2e_{cb}^- + 2H^+ \rightarrow \bullet OH + OH^- \qquad 0.18$$
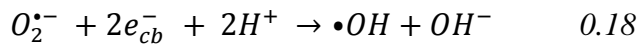
The holes in the valence bands can oxidize water (H_2O) or hydroxide ions (OH-) to form hydroxyl radicals ($\cdot OH$).

$$H_2O + h^+ \rightarrow \bullet OH + H^+ \qquad 0.19$$

$$•OH^- + h^+ \rightarrow •OH \qquad\qquad 0.20$$
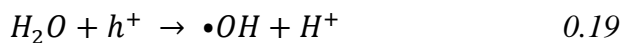
The produced ROS, particularly hydroxyl radicals (·OH) and superoxide radicals ($O_2^{·-}$) are highly reactive and target oxytetracycline molecules, resulting in their degradation.

$$OTC + h^+ \rightarrow simple\ products + H_2O + CO_2 \qquad 0.21$$

$$OTC + •OH/O_2^{·-} \rightarrow simple\ products + H_2O + CO_2 \quad 0.22$$
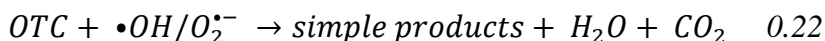
The degradation of oxytetracycline with Fe_2O_3-TiO_2 coated membranes occurs through the activation of the photocatalysts under UV and visible light, resulting in the formation of electron-hole pairs. The combination of Fe_2O_3 and TiO_2 improves charge separation, boosting the production of reactive oxygen species like hydroxyl and superoxide radicals. These ROS then oxidize and break down oxytetracycline molecules via direct and indirect pathways, converting them into less harmful substances. The synergistic interaction between the two photocatalysts significantly enhances the degradation efficiency.

The degradation mechanism of ZnO-TiO_2 coated membranes involves the activation of TiO_2 by absorbing sunlight, which excites electrons from the valence band to the conduction band, creating electron-hole pairs (equation 4-15). Likewise, ZnO absorbs sunlight and generates electron-hole pairs in a manner similar to TiO_2 and Fe_2O_3 (Shukla et al., 2021).

$$ZnO + hv \rightarrow ZnO(e_{cb}^- + h_{vb}^+) \qquad\qquad 0.23$$
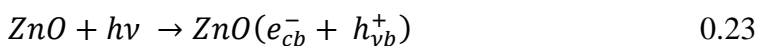
Combining ZnO and TiO_2 improves charge separation and decreases the recombination rate of electron-hole pairs. Electrons from the conduction band of ZnO can move to the conduction band of TiO_2, while holes from the valence band of TiO_2 can migrate to the valence band of ZnO.

$$ZnO(e_{cb}^-) + TiO_2 \rightarrow ZnO + TiO_2(e_{cb}^-) \qquad\qquad 0.24$$

$$TiO_2(h_{vb}^+) + ZnO \rightarrow TiO_2 + ZnO(h_{vb}^+) \qquad\qquad 0.25$$
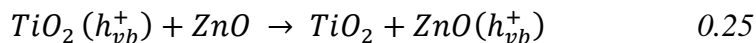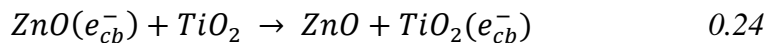
The generation of reactive oxygen species (ROS) and the degradation of oxytetracycline follow the same procedure as with Fe_2O_3-TiO_2 (equations 4.20 to 4.23).

The primary differences in the degradation mechanisms of Fe_2O_3-TiO_2 and ZnO-TiO_2 for oxytetracycline arise from their light absorption properties and band gap variations. Fe_2O_3-TiO_2 benefits from the visible light absorption capability of Fe_2O_3, enhancing photocatalytic activity across a wider light spectrum. In contrast, ZnO-TiO_2 focuses on improving efficiency under UV light through effective charge separation and transfer between ZnO and TiO_2. Consequently, Fe_2O_3-TiO_2 outperforms ZnO-TiO_2 in the initial 30 to 60 minutes of the first and second water sample collections. However, by 90 minutes, their performance levels are nearly equal as ZnO-TiO_2 optimizes its sunlight absorption.

As discussed in the section on evaluating the disinfection synergy of the photo-catalytic water treatment, direct comparisons with existing literature are not feasible due to differences in water matrix, membrane type, photocatalyst concentrations, contaminant types, initial contaminant concentrations, and contact times used by other researchers. This study is the first to utilize impregnation of doped titanium oxide with ferric and zinc oxide into polyester membranes for removing OTC. Table 4.13 provides data on OTC photodegradation using various types of photocatalysts.

Table 0-13 OTC photodegradation using several photocatalysts type

process	Source of light	(OTC) (mg L/1)	Irradiation time minutes	Removal efficiency %	Ref.
g-C$_3$N$_4$ (TCN)	visible light		60.0	93.00	(Zhang et al., 2022)
GCNQDs-CoTiO$_3$/CoFe$_2$O$_4$	Xe lamp 500 W	40	120	88.00	(C. Feng et al., 2022)
BiVO$_4$	visible light	10	240	83.00	(Senasu et al., 2021)
CoFe@NSC	visible light	50	150	90.00	(Zhang et al., 2021)
g-C$_3$N$_4$/Bi$_4$NbO$_8$Cl	visible LED light	20	60.0	87.00	(Majumdar et al., 2021)
Polypyrrole TiO$_2$@V2O$_5$	Xe lamp 300 W	50	120	85.00	(Changanaqui et al., 2020)
ZnO/TiO$_2$	Solar light	60	8.0	90.30	(Singh et al., 2020)
ZnO/TiO$_2$/Ag2Se	Blue LED 36 W	5.0	360	55.00	(Changanaqui et al., 2020)
MoS2/ZnS	visible light	20	180	81.00	(Gusain et al., 2021)
AgCl/BiVO$_4$	Xe lamp 1000W	20	120	76.50	(Dai et al., 2019)
TiO$_2$/ZnO/polyester	Solar light	1.0	90.0	86.16	This study
TiO$_2$/Fe$_2$O$_3$/polyester	Solar light	1.0	90.0	88.17	This study

4.4 Assess membrane fouling and re-use potential

4.4.1 Membrane flux performance

The flux performance of both uncoated and photocatalyst-coated membranes was assessed over a 1.00 h filtration period under sunlight radiation. The permeate flux (kg/m²h) was calculated using equation 3.14, Table 4.14, which considers the mass of permeated water (m); the density of water 1 Kg/l, the membrane's effective surface area ($A = 0.01$ m^2), and the filtration time ($\Delta t = 1$ h).

Table 0-14 the flux performance of both uncoated and photocatalyst-coated membranes

Membranes type	M (Kg)	A (m^2)	Δt (h)	JR (Kg/m^{2}h)
P	7.00	0.01	1.00	700
PTZT	8.00	0.01	1.00	800
PTZC	7.50	0.01	1.00	750
PTFT	8.60	0.01	1.00	860
PTFC	7.60	0.01	1.00	760

4.4.2 Evaluating the membranes antifouling performance

The antifouling performance of both uncoated and photocatalyst-coated membranes was evaluated using the recovery ratio of flux (RRF) as a parameter using equation 3.15; table 4.16 explained the permeate flux (JS) measured after cleaning using equation 3.14; Table 3.15, showed the permeate flux of deionized water under the same conditions was used as the reference (JR) illustrated in Table 4.14.

Table 0-15 the permeate flux (JS) after cleaning of both uncoated and photocatalyst-coated membranes

Membranes type	M (Kg)	A (m^2)	Δt (h)	JS (Kg/m^{2}h)
P	6.00	0.01	1.00	600
PTZT	7.30	0.01	1.00	730
PTZC	7.00	0.01	1.00	700
PTFT	8.30	0.01	1.00	830
PTFC	7.20	0.01	1.00	720

Table 0-16 the recovery ratio of flux (RRF) of both uncoated and photocatalyst-coated membranes

Membranes type	JS	JR	RRF %
P	600	700	85.71
PTZT	700	800	91.25
PTZC	720	750	87.50
PTFT	830	860	96.51
PTFC	700	760	94.74

Figure 4.48 illustrates the flux performance of both coated and uncoated membranes before and after fouling. The uncoated membrane (P) showed the lowest flux value, while the PTFT membrane had the highest flux value among all the membranes. This demonstrates that coating membranes with photocatalysts significantly enhances their permeability and antifouling properties.
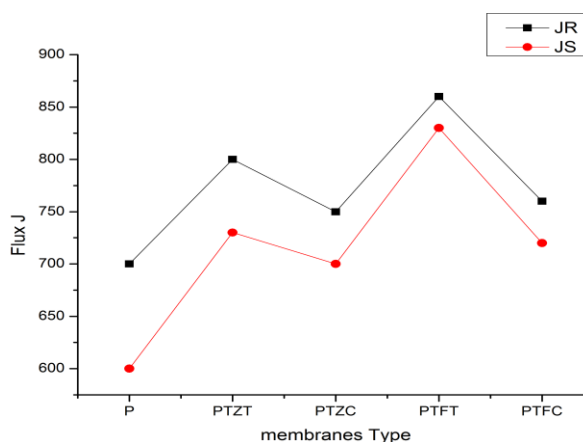
Figure 0-48 the permeate flux of the coated and uncoated membranes before and after fouling

The antifouling performance, as illustrated in the figure 4.49, indicates that the bare membrane has the lowest antifouling capability. In contrast, the membranes coated with TiO_2-ZnO and TiO_2-Fe_2O_3 exhibit higher antifouling performance, with the TiO_2-Fe_2O_3 coated membrane showing the highest antifouling value. This enhanced performance is attributed to the high band gap of Fe_2O_3, which enables the photocatalyst to efficiently absorb visible light and subsequently degrade organic and microbial contaminants more effectively.
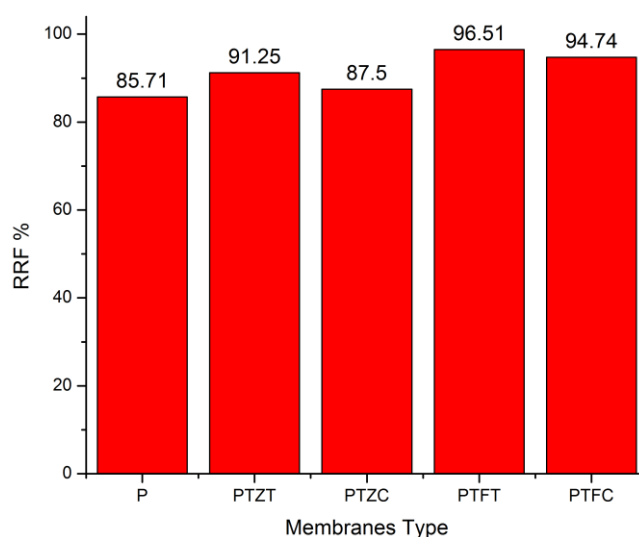
Figure 0-49 the recovery ratio of flux (RRF) of coated and uncoated membranes

4.4.3 Cleaning of the membranes

The dam water was run until a cake layer formed on each membrane. Table 4.13 indicates the number of cycles the water can run before this layer forms. The cake layer was then removed by brushing the membranes and rinsing them multiple times with water, without the need for additional physical or chemical treatments. Figure 4.46 shows the images of the uncoated and photocatalysis-coated membranes before and after cleaning. Coated membranes can run more water cycles than uncoated membranes before a cake layer forms due to the enhanced antifouling properties provided by photocatalyst nanoparticles. For uncoated membranes, the cake layer forms after 2 cycles (14 liters of water). With bare zinc oxide-coated membranes, the layer forms after 2.5 cycles (17.5 liters), an increase of 3.5 liters compared to uncoated membranes, when titanium dioxide is doped with zinc oxide, the layer forms after about 3 cycles (21 liters), an increase of approximately 7 liters. Membranes coated with titanium dioxide and ferric oxide showed the best performance: the cake layer formed after 4 cycles (28 liters) and 5 cycles (35 liters), increasing the water capacity by 14 liters and 21 liters for PTFC and PTFT coated membranes, respectively, compared to uncoated membranes. Modifying membranes by incorporating photocatalysis nanoparticles can enhance their antifouling capabilities and improve their overall properties (Choudhury et al., 2018). This modification transforms the membranes from being merely physical barriers to reactive surfaces, thereby increasing their effectiveness (Shukla et al., 2022).

Table 0-17 The No. of cycles of the several membranes before forming of cake layer

Membranes	PTFT	PTFC	PTZT	PTZC	PZ	P
No. of cycle	5	4	3	3	2.5	2
No. of liters filter	35	28	21	21	17.5	14
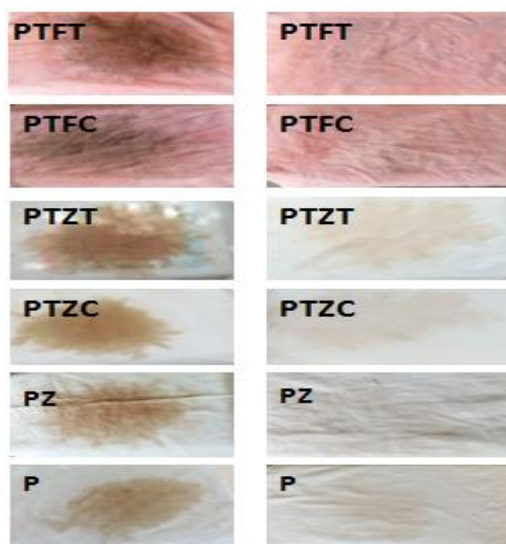
Figure 0-50 Uncoated and photocatalysis-coated membranes before and after cleaning

Table 4.14 illustrates the physicochemical properties of the raw dam water, as well as its characteristics after filtration and after cleaning the fouled membranes. The results indicate that the membranes continue to perform effectively after fouling, with their performance remaining nearly the same as before fouling.

Table 0-18 the physicochemical properties of the dam water before & after filtration and after membranes fouling

Parameter	Unit	Raw Water Value	Membranes Type (before fouling)						Membranes Type (after fouling)					
			PTFT	PTFC	PTZT	PTZC	PZ	P	PTFT	PTFC	PTZT	PTZC	PZ	P
Turbidity	NTU	16.0	0.80	0.80	0.70	0.70	1.00	4.00	0.80	0.90	0.80	0.70	0.80	3.00
pH	-	7.92	7.82	7.81	7.88	7.81	7.55	7.89	7.04	7.07	6.93	6.93	6.94	7.05
Conductivity	µS/cm	166	162	166	166	166	167	162	175	175	176	175	176	174
Total Dissolved Solids (TDS)	mg/L	83.0	81.0	83.0	83.0	83.0	83.0	81.0	77.0	76.0	79.0	78.0	78.0	82.0
Total Iron as Fe	mg/L	0.11	0.07	0.09	0.07	0.09	0.06	0.06	0.06	0.07	0.06	0.07	0.065	0.065
Zinc, as Zn^{++}	mg/L	Nil	Nil	Nil	Nil	Nil	Nil	Nil	Nil	Nil	Nil	Nil	Nil	Nil

CHAPTER FIVE

CONCLUSIONS AND RECOMMENDATION

5.1 Conclusions

This research set out to create and evaluate a novel nanoscale photo-catalytic membrane for the purification of water. This was achieved through synthesis and characterization of bare (TiO_2, Fe_2O_3 and ZnO) and codoped Fe_2O_3- TiO_2 and ZnO-TiO_2 nanphotcatalysts from Titanium precursor and commercial titanium dioxide, impregnation into polyester/ cotton membranes for application focusing on organic and microbiological contaminants in point-of-use water treatment systems using manufactured solar units.

5.1.1. Synthesis and characterization of metal-ion-doped TiO_2 photo-catalysts and impregnation to polyester based membranes

This study successfully characterized both bare and codoped photocatalysts, along with uncoated and coated membranes, using various advanced techniques including SEM, EDX, XRD, FTIR, and UVDRS. TiO_2-Fe_2O_3 photocatalysts synthesized from a titanium precursor exhibited superior properties, such as smaller particle sizes compared to commercial titanium. Extending the calcination period resulted in improved crystallinity, but at the expense of larger grains. ZnO-TiO_2 particles from commercial TiO_2 were larger and less prone to agglomeration than those from synthetic TiO_2, according to SEM examination.

The study confirmed the successful synthesis and high purity of the photocatalysts, indicated by characteristic peaks and EDX results. A significant red shift in UVDRS for α-Fe_2O_3/TiO_2 photocatalysts suggested effective utilization of sunlight for contaminant reduction. ZnO-TiO_2 photocatalysts also showed improved light absorption and reduced

band gaps, enhancing catalytic activity.

Color changes in membrane fibers indicated successful impregnation of photocatalysts. Photodegradation tests demonstrated that doping TiO_2 with other elements enhanced the removal efficiency of reactive blue dye, achieving complete removal after two hours of sunlight exposure. The degradation efficiency improved with longer exposure times and lower dye concentrations, although higher dye concentrations reduced catalyst activity due to adsorbed compound accumulation.

The pH of the solution significantly impacted dye removal, with higher efficiency observed in acidic and neutral conditions due to favorable electrostatic interactions. The photocatalysts' stability was confirmed across four cycles, showing only slight decreases in efficiency, thus affirming their stability and suitability for large-scale applications.

The immobilization of bare (TiO_2 and ZnO) and codoped TiO_2- α-Fe_2O_3 and TiO_2-ZnO photocatalysts onto the polyester membranes was achieved using an aqueous heat attachment method, resulting in obtaining different types of membranes PT and PZ using PTFT, PTFC, PTZT, and PTZC from codoped synthetic and commercial TiO_2 with Fe_2O_3 and ZnO, respectively, in addition to impregnation of pure TiO_2 and ZnO.

5.1.2. Treatment of wastewater targeting organic and microbial contaminants using photocatalytic membranes

Oxytetracycline (OTC) was utilized as an organic pollutant in the degradation experiments, conducted under sunlight for 90 minutes using a solar unit. The ability of coated and uncoated membranes to remove OTC was examined. The membrane with the highest removal efficiency was PTFT. As a result, the performance measures of PTFT served as the main basis for the experiment design. The study established that a quadratic

model effectively described and predicted OTC removal efficiency based on variations in independent variables (OTC initial concentration, water flowrate, and pH). Software calculations predicted an OTC removal efficiency of 96.308 %, closely aligning with the experimentally observed efficiency of 95 %, at pH 5, flowrate 117 ml/min, and 1 mg/L OTC concentration. This highlights the efficacy of Response Surface Methodology (RSM) in optimizing operational parameters for the heterogeneous photocatalytic process involved in OTC removal.

The introduction of α-Fe_2O_3 doping into TiO_2 leads to a shift in absorbance from the invisible to the visible region of the spectrum, this alteration enhances the absorption of sunlight irradiation, enabling the membranes to attain peak removal efficiency without the necessity of UV light. Consequently, this approach reduces costs by utilizing clean solar energy for the photocatalytic process.

The antibacterial efficacy of the coated membrane was assessed by subjecting it to two different types of medium containing *E. coli* in order to gauge its disinfection performance, using Disk diffusion test and Glass bottle test, and second, by assessing the disinfection efficacy during the filtration of water with varying concentrations of *E. coli* (flow test).

The zone of inhibition (measured in millimeters) for coated and uncoated membranes against   *E. coli* at doses of 2.45 * 105 and 2.45 * 103 CFU/ml was determined using the disk diffusion test. The uncoated membranes showed bacterial growth everywhere, including on the membrane surface, indicating no antimicrobial properties in plain polyester P. In contrast, coated membranes exhibited clear inhibition zones: 16 and 20 mm for PTFT, 17 and 19 mm for PTFC, 20 and 25 mm for PTZT, 18 and 21 mm for

PTZC, and 26 and 30 mm for PZ at the respective bacterial concentrations. Depending on the kind of photocatalyst that was utilized, the inhibition zones had different sizes. Using both coated and uncoated membranes, the glass bottle test assessed the removal efficiency of *E. coli* at a concentration of 9.8 * 105 CFU/100ml. Results indicated that uncoated membranes exhibited no antimicrobial activity, resulting in a zero removal efficiency of E. coli. In contrast, the removal efficiencies for coated membranes varied by type: PTFT achieved 92.97 %, PTFC 91.30 %, PTZT 99.99 %, PTZC 99.95 %, and PZ 100%.

For the flow test high ($12 * 10^4$ CFU/100 ml) and medium ($6 * 10^4$ CFU/100 ml) concentration of *E. coli* for synthetic feed and $13 * 10^3$ CFU/100 ml *E. coli* for dam water used to run the test. To compare the performance of coated and uncoated membranes, the removal efficiency (%) and Log Reduction Value (LRV) were computed.

When the Log Reduction Value (LRV) of uncoated membranes P (used exclusively for filtering) was calculated for synthetic feed and dam water, the results were 0.45, 0.44, and 0.46, in that order. When these membranes were coated (enabling both filtration and photodegradation), the LRV increased depending on the type of photocatalyst used. For PTFT and PTFC membranes, the LRV improved to a range of 1.6 to 1.8. The PT membranes had LRV values ranging from 3 to 3.4, indicating a greater rise. The best results were obtained by the PTZT and PTZC membranes, which attained an LRV of 5 across all bacterial concentrations.

The goal of this project was to cleanse raw water using a solar unit point-of-use system by removing chemicals and sanitizing microorganisms. Additionally, the study aimed to ensure that other physicochemical properties of the water—such as turbidity, pH,

conductivity, total dissolved solids (TDS), total iron (Fe), and zinc (Zn^{++})—met global water quality standards. The physicochemical properties of the dam water were characterized both before and after filtration to assess compliance with these standards. The study adhered to both the Kenya water quality standards and the World Health Organization (WHO) standards.

The turbidity of the dam water was initially reduced from 16 NTU to 4 NTU using uncoated polyester membranes. While this reduction met the Kenyan water quality standard of 5 NTU, it did not meet the WHO standard of less than 1 NTU. However, with the use of coated membranes, the turbidity was reduced to 1 NTU for PZ or lower for (PTFT, PTFC, PTZT, and PTZC), meeting both the Kenyan and WHO standards. Based on these findings, it can be concluded that titanium dioxide doping of the membranes led to the best turbidity reduction.

The measurements of the dam water showed that its pH was 7.92, its conductivity was 166μS/cm, its total dissolved solids (TDS) were 83 mg/l, its Fe content was 0.25 mg/l, and Zn^{++} was not present. Both international and national requirements for water quality are met by these values. Although these values were somewhat reduced when coated and uncoated membranes were used for filtering, all measures were within acceptable limits both before and after filtration. Measurements of total iron (Fe) and zinc (Zn^{++}) before and after filtration confirmed that these metals were not released from the coated membranes and remained within the acceptable water quality standards.

5.1.3. Disinfection and organic degradation kinetics and synergy of photo-catalytic membrane water treatment

The synergistic effect of combining photocatalysis and filtration was assessed,

demonstrating that the developed membrane significantly outperformed the uncoated membrane (filtration only) in removing microbial and organic contaminants. Transition metals are known to react with certain oxidants, enhancing the removal of organic pollutants and the inactivation of microorganisms. The synergistic effect was evaluated using synergy indices (SI), with a positive result indicated by SI > 1. For disinfection, the SI ranged between 1.11 and 1.24 for membranes coated with TiO_2-Zn, and between 1.07 and 1.09 for those coated with TiO_2-Fe_2O_3. In the case of TiO_2-Zn coated membranes for OTC photodegradation, the SI varied between 1.07 and 1.26, whereas for TiO_2-Fe2O3 coated membranes, it varied between 1.25 and 1.54. Together, these two factors significantly increase the efficacy and efficiency of water treatment procedures.

5.1.4. Membranes fouling, cleaning and re-use potential

Membrane systems are essential for water treatment, capable of continuous operation for over 10 cycles. On the other hand, if the membrane surface is not cleaned, a cake layer eventually forms and lowers the flow rate. Whether the membranes are coated or not, as well as their unique properties, affect this formation rate. Fouling can be efficiently removed without the use of chemicals or specialist expertise by cleaning with a bottle brush and then rinsing with water.

Coated membranes demonstrate superior durability compared to uncoated ones due to enhanced antifouling properties conferred by photocatalyst nanoparticles. Uncoated membranes typically develop a cake layer after 2 cycles (14 liters of water). In contrast, zinc oxide-coated membranes delay this process to 2.5 cycles (17.5 liters), an increase of 3.5 liters. Incorporating titanium dioxide with zinc oxide extends this further, delaying the layer formation to about 3 cycles (21 liters), and an increase of approximately 7 liters.

Membranes coated with titanium dioxide and ferric oxide perform optimally, with cake formation occurring after 4 cycles (28 liters) and 5 cycles (35 liters) for PTFC and PTFT membranes, respectively, resulting in capacity increases of 14 liters and 21 liters in contrast to membranes without coating.

Integrating photocatalyst nanoparticles into membranes enhances their antifouling capabilities and overall efficacy, transforming them from passive barriers into active surfaces that significantly improve water treatment processes.

5.2 Recommendations

Based on the findings of the study, the following recommendations are proposed:

5.2.1 Enhance the functionality of the materials by improving antimicrobial properties.

The disinfection efficiency of Titanium dioxide (TiO_2) doped with ferric oxide was lower than disinfection efficiency of the Titanium dioxide (TiO_2) doped with Zinc oxide or the bare zinc oxide. To enhance the disinfection efficiency of Titanium dioxide (TiO_2) doped with ferric oxide, one approach could involve increasing the nanoparticle coating on the membrane. Another option is to augment the photocatalyst by adding Zinc oxide (ZnO), thereby enriching its antimicrobial properties. These modifications aim to improve the membrane's ability to effectively eliminate microbial contaminants and enhance overall disinfection performance.

5.2.2 Application of the developed system in other water matrices such as textile, pharmaceutical wastewater

The study aim is the potable water and mostly the organic contaminants if available will be in low concentration because that low concentration of the blue dye and oxytetracycline were used, if another study aim to mitigate the textile or pharmaceuticals

effluents, high concentration of the dye and oxytetracycline can be used, also the concentration of the photocatalysts can be increased to get a better degradation results.

5.2.3 Automation of the process equipment to allow for solar tracking to increase absorption and utilization of sunlight

This study concern about potable water for poor people so it used manual way to adjust the dish to reflect the solar light, in case the unit used in rich area or in a big station the solar unit can improved by adding a sensor then it can follow the sun light automatically.

5.2.4 Application of rigorous experimental designs employing multiple variables to study more interactions and aid in the design of robust photocatalytic membrane systems for pilot and full scale studies

REFERENCES

Abbasi, A., Ghanbari, D., Salavati-Niasari, M., & Hamadanian, M. (2016). Photo-degradation of methylene blue: photocatalyst and magnetic investigation of Fe_2O_3–TiO_2 nanoparticles and nanocomposites. *Journal of materials science: Materials in electronics*, *27*, 4800-4809.

Abdel-Wahab, A.-M., Al-Shirbini, A.-S., Mohamed, O., & Nasr, O. (2017a). Photocatalytic degradation of paracetamol over magnetic flower-like TiO_2/Fe_2O_3 core-shell nanostructures. *J. Photochem. Photobiol. A: Chem.*, *347*, 186-198.

Abdel-Wahab, A.-M., Al-Shirbini, A.-S., Mohamed, O., & Nasr, O. (2017b). Photocatalytic degradation of paracetamol over magnetic flower-like TiO_2 /Fe_2O_3 core-shell nanostructures. *J. Photochem. Photobiol. A: Chem.*, *347*, 186-198. https://doi.org/10.1016/j.jphotochem.2017.07.030

Abdiyev, K., Azat, S., Kuldeyev, E., Ybyraiymkul, D., Kabdrakhmanova, S., Berndtsson, R., Khalkhabai, B., Kabdrakhmanova, A., & Sultakhan, S. (2023). Review of slow sand filtration for raw water treatment with potential application in less-developed countries. *Water*, *15*(11), 2007.

Achisa, C. M. (2014). *Evaluation of silver nanoparticles impregnated woven fabric microfiltration membranes for potable water treatment* [Doctoral dissertation, Durban University of Technology]. Durban University of Technology.

Adeel, S., Abrar, S., Kiran, S., Farooq, T., Gulzar, T., & Jamal, M. (2018). Sustainable application of natural dyes in cosmetic industry. *Handbook of renewable materials for coloration and finishing*, 189-211.

Adesina, O. B., William, C., & Oke, E. I. (2024). Evolution in Water Treatment: Exploring Traditional Self-Purification Methods and Emerging Technologies for Drinking Water and Wastewater Treatment: A Review. *World News of Natural Sciences*, *53*, 169-185.

Agrawal, A., Sharma, N., & Sharma, P. (2021). Designing an economical slow sand filter for households to improve water quality parameters. *Materials Today: Proceedings*, *43*, 1582-1586.

Agrawal, N., Low, P. S., Tan, J. S. J., Fong, E. W. M., Lai, Y., & Chen, Z. (2020). Durable easy-cleaning and antibacterial cotton fabrics using fluorine-free silane coupling agents and CuO nanoparticles. *Nano Materials Science*, *2*(3), 281-291.

Aguedach, A., Brosillon, S., & Morvan, J. (2005). Photocatalytic degradation of azo-dyes reactive black 5 and reactive yellow 145 in water over a newly deposited titanium dioxide. *Applied Catalysis B: Environmental*, *57*(1), 55-62.

Ahamad, T., Naushad, M., Al-Saeedi, S. I., Almotairi, S., & Alshehri, S. M. (2020). Fabrication of MoS_2/ZnS embedded in N/S doped carbon for the photocatalytic degradation of pesticide. *MatL*, *263*, 127271.

Ahammed, M. M., & Davra, K. (2011). Performance evaluation of biosand filter modified with iron oxide-coated sand for household treatment of drinking water. *Desalination*, *276*(1-3), 287-293.

Ahmadi, E., Shokri, B., Mesdaghinia, A., Nabizadeh, R., Reza Khani, M., Yousefzadeh, S., Salehi, M., & Yaghmaeian, K. (2020). Synergistic effects of α-Fe_2O_3-TiO_2 and $Na_2S_2O_8$ on the performance of a non-thermal plasma reactor as a novel catalytic oxidation process for dimethyl phthalate degradation. *Sep. Purif. Technol.*, *250*. https://doi.org/10.1016/j.seppur.2020.117185

Ahmed, H. M., Sobhy, N. A., Ibrahem, W. A., & Fawzy, M. E. (2023). Green biosynthesis of zinc oxide nanoparticles utilizing pomegranate peel extract for grey water treatment. *Solid State Phenomena*, *342*, 27-36.

Ahmed, M. A., Amin, S., & Mohamed, A. A. (2023). Fouling in reverse osmosis membranes: monitoring, characterization, mitigation strategies and future directions. *Heliyon*, *9*(4).

Akowanou, A. V. O., Aina, M. P., Groendijk, L., & Yao, B. K. (2016). Household water treatment in Benin: current/local practices. *Eur J Sci Res*, *142*(3), 246-256.

Al-Nuaim, M. A., Alwasiti, A. A., & Shnain, Z. Y. (2023). The photocatalytic process in the treatment of polluted water. *Chemical papers*, *77*(2), 677-701.

Al Zoubi, W., Salih Al-Hamdani, A. A., Sunghun, B., & Ko, Y. G. (2021). A review on TiO_2-based composites for superior photocatalytic activity. *Reviews in Inorganic Chemistry*, *41*(4), 213-222.

Ali, A., Tufa, R. A., Macedonio, F., Curcio, E., & Drioli, E. (2018). Membrane technology in renewable-energy-driven desalination. *Renewable and Sustainable Energy Reviews*, *81*, 1-21.

Ali, I., Asim, M., & Khan, T. A. (2012). Low cost adsorbents for the removal of organic pollutants from wastewater. *J. Environ. Manage.*, *113*, 170-183.

Ali, M. M., Haque, M. J., Kabir, M. H., Kaiyum, M. A., & Rahman, M. (2021). Nano synthesis of ZnO–TiO_2 composites by sol-gel method and evaluation of their antibacterial, optical and photocatalytic activities. *Results in Materials*, *11*, 100199.

Alizadeh, E., & Baseri, H. (2022). Photocatalytic degradation of sumatriptan succinate by ZnO, Fe doped ZnO and TiO_2-ZnO nanocatalysts. *Materials Chemistry Horizons*, *1*(1), 7-21.

Alosmanov, R., Buniyat-Zadeh, I., Soylak, M., Shukurov, A., Aliyeva, S., Turp, S., & Guliyeva, G. (2022). Design, Structural Characteristic and Antibacterial Performance of Silver-Containing Cotton Fiber Nanocomposite. *Bioengineering*, *9*(12), 770.

Alosmanov, R., Wolski, K., & Zapotoczny, S. (2017). Grafting of thermosensitive poly (N-isopropylacrylamide) from wet bacterial cellulose sheets to improve its swelling-drying ability. *Cellu*, *24*, 285-293.

AlSawaftah, N., Abuwatfa, W., Darwish, N., & Husseini, G. (2021). A comprehensive review on membrane fouling: Mathematical modelling, prediction, diagnosis, and mitigation. *Water*, *13*(9), 1327.

Álvarez, P. M., Jaramillo, J., López-Piñero, F., & Plucinski, P. K. (2010). Preparation and characterization of magnetic TiO_2 nanoparticles and their utilization for the degradation of emerging pollutants in water. *Applied Catalysis B: Environmental*, *100*(1-2), 338-345. https://doi.org/10.1016/j.apcatb.2010.08.010.

Amani, A., Montazer, M., & Mahmoudirad, M. (2019). Synthesis of applicable hydrogel corn silk/ZnO nanocomposites on polyester fabric with antimicrobial properties and low cytotoxicity. *Int. J. Biol. Macromol.*, *123*, 1079-1090.

Anand, A., Unnikrishnan, B., Mao, J.-Y., Lin, H.-J., & Huang, C.-C. (2018). Graphene-based nanofiltration membranes for improving salt rejection, water flux and antifouling–A review. *Desalination*, *429*, 119-133.

Anjaneyulu, B., Mittal, C., Chauhan, V., Tiwari, A., & Bhathiwal, A. S. (2024). Wastewater treatment with sustainable bionanocomposites: a comprehensive review. *Nanotechnology for Environmental Engineering*, 1-36.

Anjum, M., Miandad, R., Waqas, M., Gehany, F., & Barakat, M. (2019). Remediation of wastewater using various nano-materials. *Arabian Journal of chemistry*, *12*(8), 4897-4919.

Anjum, M., Oves, M., Kumar, R., & Barakat, M. (2017). Fabrication of ZnO-ZnS@ polyaniline nanohybrid for enhanced photocatalytic degradation of 2-chlorophenol and microbial contaminants in wastewater. *Int. Biodeterior. Biodegrad.*, *119*, 66-77.

Aremu, O., Akintayo, C., Naidoo, E., Nelana, S., & Ayanda, O. (2021). Synthesis and applications of nano-sized zinc oxide in wastewater treatment: a review. *International Journal of Environmental Science and Technology*, 1-20.

Arghavan, F. S., Al-Musawi, T. J., Allahyari, E., Moslehi, M. H., Nasseh, N., & Panahi, A. H. (2021). Complete degradation of tamoxifen using $FeNi_3$ @ SiO_2 @ ZnO as a photocatalyst with UV light irradiation: a study on the degradation process and sensitivity analysis using ANN tool. *Mater. Sci. Semicond. Process.*, *128*, 105725.

Arin, J., Thongtem, S., & Thongtem, T. (2013). Single-step synthesis of ZnO/TiO_2 nanocomposites by microwave radiation and their photocatalytic activities. *MatL*, *96*, 78-81.

Armaković, S. J., Savanović, M. M., & Armaković, S. (2022). Titanium dioxide as the most used photocatalyst for water purification: An overview. *Catalysts*, *13*(1), 26.

Asadzadeh Patehkhor, H., Fattahi, M., & Khosravi-Nikou, M. (2021). Synthesis and characterization of ternary chitosan–TiO_2–ZnO over graphene for photocatalytic degradation of tetracycline from pharmaceutical wastewater. *Scientific reports*, *11*(1), 24177.

Asoufi, H. M., Al-Antary, T. M., & Awwad, A. M. (2018). Green route for synthesis hematite (α-Fe_2O_3) nanoparticles: Toxicity effect on the green peach aphid, Myzus persicae (Sulzer). *Environmental Nanotechnology, Monitoring & Management*, *9*, 107-111.

Ayar, V., & Sutaria, M. (2021). Comparative evaluation of ex situ and in situ method of fabricating aluminum/TiB_2 composites. *International Journal of Metalcasting*, *15*(3), 1047-1056.

Backer, H. D., Derlet, R. W., & Hill, V. R. (2024). Wilderness Medical Society Clinical Practice Guidelines on Water Treatment for Wilderness, International Travel, and Austere Situations: 2024 Update. *Wilderness Environ. Med.*, *35*(1_suppl), 45S-66S.

Bagheri, M., Najafabadi, N. R., & Borna, E. (2020). Removal of reactive blue 203 dye photocatalytic using ZnO nanoparticles stabilized on functionalized MWCNTs. *Journal of King Saud University-Science*, *32*(1), 799-804.

Bahrudin, N. (2022). Evaluation of degradation kinetic and photostability of immobilized TiO_2/activated carbon bilayer photocatalyst for phenol removal. *Applied Surface Science Advances*, *7*, 100208.

Behera, M., Nayak, J., Banerjee, S., Chakrabortty, S., & Tripathy, S. K. (2021). A review on the treatment of textile industry waste effluents towards the development of efficient mitigation strategy: An integrated system design approach. *Journal of Environmental Chemical Engineering*, *9*(4), 105277.

Behroozi, A. H., & Xu, R. (2023). Photocatalytic CO_2 reduction: Photocatalysts, membrane reactors, and hybrid processes. *Chem Catalysis*, *3*(3).

Bhanvase, B., Shende, T., & Sonawane, S. (2017). A review on graphene–TiO_2 and doped graphene–TiO_2 nanocomposite photocatalyst for water and wastewater treatment. *Environmental Technology Reviews*, *6*(1), 1-14.

Bhatta, R., Kayastha, R., Subedi, D. P., & Joshi, R. (2015). Treatment of wastewater by ozone produced in dielectric barrier discharge. *Journal of Chemistry*, *2015*(1), 648162.

Binazadeh, M., Rasouli, J., Sabbaghi, S., Mousavi, S. M., Hashemi, S. A., & Lai, C. W. (2023). An overview of photocatalytic membrane degradation development. *Materials*, *16*(9), 3526.

Biswajit, Biswas, N. T., Baidya, R., & Ghosh, S. K. J. E. U. A. (2014). Nanotechnology in waste water treatment: a review. IV International Conference „Ecology Of Urban Areas 2014", University Of Novi Sad.

Biswal, A. K., & Misra, P. K. (2020). Biosynthesis and characterization of silver nanoparticles for prospective application in food packaging and biomedical fields. *MCP*, *250*, 123014.

Bitton, G. (2014). *Microbiology of drinking water: production and distribution*. John Wiley & Sons.

Bodzek, M. (2019). Membrane separation techniques: removal of inorganic and organic admixtures and impurities from water environment. *Archives of Environmental Protection*, *45*(4), 4--19.

Bodzek, M., Konieczny, K., & Kwiecińska-Mydlak, A. (2020). Application of nanotechnology and nanomaterials in water and wastewater treatment: membranes, photocatalysis and disinfection. *Desalination and Water Treatment*, *186*, 88-106.

Bootluck, W., Chittrakarn, T., Techato, K., & Khongnakorn, W. (2021). Modification of surface α-Fe_2O_3/TiO_2 photocatalyst nanocomposite with enhanced photocatalytic activity by Ar gas plasma treatment for hydrogen evolution. *Journal of Environmental Chemical Engineering*, *9*(4), 105660.

Bourne, D. G., Blakeley, R. L., Riddles, P., & Jones, G. J. (2006). Biodegradation of the cyanobacterial toxin microcystin LR in natural water and biologically active slow sand filters. *Water Res.*, *40*(6), 1294-1302.

Bouziane Errahmani, K., Benhabiles, O., Bellebia, S., Bengharez, Z., Goosen, M., & Mahmoudi, H. (2021). Photocatalytic nanocomposite polymer-TiO_2 membranes for pollutant removal from wastewater. *Catalysts*, *11*(3), 402.

Bouziani, A., Park, J., & Ozturk, A. (2020). Synthesis of α-Fe$_2$O$_3$/TiO$_2$ heterogeneous composites by the sol-gel process and their photocatalytic activity. *J. Photochem. Photobiol. A: Chem.*, *400*, 112718.

Briffa, J., Sinagra, E., & Blundell, R. (2020). Heavy metal pollution in the environment and their toxicological effects on humans. *Heliyon*, *6*(9), e04691. https://doi.org/10.1016/j.heliyon.2020.e04691

Cao, X.-L., Zhou, F.-Y., Cai, J., Zhao, Y., Liu, M.-L., Xu, L., & Sun, S.-P. (2021). High-permeability and anti-fouling nanofiltration membranes decorated by asymmetric organic phosphate. *J. Membr. Sci.*, *617*, 118667.

Chabalala, M. B., Gumbi, N. N., Mamba, B. B., Al-Abri, M. Z., & Nxumalo, E. N. (2021). Photocatalytic nanofiber membranes for the degradation of micropollutants and their antimicrobial activity: recent advances and future prospects. *Membranes*, *11*(9), 678.

Chadha, U., Selvaraj, S. K., Thanu, S. V., Cholapadath, V., Abraham, A. M., Manoharan, M., & Paramsivam, V. (2022). A review of the function of using carbon nanomaterials in membrane filtration for contaminant removal from wastewater. *Materials Research Express*, *9*(1), 012003.

Chand, K., Cao, D., Fouad, D. E., Shah, A. H., Lakhan, M. N., Dayo, A. Q., Sagar, H. J., Zhu, K., & Mohamed, A. M. A. (2020). Photocatalytic and antimicrobial activity of biosynthesized silver and titanium dioxide nanoparticles: a comparative study. *J. Mol. Liq.*, *316*, 113821.

Changanaqui, K., Brillas, E., Alarcón, H., & Sirés, I. (2020). ZnO/TiO$_2$/Ag$_2$Se nanostructures as photoelectrocatalysts for the degradation of oxytetracycline in water. *Electrochim. Acta*, *331*, 135194.

Chen, W., Zeng, M., & Yang, J. (2023). Preparation of Fenton Catalysts for Water Treatment. *Catalysts*, *13*(11), 1407.

Chhabra, R. P., & Gurappa, B. (2019). *Coulson and Richardson's chemical engineering* (Vol. volume 2A). Butterworth-Heinemann.

Chorawalaa, K. K., & Mehta, M. J. (2015). Applications of nanotechnology in wastewater treatment. *Int J Innov Emerg Res Eng*, *2*(1), 21-26.

Choudhury, R. R., Gohil, J. M., Mohanty, S., & Nayak, S. K. (2018). Antifouling, fouling release and antimicrobial materials for surface modification of reverse osmosis and nanofiltration membranes. *Journal of Materials Chemistry A*, *6*(2), 313-333.

Ciawi, Y., & Khoiruddin, K. (2024). Low-Cost Antibacterial Ceramic Water Filters for Decentralized Water Treatment: Advances and Practical Applications. *ACS omega*, *9*(11), 12457-12477.

Çolak, F., Atar, N., & Olgun, A. (2009). Biosorption of acidic dyes from aqueous solution by Paenibacillus macerans: Kinetic, thermodynamic and equilibrium studies. *Chem. Eng. J.*, *150*(1), 122-130.

Correa, M. G., Martínez, F. B., Vidal, C. P., Streitt, C., Escrig, J., & de Dicastillo, C. L. (2020). Antimicrobial metal-based nanoparticles: A review on their synthesis, types and antimicrobial action. *Beilstein journal of nanotechnology*, *11*(1), 1450-1469.

Cuerda-Correa, E. M., Alexandre-Franco, M. F., & Fernández-González, C. (2019). Advanced oxidation processes for the removal of antibiotics from water. An overview. *Water*, *12*(1), 102.

Da Silva, R. L., Fumagalli, M., & Krumholz, M. (2012). Slug—stochastically lighting up galaxies. I. Methods and validating tests. *The Astrophysical Journal*, *745*(2), 145.

Dai, Y., Liu, Y., Kong, J., Yuan, J., Sun, C., Xian, Q., Yang, S., & He, H. (2019). High photocatalytic degradation efficiency of oxytetracycline hydrochloride over $Ag/AgCl/BiVO_4$ plasmonic photocatalyst. *Solid State Sciences*, *96*, 105946.

Daneshvar, N., Salari, D., & Khataee, A. (2003). Photocatalytic degradation of azo dye acid red 14 in water: investigation of the effect of operational parameters. *J. Photochem. Photobiol. A: Chem.*, *157*(1), 111-116.

Dankovich, T. (2012). Bactericidal paper containing silver nanoparticles for water treatment.

Dankovich, T. A. (2014). Microwave-assisted incorporation of silver nanoparticles in paper for point-of-use water purification. *Environmental Science: Nano*, *1*(4), 367-378.

Dankovich, T. A., & Gray, D. G. (2011). Bactericidal paper impregnated with silver nanoparticles for point-of-use water treatment. *Environ. Sci. Technol.*, *45*(5), 1992-1998.

Dehbi, A., Dehmani, Y., Omari, H., Lammini, A., Elazhari, K., & Abdallaoui, A. (2020). Hematite iron oxide nanoparticles (α-Fe_2O_3): synthesis and modelling adsorption of malachite green. *Journal of environmental chemical engineering*, *8*(1), 103394.

Dharma, H. N. C., Jaafar, J., Widiastuti, N., Matsuyama, H., Rajabsadeh, S., Othman, M. H. D., Rahman, M. A., Jafri, N. N. M., Suhaimin, N. S., & Nasir, A. M. (2022). A review of titanium dioxide (TiO_2)-based photocatalyst for oilfield-produced water treatment. *Membranes*, *12*(3), 345.

Dochia, M., Chambre, D., Gavrilaş, S., & Moisă, C. (2018). Characterization of the complexing agents' influence on bioscouring cotton fabrics by FT-IR and TG/DTG/DTA analysis. *JTAC*, *132*, 1489-1498.

Dong, H., Zeng, G., Tang, L., Fan, C., Zhang, C., He, X., & He, Y. (2015). An overview on limitations of TiO_2-based particles for photocatalytic degradation of organic pollutants and the corresponding countermeasures. *Water Res.*, *79*, 128-146.

Dong, W., Zhou, M., Li, Y., Zhai, S., Jin, K., Fan, Z., Zhao, H., Zou, W., & Cai, Z. (2020). Low-salt dyeing of cotton fabric grafted with pH-responsive cationic polymer of polyelectrolyte 2-(N, N-dimethylamino) ethyl methacrylate. *Colloids Surf. Physicochem. Eng. Aspects*, *594*, 124573.

Dos Santos, P. R., de Souza Leite, L., & Daniel, L. A. (2022). Performance of biological activated carbon (BAC) filtration for the treatment of secondary effluent: A pilot-scale study. *J. Environ. Manage.*, *302*, 114026.

EAS, K. (2014). Kenya Standard potable water specification. ICS,

Ebele, A. J., Abdallah, M. A.-E., & Harrad, S. (2017). Pharmaceuticals and personal care products (PPCPs) in the freshwater aquatic environment. *Emerging contaminants*, *3*(1), 1-16.

El-Naggar, H., Abd Al-Halim, M., Gaballa, A. S., & Hassouba, M. (2021). Surface improvement of cotton/polyester blend textile using DC air glow discharge plasma. *PhyS*, *96*(12), 125712.

El-Nahhal, I. M., Elmanama, A. A., & Amara, N. M. (2016). Synthesis of nanometal oxide–coated cotton composites. *Cotton Research*, 279-297.

El-taweel, R. M., Mohamed, N., Alrefaey, K. A., Husien, S., Abdel-Aziz, A., Salim, A. I., Mostafa, N. G., Said, L. A., Fahim, I. S., & Radwan, A. G. (2023). A review of coagulation explaining its definition, mechanism, coagulant types, and optimization models; RSM, and ANN. *Current Research in Green and Sustainable Chemistry*, *6*, 100358.

El Jabbar, Y., ElHafdi, M., Benchikhi, M., El Ouatib, R., Er-Rakho, L., & Essadki, A. (2019). Photocatalytic degradation of navy blue textile dye by nanoscale cobalt aluminate prepared by polymeric precursor method. *Environmental Nanotechnology, Monitoring & Management*, *12*, 100259.

Elbana, M., de Cartagena, F. R., & Puig-Bargués, J. (2012). Effectiveness of sand media filters for removing turbidity and recovering dissolved oxygen from a reclaimed effluent used for micro-irrigation. *Agric. Water Manage.*, *111*, 27-33.

Epelle, E. I., Macfarlane, A., Cusack, M., Burns, A., Okolie, J. A., Mackay, W., Rateb, M., & Yaseen, M. (2023). Ozone application in different industries: A review of recent developments. *Chem. Eng. J.*, *454*, 140188.

Esfahani, A. R., Firouzi, A. F., Sayyad, G., Kiasat, A., Alidokht, L., & Khataee, A. (2014). Pb (II) removal from aqueous solution by polyacrylic acid stabilized zero-valent iron nanoparticles: process optimization using response surface methodology. *Res. Chem. Intermed.*, *40*, 431-445.

Eskandari, P., Amarloo, E., Zangeneh, H., Rezakazemi, M., & Aminabhavi, T. M. (2023). Photocatalytic degradation of metronidazole and oxytetracycline by novel l-Arginine (C, N codoped)-TiO_2/g-C_3N_4: RSM optimization, photodegradation mechanism, biodegradability evaluation. *Chemosphere*, *337*, 139282.

Etemadi, H., Yegani, R., & Babaeipour, V. (2017). Performance evaluation and antifouling analyses of cellulose acetate/nanodiamond nanocomposite membranes in water treatment. *J. Appl. Polym. Sci.*, *134*(21).

Ezealigo, U. S., Ezealigo, B. N., Aisida, S. O., & Ezema, F. I. (2021). Iron oxide nanoparticles in biological systems: Antibacterial and toxicology perspective. *JCIS Open*, *4*, 100027.

Felis, E., Kalka, J., Sochacki, A., Kowalska, K., Bajkacz, S., Harnisz, M., & Korzeniewska, E. (2020). Antimicrobial pharmaceuticals in the aquatic environment-occurrence and environmental implications. *Eur. J. Pharmacol.*, *866*, 172813.

Feng, C., Lu, Z., Zhang, Y., Liang, Q., Zhou, M., Li, X., Yao, C., Li, Z., & Xu, S. (2022). A magnetically recyclable dual Z-scheme GCNQDs-$CoTiO_3$/$CoFe_2O_4$ composite photocatalyst for efficient photocatalytic degradation of oxytetracycline. *Chem. Eng. J.*, *435*, 134833.

Feng, J., Ran, X., Wang, L., Xiao, B., Lei, L., Zhu, J., Liu, Z., Xi, X., Feng, G., & Dai, Z. (2022). The synergistic effect of adsorption-photocatalysis for removal of organic pollutants on mesoporous $Cu_2V_2O_7$/$Cu_3V_2O_8$/g-C_3N_4 heterojunction. *International Journal of Molecular Sciences*, *23*(22), 14264.

Fernando, S., Gunasekara, T., & Holton, J. (2018). Antimicrobial nanoparticles: applications and mechanisms of action. *Sri Lankan Journal of Infectious Diseases Vol.8 (1):2-11*

Frisbie, S. H., Mitchell, E. J., Dustin, H., Maynard, D. M., & Sarkar, B. (2012). World Health Organization discontinues its drinking-water guideline for manganese. *Environ. Health Perspect.*, *120*(6), 775-778.

Ganjoo, R., Sharma, S., Kumar, A., & Daouda, M. (2023). Activated carbon: Fundamentals, classification, and properties.

Gareso, P., Heryanto, H., Sampebatu, E., Sampe, N., Palentek, V., Taba, P., Juarlin, E., & Aryanto, D. (2021). Synthesis and material characterization of TiO2 nanoparticles doped with iron (Fe). Journal of Physics: Conference Series,

Garrido-Cardenas, J. A., Esteban-García, B., Agüera, A., Sánchez-Pérez, J. A., & Manzano-Agugliaro, F. (2020). Wastewater treatment by advanced oxidation process and their worldwide research trends. *Int. J. Env. Res. Public Health*, *17*(1), 170.

Gottesman, R., Shukla, S., Perkas, N., Solovyov, L. A., Nitzan, Y., & Gedanken, A. (2011). Sonochemical coating of paper by microbiocidal silver nanoparticles. *Langmuir*, *27*(2), 720-726.

Granados, A., Pleixats, R., & Vallribera, A. (2021). Recent advances on antimicrobial and anti-inflammatory cotton fabrics containing nanostructures. *Molecules*, *26*(10), 3008.

Grignani, E., Mansi, A., Cabella, R., Castellano, P., Tirabasso, A., Sisto, R., Spagnoli, M., Fabrizi, G., Frigerio, F., & Tranfo, G. (2020). Safe and effective use of ozone as air and surface disinfectant in the conjuncture of Covid-19. *Gases*, *1*(1), 19-32.

Gul, A., Hruza, J., & Yalcinkaya, F. (2021). Fouling and chemical cleaning of microfiltration membranes: A mini-review. *Polymers*, *13*(6), 846.

Gupta, B. G., Agrawal, K., & Biswas, J. K. (2018). Conservation of ground water at Maheshtala bleaching and dyeing cluster, a populated area in West Bengal, India by implementing ultra filtration and reverse osmosis based effluent treatment plant—A case study. *Journal of The Institution of Engineers (India): Series A*, *99*, 705-718.

Gurlhosur, S. H., & Sreekanth, B. (2018). Synthesis, Characterization Of Iron Oxide (α-Fe_2O_3) Nanoparticles And Its Application In Photocatalytic Reduction Of Chromium (VI). *Rasāyan Journal of Chemistry*, *11*(4), 1678-1685.

Gusain, R., Kumar, N., Opoku, F., Govender, P. P., & Ray, S. S. (2021). MoS_2 nanosheet/ZnS composites for the visible-light-assisted photocatalytic degradation of oxytetracycline. *ACS Applied Nano Materials*, *4*(5), 4721-4734.

Haig, S.-J., Collins, G., Davies, R., Dorea, C., & Quince, C. (2011). Biological aspects of slow sand filtration: past, present and future. *Water Science and Technology: Water Supply*, *11*(4), 468-472.

Hamouda, M., Anderson, W., & Huck, P. (2012). Employing multi-criteria decision analysis to select sustainable point-of-use and point-of-entry water treatment systems. *Water Science and Technology: Water Supply*, *12*(5), 637-647.

Haque, F. Z., Nandanwar, R., & Singh, P. (2017). Evaluating photodegradation properties of anatase and rutile TiO_2 nanoparticles for organic compounds. *Optik*, *128*, 191-200.

Hernández-Téllez, C. N., Plascencia-Jatomea, M., & Cortez-Rocha, M. O. (2016). *Chitosan-based bionanocomposites: development and perspectives in food and agricultural applications.*

Ho, P. L., Hung, L. D., Minh, V. T., Chinh, D. V., Thanh, T. T., & Tao, C. V. (2020). Simultaneous determination of gross alpha/beta activities in groundwater for ingestion effective dose and its associated public health risk prevention. *Scientific Reports*, *10*(1), 4299.

Horikoshi, S., & Serpone, N. (2020). Can the photocatalyst TiO_2 be incorporated into a wastewater treatment method? Background and prospects. *Catal. Today*, *340*, 334-346. https://doi.org/10.1016/j.cattod.2018.10.020

Huang, C., Fang, N., Yu, W., Wang, R., Chu, Y., & Li, J. (2024). Photodegradation of halogenated organic pollutants in wastewater: A review. *Journal of Industrial and Engineering Chemistry*.

Ijadpanah-Saravy, H., Safari, M., Khodadadi-Darban, A., & Rezaei, A. (2014). Synthesis of titanium dioxide nanoparticles for photocatalytic degradation of cyanide in wastewater. *Anal. Lett.*, *47*(10), 1772-1782.

Irani, E., & Amoli-Diva, M. (2020). Hybrid adsorption–photocatalysis properties of quaternary magneto-plasmonic ZnO/MWCNTs nanocomposite for applying synergistic photocatalytic removal and membrane filtration in industrial wastewater treatment. *J. Photochem. Photobiol. A: Chem.*, *391*, 112359.

Irfan, M., Nawaz, R., Khan, J. A., Ullah, H., Haneef, T., Legutko, S., Rahman, S., Józwik, J., Alsaiari, M. A., & Khan, M. K. A. (2021). Synthesis and characterization of manganese-modified black TiO_2 nanoparticles and their performance evaluation for the photodegradation of phenolic compounds from wastewater. *Materials*, *14*(23), 7422.

Iwuozor, K. O. (2019). Prospects and challenges of using coagulation-flocculation method in the treatment of effluents. *Advanced Journal of Chemistry-Section A*, *2*(2), 105-127.

Jackson, K. N., & Smith, J. A. (2018). A new method for the deposition of metallic silver on porous ceramic water filters. *Journal of nanotechnology*, *2018*, 1-9.

Jaeel, A. J., & Abdulkathum, S. (2018). Sustainable pollutants removal from wastewater using sand filter: A review. 2018 International Conference on Advance of Sustainable Engineering and its Application (ICASEA),

Jaiaue, P., Piluk, J., Sawattrakool, K., Thammakes, J., Malasuk, C., Thitiprasert, S., Thongchul, N., & Siwamogsatham, S. (2022). Mathematical modeling for evaluating inherent parameters affecting UVC decontamination of indicator bacteria. *Appl. Environ. Microbiol.*, *88*(7), e02148-02121.

Jamkhande, P. G., Ghule, N. W., Bamer, A. H., & Kalaskar, M. G. (2019). Metal nanoparticles synthesis: An overview on methods of preparation, advantages and disadvantages, and applications. *J. Drug Deliv. Sci. Technol.*, *53*, 101174.

Jang, H., Lee, C. S., Kim, J. H., & Kim, J. (2024). Optimization of photocatalytic ceramic membrane filtration by response surface methodology: Effects of hydrodynamic conditions on organic fouling and removal efficiency. *Chemosphere*, *356*, 141885.

Jasso-Salcedo, A. B., Palestino, G., & Escobar-Barrios, V. A. (2014). Effect of Ag, pH, and time on the preparation of Ag-functionalized zinc oxide nanoagglomerates as photocatalysts. *JCat*, *318*, 170-178.

Jayawardena, A. (2021). An inconvenient truth about access to safe drinking water. *International Journal of Environment and Climate Change*, *11*(10), 158-168.

Jiang, Q., Ji, Y., Zheng, T., Li, X., & Xia, C. (2023). The nexus of innovation: Electrochemically synthesizing H2O2 and its integration with downstream reactions. *ACS Materials Au*, *4*(2), 133-147.

Jimenez-Relinque, E., Lee, S. F., Plaza, L., & Castellote, M. (2022). Synergetic adsorption–photocatalysis process for water treatment using TiO_2 supported on waste stainless steel slag. *Environmental Science and Pollution Research*, *29*(26), 39712-39722.

Kalita, I., Kamilaris, A., Havinga, P., & Reva, I. (2024). Assessing the Health Impact of Disinfection Byproducts in Drinking Water. *ACS Es&t Water*, *4*(4), 1564-1578.

Karim, K., Guha, S., & Beni, R. (2020). Comparative Analysis of Water Quality Disparities in the United States in Relation to Heavy Metals and Biological Contaminants. *Water*, *12*(4), 967.

Karthikeyan, C., Arunachalam, P., Ramachandran, K., Al-Mayouf, A. M., & Karuppuchamy, S. (2020). Recent advances in semiconductor metal oxides with enhanced methods for solar photocatalytic applications. *JAllC*, *828*, 154281.

Kaur, N., Shahi, S. K., & Singh, V. (2015). Anomalous behavior of visible light active TiO_2 for the photocatalytic degradation of different Reactive dyes. *Photochemical & Photobiological Sciences*, *14*, 2024-2034.

Khader, E. H., Muslim, S. A., Saady, N. M. C., Ali, N. S., Salih, I. K., Mohammed, T. J., Albayati, T. M., & Zendehboudi, S. (2024). Recent Advances in Photocatalytic Advanced Oxidation Processes for Organic Compound Degradation: A Review. *Desalination and Water Treatment*, 100384.

Khan, Z. U. H., Gul, N. S., Sabahat, S., Sun, J., Tahir, K., Shah, N. S., Muhammad, N., Rahim, A., Imran, M., & Iqbal, J. (2023). Removal of organic pollutants through hydroxyl radical-based advanced oxidation processes. *Ecotoxicol. Environ. Saf.*, *267*, 115564.

Khasawneh, O. F. S., Palaniandy, P., Ahmadipour, M., Mohammadi, H., & Bin Hamdan, M. R. (2021). Removal of acetaminophen using Fe_2O_3-TiO_2 nanocomposites by photocatalysis under simulated solar irradiation: Optimization study. *Journal of Environmental Chemical Engineering*, *9*(1). https://doi.org/10.1016/j.jece.2020.104921.

Khasawneh, O. F. S., Palaniandy, P., & Teng, L. P. (2019). Large-scale study for the photocatalytic degradation of paracetamol using Fe_2O_3/TiO_2 nanocomposite catalyst and CPC reactor under natural sunlight radiations. *MethodsX*, *6*, 2735-2743. https://doi.org/10.1016/j.mex.2019.11.016.

Khasawneh, O. F. S., Palaniandy, P. J. E. T., & Innovation. (2021). Removal of organic pollutants from water by Fe_2O_3/TiO_2 based photocatalytic degradation: A review. *Environmental Technology & Innovation*, *21*, 101230.

Khashan, K. S., Sulaiman, G. M., Abdulameer, F. A., Albukhaty, S., Ibrahem, M. A., Al-Muhimeed, T., & AlObaid, A. A. (2021). Antibacterial activity of TiO_2 nanoparticles prepared by one-step laser ablation in liquid. *Applied Sciences*, *11*(10), 4623.

Khataee, A. (2009). Application of central composite design for the optimization of photo-destruction of a textile dye using UV/SO process. *Polish Journal of Chemical Technology*, *11*(4), 38-45.

Kim, S. P., Choi, M. Y., & Choi, H. C. (2015). Characterization and photocatalytic performance of SnO_2–CNT nanocomposites. *ApSS*, *357*, 302-308.

Koruyucu, A., Erdal, B., Aydin KurÇ, M., & GÜLen, D. (2021). Antibacterial and Washing Resistance Improvement of Cotton Fabric Using Some Metal Oxides. *Tekstil ve Konfeksiyon*, *31*(1), 19-26. https://doi.org/10.32710/tekstilvekonfeksiyon.724693.

Krishnamoorthy, K., Navaneethaiyer, U., Mohan, R., Lee, J., & Kim, S.-J. (2012). Graphene oxide nanostructures modified multifunctional cotton fabrics. *Applied Nanoscience*, *2*, 119-126.

Kumar, M. A., Abebe, B., Nagaswarupa, H., Murthy, H. A., Ravikumar, C., & Sabir, F. K. (2020). Enhanced photocatalytic and electrochemical performance of TiO_2-Fe_2O_3 nanocomposite: Its applications in dye decolorization and as supercapacitors. *Scientific Reports*, *10*(1), 1249.

Kumar, P. S., & Saravanan, A. (2017). Sustainable wastewater treatments in textile sector. In *Sustainable fibres and textiles* (pp. 323-346). Elsevier.

Kurniawan, S. B., Abdullah, S. R. S., Imron, M. F., Said, N. S. M., Ismail, N. I., Hasan, H. A., Othman, A. R., & Purwanti, I. F. (2020). Challenges and opportunities of biocoagulant/bioflocculant application for drinking water and wastewater treatment and its potential for sludge recovery. *Int. J. Env. Res. Public Health*, *17*(24), 9312.

Kuvarega, A. T., & Mamba, B. B. (2016). Photocatalytic membranes for efficient water treatment. In *Semiconductor photocatalysis-materials, mechanisms and applications*. IntechOpen.

Lassoued, A., Lassoued, M. S., Dkhil, B., Ammar, S., & Gadri, A. (2018). Synthesis, photoluminescence and Magnetic properties of iron oxide (α-Fe_2O_3) nanoparticles through precipitation or hydrothermal methods. *Physica E: Low-dimensional Systems and Nanostructures*, *101*, 212-219.

Le, H. N. (2018). *A concept for nanoparticle-based photocatalytic treatment of wastewater from textile industry* Hanoi University of Science and Technology.

Leary, R., & Westwood, A. (2011). Carbonaceous nanomaterials for the enhancement of TiO_2 photocatalysis. *Carbon*, *49*(3), 741-772.

LeChevallier, M. W., & Au, K.-K. (2004). *Water treatment and pathogen control*. Iwa Publishing.

Lee, K. M., Lai, C. W., Ngai, K. S., & Juan, J. C. (2016). Recent developments of zinc oxide based photocatalyst in water treatment technology: a review. *Water Res.*, *88*, 428-448.

Liang, Y., Huang, G., Li, Y., Yao, Y., Xin, X., Li, X., Yin, J., Gao, S., Wu, Y., & Chen, X. (2022). Photocatalytic disinfection for point-of-use water treatment using $Ti3^+$ self-doping TiO_2 nanoparticle decorated ceramic disk filter. *Environ. Res.*, *212*, 113602.

Liu, J., Wang, Z., Dong, B., & Zhao, D. (2016). Fouling behaviors correlating to water characteristics during the ultrafiltration of micro-polluted water with and without the addition of powdered activated carbon. *Colloids Surf. Physicochem. Eng. Aspects*, *511*, 320-328.

Liu, Y., Zhao, Y., & Wang, J. (2021). Fenton/Fenton-like processes with in-situ production of hydrogen peroxide/hydroxyl radical for degradation of emerging contaminants: Advances and prospects. *J. Hazard. Mater.*, *404*, 124191.

Lotfi, H., Nademi, M., Mansouri, M., & Olya, M. E. (2016). Employing response surface analysis for photocatalytic degradation of MTBE by nanoparticles. *Adv. Environ. Sci. Technol*, *3*, 127-135.

Lu, P., Wang, X., Tang, Y., Ding, A., Yang, H., Guo, J., Cui, Y., & Ling, C. (2020). Granular activated carbon assisted nitrate-dependent anaerobic methane oxidation-membrane bioreactor: Strengthening effect and mechanisms. *Environ. Int.*, *138*, 105675.

Lu, Z., Sun, W., Li, C., Cao, W., Jing, Z., Li, S., Ao, X., Chen, C., & Liu, S. (2020). Effect of granular activated carbon pore-size distribution on biological activated carbon filter performance. *Water Res.*, *177*, 115768.

Lucarelli, L., Nadtochenko, V., & Kiwi, d. J. (2000). Environmental photochemistry: quantitative adsorption and FTIR studies during the TiO_2-photocatalyzed degradation of orange II. *Langmuir*, *16*(3), 1102-1108.

Ma, H., Cheng, X., Ma, C., Dong, X., Zhang, X., Xue, M., Zhang, X., & Fu, Y. (2013). Synthesis, characterization, and photocatalytic activity of N-doped ZnO/ZnS composites. *International Journal of Photoenergy*, *2013*(625024,), 8.

Ma, Z., Liu, J., Shen, G., Zheng, X., Pei, Y., & Tang, K. (2021). In-situ synthesis and immobilization of silver nanoparticles on microfibrillated cellulose for long-term antibacterial applications. *Cellu*, *28*(10), 6287-6303.

Mahmoodi, V., Bastami, T. R., & Ahmadpour, A. (2018). Solar energy harvesting by magnetic-semiconductor nanoheterostructure in water treatment technology. *Environmental Science and Pollution Research*, *25*, 8268-8285.

Maiyo, J. K., Dasika, S., & Jafvert, C. T. (2023). Slow sand filters for the 21st century: A review. *Int. J. Env. Res. Public Health*, *20*(2), 1019.

Majumdar, A., Ghosh, U., & Pal, A. (2021). Novel 2D/2D g-C_3N_4/Bi_4NbO_8Cl nano-composite for enhanced photocatalytic degradation of oxytetracycline under visible LED light irradiation. *J. Colloid Interface Sci.*, *584*, 320-331.

Malvestiti, J. A., Cavalcante, R. P., Bacellar, P. F., Tornisielo, V. L., & Dantas, R. F. (2024). Modelling ozone disinfection of secondary effluents in presence of scavengers and metal catalyst: Synergistic effect and regrowth. *Journal of Water Process Engineering*, *57*, 104650.

Manzoor, A., Jan, B., Zahoor, I., Anjum, N., Nabi, A., Allai, F. M., Rizvi, Q. U. E. H., Shiekh, R. A., Sheikh, M. A., & Ahmad, S. (2022). Thermal treatment of foods: science, shelf life, and quality. In *Shelf Life and Food Safety* (pp. 165-180). CRC Press.

Marra, A., Rollo, G., Cimmino, S., & Silvestre, C. (2017). Assessment on the effects of ZnO and Coated ZnO particles on iPP and PLA properties for application in food packaging. *Coatings*, *7*(2), 29.

Martinaga Pintarić, L., Somogi Škoc, M., Ljoljić Bilić, V., Pokrovac, I., Kosalec, I., & Rezić, I. (2020). Synthesis, modification and characterization of antimicrobial textile surface containing ZnO nanoparticles. *Polymers*, *12*(6), 1210.

Masindi, V., & Muedi, K. L. (2018). Environmental contamination by heavy metals. *Heavy metals*, *10*, 115-132.

Mazhar, M. A., Khan, N. A., Ahmed, S., Khan, A. H., Hussain, A., Changani, F., Yousefi, M., Ahmadi, S., & Vambol, V. (2020). Chlorination disinfection by-products in municipal drinking water–a review. *Journal of Cleaner Production*, *273*, 123159.

Mecha, A., Onyango, M., Ochieng, A., & Momba, M. (2019). UV and solar photocatalytic disinfection of municipal wastewater: inactivation, reactivation and regrowth of bacterial pathogens. *International journal of environmental science and technology*, *16*, 3687-3696.

Mecha, A. C., Onyango, M. S., Ochieng, A., Fourie, C. J. S., & Momba, M. N. B. (2016). Synergistic effect of UV–vis and solar photocatalytic ozonation on the degradation of phenol in municipal wastewater: A comparative study. *JCat*, *341*, 116-125. https://doi.org/10.1016/j.jcat.2016.06.015.

Mecha, A. C., Onyango, M. S., Ochieng, A., Jamil, T. S., Fourie, C. J., & Momba, M. N. (2016). UV and solar light photocatalytic removal of organic contaminants in municipal wastewater. *SS&T*, *51*(10), 1765-1778.

Mecha, A. C., Onyango, M. S., Ochieng, A., & Momba, M. N. B. (2017). Evaluation of synergy and bacterial regrowth in photocatalytic ozonation disinfection of municipal wastewater. *Sci. Total Environ.*, *601-602*, 626-635. https://doi.org/10.1016/j.scitotenv.2017.05.204

Mecha, A. C., Onyango, M. S., Ochieng, A., & Momba, M. N. B. (2018). UV and solar photocatalytic disinfection of municipal wastewater: inactivation, reactivation and regrowth of bacterial pathogens. *International Journal of Environmental Science and Technology*, *16*(7), 3687-3696. https://doi.org/10.1007/s13762-018-1950-1

Mecha, A. C., Onyango, M. S., Ochieng, A., & Momba, M. N. B. (2019). Modelling inactivation kinetics of waterborne pathogens in municipal wastewater using ozone. *Environmental Engineering Research*, *25*(6), 890-897. https://doi.org/10.4491/eer.2019.432

Mecha, A. C., Otieno, F. A. O., & Pillay, V. L. (2014). Long-term disinfection performance of silver nanoparticles impregnated membranes. *Desalination and Water Treatment*, *57*(11), 4906-4912. https://doi.org/10.1080/19443994.2014.996778

Mecha, C. A., & Pillay, V. L. (2014). Development and evaluation of woven fabric microfiltration membranes impregnated with silver nanoparticles for potable water treatment. *J. Membr. Sci.*, *458*, 149-156. https://doi.org/10.1016/j.memsci.2014.02.001

Mehmood, T., Ahmed, A., Ahmad, A., Ahmad, M. S., & Sandhu, M. A. (2018). Optimization of mixed surfactants-based β-carotene nanoemulsions using response surface methodology: An ultrasonic homogenization approach. *Food Chem.*, *253*, 179-184.

Mishra, R. K. (2023). Fresh water availability and its global challenge. *British Journal of Multidisciplinary and Advanced Studies*, *4*(3), 1-78.

Mohamadi Zalani, N., Koozegar Kaleji, B., & Mazinani, B. (2020). Synthesis and characterisation of the mesoporous ZnO-TiO$_2$ nanocomposite; Taguchi optimisation and photocatalytic methylene blue degradation under visible light. *Materials Technology*, *35*(5), 281-289.

Mohammadi, H., & Ghorbani, M. (2018). Synthesis photocatalytic TiO$_2$/ZnO nanocomposite and investigation through anatase, wurtzite and ZnTiO$_3$ phases antibacterial behaviors. *Journal of Nano Research*, *51*, 69-77.

Mohsenzadeh, M., Mirbagheri, S. A., & Sabbaghi, S. (2019). Photocatalytic degradation of 1, 2-dichloroethane using immobilized PAni-TiO$_2$ nanocomposite in a pilot-scale packed bed reactor. *Desalination and Water Treatment*, *155*, 72-83.

Mohsin, A. K. (2020). Preparation TiO$_2$ and Zno/TiO$_2$ nanocomposites locally and use against Staphylococcus aureus. IOP Conference Series: Materials Science and Engineering,

Moradi, H., Eshaghi, A., Hosseini, S. R., & Ghani, K. (2016). Fabrication of Fe-doped TiO_2 nanoparticles and investigation of photocatalytic decolorization of reactive red 198 under visible light irradiation. *Ultrason. Sonochem.*, *32*, 314-319.

Moradi, S., Aberoomand-Azar, P., Raeis-Farshid, S., Abedini-Khorrami, S., & Givianrad, M. H. (2016). The effect of different molar ratios of ZnO on characterization and photocatalytic activity of TiO_2/ZnO nanocomposite. *Journal of Saudi Chemical Society*, *20*(4), 373-378.

Moreira, N. F. F., Sampaio, M. J., Ribeiro, A. R., Silva, C. G., Faria, J. L., & Silva, A. M. T. (2019). Metal-free g-C_3N_4 photocatalysis of organic micropollutants in urban wastewater under visible light. *Applied Catalysis B: Environmental*, *248*, 184-192. https://doi.org/10.1016/j.apcatb.2019.02.001

Msomi, P. F. (2015). *Electrospun nanofibers decorated with silver nanoparticles for fouling control* University of Johannesburg (South Africa).

Mufungizi, I., Okon, I., Nkundakozera, M., & Akilimali, A. (2024). Supporting health systems and environment in the Democratic Republic of Congo: A call for action. *Health Science Reports*, *7*(7), e2257.

Munguti, L., & Dejene, F. (2020). Influence of annealing temperature on structural, optical and photocatalytic properties of ZnO–TiO_2 composites for application in dye removal in water. *Nano-Structures & Nano-Objects*, *24*, 100594.

Muthukumar, N., & Thilagavathi, G. (2012). Development and characterization of electrically conductive polyaniline coated fabrics.

Najafi, M., Bastami, T. R., Binesh, N., Ayati, A., & Emamverdi, S. (2022). Sono-sorption versus adsorption for the removal of congo red from aqueous solution using NiFeLDH/Au nanocomposite: Kinetics, thermodynamics, isotherm studies, and optimization of process parameters. *Journal of Industrial and Engineering Chemistry*, *116*, 489-503.

Nascimben Santos, E., László, Z., Hodúr, C., Arthanareeswaran, G., & Veréb, G. (2020). Photocatalytic membrane filtration and its advantages over conventional approaches in the treatment of oily wastewater: a review. *Asia‑Pacific Journal of Chemical Engineering*, *15*(5), e2533.

Naseem, T., & Durrani, T. (2021). The role of some important metal oxide nanoparticles for wastewater and antibacterial applications: A review. *Environmental Chemistry and Ecotoxicology*, *3*, 59-75.

Naseem, T., & Waseem, M. (2022). A comprehensive review on the role of some important nanocomposites for antimicrobial and wastewater applications. *International Journal of Environmental Science and Technology*, 1-26.

Nasrollahzadeh, M., Sajjadi, M., Iravani, S., & Varma, R. S. (2021a). Green-synthesized nanocatalysts and nanomaterials for water treatment: Current challenges and future perspectives. *J. Hazard. Mater.*, *401*, 123401.

Nasrollahzadeh, M., Sajjadi, M., Iravani, S., & Varma, R. S. J. J. o. H. M. (2021b). Green-synthesized nanocatalysts and nanomaterials for water treatment: Current challenges and future perspectives. *401*, 123401.

Nelson, K., Mecha, A. C., & Kumar, A. (2024). Characterization of novel solar based nitrogen doped titanium dioxide photocatalytic membrane for wastewater treatment. *Heliyon*, *10*(8).

Nemiwal, M., Zhang, T. C., & Kumar, D. (2021). Recent progress in g-C_3N_4, TiO_2 and ZnO based photocatalysts for dye degradation: Strategies to improve photocatalytic activity. *Sci. Total Environ.*, *767*, 144896.

Nunes, D., Pimentel, A., Branquinho, R., Fortunato, E., & Martins, R. (2021). Metal oxide-based photocatalytic paper: A green alternative for environmental remediation. *Catalysts*, *11*(4), 504.

Nunnelley, K. (2018). *Metal Nanopatch Formation in Ceramic Porous Media for Point-Of-Use Water Filtration* University of Virginia. https://libraetd.lib.virginia.edu/public_view/pn89d6877

Odonkor, S. T., & Ampofo, J. K. (2013). Escherichia coli as an indicator of bacteriological quality of water: an overview. *Microbiology research*, *4*(1), e2.

Oh, J., Salcedo, D. E., Medriano, C. A., & Kim, S. (2014). Comparison of different disinfection processes in the effective removal of antibiotic-resistant bacteria and genes. *JEnvS*, *26*(6), 1238-1242.

Organization, W. H. (2021). A global overview of national regulations and standards for drinking-water quality.

Organization, W. H. (2022). *Guidelines for drinking-water quality: incorporating the first and second addenda*. World Health Organization.

Organization, W. H. (2024). Guidelines for drinking-water quality: small water supplies.

Osuolale, O., & Okoh, A. (2017). Human enteric bacteria and viruses in five wastewater treatment plants in the Eastern Cape, South Africa. *Journal of infection and public health*, *10*(5), 541-547.

Pang, W. Y., Ahmad, A. L., & Zaulkiflee, N. D. (2019). Antifouling and antibacterial evaluation of ZnO/MWCNT dual nanofiller polyethersulfone mixed matrix membrane. *J. Environ. Manage.*, *249*, 109358.

Parra-Ortiz, E., & Malmsten, M. (2022). Photocatalytic nanoparticles–from membrane interactions to antimicrobial and antiviral effects. *Adv. Colloid Interface Sci.*, *299*, 102526.

Pei, L., Wei, T., Lin, N., & Yu, H. (2016). Synthesis of zinc oxide and titanium dioxide composite nanorods and their photocatalytic properties. *AdCoL*, *25*(1), 096369351602500102.

Peiris, S., de Silva, H. B., Ranasinghe, K. N., Bandara, S. V., & Perera, I. R. (2021). Recent development and future prospects of TiO2 photocatalysis. *J. Chin. Chem. Soc.*, *68*(5), 738-769.

Peleg, M. (2021). Modeling the dynamic kinetics of microbial disinfection with dissipating chemical agents—a theoretical investigation. *Appl. Microbiol. Biotechnol.*, *105*, 539-549.

Pelosato, R., Bolognino, I., Fontana, F., & Sora, I. N. (2022). Applications of heterogeneous photocatalysis to the degradation of oxytetracycline in water: A review. *Molecules*, *27*(9), 2743.

Pillay, V. (2009). The Development of an Immersed Membrane Microfiltration System for the Treatment of Rural Waters and Industrial Waters. *Water Research Commission*.

Pillay, V., & Jacobs, E. (2005). *The development and evaluation of a reverse flow microfilter*.

Pillay, V., & Kalu, A. (2012). A sustainable and robust membrane water treatment unit for potable water production in remote rural areas. Accra, Ghana 4th international appropriate technology conference,

Pizzi, N. G. (2010). Water treatment: Principles and practices of water supply operations. *American Water Works Association, Denver, Colorado*.

Prorokova, N., Kumeeva, T., & Kholodkov, I. (2020). Formation of coatings based on titanium dioxide nanosolson polyester fibre materials. *Coatings*, *10*(1), 82.

Ramírez-Ortega, D., Meléndez, A. M., Acevedo-Peña, P., González, I., & Arroyo, R. (2014). Semiconducting properties of ZnO/TiO_2 composites by electrochemical measurements and their relationship with photocatalytic activity. *Electrochim. Acta*, *140*, 541-549.

Ranjan, P., & Prem, M. (2018). Schmutzdecke-a filtration layer of slow sand filter. *International Journal of Current Microbiology and Applied Sciences*, *7*(07), 637-645.

Rao, A. P., Desai, N., & Rangarajan, R. (1997). Interfacially synthesized thin film composite RO membranes for seawater desalination. *J. Membr. Sci.*, *124*(2), 263-272.

Rastgoo, M., Montazer, M., Harifi, T., & Rad, M. M. (2017). In-situ sonosynthesis of cobblestone-like ZnO nanoparticles on cotton/polyester fabric improving photo, bio and sonocatalytic activities along with low toxicity and enhanced mechanical properties. *Mater. Sci. Semicond. Process.*, *66*, 92-98.

Razani, A., Abdullah, A. H., Fitrianto, A., Yusof, N. A., & Gaya, U. I. (2017). Sol-gel synthesis of Fe_2O_3-doped TiO_2 photocatalyst for optimized photocatalytic degradation of 2, 4-dichlorophenoxyacetic acid. *Oriental Journal of Chemistry*, *33*(4), 1959.

Rheima, A. M., Hussain, D. H., & Abed, H. J. (2020). Fabrication of a new photo-sensitized solar cell using TiO2\ZnO Nanocomposite synthesized via a modified sol-gel Technique. IOP Conference Series: Materials Science and Engineering,

Rienzie, R., Sendanayake, L., & Adassooriya, N. M. (2020). Nanotechnology applications for removal of disinfection by-products from water. In *Disinfection By-products in Drinking Water* (pp. 253-277). Elsevier.

Román, L. E., Gomez, E. D., Solís, J. L., & Gómez, M. M. (2020). Antibacterial cotton fabric functionalized with copper oxide nanoparticles. *Molecules*, *25*(24), 5802.

Rosa, G., Miller, L., & Clasen, T. (2010). Microbiological effectiveness of disinfecting water by boiling in rural Guatemala. *The American journal of tropical medicine and hygiene*, *82*(3), 473.

Sadeghi-Aghbash, M., & Rahimnejad, M. (2022). Zinc phosphate nanoparticles: a review on physical, chemical, and biological synthesis and their applications. *Curr. Pharm. Biotechnol.*, *23*(10), 1228-1244.

Salama, A., & El-Sakhawy, M. (2016). Regenerated cellulose/wool blend enhanced biomimetic hydroxyapatite mineralization. *Int. J. Biol. Macromol.*, *92*, 920-925.

Saluja, K., Reddy, K. S., Wang, Q., Zhu, Y., Li, Y., Chu, X., Li, R., Hou, L., Horsley, T., & Carden, F. (2022). Improving WHO's understanding of WHO guideline uptake and use in Member States: a scoping review. *Health research policy and systems*, *20*(1), 98.

Samsudin, E. M., Goh, S. N., Wu, T. Y., Ling, T. T., Hamid, S. B. A., & Juan, J. C. (2015). Evaluation on the photocatalytic degradation activity of reactive blue 4 using pure anatase nano-TiO2. *Sains Malaysiana*, *44*(7), 1011-1019.

Samuel, J. J., & Yam, F. (2020). Photocatalytic degradation of methylene blue under visible light by dye sensitized titania. *Materials Research Express*, *7*(1), 015051.

Santos, É. N., László, Z., Hodúr, C., Arthanareeswaran, G., & Veréb, G. (2020). Photocatalytic membrane filtration and its advantages over conventional approaches in the treatment of oily wastewater: a review. *methods*, *13*, 14.

Saravanan, A., Kumar, P. S., Jeevanantham, S., Karishma, S., Tajsabreen, B., Yaashikaa, P., & Reshma, B. (2021). Effective water/wastewater treatment methodologies for toxic pollutants removal: Processes and applications towards sustainable development. *Chemosphere*, *280*, 130595.

Sarmah, A. K., Meyer, M. T., & Boxall, A. B. (2006). A global perspective on the use, sales, exposure pathways, occurrence, fate and effects of veterinary antibiotics (VAs) in the environment. *Chemosphere*, *65*(5), 725-759.

Satti, U. Q., Zaidi, S. J. A., Riaz, A., ur Rehman, M. A., Li, C. X., & Basit, M. A. (2023). Simple two-step development of TiO2/Fe2O3 nanocomposite for oxygen evolution reaction (OER) and photo-bio active applications. *Colloids Surf. Physicochem. Eng. Aspects*, *671*, 131662.

Semblante, G. U., Lee, J. Z., Lee, L. Y., Ong, S. L., & Ng, H. Y. (2018). Brine pre-treatment technologies for zero liquid discharge systems. *Desalination*, *441*, 96-111.

Senasu, T., Youngme, S., Hemavibool, K., & Nanan, S. (2021). Sunlight-driven photodegradation of oxytetracycline antibiotic by BiVO4 photocatalyst. *J. Solid State Chem.*, *297*, 122088.

Seneviratne, K. L., Munaweera, I., Peiris, S. E., Peiris, C. N., & Kottegoda, N. (2021). Recent progress in visible-light active (VLA) TiO2 nano-structures for enhanced photocatalytic activity (PCA) and antibacterial properties: a review. *Iranian Journal of Catalysis*, *11*(3), 217-245.

Sethi, D., & Sakthivel, R. (2017). ZnO/TiO$_2$ composites for photocatalytic inactivation of Escherichia coli. *J. Photochem. Photobiol. B: Biol.*, *168*, 117-123.

Shafiee, A., Rabiee, N., Ahmadi, S., Baneshi, M., Khatami, M., Iravani, S., & Varma, R. S. (2022). Core–shell nanophotocatalysts: review of materials and applications. *ACS Applied Nano Materials*, *5*(1), 55-86.

Sharma, S., & Bhattacharya, A. (2017). Drinking water contamination and treatment techniques. *Applied water science*, *7*(3), 1043-1067.

Sharma, S., Mehta, S., & Kansal, S. (2017a). N doped ZnO/C-dots nanoflowers as visible light driven photocatalyst for the degradation of malachite green dye in aqueous phase. *JAllC*, *699*, 323-333.

Sharma, S., Mehta, S. K., & Kansal, S. K. (2017b). N doped ZnO/C-dots nanoflowers as visible light driven photocatalyst for the degradation of malachite green dye in aqueous phase. *JAllC*, *699*, 323-333. https://doi.org/10.1016/j.jallcom.2016.12.408

Sharmin, S., Rahaman, M. M., Sarkar, C., Atolani, O., Islam, M. T., & Adeyemi, O. S. (2021). Nanoparticles as antimicrobial and antiviral agents: A literature-based perspective study. *Heliyon*, *7*(3).

Shathy, R. A., Fahim, S. A., Sarker, M., Quddus, M. S., Moniruzzaman, M., Masum, S. M., & Molla, M. A. I. (2022). Natural sunlight driven photocatalytic removal of toxic textile dyes in water using B-doped ZnO/TiO$_2$ nanocomposites. *Catalysts*, *12*(3), 308.

Shekofteh-Gohari, M., Habibi-Yangjeh, A., Abitorabi, M., & Rouhi, A. (2018). Magnetically separable nanocomposites based on ZnO and their applications in photocatalytic processes: a review. *Crit. Rev. Environ. Sci. Technol.*, *48*(10-12), 806-857.

Shelke, H. D., Machale, A. R., Surwase, A. A., Shaikh, S. F., Rana, A. u. H. S., & Pathan, H. M. (2023). Enhanced Photocatalytic Activity of the Cu$_2$SnS$_3$+ GO Composite for the Degradation of Navy Blue ME2RL Industrial Dye. *Coatings*, *13*(3), 522.

Shi, Q., Chen, Z., Liu, H., Lu, Y., Li, K., Shi, Y., Mao, Y., & Hu, H.-Y. (2021). Efficient synergistic disinfection by ozone, ultraviolet irradiation and chlorine in secondary effluents. *Sci. Total Environ.*, *758*, 143641
.
Shmeis, R. M. A. (2018). Water chemistry and microbiology. In *Comprehensive analytical chemistry* (Vol. 81, pp. 1-56). Elsevier.

Shukla, A. K., Alam, J., & Alhoshan, M. (2022). Recent advancements in polyphenylsulfone membrane modification methods for separation applications. *Membranes*, *12*(2), 247.

Shukla, S., Pandey, H., Singh, P., Tiwari, A. K., Baranwal, V., & Pandey, A. C. (2021). Synergistic impact of photocatalyst and dopants on pharmaceutical-polluted waste water treatment: a review. *Environmental Pollutants and Bioavailability*, *33*(1), 347-364.

Siddique, M., Farooq, R., & Shaheen, A. (2011). Removal of Reactive Blue 19 from wastewaters by physicochemical and biological processes-a review. *J. Chem. Soc. Pak.*, *33*.

Singh, J., Dutta, T., Kim, K. H., Rawat, M., Samddar, P., & Kumar, P. (2018). 'Green' synthesis of metals and their oxide nanoparticles: applications for environmental remediation. *J Nanobiotechnology*, *16*(1), 84. https://doi.org/10.1186/s12951-018-0408-4

Singh, J., Kumar, S., Manna, A. K., & Soni, R. (2020). Fabrication of ZnO–TiO$_2$ nanohybrids for rapid sunlight driven photodegradation of textile dyes and antibiotic residue molecules. *OptMa*, *107*, 110138.

Slavik, I., Oliveira, K. R., Cheung, P. B., & Uhl, W. (2020). Water quality aspects related to domestic drinking water storage tanks and consideration in current standards and guidelines throughout the world–a review. *J. Water Health*, *18*(4), 439-463.

Soleimani, M., Ghasemi, J. B., Ziarani, G. M., Karimi-Maleh, H., & Badiei, A. (2021). Photocatalytic degradation of organic pollutants, viral and bacterial pathogens using titania nanoparticles. *Inorg. Chem. Commun.*, *130*, 108688.

Song, N., Gao, X., Ma, Z., Wang, X., Wei, Y., & Gao, C. (2018). A review of graphene-based separation membrane: Materials, characteristics, preparation and applications. *Desalination*, *437*, 59-72.

Song, X., Bayati, P., Gupta, M., Elahinia, M., & Haghshenas, M. (2021). Fracture of magnesium matrix nanocomposites-a review. *International Journal of Lightweight Materials and Manufacture*, *4*(1), 67-98.

Soni, R., Bhardwaj, S., & Shukla, D. P. (2020). Various water-treatment technologies for inorganic contaminants: current status and future aspects. *Inorganic Pollutants in water*, 273-295.

Sridevi, K., Sivakumar, S., Sangeetha, B., Saravanan, K., & Praveen, H. (2021). Zno-Tio2 Nanocomposites Synthesized By Sol-Gel Route: Study Of Their Structural And Optical Properties. *NVEO-NATURAL VOLATILES & ESSENTIAL OILS Journal| NVEO*, 4840–4853-4840–4853.

Srivastav, A. L., Patel, N., & Chaudhary, V. K. (2020). Disinfection by-products in drinking water: occurrence, toxicity and abatement. *Environ. Pollut.*, *267*, 115474.

STANDARD, D. E. A. (2018). Draft East African Standard. *Draft East African Standards*, *3*(9).

Standardization, I.-I. O. f. (2017). International Standard ISO 7001, Graphical symbols–Public information symbols. In.

Sudrajat, H. J. J. o. C. P. (2018). Superior photocatalytic activity of polyester fabrics coated with zinc oxide from waste hot dipping zinc. *172*, 1722-1729.

Suliman, Z. A., Mecha, A. C., & Mwasiagi, J. I. (2024). Effect of TiO_2/Fe_2O_3 nanopowder synthesis method on visible light photocatalytic degradation of reactive blue dye. *Heliyon*.

Sun, Y., Zhang, W., Li, Q., Liu, H., & Wang, X. (2023). Preparations and applications of zinc oxide based photocatalytic materials. *Advanced Sensor and Energy Materials*, 100069.

Tahir, K., Nazir, S., Li, B., Ahmad, A., Nasir, T., Khan, A. U., Shah, S. A. A., Khan, Z. U. H., Yasin, G., & Hameed, M. U. (2016). Sapium sebiferum leaf extract mediated synthesis of palladium nanoparticles and in vitro investigation of their bacterial and photocatalytic activities. *J. Photochem. Photobiol. B: Biol.*, *164*, 164-173.

Talebi, S., Chaibakhsh, N., & Moradi-Shoeili, Z. (2017). Application of nanoscale ZnS/TiO_2 composite for optimized photocatalytic decolorization of a textile dye. *Journal of applied research and technology*, *15*(4), 378-385.

Tang, S., Meng, X., Lu, H., & Zhu, S. (2009). PVP-assisted sonoelectrochemical growth of silver nanostructures with various shapes. *MCP*, *116*(2-3), 464-468.

Tapia-Tlatelpa, T., Trull, J., & Romeral, L. (2019). In situ decolorization monitoring of textile dyes for an optimized UV-LED/TiO2 reactor. *Catalysts*, *9*(8), 669.

Terán Hilares, R., Singh, I., Tejada Meza, K., Colina Andrade, G. J., & Pacheco Tanaka, D. A. (2022). Alternative methods for cleaning membranes in water and wastewater treatment. *Water Environ. Res.*, *94*(4), e10708.

Theerthagiri, J., Chandrasekaran, S., Salla, S., Elakkiya, V., Senthil, R., Nithyadharseni, P., Maiyalagan, T., Micheal, K., Ayeshamariam, A., & Arasu, M. V. (2018). Recent developments of metal oxide based heterostructures for photocatalytic applications towards environmental remediation. *J. Solid State Chem.*, *267*, 35-52.

Theivasanthi, T., & Alagar, M. (2013). Titanium dioxide (TiO_2) nanoparticles XRD analyses: an insight. *arXiv preprint arXiv:1307.1091*.

Thokchom, B., Radhapyari, K., & Dutta, S. (2020). Occurrence of trihalomethanes in drinking water of Indian states: a critical review. *Disinfection by-products in drinking water*, 83-107.

Tlili, I., & Alkanhal, T. A. (2019). Nanotechnology for water purification: electrospun nanofibrous membrane in water and wastewater treatment. *Journal of Water Reuse and Desalination*, *9*(3), 232-248.

Torrades, F., & García-Montaño, J. (2014). Using central composite experimental design to optimize the degradation of real dye wastewater by Fenton and photo-Fenton reactions. *Dyes and pigments*, *100*, 184-189.

Touati, K., & Tadeo, F. (2017). Pressure retarded osmosis as renewable energy source. In *Pressure Retarded Osmosis* (pp. 1-54). Elsevier.

Tripathi, S., & Hussain, T. (2022). Water and wastewater treatment through ozone-based technologies. In *Development in wastewater treatment research and processes* (pp. 139-172). Elsevier.

Umar, K., Aris, A., Parveen, T., Jaafar, J., Majid, Z. A., Reddy, A. V. B., & Talib, J. (2015). Synthesis, characterization of Mo and Mn doped ZnO and their photocatalytic activity for the decolorization of two different chromophoric dyes. *Applied Catalysis A: General*, *505*, 507-514.

Upadhyay, G. K., Rajput, J. K., Pathak, T. K., Kumar, V., & Purohit, L. (2019). Synthesis of ZnO: TiO_2 nanocomposites for photocatalyst application in visible light. *Vacuu*, *160*, 154-163.

Vacs Renwick, D. A. (2013). *The effects of an intermittent piped water network and storage practices on household water quality in Tamale, Ghana* Massachusetts Institute of Technology.

Van Thuan, D., Ngo, H. L., Thi, H. P., & Chu, T. T. H. (2023). Photodegradation of hazardous organic pollutants using titanium oxides-based photocatalytic: A review. *Environ. Res.*, *229*, 116000.

Verma, S., Daverey, A., & Sharma, A. (2017). Slow sand filtration for water and wastewater treatment–a review. *Environmental Technology Reviews*, *6*(1), 47-58.

Verma, S. K., Singhal, P., & Chauhan, D. S. (2019). A synergistic evaluation on application of solar-thermal energy in water purification: Current scenario and future prospects. *Energy Convers. Manage.*, *180*, 372-390.

Wang, C.-y., Böttcher, C., Bahnemann, D. W., & Dohrmann, J. K. (2003). A comparative study of nanometer sized Fe (III)-doped TiO_2 photocatalysts: synthesis, characterization and activity. *JMCh*, *13*(9), 2322-2329.

Wang, L., Fu, X., Han, Y., Chang, E., Wu, H., Wang, H., Li, K., & Qi, X. (2013). Preparation, characterization, and photocatalytic activity of TiO_2/ZnO nanocomposites. *Journal of nanomaterials*, *2013*, 15-15.

Wang, L., Kahrizi, M., Lu, P., Wei, Y., Yang, H., Yu, Y., Wang, L., Li, Y., & Zhao, S. (2021). Enhancing water permeability and antifouling performance of thin–film composite membrane by tailoring the support layer. *Desalination*, *516*, 115193.

Wang, W., Yu, Y., An, T., Li, G., Yip, H. Y., Yu, J. C., & Wong, P. K. (2012). Visible-light-driven photocatalytic inactivation of *E. coli* K-12 by bismuth vanadate nanotubes: bactericidal performance and mechanism. *Environ. Sci. Technol.*, *46*(8), 4599-4606. https://doi.org/10.1021/es2042977

Wang, X., Yao, S., & Li, X. (2009). Sol-gel preparation of CNT/ZnO nanocomposite and its photocatalytic property. *Chin. J. Chem .* *27*(7), 1317-1320.

Wei, F.-Q., Lu, Y., Shi, Q., Chen, Z., Li, K.-X., Zhang, T., Shi, Y.-L., Xu, Q., & Hu, H.-Y. (2022). A dose optimization method of disinfection units and synergistic effects of combined disinfection in pilot tests. *Water Res.*, *211*, 118037.

Woolf, A. D., Stierman, B. D., Barnett, E. D., Byron, L. G., Bole, A., Balk, S. J., Huerta-Montañez, G. M., Landrigan, P. J., Marcus, S. M., & Nerlinger, A. L. (2023). Drinking water from private wells and risks to children. *Pediatrics*, *151*(2).

Wydro, U., Wołejko, E., Luarasi, L., Puto, K., Tarasevičienė, Ž., & Jabłońska-Trypuć, A. (2023). A Review on Pharmaceuticals and Personal Care Products Residues in the Aquatic Environment and Possibilities for Their Remediation. *Sustainability*, *16*(1), 169.

Xia, X., Lan, S., Li, X., Xie, Y., Liang, Y., Yan, P., Chen, Z., & Xing, Y. (2018). Characterization and coagulation-flocculation performance of a composite flocculant in high-turbidity drinking water treatment. *Chemosphere*, *206*, 701-708.

Yang, H., Xu, S., Chitwood, D. E., & Wang, Y. (2020). Ceramic water filter for point-of-use water treatment in developing countries: Principles, challenges and opportunities. *Frontiers of Environmental Science & Engineering*, *14*, 1-10.

Yang, T., Peng, J., Zheng, Y., He, X., Hou, Y., Wu, L., & Fu, X. (2018). Enhanced photocatalytic ozonation degradation of organic pollutants by ZnO modified TiO_2 nanocomposites. *Applied Catalysis B: Environmental*, *221*, 223-234.

Yang, X., Cao, C., Erickson, L., Hohn, K., Maghirang, R., & Klabunde, K. (2008). Synthesis of visible-light-active TiO2-based photocatalysts by carbon and nitrogen doping. *JCat*, *260*(1), 128-133

Yaqoob, A. A., Parveen, T., Umar, K., & Mohamad Ibrahim, M. N. (2020). Role of nanomaterials in the treatment of wastewater: A review. *Water*, *12*(2), 495.

Yeneneh, A. M., Al Balushi, K., Jafary, T., & Al Marshudi, A. S. (2024). Hydrodynamic Cavitation and Advanced Oxidation for Enhanced Degradation of Persistent Organic Pollutants: A Review. *Sustainability*, *16*(11), 4601.

Yu, R., Chen, W., Zhang, J., Liu, J., Li, X.-y., & Lin, L. (2024). Catalytic membranes for water treatment: Perspectives and challenges. *Journal of Hazardous Materials Advances*, 100414.

Zarei, N., & Behnajady, M. A. (2019). Optimization of photocatalytic activity of Mg/ZnO nanoparticles in the removal of a model contaminant using response surface methodology. *Environmental Engineering & Management Journal (EEMJ)*, *18*(2).

Zhang, C., Ouyang, Z., Yang, Y., Long, X., Qin, L., Wang, W., Zhou, Y., Qin, D., Qin, F., & Lai, C. (2022). Molecular engineering of donor-acceptor structured g-C3N4 for superior photocatalytic oxytetracycline degradation. *Chem. Eng. J.*, *448*, 137370.

Zhang, G., Wang, D., Yan, J., Xiao, Y., Gu, W., & Zang, C. (2019). Study on the photocatalytic and antibacterial properties of TiO_2 nanoparticles-coated cotton fabrics. *Materials*, *12*(12), 2010.

Zhang, H., Luo, Y., Wu, L., Huang, Y., & Christie, P. (2015). Residues and potential ecological risks of veterinary antibiotics in manures and composts associated with protected vegetable farming. *Environmental Science and Pollution Research*, *22*, 5908-5918.

Zhang, J., Wu, H., Shi, L., Wu, Z., Zhang, S., Wang, S., & Sun, H. (2023). Photocatalysis coupling with membrane technology for sustainable and continuous purification of wastewater. *Sep. Purif. Technol.*, 125225.

Zhang, Q.-Q., Ying, G.-G., Pan, C.-G., Liu, Y.-S., & Zhao, J.-L. (2015). Comprehensive evaluation of antibiotics emission and fate in the river basins of China: source analysis, multimedia modeling, and linkage to bacterial resistance. *Environ. Sci. Technol.*, *49*(11), 6772-6782.

Zhang, S., Zhao, S., Huang, S., Hu, B., Wang, M., Zhang, Z., He, L., & Du, M. (2021). Photocatalytic degradation of oxytetracycline under visible light by nanohybrids of CoFe alloy nanoparticles and nitrogen-/sulfur-codoped mesoporous carbon. *Chem. Eng. J.*, *420*, 130516.

Zhao, X., Castka, P., & Searcy, C. (2020). ISO standards: a platform for achieving sustainable development goal 2. *Sustainability*, *12*(22), 9332.

Zhu, J., Zheng, W., He, B., Zhang, J., & Anpo, M. (2004). Characterization of Fe–TiO_2 photocatalysts synthesized by hydrothermal method and their photocatalytic reactivity for photodegradation of XRG dye diluted in water. *J. Mol. Catal. A: Chem.*, *216*(1), 35-43.

Zúñiga-Miranda, J., Guerra, J., Mueller, A., Mayorga-Ramos, A., Carrera-Pacheco, S. E., Barba-Ostria, C., Heredia-Moya, J., & Guamán, L. P. (2023). Iron oxide nanoparticles: green synthesis and their antimicrobial activity. *Nanomaterials*, *13*(22), 2919.

APPENDIXES

Appendix A. Chemical characteristics affecting the safety of potable water according to

WHO standard (Organization, 2021)

Appendix A.1 Inorganic contaminants Limits for inorganic contaminants in natural and

treated potable water

Sl. No.	Element	WHO Guideline value mg/l	Maximum value set mg/l	Minimum value set mg/l	Median value mg/l
1	Antimony	0.020	0.050	0.003	0.005
2	Arsenic	0.010	0.500	0.007	0.010
3	Barium	0.700	2.000	0.10	0.700
4	Beryllium	None specified	0.060	0.0002	0.004
5	Boron	2.400	5.000	0.200	1.000
6	Bromate	0.010	0.025	0.005	0.010
7	Cadmium	0.003	0.050	0.001	0.050
8	Chlorate	0.070	1.000	0.050	0.700
9	Chlorine	5.000	5.000	0.100	0.900
10	Chlorite	0.700	1.000	0.050	0.700
11	Chromium (total)	0.050	0.500	0.040	0.050
12	Copper	2.000	3.000	0.050	1.500
13	Fluoride	1.500	4.000	0.600	1.500
14	Lead	0.010	0.100	0.005	0.010
15	Mercury	0.006	0.007	0.0005	0.001
16	Nickel	0.070	0.100	0.010	0.020
17	Nitrate (as NO^{3-})	50.00	75.00	40.00	50.00
18	Selenium	0.040	0.050	0.007	0.010
19	Uranium	0.030	0.100	0.002	0.015
20	Molybdenum	0.070	0.250	0.050	0.070
21	Manganese	0.400	0.500	0.05	0.100
22	Glyphosate	0.900	1.000	0.010	0.700
23	Cyanide	0.070	0.600	0.010	0.050

Appendix A.2 Organic contaminants Limits for organic contaminants in treated and

natural potable water

Sl. No.	Element	WHO Guideline value mg/l	Maximum value set mg/l	Minimum value set mg/l	Median value mg/l
1	Alachlor	0.020	0.150	0.002	0.020
2	Bentazone	None specified	0.400	0.030	0.030
3	Benzene	0.010	0.030	0.001	0.005
4	Carbofuran	0.007	0.090	0.004	0.007
5	Carbon tetrachloride	0.004	0.005	0.001	0.004
6	Chloral hydrate	0.100	0.100	0.010	0.010
7	Chloroform	0.300	0.400	0.030	0.200
8	Cyanuric Acid	40.00	0.000	0.000	0.000
9	Dichloroacetic acid	0.050	0.050	0.020	0.050
10	1,4-Dioxane	0.050	0.050	0.050	0.050
11	Edetec Acid (EDTA)	0.600	0.700	0.150	0.425
12	Ethylbenzene	0.300	0.700	0.002	0.030
13	Fenoprop	0.009	0.010	0.006	0.009
14	Hydroxyatrazine	0.200	0.000	0.000	0.000
15	Isoproturon	0.009	0.010	0.007	0.009
16	Mecoprop	0.010	0.010	0.001	0.010
17	Methoxychlor	0.020	0.900	0.015	0.020
18	Molinate	0.006	0.007	0.004	0.006
19	Parathion	None	0.050	0.003	0.020
20	Pendimethalin	0.020	0.400	0.015	0.020
21	Simazine	0.002	0.020	0.002	0.002
22	Styrene	0.020	0.100	0.015	0.020
23	Terbuthylazine	0.007	0.010	0.007	0.007
24	Trifluralin	0.020	0.090	0.020	0.020

Appendix A.3 Radiological parameters Limits for radioactive materials in treated and natural potable water

Sl. No.	Element	WHO Guideline value	Maximum value set	Minimum value set	Median value set
1	Total Dose	0.1 mSv/year	1.0 mSv/year	0.1 mSv/year	0.1 mSv/year
2	Gross alpha activity	0.5 Bq/l	0.56 Bq/l	0.01 Bq/l	0.1 Bq/l
3	Gross beta activity	1 Bq/l	2.0Bq/l	0.1 Bq/l	1 Bq/l

Appendix B Chemical characteristics affecting the safety of potable water according to

Kenya standard (EAS, 2014)

Appendix B.1 Inorganic contaminants Limits for inorganic contaminants in natural and

treated potable water

Sl. No.	Substance	Treated potable water limit of concentration mg/L, max.	Natural potable water	Method of test
1	Arsenic, as As	0.01	0.01	ISO 11969
2	Cadmium, as Cd	0.003	0.003	ISO 5961
3	Lead, as Pb	0.01	0.01	ISO 8288
4	Copper, as Cu	1.000	1.000	ISO 8288
5	Mercury (total as Hg)	0.001	0.001	ISO 12846
6	Manganese, as Mn	0.1	0.1	ISO 6333
7	Selenium, as Se	0.01	0.01	ISO 9965
8	Ammonia (NH3)	0.5	0.5	ISO 11732
9	Chromium Total, as Cr		0.05	ISO 9174
10	Nickel, as Ni	0.02	0.02	ISO 8288
11	Cyanide, as CN	0.01	0.01	ISO 6703
12	Barium, as Ba	0.7	0.7	ISO 14911
13	Nitrate as NO3-	45	45	ISO 7890
14	Boron,as Boric acid	2.4	2.4	ISO 9390
15	Fluoride, as F	1.5	1.5	ISO 10359
16	Bromate, as BrO3-	0.01	0.01	ISO 15061
17	Nitrite	0.003	0.003	ISO 6777
18	Molybdenum	0.07	0.07	ISO 11885
19	Phosphates, as PO4-3	2.2	2.2	ISO 15681
20	Residual free Chlorine	0.2-0.5 [a]	Absent	ISO 7393

[a] Under conditions of epidemic diseases, it may be necessary to increase the residual chlorine temporarily.

Appendix B.2 Organic contaminants Limits for organic contaminants in treated and

natural potable water

l. No.	Substance (Arrange alphabetical order)	Limit µg/L max.	Method of test
1	Aromatics		
	Benzene	10	ISO 11423
	Toluene	700	-
	Xylene	500	-
	Polynuclear aromatic hydrocarbon	0.7	ISO 13877
2	Chlorinated Alkanes and Alkenes		
	Carbon tetrachloride	2	-
	1,2-Dichloroethane	30	-
	1,1-Dichloroethylene	0.3	-
	1,1-Dichloroethene	30	-
	Tetrachloroethene	40	-
3	Phenolic substances		
	Phenols	2	ISO 8165
	2,4,6-Trichlorophenol	200	ISO 14402
4	Trihalomethanes		
	Chloroform	30	-
5	Pesticides		
	Aldrin/Dieldrin	0.03	ISO 15089
	Chlordane (total)	0.3	
	2,4- Dichlorophenoxyacetic acid	30	
	DDT (total)	1	
	Heptachlor and Heptachlor Epoxide	0.03	
	Hexachlorobenzene	1	
	Lindane BHC	2	
	Methoxychlor	20	
6	Surfactants (reacting with methylene Blue)	200	ISO 16265
7	Mineral oil	0.01	-
8	Organic matter	3	-

Appendix B.3 Radioactive characteristics Limits for radioactive materials in treated and

natural potable water

Sl. No.	Radioactive material	Limits in Bq/L	Method of test
1	Gross alpha activity	0.5	ISO 9696
2	Gross beta activity	1	ISO 9697

Appendix C1 Disinfection By-products limits by different organizations (A)

Disinfectant	DBPs		Cancer Group	WHO	US EPA	United Kingdom	Canada	European Union	South Africa	Japan	China	Korea	Australia	New Zealand	India
Chlorine or Chloramine	Trihalo Methanes	Chloroform	2B	0.30	0.08	-	-	-	0.30	0.06	0.06	0.08	-	0.40	0.20
		Bromodi chloro methane	2B	0.06	0.80	-	-	-	0.06	0.03	0.06	-	-	0.06	0.06
		Dibromo chloro methane	3	0.10	0.08	-	-	-	0.1	0.1	0.1	-	-	0.15	0.10
		Bromoform	3	0.10	0.08	-	-	-	0.1	0.09	0.1	-	-	0.10	0.10
		Total THM		*	0.08	0.10	0.10	0.10	*	0.10	*	0.10	0.25	*	-
	Halo acetic Acids	Mono chloro acetic acid		0.02	0.06	-	-	-	-	0.02	-	-	0.15	0.02	-
		Dichloro acetic acid	2B	0.05	0.06	-	-	-	-	0.03	0.05	-	0.10	0.05	-
		Trichloro acetic acid	2B	0.20	0.06	-	-	-	-	0.03	0.1	-	0.10	0.20	-
		Dibromo acetic acid	-	-	-	-	-	-	-	-	-	-	-	-	-
		Bromochloro acetic acid	-	-	-	-	-	-	-	-	-	-	-	-	-
		Total HAA		-	0.06	-	0.08	0.06	-	-	-	0.10	-	-	-
	Chlora mines	Monochlo ramines	3.00	3.00	4.00	-	3.00	-	3.00	-	3.00	-	3.00	3.00	-
	NDMA	N-Nitroso dimethyla mine	2A	0.0001	-		0.00004							0.0001	
	Halo aceto nitrile	Dichloroace tonitrile	3.00	0.02	-	-	-	-	-	0.04	-	0.09	-	0.02	-
		Trichloro acetonitrile	3.00	-	-	-	-	-	-	-	-	0.004	-	-	-
		Dibromoace tonitrile	2B	0.07	-	-	-	-	-	-	-	0.10	-	0.08	-
		Bromochloro acetonitrile	3.00	-	-	-	-	-	-	-	-	-	-	-	-
	Cyanide	Cyanogen chloride as cyanide	-	-	-	-	-	-	0.01	0.07	-	0.08		0.40	-
		Cyanide		-	0.20	0.05	0.20	0.05	0.20	-	0.05	0.01	0.08	0.40	-
		Nitrite	2A	3.00	1.00	0.50	3(a)	0.50	0.90		1.00		3.00	3.00	
		Nitrate	2A	50.0	10.0	50.0	45(a)	50.0	11.0	10.0	10.0		50.0	50.0	

280

Appendix C2 Disinfection By-products limits by different organizations (B)

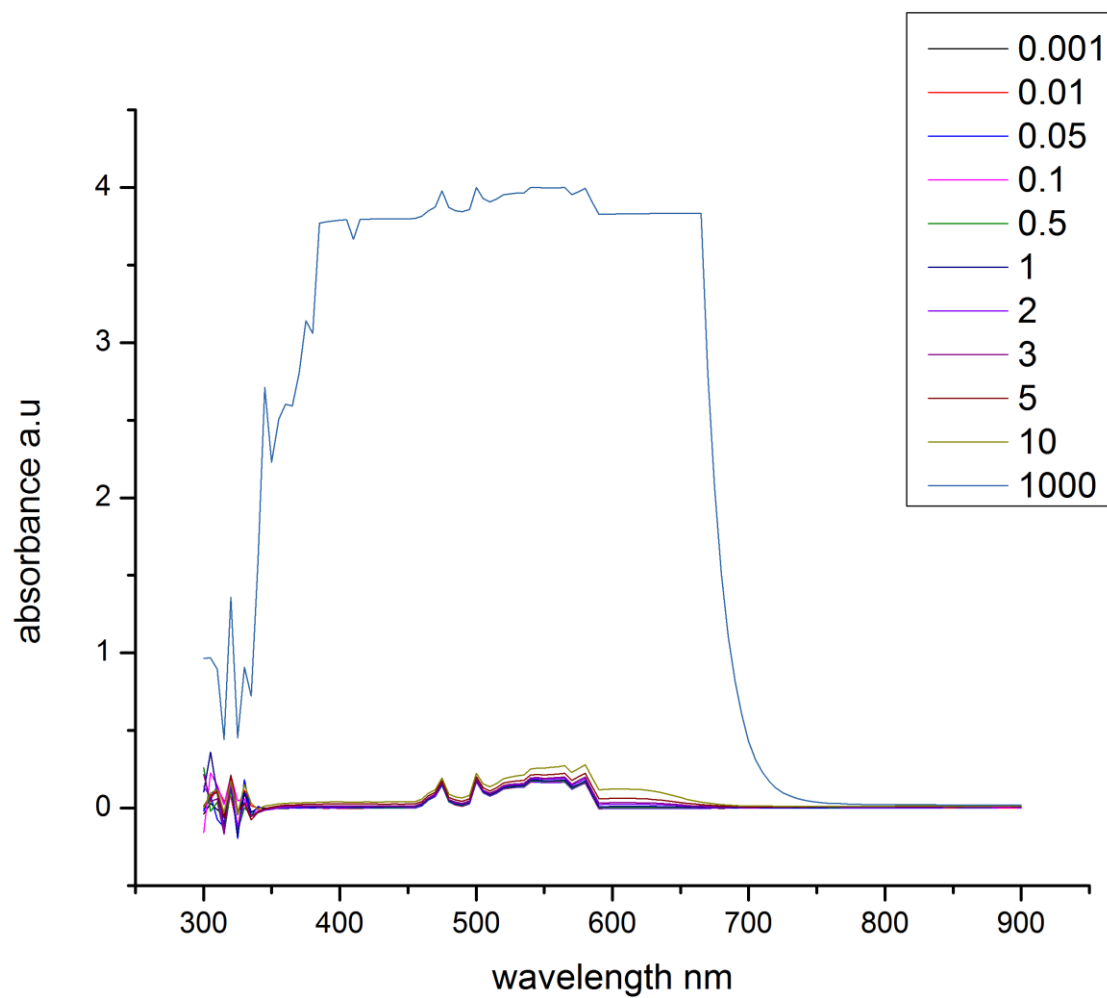| Disinfectant	DBPs		Cancer Group	WHO	US EPA	United Kingdom	Canada	European Union	South Africa	Japan	China	Korea	Australia	New Zealand	India
Chlorine or Chloramine	Chloral hydrate	Trichloro acetaldehyde	2A	-	-	-	0.20	-	-	-	0.03	0.01	0.03	0.001(c)	
Chlorine dioxide	Choloro phenols		-	-	-	-	-	-	-	-	-	0.30	0.0001(c)	-	
			-	-	-	0.90	-	-	-	-	-	0.20	0.0003(c) 0.04(d)	-	
		2,4,6-tricholoro phenol	2B	-	-	0.005	-	-	-	0.20	-	0.02	0.0002(a) 0.3(b)	-	
		2,3,4,6-tetra choloro phenol	-	-	-	0.10	-	-	-	-	-	-	-	-	
	Pentachloro phenol	1.00	0.009	0.001	-	0.06	-	-	-	0.009	-	-	0.009	-	
Oxy halides	Chlorite			0.70	1.00	-	1.00	0.25	-	0.60	0.70	-	0.80	0.80	-
	Chlorate			0.70	-	-	1.00	0.25	-	0.60	0.70	-	-	0.80	-
	Bromate	2B	0.01	0.01	0.01	0.01	0.01	0.01	-	0.01	0.01	-	0.02	0.01	-
Ozone	Formaldehyde	1.00	-	-	-	-	-	-	0.08	0.90	-	0.50	-	-	

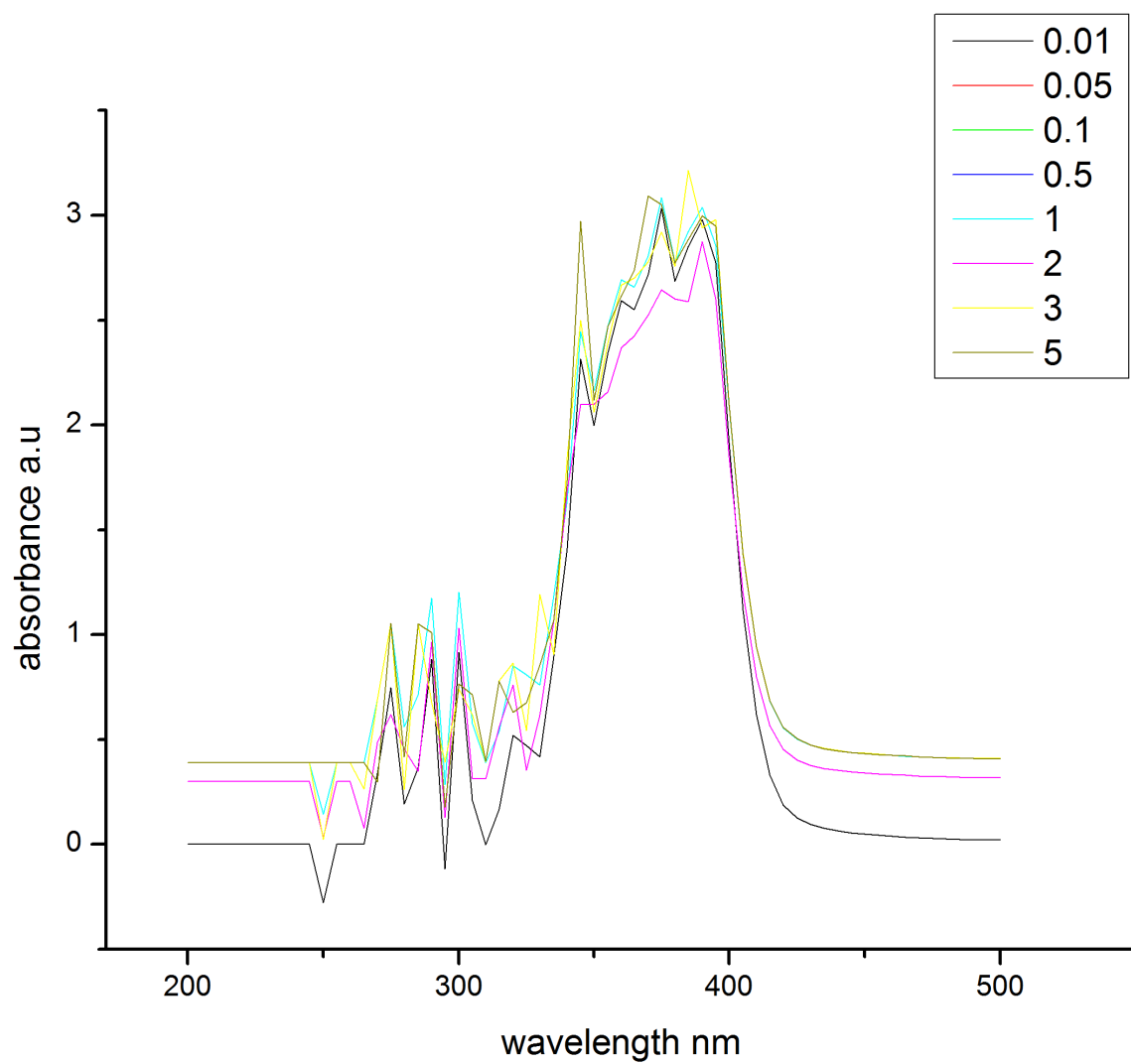**Appendix D.** Raw data the removal efficiency % of different concentration of blue dye (1, 2 and 3) ppm using bare TiO_2 and codoped photocatalysts for 1and 2 hr irradiation time

Photocatalyst type	Concentration ppm	1 hr irradiation Removal Efficiency %	2 hr irradiation Removal Efficiency %
TiO_2	1	87.00	96.26
	2	88.77	98.15
	3	92.6	98.77
α-Fe_2O_3-TiO_2 (TFC)	1	98.75	100.0
	2	88.80	100.0
	3	88.00	100.0
α-Fe_2O_3-TiO_2 (TFT)	1	92.50	100.0
	2	88.50	100.0
	3	88.00	100.0
ZnO	1	68.00	85.00
	2	69.00	81.50
	3	65.00	81.30
ZnO-TiO_2 (TZC)	1	68.00	87.00
	2	67.70	84.00
	3	65.20	82.00
ZnO-TiO_2 (TZT)	1	95.00	100.0
	2	93.48	100.0
	3	91.00	100.0

Appendix E. Raw data the removal efficiency % of pH (3, 7, and 11) of blue dye (3, 7 and 11) using bare TiO_2 and codoped photocatalysts for 1and 2 hr irradiation time

Photocatalyst type	pH	1 hr irradiation Removal Efficiency %	2 hr irradiation Removal Efficiency %
TiO_2	3	85	94
	7	87	96.26
	11	22.7	30
$\alpha\text{-}Fe_2O_3\text{-}TiO_2$	3	96	100
(TFC)	7	98.75	100
	11	30	36.3
$\alpha\text{-}Fe_2O_3\text{-}TiO_2$	3	89.4	100
(TFT)	7	92.5	100
	11	29.5	37
ZnO	3	65	84
	7	68	85
	11	20	30.4
$ZnO\text{-}TiO_2$	3	65	86
(TZC)	7	68	87
	11	28	34
$ZnO\text{-}TiO_2$	3	93	100
(TZT)	7	95	100
	11	30	36

Appendix F. UV spectroscopy results for the reactive blue dye concentrations ranging from 0.001 to 10 ppm, plus an additional concentration of 1000 ppm,

Appendix G. UV spectroscopy results for oxytetracycline OTC concentrations ranging from 0.001 to 5 ppm,

Research Outputs of this Study

Publications

1. Suliman, Z. A., Mecha, A. C., & Mwasiagi, J. I. (2024). Effect of TiO_2/Fe_2O_3 nanopowder synthesis method on visible light photocatalytic degradation of reactive blue dye. *Heliyon, 10(8).* https://doi.org/10.1016/j.heliyon.2024.e29648

2. Zeinab, S., Mecha, A., & Mwasiagi, J. (2024). Development of Wash-Durable Antimicrobial Polyester/Cotton Fabrics by Impregnation with Zinc-Oxide Nanoparticles. Fascicle of Textiles, Leatherwork, 87.

3. Suliman, Z. A., Mecha, A. C., & Mwasiagi, J. I. (2024). Characterization and growth inhibition of *Escherichia Coli* bacteria using cotton fabrics coated with Zinc Oxide nanoparticles. Industria textila journal (Accepted for puplication)

4. Suliman, Z. A., Mecha, A. C., & Mwasiagi, J. I. (2024). Characterization and Disinfection Performance of α-Fe_2O_3-TiO_2 Based Polyester Membranes for Water Treatment. Universal Journal of Green Chemistry, 336-346.
   DOI: https://doi.org/10.37256/ujgc.2220245851

Conferences

1. Development of wash-durable antimicrobial polyester fabrics by impregnation with zinc-oxide based nanoparticles, **SAISTA**, 2023. Mombasa, Kenya

2. Characterization and Antibacterial Properties of ZnO Nanoparticles-Coated Cotton Fabrics, **ICKT**, 2024. Faisal Abad, Pakistan

3. Suliman, Z., Mecha, C., & Mwasiagi, J. (2024). Photo-degradation of reactive blue dye (171) by TiO_2/Fe_2O_3 photocatalysis under visible light irradiation. **MDPI** in The 8th International Electronic Conference on Water Sciences session Urban Water, Treatment Technologies, Systems Efficiency and Smart Water Grids